Development of a protein-protein displacement platform using an anti-minocycline single domain antibody and a dedicated displaceable peptide for the generation of an OFF-switch CAR T cell

Ram Jha

University College London

UCL Cancer Institute

Department of Haematology

A thesis submitted to University College London (UCL) for the degree of Doctor of Philosophy

2022

Supervised by Dr Martin Pule & Dr Simon Thomas

Declaration

I, Ram Jha confirm that the work presented in this thesis is my own. Where information has been derived from other sources, I confirm that this has been indicated in the thesis.

Acknowledgements

ABSTRACT

Chimeric antigen receptor (CAR) T cell therapy has shown remarkable success in the clinic; however, the treatment carries potential risks of significant toxicities. A versatile small-molecule control system is desirable to increase control and mitigate toxicity in clinical settings. I set about creating a two-component small-molecule control system based on disruption of protein-protein interactions. Given its wide availability, excellent bio-distribution, and lack of toxicity, this system was developed around minocycline.

The protein-protein displacement system was composed of an anti-minocycline single-domain antibody (sdAb) and a minocycline displaceable sdAb-specific cyclic peptide. Minocycline-specific sdAbs were generated by immunising an alpaca with KLH-conjugated minocycline. The highest affinity sdAb-minocycline binding was measured at 31 nM. Displaceable cyclic peptides were isolated by panning a cysteine-constrained heptapeptide phage library against the sdAb and eluted using minocycline. Peptide sequence, ACPGWARAFC, presented the highest affinity sdAb binding at 111 nM. Utilising the displacement system, an OFF-switch split CAR was developed, made up of a physically separated antigen-binding chain bearing a tumour-specific sdAb and the anti-minocycline sdAb which interacts with a cyclic peptide bearing signaling chain forming a functional CAR heterodimer (MinoCAR). MinoCAR showed cytotoxicity and cytokine release against tumour cells comparable to a conventional CAR. Transient suppression of MinoCAR was achieved via the administration of minocycline in a dose-dependent and reversible manner. To apply the system to control secretion of cellular payloads, the KDEL retention motif was fused to the sdAb thus anchoring it to the ER/Golgi. The pro-inflammatory cytokine IL-12 was fused to ACPGWARAFC thus causing its cellular retention. Upon the addition of minocycline, the sdAb-peptide complex was displaced, enabling the secretion of IL-12.

This work allows remote-controlled regulation of a novel minimally immunogenic OFF-switch CAR using an FDA approved drug which may permit clinicians to precisely control the timing, intensity and safety of the tumour targeted response.

Impact Statement

Cancer is a broad disease defined by the rapid growth of abnormal cells, which can occupy neighbouring tissue or metastasise to other tissue and organs. Cancer is one of the leading causes of death worldwide. In 2020, 1 in 6 deaths or approximately 10 million deaths worldwide were directly caused by the disease. Chimeric antigen receptor (CAR) T cell therapy has demonstrated significant clinical efficacy in the treatment of haematological malignancies and is being developed to target solid tumours. However, the therapy has the potential to induce life-threatening toxicities such as cytokine release syndrome (CRS), neurotoxicity and on-target off-tumour toxicities.

Current strategies to control such toxicities is based on the selective ablation of the therapy or dampening of T cells using steroids, although useful in controlling toxicities, the therapy is permanently destroyed which may lead to disease relapse. Therefore, re-administration of CAR T cell therapy as a treatment option may be restricted due to economic implications to the patient or the health care provider.

The work carried out in the thesis describes a protein displacement platform and its application as an OFF-switch CAR T cell, where it's activity can be modulated using a safe and well-tolerated antibiotic drug minocycline. This technology has the potential to have a significant impact on patient safety and treatment outcome by precisely controlling the timing of CAR T cell activation in response to real-time adverse effects. Moreover, the minimally immunogenic components utilised in this work may also reduce potential adverse immune reactions, further improving patient care and treatment outcome.

Besides enhancing patient safety, CAR T cell-based therapeutics is one of the fastest immerging fields in cancer therapy and has generated immense media and commercial interest over the past decade. The technology described in this thesis also has the potential to reduce the cost associated with intensive care management of patients suffering from treatment induced toxicities. Moreover, the use of a cheap, widely available antibiotic which does not require trained personnel to administer also has many commercial

advantages. The CAR architecture presented here can be used as a foundation for the targeting of a range of novel tumour antigens, opening the potential for commercial partnerships.

In an academic context, the work carried out in this thesis contributes to the field of antibody engineering, synthetic biology, and immunotherapy via i) the generation of a single domain antibody capable of binding to a small molecule drug with high affinity and ii) the generation of a protein displacement platform suitable for use in numerous synthetic biology and engineered cellular therapy applications.

Lastly, results from this thesis will be presented at scientific conferences and published in a manuscript to share the novel protein-protein displacement platform and its immunotherapeutic applications. This will not only enhance the understanding of the scientists within the field but will provide a new tool for other potential research methods such as protein purification to the greater scientific community.

Table of Contents

INDEX OF FIGURES

INDEX OF TABLES

ABBREVIATIONS

2-D	Two-dimensional
3-D	Three-dimensional
Å	Angstrom
aa	Amino Acids
ACT	Adoptive Cell Therapy
Ag	Antigen
ALL	Acute Lymphoblastic Leukaemia
APC	Antigen presenting cell
APC	Allophycocyanin
APC-Cy7	Allophycocyanin-Cyanine7
BSA	Bovine Serum Albumin
CAIX	Carbonic Anhydrase IX
CAR	Chimeric Antigen Receptor
CLL	Chronic Lymphocytic Leukemia
CRS	Cytokine Release Syndrome
C-terminal	Carboxyl terminal
Cys	Cysteine
dCD34	Truncated CD34
DLBCL	Diffuse Large B Cel Lymphoma
DMEM	Dulbecco's Modified Eagle Medium
DMSO	Dimethyl Sulfoxide
DNA	Deoxyribonucleic acid
E:T	Effector:Target Ratio

EGFR.	Epidermal Growth Factor Receptor
ELISA	Enzyme-Linked Immunosorbent Assay
EPO	Erythropoietin
Fab	Fragment Antigen-Binding
FACS	Fluorescence-Activated Cell Sorting
FCS	Foetal Calf Serum
FDA	Food and Drug Administration
FITC	Fluorescein Isothiocyanate
FKBP	FK506-Binding Protein
FRB	FKBP12-Rapamycin Binding
FSC	Forward Scatter
g	G-force
GFP	Green Fluorescent Protein
GVHD	Graft Versus Host Disease
HA	Haemagglutinin
HER2	Human Epidermal Growth Factor Receptor 2
HLA	Human Leukocyte Antigen
HRP	Horseradish Peroxidase
ICANS	Immune effector cell associated neurotoxicity syndrome
iCasp9	Inducible caspase 9
i.v.	Intravenous
i.m.	Intramuscular
IFN	Interferon
Ig	Immunoglobulin

IL	Interleukin
IMDM	Iscove Modified Dulbecco Media
ITAMs	Immune-receptor Tyrosine-based Activation Motifs
JAK	Janus Kinase
KD	Dissociation Constant
ka	Rate of dissociation
kd	Rate of association
LAT	Linker of activated T cells
LCK	Lymphocyte-specific Protein Tyrosine Kinase
LV	Lentivirus
mAb	Monoclonal Antibody
MART-1	Melanoma Antigen Recognised by T cells
MFI	Mean Fluorescent Value
MHC	Major Histocompatibility Complex
MoMLV	Moloney Murine Leukaemia Virus
mu	Murine
NFAT	Nuclear Factor of Activated T cells
NK	Natural Killer Cells
PBMCs	Peripheral Blood Mononuclear Cells
PBS	Phosphate Buffered Saline
PCR	Polymerase Chain Reaction
PE	Phycoerythrin
PI3K	Phosphoinositide 3-Kinase
PIAS	Protein inhibitor of activated STAT

RNA	Ribonucleic Acid
RPM	Revolutions per minute
RPMI	Roswell Park Memorial Institute
Scfv	Single Chain Variable Fragment
SDS-PAGE	Sodium Dodecyl Sulphate-Polyacrylamide Gel Electrophoresis
SH2	Src Homology 2
SPR	Surface plasmon resonance
STAT	Signal Transducer and Activator of Transcription
TAA	Tumour Associate Antigen
TCR	T Cell Receptor
TEFF	Effector T cells
Th	T Helper Cells
TILs	Tumour Infiltrated Lymphocytes
TRUCKs Killing	T cells Redirected for Antigen-Unrestricted Cytokine-Initiated
VB	Vector Backbone
VDJ	Variable, diversity, joining
VEGF	Vascular Endothelial Growth Factor
VH	Variable Heavy chain
VHH	Single-Domain Antibody
Vk	Variable kappa chain
VL	Variable Light chain
WT	Wild Type
ZAP70	Zeta-Associated Protein of 70 kDa
γ-RV	Gamma Retrovirus

1 INTRODUCTION

1.1 Antibodies

Antibodies were first discovered in the 1890s by a German physiologist, Emil von Behring, along with Japanese physician and bacteriologist Kitasato Shibasaburo. Behring and Shibasaburo described a substance, which they initially referred to as a neutralizing agent and later an antibody, that was produced by sick animals to neutralise and eradicate *C. diphtheriae* infection. Based on their work, Behring and Kitasato formed the foundation for subsequent researchers to characterise the mechanism of antibody function and are accredited with inventing the field of immunology. The 1901 Nobel Prize in Physiology and Medicine was awarded to Behring for his work. Since Behring and Shibasaburo's time, antibodies have become one of the most well characterised and intensely studied proteins in medical biology.[1] Traditionally, this was mainly due to their roles as the primary defence mechanism against pathogens in humans and in autoimmune diseases. Although in the recent decades, their vast array of applications in therapeutics, diagnostics, and research has further intensified research and development into antibodies and garnered searches for novel applications using antibodies and antibody fragments.

1.1.1 Introduction to Antibodies

The mammalian immune system protects organisms against a vast collection of pathogenic agents. Through an "evolutionary arms race", the immune system has developed a highly intricate defence mechanism composed of the innate and adaptive immune arms with the key feature of discrimination of self from non-self-material. Broadly defined, the innate responses are germline encoded and are rapidly recruited upon exposure to foreign bodies. Specifically, the innate effector cells recognise molecular patterns conserved within invading pathogens to trigger an immune response. On the other hand, the adaptive immune response, consisting of B and T lymphocytes, possess the capacity for somatic rearrangement of the germ-line gene segments to produce a vast repertoire of antigen binding molecules in the form of the T cell receptor (TCR) and B-cell immunoglobulins (Ig) which are involved in the cellular immune and humoral immune response, respectively. Although both

arms of the immune systems have a fundamentally different mechanism of action, interaction between each is necessary for an effective immune response. The TCR recognises antigenic peptide sequences presented by the major histocompatibility complex (MHC) proteins. Upon engagement, the T cells are triggered through the CD3 signal cascade consisting of multiple biochemical reactions mediated through co-receptors, enzymes, and transcriptional activators. Co-receptors CD8, expressed by cytotoxic T cells, and CD4, expressed by T helper cells, also amplify T cell activation by engaging with MHC class I and II, respectively. Antigen-specific T lymphocytes require several days of clonal expansion and proliferation to exhibit an effective immune response. Furthermore, T cells reinforce their immune responses by recruiting the effector functions of the innate immune system. Upon B-cell recognition of antigens via the B cell receptor (BCR), the antigen is internalised and degraded into peptide sequences which are then transported to the B-cell surface in the form of a peptide-MHCII complex. The peptide-MHCII complex is then presented to helper T cells resulting in the secretion of interleukins such as IL-4, IL-5 and IL-6 which are involved in B-cell clonal expansion and differentiation.[2] B-cell differentiation results in the formation of memory B-cells or plasma cells which provide long-lasting protection and antibody secretion respectively.[3] Antibodies function by recognising and binding to antigenic material. In doing so, antibodies neutralise the pathogens, recruit professional phagocytes to carry out phagocytosis and recruit natural killer (NK) cells to carry out antibody-dependent cell-mediated cytotoxicity (ADCC).[4]

1.1.2 Structure and Function of Antibodies

Conventional antibodies (Ab), also termed immunoglobulins (Ig), are Y-shaped molecules composed of a ~150kDa polypeptide tetramer consisting of identical pairs of heavy polypeptide chains (HC) and light polypeptide chains (LC) of ~50kDa and ~25kDa, respectively. Five isotypes of HCs are present which are denoted by α, μ, δ, γ and ε, and two types of LCs denoted by κ and λ. Abs can recognise and bind to an enormous number of a unique pathogens, specifically to regions known as antigen epitopes. The generation of such a

diverse range of antibodies is due to the modular structure of the Y-shaped protein, allowing host organisms to produce ~10^{18} unique antibodies. The HCs and LCs are made up of two distinguishable regions: An N-terminal variable (V) region and a C-terminal constant (C) region.[5] The HC is made up of one variable domain (VH) and three/four constant domains (CH1-CH2-CH3/-CH4) depending on the antibody isotype. Whereas the LC is made up of one variable domain (VL) and one constant domain (CL). The two identical chains form a homodimer via covalent linkage achieved through disulphide bond formation between the flexible hinge region located between the CH1 and CH2 domains.[6] Antibodies serve two important functions within the host organism; firstly, to bind antigenic epitopes of foreign material and secondly, to initiate antigen-independent downstream effector functions of the immune response. With each respective function attributed to different regions of the antibody; the fragments antigen-binding (Fab) region and the fragment crystallizable (Fc) region. The Fab and Fc portions are linked by hinge region which permits each Fab region a great degree of mobility relative to the Fc region.[7] Cleavage of the conventional antibody structure at the hinge region results in the two distinctive fragments.
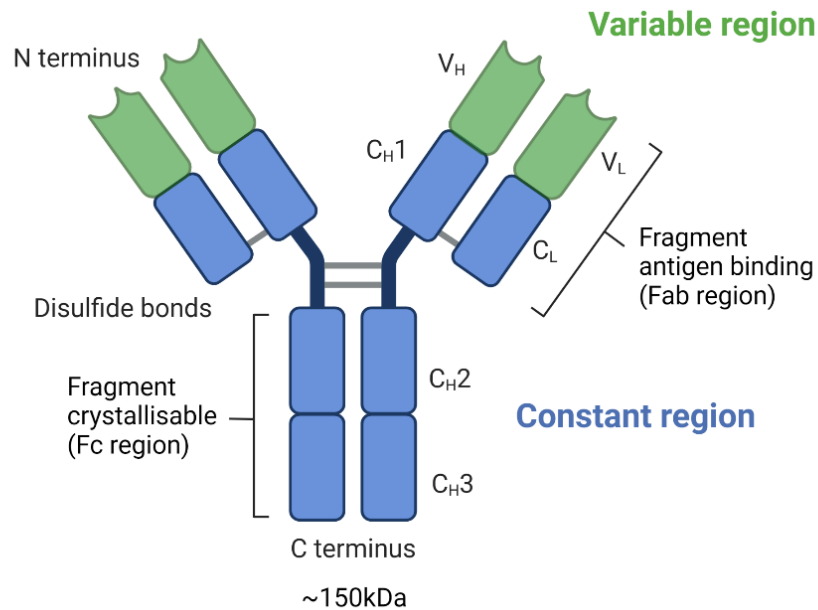
Figure 1.1. Structure of a conventional antibody.

A polypeptide tetramer consisting of identical pairs of heavy chains and light chains. The heavy chain is composed of one variable domain (VH) and three/four constant domains (CH1-CH2-CH3/-CH4). The light chain is made up of one variable domain (VL) and one constant domain (CL). Functional homodimer is formed through disulphide bond formation between the hinge region of the heavy chain.

1.1.2.1 The Fragment variable (Fc) region

The 3D structure of the Fragment variable (Fc) region is made up of CH2-CH3 domains from separate heavy chains. The CH2 chains are closely associated whereas the CH3 domains lack clear residue interactions. A biantennary interaction is achieved through the carbohydrate (glycan) groups fused at position Asn297 of CH2, followed by hydrogen bond formations.[8] As a result, increased conformational flexibility of the Fc region aids in the recruitment of cytotoxic effector functions via antibody-dependent cellular cytotoxicity (ADCC) and complement-dependent cytotoxicity (CDC). ADCC is characterised by engagement of the Fc region with Fc receptors (FcγR) expressed on NK cells, dendritic cells and macrophages which subsequently triggers phagocytosis of target cells. Whereas in the case of CDC, Fc engagement with the first subcomponent of the C1 complex (C1q) leads to the

target cell lysis via triggering of the complement cascade. The various Ig classes, subclasses and origin species express different Fc fragments exhibiting unique set of properties. Substantial engineering efforts have been made to modulate the effector function of the Fc region found on effector cells such as macrophages, dendritic cells, NK cells and T and B lymphocytes.[9]

1.1.2.2 The Fragment antigen binding (Fab) region

The Fragment antigen binding (Fab) region is formed through the joining of VL-CL and VH-CH1 domains, with each domain made up of approximately 110 amino acids. The antigen binding capacity is solely imparted through the engagement of the two variable fragments, VL and VH which make up the variable fragment (Fv). The Fv region is composed of two anti-parallel β-sheets fused by an intramolecular disulphide bond. The highest sequence diversity is concentrated in three hypervariable regions belonging to each VH and VL domain. VH-VL pairing results in six hypervariable loops being positioned such that a single hypervariable antigen-binding site is generated. Looping the β-sheet structures of each variable domain these three hypervariable sequences are known as the complementarity determining regions (CDRs). The CDRs are distributed evenly between each of the variable domains and are denoted as CDR-L1, CDR-L2, CDR-L3, CDR-H1, CDR-H2 and CDR-H3. Historically, the CDR regions were identified based on highly variable amino acid sequence analysis prior to deciphering the complete immunoglobulin structure.[7] As a result of the noncovalent interaction between the variable domains, the six CDRs cluster in proximity at the N-terminus of the Fv fragment forming an interface for antigen-binding specificity. The CDRs are separated by invariant sequence stretches of two β-sheets and non-hypervariable loops known as the framework regions (FRs); these provide a scaffold for the CDRs.

A combination of the loop length and amino acid residues positioned at key residues within the framework and hypervariable regions means the CDRs can orientate into an unlimited number of canonical loops.[10] The greatest variation in CDR length and amino acid profile is observed at the CDR-H3 region

making it the most challenging CDR structure to predict. Antigen binding is primarily facilitated by noncovalent interactions of the CDR amino acids, although amino acid residues of the FR may directly or indirectly be involved in antigen recognition through their role in the structural conservation and stability of the antibody.[11] All amino acid residues interacting with the antigen have been termed the specificity-determining residues (SDRs).[12] For conventional antibodies, the LC CDRs are generally 6-10 amino acids in length and HC CDRs are generally 5-15 amino acid in length,[13,14] although the length of the CDRs, particularly of CDR-H3, vary dramatically from species to species as they generate the greatest diversity and influence antigen-binding the most.[11,13,15] Antibody-antigen binding interaction occurs through non-covalent interactions such as hydrogen bonding, salt bridges and van der Waals interactions.[16] The strength of an antibody-epitope interaction is known as the binding affinity. Whereas, as antibodies arise as homodimers/bivalent structures in their native form, two identical Fv regions impart identical antigen specificity allowing a tendency for antibodies to simultaneously bind two identical epitopes at once, this joint interface of binding is known as avidity. Interestingly, modelling of antibodies in complex with peptides and proteins present distinctive SDR properties and structures.[12,17] The antigen-binding interface targeting peptides are groove-shaped depressions, whereas antibodies targeting protein molecules generally have protracted and larger VL-VH binding interface. Such structural features of antibody CDRs for different antigens have been utilised in the development of synthetic libraries for generating affinity against haptens, peptides, and proteins.[18–20]

VH gene fragment

| 1 | 30 | 35 | 50 | 65 | 95 | 102 | 120 |

| FR1 | CD1 | FR2 | CDR2 | FR3 | CDR3 | FR4 |
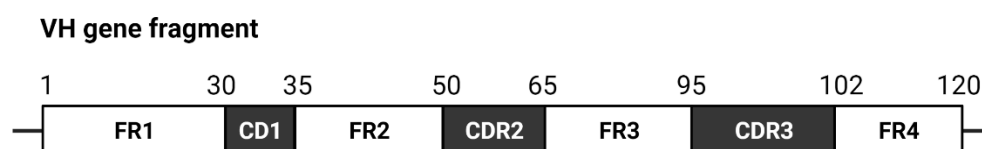
Figure 1.2. Schematic of the variable-heavy gene segment.

Three CDR regions and four flanking FR regions. Amino acid number referencing is based on the Kabat number system.[13]

1.1.2.3 Antibody classes

Five immunoglobin classes known as IgA, IgD, IgE, IgG and IgM have been characterised and grouped based on the constituent heavy chain (HC) isotypes; The heavy chain isotypes are assigned by the Greek letters α, δ, ε, γ and μ, respectively. IgA, IgD, IgE, IgG and IgM each possess unique structural characteristics as well as each possessing a distinctive role within the adaptive arm of the immune system. IgA, IgD and IgG antibody consist of four or five HC domains with one variable domain (VH) and three/four constant domains (CH1, CH2, CH3 and potentially CH4). Moreover, IgA and IgM express an additional joining (J) chain resulting in the formation of antibody dimers and pentamers.

Upon initial exposure to antigen, B-cell activation results in the production and secretion of the IgM isotype.[21] Through the process of somatic recombination known as class switching, the CH encoding region is switched from μ to α, δ, ε or γ thus generating either IgA, IgD, IgE or IgG, respectively. Thus, class switching of HC isotypes leads to distinctive changes in the antibody effector function.[22]

As IgM are the first isotypes to be secreted upon pathogen exposure, IgMs are involved in the process of phagocytosis. Whereas IgAs are primarily concentrated in the mucous membranes and provide first line defence against pathogens through the prevention of viral or bacterial adhesion to epithelial membranes.

IgDs are only present in extremely low levels in the serum with their function centred around enhancing mucosal homeostasis and activating myeloid effector cells such as mast cells and basophils with IgDs targeting mucosal antigens.[23] IgEs is key to defence against parasitic diseases and is thought to play an essential role in the pathogenesis of allergies. Above all other classes, the IgG isotype is the most abundant isotype found in the serum upon the initiation of an immune response in high vertebrates.[24] Apart from differences in the HC isotypes described previously, each isotype is expressed as various

structural formats based on the number of CH domains, length of the hinge and number of disulphide bond formations (Fig. 1.3).

Class	Subclass	H chain	L chain	Structure	Key function
IgG	IgG1, IgG2, IgG3, IgG4	γ	λ or κ		Neutralisation, complement activation and opsonisation
IgA	IgA1, IgA2	α	λ or κ		Mucosal defense preventing bacterial or viral attachment
IgM	None	μ	λ or κ		Complement activation, agglutination
IgD	None	δ	λ or κ		Activation of lymphocytes
IgE	None	ε	λ or κ		Involved in allergies, prevent parasites

Figure 1.3. Class and function of IgG, IgA, IgM, IgD and IgE.

The IgG isotype antibody exists in four subclasses, named based in the order of decreasing abundance in the serum, as IgG1, IgG2, IgG3 and IgG4. Each isotype is highly conserved with structural variations found in the constant regions, specifically the CH2 domain and hinge region leading to differences in the disulphide bond formations and allocation.[24] This portion of each IgG subclass is involved in the binding to IgG-Fc receptors (FcγR) and C1q therefore resulting in each subclass presenting a range of effector functions, such as activating FcγR-expressing cells to carry out phagocytosis, ADCC or activating complement.[24]

1.1.3 Antibody-based Applications

Due to their extraordinary ability to specifically bind to epitopes with high selectivity and sensitivity as well as the capacity to be produced in unlimited quantities, a host of recombinant antibodies and antibody-based applications

have been developed. Prior to the advent of hybridoma technology, polyclonal antibodies targeted multiple epitopes within target molecules. However, the creation of hybridomas, a fusion of a short-lived B cell and an immortal myeloma cell line, results in a cell line which constitutively expresses and secretes a single antibody clone with specificity against a single target epitope. These antibodies were termed as monoclonal antibodies (mAbs).[25]

Advancements in monoclonal antibody production methods and genetic engineering techniques have allowed researchers to efficiently develop and design a range of robust novel monoclonal antibodies compared to those generated through hybridoma technology. In all, humanized antibodies, chimeric antibodies and bispecific antibodies have been developed. These various formats of monoclonal antibodies have been extensively used in research, diagnostics, and therapeutics with remarkable success. Monoclonal antibodies have played an irreplaceable role in and have revolutionised research and medicine with a host of applications. In research, scientists have utilised mAbs to develop key biological techniques, such as enzyme-linked immunosorbent assay (ELISA), western blot, mass cytometry, immunohistochemistry, protein purification, and flow cytometry.

The typical use of mAbs in research techniques is centred around immobilised antibody binding assays. For example, target protein purification can be achieved through affinity chromatography using an agarose or sephadex matrix-immobilised mAb targeting distinct epitopes within the protein. For instance, the hormones such as chorionic gonadotropin (CG), thyrotropin, lutropin, and follitropin are composed of a conserved α-chain, and a unique β-chain for each hormone. Using an mAb specific to a single unique β-chain epitope of each respective hormone, the immobilised mAb acts as an immunosorbent column to bind the protein of interest and retain it within the column, whist non-specific proteins are washed away.[26] The desired protein can then be eluted with high purity. Furthermore, because of the intrinsic high sensitivity and selectivity of mAbs, the same principles are also applied for diagnostic tests for the detection of trace amounts of drugs or proteins such as the detection of GC in pregnancy diagnostic tests.[27] Such distinctive

properties have also aided the invention of ELISA to detect and measure with high precision the quantity of antibodies, disease antigens, cytokines, glycoproteins, and other biological markers in a given sample.[28] In medical diagnostics, mAbs have allowed non-invasive disease diagnosis by analysis of biomarkers and immune imaging. For example, conjugation of a mAb to a gamma-emitting radionuclides or fluorophores can be used as imaging probes for detecting disease tissue.[29]

35 years since the first mAb approval from the Food and Drug Administration (FDA), more than 100 antibodies in various formats are now FDA-approved with more than 870 antibody candidates currently in clinical development. In total, this accounts for approximately a fifth of all new drug approvals FDA permits each year. Furthermore, since 2020, approximately twice as many programmes containing one format of antibody structure targeting cancers were in the clinic compared to non-cancer targets. The success of antibody-based binding moieties in cancer therapy is due to their ability to differentiate low copy number tumour-associated antigens.[30]

1.1.4 Recombinant antibodies

As previously mentioned, antibody-based therapeutics are one of the fastest growing products in clinical development accounting for a fifth of all new drug approvals by the FDA. Despite widespread use, conventional antibodies bear inherent disadvantages. In their native state, antibodies are secreted or fused to the cell-membrane as a key mechanism of defence against foreign material. As the formation of a functional antibody requires an oxidative environment for appropriate intermolecular and intramolecular disulphide bond formation, many intracellular therapeutic applications have been restricted.[31] Furthermore, a combination of its bulky protein structure and the limited real estate of the DNA plasmid cassette for T cell based therapeutic applications, have meant the use of simpler pre-existing antibody-based antigen-binding fragments have been advantageous.

1.1.4.1 Recombinant Antibody Formats

Genetic engineering techniques have allowed for the design and expression of recombinant antibody formats not found in nature. With advancements in molecular biology and genetic engineering techniques, recombinant antibodies structures such as single-chain variable Fragment (ScFv) and fragment antigen binding (Fab) have been developed.
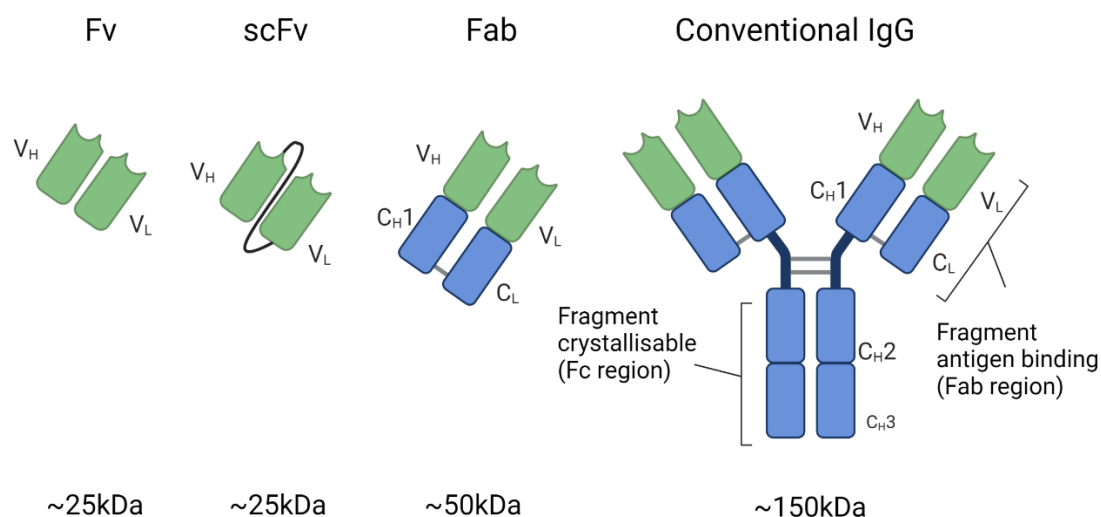
Figure 1.4. Illustration of variable Fragment (Fv), single-chain variable Fragment (ScFv), fragment antigen binding (Fab) and conventional IgG antibody.

1.1.4.2 Single-chain variable fragment (ScFv)

As previously mentioned, the variable fragment (Fv), composed of the VL and VH domains, is the smallest antigen-binding region of the antibody. In conventional antibodies, VH and VL pairing is maintained through hydrophobic interactions and hydrogen bonding. The stable recombinant format of the Fv, is the single-chain variable fragment (ScFv). The ScFv is generated through the fusion of VH and VL via a flexible peptide linker made up of glycine and serine, usually of the sequence Gly4-Ser, up to 25 amino acids long and ~25 kDa in size. Glycine provides the flexibility whilst serine allows for solubility. Based on where the linker is used to fuse the VH and VL, either N-terminus of VH and C-terminal of VL or C-terminus of VH and N-terminus of VL, two formats known as Heavy-Light or Light-Heavy can be formed with

varying binding characteristics. The small size of the scFv means the orientation of binding is greatly improved for targeting epitopes inaccessible by conventional antibodies.[32] Furthermore, the small size is ideal for introducing target specificity in modular adoptive T cell technologies such as chimeric antigen receptors (CAR) where the real-estate of the DNA cassette limited. Nevertheless, scFvs also have many disadvantages for use as therapeutics. For example, relative to IgGs, which have a longer serum half-life due to their larger size and FcRn recycling, the improved absorption and tissue penetration of ScFvs mean the serum half-life is poor and readily secreted.[33,34] Furthermore, the aggregation propensity of scFv fragments is high as a result of hydrophobic interactions of the VH domain in a hydrophilic setting.[35]

1.1.4.3 Fab fragments

The Fab fragment can be isolated through the proteolytic cleavage of the conventional antibody structure. The Fab fragment is made up of paired VL-CL and VH-CH1 domains with linkage taking place via a disulphide bond between each respective constant domain. The Fab fragment, which is approximately 50 kDa in size and the F(ab)2 fragment, which is approximately 100 kDa in size, are also widely used antibody formats.

1.2 In vitro Antibody Display Technology

Monoclonal antibodies (mAbs) have shown to be efficacious against a range of diseases such as cancer and autoimmune conditions, with over 100 antibody-based therapeutics having FDA approval. One example is the human IgG1 mAb adalimumab used in the treatment of arthritis therapy by specifically targeting the tumour necrosis factor α (TNFα).[36] Based on experimentally-derived data and theoretical combinatorial data, a vast human antibody naïve repertoire is shown to be present, although the generation and isolation of mAbs with desired structural and specificity features is challenging. Therefore, antibody engineers have developed methods such as immunization and in vitro display technology such as phage display. Phage display technology involves the in vitro selection of antibody sequences from a naïve library, an immunized library or from a completely synthetic library.[37] Whereby the in vitro

process achieved artificially applies a selection pressure to simulate processes occurring during B-cell maturation in vivo. These include generating genetic diversity, linking genotype to phenotype, imparting a selection pressure, and isolation and amplification of binder sequences with desired properties. The use of a display technology for the isolation and selection of antibody sequences was first reported in 1990.[38] Typically, the display of antibody fragments such as fragment antigen binding (Fab) or single chain Fragment variable (scFv) is favoured as conventional antibody display is challenging.

In addition to selecting antibody sequences targeting protein antigens, in vitro display can also be employed to screen for binders targeting small molecule drugs, chemical modifications, and toxins.[39] In this work, phage display technology was utilised in the generation of an antibody targeting the small molecule antibiotic drug, minocycline. Furthermore, phage display was also used to select a peptide sequence specifically targeting the previously generated minocycline specific antibody. Therefore, in this section, details of the history, function, fundamental principles, and application of phage display technology will be covered.

1.2.1 Phage display technology

Phage display technology was first described by George P. Smith in 1985 and was based on the fusion of a peptide to the exterior coat protein of the filamentous bacteriophage M13. Fusion of genes encoding for a foreign oligopeptide to the M13 coat protein, resulted in the coupling the genotype and phenotype, thus allowing for selection via affinity purification of phage particles bearing unique peptides.[40] Based on this principle, Sir Gregory P. Winter developed antibody phage display to generate a vast collection of therapeutic antibodies, due to the technology being able to access the diverse antibody sequence repertoire.[38,41] Since its discovery, the technology has become the most widely used in vitro evolution strategy and has been proven to be one of the most tried and tested methodologies in the discovery of human antibodies. As a result, George P. Smith and Sir Gregory P. Winter were awarded the 2018 Nobel Prize in Chemistry.[42]

A
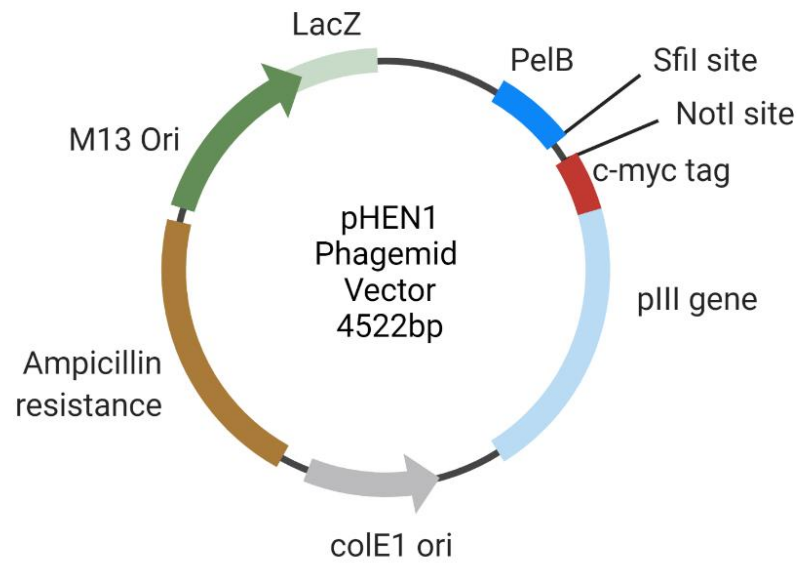
B
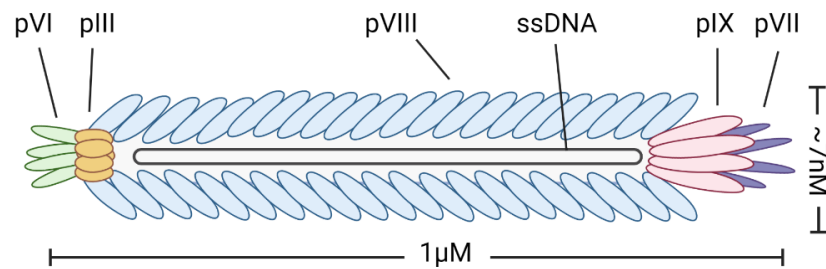
Figure 1.5. Schematic illustration of the phagemid vector map and whole M13 phage structure.

(A) Vector map of the pHEN phagemid vector composed of the antibiotic resistance gene for selection in E. coli. A PelB leader sequence in-frame with the gene encoding the displayed antibody, myc-tag and the pIII phage coat protein fusion. Phagemid vector also contains the plasmid origin of replication and the M13 replication origin. SfiI and NotI restriction sites are used to subclone the antibody coding genes into the phagemid vector. Phagemid is integrated into progeny phage through the helper phage co-infection of E. coli. (B) Structure of the filamentous M13 bacteriophage. Belongs to Family: Inoviridae, Genus: Inovirus, Species: Enterobacteria phage M13. M13 bacteriophage genome is composed of a circular single-stranded DNA which is 6400 nucleotides in length and encodes 11 proteins. One major coat protein,

pVIII, is the most abundant protein making up ~2700 copies and forms the filamentous outer coat along the length of the virion particle. Four minor coat proteins, pIII, pVI, pVII and pIX. The pIII and pVI proteins are assembled at one end of the filament and are involved in recognition of sex pilus in E. coli. The pVII and pIX proteins are assembled at the opposite end and interact with the packaging signal of the supercoiled single-stranded DNA. Three proteins involved in bacteriophage replication: pII, pV and pX. Three proteins involved in the assembly of progeny bacteriophage: pI, pIV and pXI.

Phage display allows for the selection of peptides or antibodies with ideal binding characteristics from a large and diverse sequence repertoire known as the library. These libraries are generated through the fusion of the antibody genes to the minor coat protein III (pIII) gene enabling the affinity selection of antibodies and their respective genes through the transformation of *E. coli* (Fig. 1.5).[40] Crucially, phage display benefits from an essential property the M13 phage to infect *E. coli* without rupturing the host cells. To date, many variations in phage display systems have been developed and currently used, with most systems utilising the integration of antibody-pIII gene fusion.[38] It has been shown the direct fusion of the antibody-pIII gene with the whole phage genome is not as versatile compared to the phagemid system.[43] Whereas, using the phagemid system, the antibody-pIII gene fusion is expressed in a separate vector known as a phagemid display vector (e.g. pHEN) from the rest of the phage genes encoding the structural proteins and genes involved in phage expression and replication. Thus, coinfection of *E. coli* with a helper phage vector (e.g. M13KO7) is required to encode the rest of the proteins for the formation of a whole phage particles displaying the antibody on the exterior of the phage.[43–46] The phagemid vector is composed of a selection marker (typically an antibiotic resistance gene), an *E. coli*. and phage replicon and morphogenetic packing signal which allows packing within the phage particles upon assembly, thus enabling the genotype-phenotype link.

For antibody phage display, antibody fragments such as scFv, Fab and VHH antibodies are typically used over full-length conventional antibodies due to the restricted folding machinery of *E. coli*.[46,47] The antibody repertoire is

sourced from either the immune antibody library or a universal antibody library. Immune libraries are generated through the isolation of B-cells from vaccinated wild-type animals or transgenic animals bearing the human immunoglobulin V-genes as well as B-cells from infected patients.[48] Immune libraries provide hypermutated V-gene sequences which are likely to have undergone the process of affinity maturation. On the other hand, universal libraries encompass naïve libraries or semi-synthetic/synthetic libraries. Naïve libraries are constructed from rearranged V-genes from isolated B-cells of unvaccinated donors/humans. These libraries are antigen-independent and thus a single naïve library can theoretically show specificity against virtually any antigen. Semi-synthetic libraries are generated by introducing diversity using oligonucleotides. Semi-synthetic libraries are obtained from unrearranged V-genes from pre-B-cell germline cells or via the use of an antibody framework where the sequence of one CDR region is randomised, typically the CDR-H3 as it imparts the greatest diversity.[49] Whereas synthetic libraries are constructed from synthetic DNA using a human framework and randomisations at the CDR coding regions using oligonucleotides.[50]

Library construction is the initial step of phage display and involves the isolation and cloning of the antibody repertoire into an appropriate phagemid vector such as pHEN followed by infection of *E. coli*. Later, the library is further infected with M13KO7 helper phage which provides all viral structural and accessory proteins for single-stranded DNA replication and phagemid DNA packaging into each phage particle. This results in the phage particles displaying the antibody on the exterior of the phage with its corresponding antibody coding sequence within the phage. Upon the expression of phage particles each displaying a unique antibody variant, the process of antibody selection known as 'panning' is carried out by exposing the pool of phage particles to an immobilized antigen (incubation step).[38] During the 'panning' step, phage displaying antibodies specific for the immobilized antigen are preserved whilst non-specific phage-antibodies are washed away. In addition to antigen specificity, many factors affecting antibody selection can be applied such as temperature, pH or the presence of a competitor. Furthermore, altering the stringency during the wash steps means only the phage-antibodies

with requisite characteristics of specificity and affinity can be preserved whilst the rest of the antibody population is removed. Upon enrichment of the desired phage pool, the bound phage is eluted, typically via trypsinisation or altering the pH, and used to reinfect bacteria for another round of enrichment (Fig. 1.6).[51] Infected cells are further infected with helper phage to express enriched phage for further panning. In total, 2-3 rounds of panning are sufficient to obtain an enriched but diverse library of antibody sequences. The assessment of individual antibodies against target antigen can be carried out by ELISA, followed by sequencing individual clones to determine sequence diversity. The candidate sequences are then expressed as one of the recombinant antibody formats for further biophysical characterisation to assess the affinity, stability, and aggregation propensity.
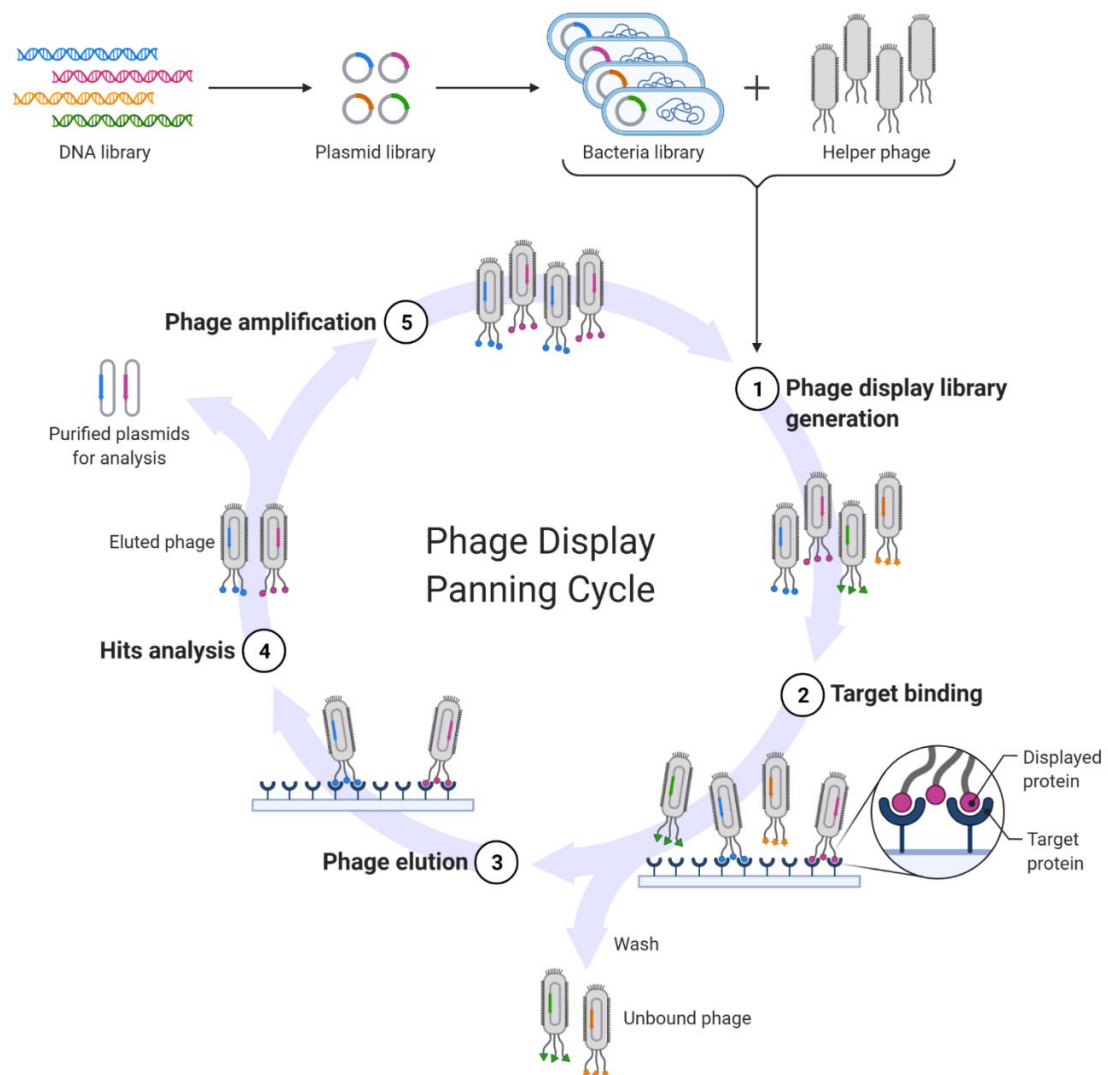
Figure 1.6. Schematic of phage display biopanning and selection.

Phage display library containing phage particles each expressing unique antibody on its exterior is incubated with immobilized antigen. Washing step is carried out to remove non-specific phage. Antigen-specific bound phage is eluted using trypsinisation or altering the pH. Enriched phage are then amplified by reinfection of E. coli. Typically, 2-3 rounds of panning are sufficient to enrich for high affinity binders. Individual clones are sequenced, and further characterisation is carried out by fusing the antibody sequence in various antibody formats.

1.3 Single domain antibodies (sdAb)

While the antibody engineering field progressed in designing intricate antibody fragments to overcome the shortcoming of mAbs, a chance discovery showed camelid and cartilaginous fish, as a part of their natural immune defences, expressed heavy chain isotype antibodies as well as conventional antibodies. These heavy chain antibodies (HCAbs) achieved antigen recognition through a single heavy chain variable domain only. In addition to their monosteric nature and small size, extensive characterisation of sdAb fragments have shown sdAbs to be highly stable with high affinity and specificity towards their target antigen. Such properties have been sought after in cellular therapy applications.

The conventional heterotetrametric structure of antibodies is extremely well conserved between mammal species with only three variations from the conventional structure described. Each of these variations have iterations centred around a homodimer of the Ig heavy chain. The initial discovery of heavy chain antibody fragments was made in sera of patients with a disorder later termed heavy chain disease (HCD).[52] Such proliferative disorders involve B-lymphoid cells expressing truncated heavy chain variations due to a somatic event, through deletion or splicing, which eliminates parts of the *VH-CH1* from the full Ig gene expression. These heavy chain antibody variants are non-functional in binding to target antigens due to lack of VL-CDRs and parts of the VH-CDRs. A serendipitous discovery of a unique class of natively occurring heavy chain antibody (HCAbs) was also observed in species of the Camelidae family.[53] The Camelidae family (residing in the suborder Tylopoda and the order Artiodactyla) is made up of the Old and New World camelids. The Old-World camelids consist of the dromedary camel (*C. dromedarius*), the domestic Bactrian camel (*C. bactrianus)*, and the wild Bactrian camel (*C. ferus)*. On the other hand, the New-World camelids consist of the llama (*L. glama*) and guanaco (*L. guanicoe*) which belong to the genus Lama, and the vicuña (*V. vicugna*) and alpaca (*V. pacos*) which belong to the genus Vicugna. These camelid HCAbs are expressed in addition to conventional antibody isotypes and play a typical role in the normal functioning of the immune

response against invading pathogens.[53] Furthermore, HCAbs have also been discovered in cartilaginous fish such as Sharks and have shown to have evolved independently from Camelids.[54,55] The independent emergence of HCAb in Camelids and cartilaginous fish suggests that small antibody fragments targeting cryptic epitopes of enzymes or pathogens were evolutionary advantageous and thus selected.[56]

1.3.1 Camelidae heavy chain antibodies (HCAbs)

Camelidae heavy chain antibodies (HCAbs) originate from the conventional IgG and makes up half of circulating serum antibodies in Camelidae.[57] HCAbs are composed of a homodimeric structure made up of two chains fused together via a disulphide bridge at the hinge region. Each chain is composed of two C-terminal constant (CH2 and CH3) domains and one N-terminal variable domain of heavy chain antibody (VHH). Unlike conventional antibodies, the antigen-binding specificity is solely imparted through a single VH domain only. Therefore, expression of a recombinant VHH produces single domain antibody fragments (sdAb), making the sdAb the smallest functional antigen targeting fragment (~15 kDa) of a naturally occurring antibody. Thus, VHH domains have evolved a host of unique properties.

Antibody	gDNA	mRNA
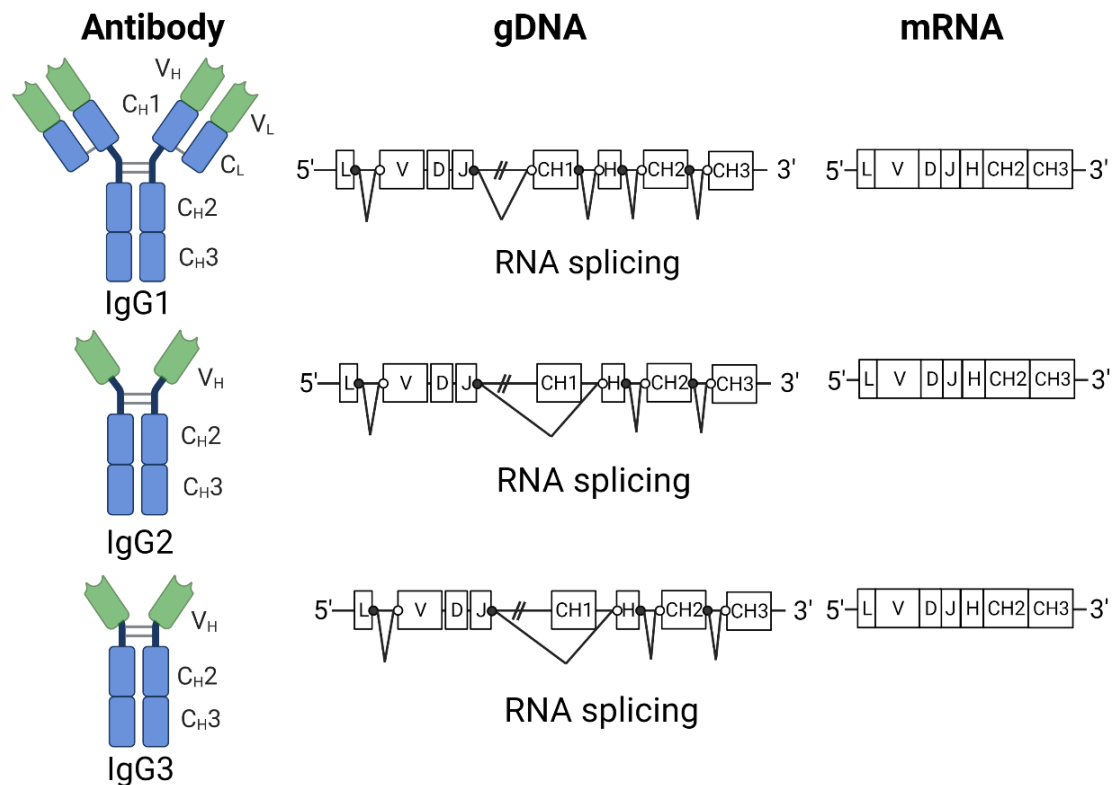
Figure 1.7. Illustration of a conventional Camelidae antibody and a Camelidae heavy chain antibody (HCAb).

HCAbs are composed of a homodimer of two chains fused together via a disulphide bridge at the hinge region. Each chain is composed of an Fc region made up of CH2 and CH3 domains with high sequence homology to the domains found in conventional antibodies. The Fc-region is fused, via a hinge region, to a single variable domain of heavy chain antibody, known as VHH. VHH domains recognise and bind to antigens without the requirement of light chain pairing. In all, HCAb are devoid of a light chain and the CH1 domain typically found in conventional antibodies with the hinge length being the key difference between IgG2 and IgG3 antibodies.

1.3.1.1 Genetic and structural properties of heavy chain antibodies

The presence of the light chain interacting with the heavy chain is essential for functionalisation in conventional antibodies. Therefore, HCAbs have gone through many genetic and structural adaptions in order to function appropriately in the absence of a light chain. It has been shown using Protein A/Protein G purification of the camelid sera, that three distinct IgG molecular weight fractions exist which are divided into subclasses known as IgG1, IgG2

and IgG3. IgG1 is the full-length antibody whereas the IgG2 and IgG3 are devoid of the light chain and the CH1 domain (Fig. 1.7).[53]

The first modification of HCAbs is the loss of the CH1 domain. The CH1 domain typically joins the kappa/lambda light chains in conventional antibodies and is encoded as a part of the HCAb gene but is spliced out as a result of a point mutation at the 3' splice signal of the CH1 exon.[58,59] As a result of the splicing event, HCAb structures show the VH domain to be directly fused with the hinge region. The CH1 is involved in the retention of the heavy chain within the endoplasmic reticulum through interacting chaperones (heavy-chain binding protein (BiP)), and secretion of the full-length antibody is dependent on the dislocation of these chaperones mediated through light chain joining. Therefore, splicing of the CH1 gene is an essential modification to allow for the secretion of HCAbs in the absence of the light chain.[60] Based on the hinge region amino acid length, the camelid IgG2 is divided into two isotypes, known as IgG2a and IgG2c, with the amino acid length being 35aa and 15aa, respectively. A further isotype known as IgG2b has been discovered in *L. glama* and bears a hinge region of 29aa.[61] The IgG3 HCAb bears a hinge region of 12aa in length. Although the general expression profile of classical antibodies to HCAbs in the sera of camelid species varies, an approximate 1:1 ratio is observed in *C. dromedarius*, *C. bactrianus*, *C. ferus*, and 3:1 in *L. glama* and *L. guanicoe*.

Typically, the framework regions of conventional antibody VH domains have key hydrophobic residues which interact with the VL domains. However, in VHH antibodies, the lack of VL interaction means such residues would lead the instability and aggregation upon exposure to aqueous conditions. Although the framework region (FR) of VHH antibodies is highly homologous to VH domains, VHH antibodies have evolved the amino acid residue substitution to more hydrophilic residues at conserved residues within the FR2 region (known as hallmark residues). This enables VHH domains to be expressed with increased stability and a lower aggregation propensity. The hallmark residue substitutions (from the FR2 region of VH to VHH) are as follows: Leu12→Ser, Val42→Phe/Tyr, Gly49→Glu, Leu50→Arg/Cys and Trp52→Gly.[62,63] The

amino acid positions were numbered in accordance with the IMGT numbering system. The hallmark residue amino acid substitutions using the Kabat numbering system is as follows: Leu7→Ser, Val37→Phe/Tyr, Gly44→Glu, Leu45→Arg or Leu45→Cys and Trp47→Gly.[13] Although a small percentage of camelid VHH domains possess the Leu12→Ser substitution, is it is believed the modification from a hydrophobic residue to a hydrophilic serine amino acid aids in solubility due to a missing CH1 domain.[61]

Sequence analysis of the flanking region between VHH and VH domains, show conservation of all elements within the V-gene segment, involving the conventional Ig promoter as well as the recombination signal sequences. Indicating the VHH germline genes are involved in somatic rearrangement of VDJ upon B-cell differentiation.[64]
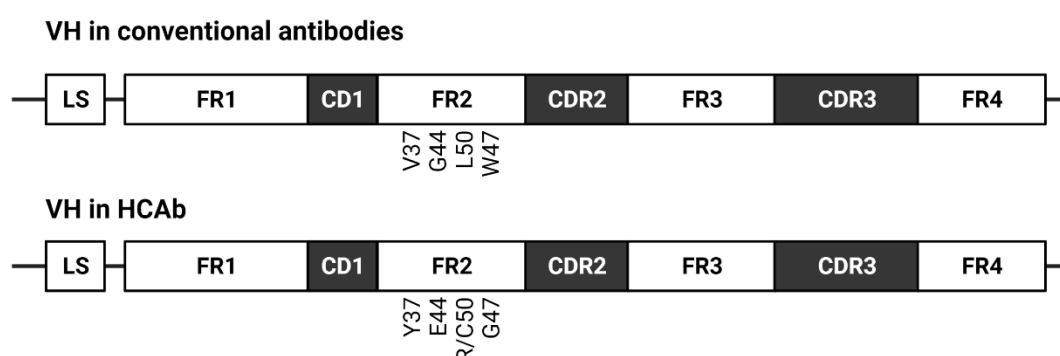
Figure 1.8. Conventional VH and HCAb VHH germline gene segments.
Ig-promoter sequence. LS, the leader sequence is split from the V-exon. The recombination signal sequences are indicated before the CDR3. Hallmark residues within the FR2 region indicated showing hydrophobic amino acid residue of VH substituted to hydrophilic amino acid residues in VHH antibodies. Hallmark residue substitutions minimise hydrophobicity and compensate for lack of VL pairing, decrease aggregation propensity and increase solubility and stability in VHH antibodies. Novel cysteine residue codons within the VHH CDR1 region and FR2 region also indicated. Compared to the VH domain, the VHH domain bears interloop disulphide bridges. The VH and VHH amino acid position number is based on the IMGT numbering system.

Solved X-ray crystallography structures have confirmed that sdAbs take on the typical conventional antibody variable domain fold composed of two anti-parallel β-sheets fused by a conserved intramolecular disulphide bond.[65] However, as mentioned, VHHs bear a cluster of amino acid substitutions at the interface where a VH would typically interact with VL, thus resulting in structural differences. Substitutes of non-polar residues (Gly and Leu) to polar residues (Glu and Arg) at positions 49 and 50, not only increases the hydrophobic nature of hallmark residue interface but results in the exposure of more hydrophilic regions of adjacent amino acids to become solvent accessible.[66] The greatest deviations of VH domains from VHH occur at the CDR1 and CDR2 canonical loops, with VHHs capable of generating far more diverse structures due to novel amino acid sequences at locations which are significant in CDR length, interfacial disulphide bond through additional cysteine residues and loop conformation.[10]

Depending on the target antigen and epitope size, structure, and conformation, sdAbs display a drastically different antigen-binding site. For example, sdAb targeting bulky protein antigens express flat 2D antigen-binding sites.[64] Whereas, cavities, grooves and extensive protruding structures are formed from all three CDR loops to accommodate binding to challenging antigens such as haptens.[67,68] For example, part of the long CDR3 of a lysozyme-specific sdAb folds over the former VL side while the other section protrudes from the remaining paratope and penetrates the active site of lysozyme. This large convex paratope provides over 70% of the contacts with lysozyme and the interaction area with lysozyme is as large as the interface between an antigen and a VH–VL pair. This feature allows sdAbs to recognize epitopes that are usually not antigenic for classical antibodies, such as the catalytic site of enzymes and canyons in viral and infectious disease biomarkers.[68]

1.3.2 Generation of CDR site diversity

The effectiveness of the adaptive immune response depends on the genetic capability to generate an immense repertoire of variable domain sequences to target a vast number of antigens. The VH and VHH domains are encoded by

multiple gene segments rather than just one.[61,69] The germline encoded immunoglobulin V genes are gene clusters of the following gene segments; variable (V), diversity (D), and joining (J) genes.[70] The combinatorial diversity of the antigen-binding sequences is generated through the rearrangement of the V(D)J gene segments (known as VDJ recombination) carried out during the process of B cell differentiation. The VH, D and JH gene segments are selected and joined to generate a complete VH polypeptide chain where the V gene segments encode for CDR1 and CDR2, whilst the joining of all segments generates CDR3. In the case of conventional antibodies, the VL and JL rearrangement results in the VL polypeptide chain formation. Upon assembly of a functional VH or VL gene, the *V(D)J* rearrangement apparatus present on the second allele is switched off, ensuring each cell generates a single clone of an antibody. Further diversity is generated due to an inaccurate DNA recombination mechanism in combination with nucleotide deletions at the *VH-(D)-JH/VL-JL* splice junctions. Furthermore, during rearrangement and assembly of the VH, D and JH gene segments, non-templated nucleotides, aided by a DNA polymerase known as terminal deoxynucleotidyl transferase (TdT), are added between the gene segment junctions.[71] Moreover, palindromic nucleotide sequences and deletions at junctional region contributes to diversity of the CDR3.[11]

As previously mentioned, camelid serum contains conventional Abs and HCAb, however the process of V(D)J gene recombination is very distinct in the generations of the HCAb heavy chain. In order attain the VHH specific amino acid substitutions in the hydrophobic regions, HCAbs utilise a different V gene segment to that used to generate the VH of conventional antibodies.[59]

The random VH and VL pairing in the generation of conventional antibodies increases the binding diversity in higher vertebrates. However, due to the fact HCAbs lack the light chain pairing, additional sequence adaptions to increase VHH repertoire diversity in HCAb have been described. VHH repertoire diversity is enhanced using a total of 42 VHH gene segments which possess modifications to enhance the stability and solubility of VHHs.[72]

Further VH and VL binding diversity is introduced post B-cell activation and VDJ recombination via the process of somatic hypermutation of favoured sequence motifs known as mutational hotspots.[73] Point mutations at the mutational hotspots are clustered within the antigen binding region, occurring at a higher frequency within the CDR regions, and accordingly enhance the affinity of antibodies against their target epitopes. The mutation rate in the V gene segments is $\sim10^{-5}$ kb per replication round which is substantially higher compared to mutation rate in other genes.[74] Over time, a positive selection pressure will be imposed on cells expressing high affinity antibodies because of increased levels of cellular proliferation, limited by antigen density, a process known as affinity maturation. In HCAbs, the VHH CDR1 region possess a higher number of these mutational hotspots which enhances the process of somatic hypermutation thus increasing diversity in HCAbs compared to conventional VH domains.[64,72]

Another key adaption of VHH domains to increase the antibody diversity/counteract loss of diversity in the absence of a paired light chain, is the evolution of long CDR3 regions. The CDR3 region in the VH domain of conventional antibodies is typically up to 11 amino acids long, whereas the CDR3 region of VHH antibodies is up to 17 amino acids in length.[64] The presence of an extra cysteine residue within the FR2, CDR1 or CDR2, in conjunction with an increased length of the CDR3 region can further form secondary loop structures through interfacial disulphide bond formation between CDR3 and CDR1 or CDR2.[72] Thus further increasing the diversity and stability of the VHH-epitope binding interface.

The emergence of such mechanisms to overcome the lack of VH–VL combinatorial binding diversity has meant HCAbs can attain a complex and diverse repertoire of binding sites. So much so that analysis shows the diversity of the VHH gene is in fact greater than the VH gene due to the greater rate of mutational hotspots and DNA recombination events at the germline sequences.

1.3.3 Distinctive VHH antibody characteristics

VHH antibodies have unique characteristics compared to conventional antibodies and recombinant antibody formats, which make them ideal candidates for a multitude of applications to overcome the limitations of conventional antibodies. Among the peculiar VHH characteristics, the first is the small size (12-15 kDa) which aids in efficient and rapid tissue penetration. Additionally, as VH-VL pairing is not an essential in VHH functionality, the probability of successful construction of a phage display library with ideal binder properties is greater for VHH based phage libraries over ScFv and Fab antibody-based libraries.[75] Furthermore, VHH have shown enhanced thermal stability maintaining antigen binding at high temperatures (up to 90°C) and at pH extremes[62,76] coupled with a higher hydrophilicity resulting in improved water solubility and lower aggregation propensity. Finally, an extended CDR3 of VHH antibodies means VHHs can not only bind to epitopes inaccessible to conventional antibodies, but with high affinity in the nanomolar range.[62,77]

1.4 Cancer immunotherapy

Accounts of tumour regression/remission post infection and/or a pyrexia episode have been documented throughout history, from ancient Egypt to 18th century Europe. Although the scientific rationale behind the phenomenon of modulating the immune system to treat tumour growth was only realised in the late 19th century. From 1867, German physicians Wilhelm Busch and Friedrich Fehleisen independently described tumour regression in cancer patients following infection with *Streptococcus pyogenes* and the development of erysipelas. Later in 1891, Dr William B. Coley followed up with independent observations of cancer patients diagnosed with bacterial infection showing tumour regression and improved prognosis.[78] He reasoned that the infections and the activated immune response may, in fact, be associated with tumour regression. As such, Coley aimed to verify his epidemiological association between the immune system and neoplastic disease by administering cultures of heat-inactivated *Streptococcus pyogenes* and *Serratia marcescens*, termed 'Coley's toxins', to his cancer patients with a view to induce tumour regression.[79] Indeed, these cultures triggered a potent immunostimulatory

response against a range of cancers. Nevertheless, the lack of controlled trials and the discovery of chemotherapy and radiotherapy halted the use of 'Coley's toxins' as standard treatments. Although controversial at the time, Coley's ideas proved to be ahead of their time and today form the foundation of modern immunotherapy. Since Coley's time, both the humoral and cellular immune mechanisms have been researched extensively to show potent anti-tumour responses.

Immunotherapy is the use of substances to illicit or suppress immune response in order to combat diseases such as cancer and infection.[80] It benefits from immune memory that can produce sustained responses even after termination of the therapy. Advances in genetic engineering have resulted in the emergence of a scientific field known as cancer immunotherapy. It aims to regulate the immune response to enhance the anti-tumour activity against tumour cells, while avoiding unwanted autoimmune responses.[81] Cancer immunotherapy encompasses a broad spectrum of therapeutic approaches which aim to modulate the native immune responses for a therapeutic outcome. Use of monoclonal antibodies, cancer vaccines, adoptive transfer of T and natural killer cells, as well as administration of recombinant proteins and cytokines are strategies used in cancer immunotherapy. There are broadly two categories of immunotherapies: direct activation of the immune system that produces long lasting memory immune response, such as with cancer vaccines and oncolytic viruses;[82] and indirect activation of immune system that relies on injection of cells or biomolecules to specifically target antigens on or associated with tumour cells. These include monoclonal antibody therapy, adoptive T cell therapy and checkpoint inhibitors.[82]

1.4.1 Cancer vaccines

Therapeutic cancer vaccines are used to activate the adaptive immune system by administration of specific tumour antigens, along with adjuvants to activate antigen presenting cells such as dendritic cells. The key concepts of successful therapeutic vaccines are delivery of sufficient antigen to antigen presenting cells, to induce strong and durable immune response from CD4+ T helper cells and cytotoxic T lymphocytes.[83] The first cancer vaccine,

sipuleucel-T (Provenge®), was approved by the FDA in 2010. It aims to activate dendritic cells in castrate-resistant prostate cancer, in a clinical study it has reduced risk of death by 25%, however the exact mechanism of action is not fully clear, which limits its applicability.[84]

1.4.2 Oncoloytic virus therapy

Oncolytic viruses can selectively replicate inside cancer cells, leading to cell destruction, while sparing healthy tissue.[85] They can be genetically engineered or naturally occurring viruses that are non-pathogenic, have the ability to specifically target cancer cells and cause cell death.[86] The only FDA approved oncolytic virus therapy is Talimogene laherparepvec (T-VEC). However, toxicities and efficacy have been a concern, as the circulating antibodies can decrease effectiveness of the therapy.[86]

1.4.3 Monoclonal antibody therapy

Monoclonal antibodies (mAb) are produced by unique B cell clones, they bind to specific parts of an antigen called an epitope. Human derived hybridomas have been used to generate therapeutic antibodies since they were identified in 1973 by Schwaber, this technique has been the main method for large scale production of antibodies.[87] The first human trial of using mAb to treat cancer was carried out in a patient with lymphoma, however these antibodies were immunogenic in patients due to their murine origins, therefore toxicity was a concern for the therapy, and the antibodies did not induce sufficient immune responses to demonstrate their clinical activity.[88] New techniques such as phage display have enabled fully-human antibodies to be produced, this has greatly decreased immunogenicity of the mAbs and increased their clinical applicability in treating cancer.[82] In 1997, the FDA approved the use of rituximab for the treatment of relapsed or refractory non-Hodgkin's lymphoma, the antibody binds to CD20 on B cells resulting in tumour clearance via induction of apoptosis, cell-mediated cytotoxicity and complement activation.[89,90] Since then many more mAbs have been approved for the treatment of various cancers, such as colorectal, lung, Hodgkin's lymphoma and breast cancer.[85] The ability of antibodies to specifically target and kill tumour cells while activating the immune system to induce lasting response

against the tumour distinguishes mAb therapy from other therapies for minimal toxicity and adverse events.

1.4.4 Checkpoint inhibitors

Cytotoxic T lymphocyte antigen 4 (CTLA-4) was discovered to block T cell immune responses by Dr James Allison, who demonstrated that inhibiting CTLA-4 molecules in vivo can increase the immune system's anti-tumour response.[91] CTLA-4 is a homolog of CD28, both are expressed on T cells and both bind to B7-1 (CD80) and B7-2 (CD86). CD28 is a co-stimulatory molecule for T cell activation, CTLA-4 has a higher binding affinity for the ligands compared to CD28 and hence acts to supress T cell activation.[92] In 2011, the FDA approved the anti-CTLA-4 antibody ipilimumab for the treatment of advanced melanoma, it was the first therapeutic agent to have shown to improve overall survival of patients with melanoma.[93]

Programmed death-1 (PD-1) and its ligand PD-L1 were also discovered to exert negative immunomodulation. Supressing PD-1 and PD-L1 have been shown to increase T cell penetration of solid tumours such as lung cancer, as well as melanoma. There are many other studies investigating combining different checkpoint inhibitors or using checkpoint inhibitors in conjunction with other treatments such as radiotherapy.[85]

1.4.5 Adoptive T cell therapy

The goal of adoptive T cell therapy is the enhancement of immune mediated anti-tumour activity through the reinfusion of isolated and ex vivo-expanded tumour-specific T cells into patients. Early work in the field focused on the transfer of non-genetically modified T cells for the treatment of viral and non-viral malignancies. During the nineties, tumour infiltrating lymphocyte (TIL) infusion was explored as a means of controlling immune responses against non-viral malignancies. Many reports described patient-derived TILs mediating tumour clearance in malignant melanoma, as well as efficacy of TILs derived from surgical donor samples used as a treatment option for patients with chronic myelogenous leukaemia. Improved patient prognosis has been linked to higher levels of TILs, exemplifying the importance of immune surveillance and tumour control.[94] Successful transfer of antigen-specific T

cells has also shown to avert the reactivation of EBV upon haematopoietic stem cell transplantation (HSCT).

1.4.5.1 Chimeric Antigen Receptor (CAR) T cells

Many advancements in the field of adoptive T cell therapy were made in the early 1990s, with multiple reports describing the use of engineered tumour associated antigen (TAA)-specific TCRs introduced into patient T cells through gamma-retroviral transduction. Although TCR-based immunotherapy has been researched extensively and shown promise as a treatment option, the MHC-dependent restriction and co-receptor downregulation on tumour cells limits the effectiveness of TAA specific TCRs. In addition, mispairing between the α and β chains of the engineered and endogenous TCR resulted in lethal autoimmune diseases in mice and could result in similar toxicities in patients. Such obstacles drove the development of chimeric receptors consisting of an antibody-derived extracellular tumour antigen recognition domain fused to an intracellular TCR activation CD3ζ moiety to facilitate targeting of a pre-determined tumour antigen using the T lymphocytes in an MHC-independent manner. Such receptors were later described as Chimeric Antigen Receptors (CARs).

The first CAR T cell structures were described by Eshhar Z. et al and were composed of a chimeric T cell receptor. These structures were made up of the VH and VL antibody domains fused to either the α or β TCR domains to form VHCα or VH-Cβ/ VLCα or VL-Cβ chimeric chains. The VH and VL domains were specific for the 2,4,6-trinitrophenyl (TNP) antigen and provided the engineered T cells with specificity for the TNP in an MHC-independent manner, thus permitting the T cells to carry out signal transduction, activation and effector function.[95] Further developments were carried out by Eshhar Z. et al; Instead of fusing the VH and VL domains to the constant domains of the TCRα and β, a TNP specific single-chain variable fragment (scFv) was used to provide the T cell with antibody-like specificity towards its target antigen. This was fused directly to the CD3ζ intracellular signalling domain due to the fact it provided the robust and potent signalling within TCR complex.[96] Such structures presented effective cytotoxic killing of antigen-expressing target cells.[96]

These artificial receptor structures have the primary aim of redirecting T cell specificity towards a defined antigen. CARs are typically made up of four distinct regions: an antigen binding region, a spacer region, the transmembrane region, and an intracellular signalling domain region (Fig. 1.9).

The antigen binding region is typically a single chain fragment of the variable region (scFv) derived from the VH and VL domains of a monoclonal antibody. The binding region acts as the extracellular binding portion against a predetermined tumour antigen and binding is the initial step of downstream signalling. The binding affinity and kinetics of the scFv are thoroughly considered based on the antigen density of the chosen target antigen.[97] For example, it has been shown low affinity antigen-binding domains results in CAR T cell activation only once a high threshold of antigen density has been reached.[98,99] In addition to low antibody affinity, the component kinetics such as fast off-rates have been linked to a reduction in CAR T cell mediated toxicities and improved serial tumour cell killing.[100]. Utilising scFv antibody fragments allow the CAR to function independent of MHC-mediated antigen presentation and are not affected by HLA down-regulation observed in many tumours.[101] Although to date, scFv is the most utilised antigen binding domain of the CAR structure, alternative binding domains such as the VHH domain of HCAbs and the IgG Fab domains (VH-CH and VL-CL heterodimer) have been explored for use in CAR T cells.[102] VHH antibodies, devoid of light chains, maintain full antigen-specific binding capacity while only having a molecular weight ranging from 12–15 kDa, significantly less than Fab fragments (~50 kDa) and scFv fragments (~25 kDa) traditionally used in CAR architectures. Developments in the use of VHH antibodies in CAR T cell therapy is of particular significance due to the limited DNA encoding space available for efficient viral vector gene transfer required, as well as the unique immunological and biophysical characteristics exhibited by VHH antibodies.[103]

The antigen-binding region of the CAR is fused to the membrane via a spacer and transmembrane region. The spacer region confers the distance and flexibility of the binding domains from the T cell plasma membrane[104,105] and is commonly composed of an IgG hinge region, a CD8α or CD28 spacer or IgG constant domains.[97] Several considerations are taken into account when

choosing the spacer type and length. Generally, it is thought maintaining the native immunological synapse dimensions of the TCR and peptide-bound MHC interaction is desirable.[97] Therefore, a longer spacer region is favoured for membrane-proximal epitopes whereas a shorter spacer region is favoured for membrane-distal epitopes.[106] Beyond fusing the CAR structure to the T cell membrane, the role of the transmembrane region was the least well characterised out of the four broad regions of the CAR structure. However, recent work has shown the importance of the transmembrane region on CAR function. It has been reported the use of the CD28 transmembrane (CD28TM) enhanced the CAR T cell sensitivity through the stabilisation of the immune synapse.[107]

Finally, the combination of intracellular co-stimulatory and signalling domains of the intracellular signalling region confers the potency of the T cell signalling cascade. Over the years, various combinations of intracellular co-stimulatory and signalling domains has led to the evolution of first, second, third and fourth-generation CAR T cells (Fig. 1.9).[97]
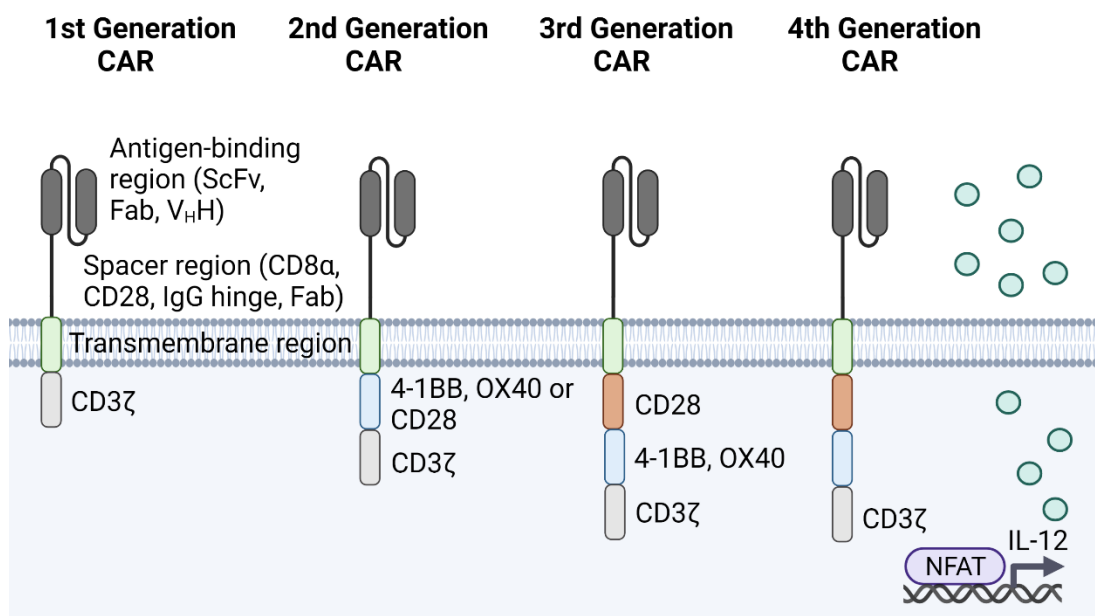
Figure 1.9. Evolution of chimeric antigen receptors (CARs).

A Chimeric antigen receptor (CAR) is an artificial receptor which redirects T cell specificity towards a defined tumour antigen. First generation CARs consist of four segments: (i) An antigen specific single chain variable fragment (scFv), (ii) the spacer domain, linking the scFv to the (iii) transmembrane (TM)

domain which is linked to the CD3ζ endodomain derived from the TCR. Addition of one or more costimulatory domain(s) such as CD28, 4-1BB or OX40 alongside the CD3ζ moiety form second-generation and third-generation CARs, respectively. Second or third generation CARs with inducible expression cassettes for a therapeutic transgene protein or pro-inflammatory cytokines such as IL-12 are termed as fourth-generation CARs.

First-generation CARs incorporated an individual CD3ζ signalling chain from the TCR complex, which proved to be sufficient to mediate target cell killing upon antigen engagement.[96,108] However, early trials and animal models using 'first-generation' CARs, which lacked co-stimulatory domains, showed poor cytokine production, T cell activation, proliferation, poor persistence[109], premature anergy[110] and anti-tumour activity.[111–113] For example, a group of patients treated with a first-generation CAR against the renal cell carcinoma antigen Carboxy-Anhydrase-IX (CAIX) presented poor CAR-T cell persistence.[114] Moreover, patients also developed unexpected treatment-related on-target off-tumour limiting biliary toxicity due to CAIX expression on the bile duct epithelium.[114] The limitations mentioned above have also been reported with the use of a first-generation CAR T cells for the treatment of paediatric metastatic neuroblastoma,[115] ovarian cancer,[116] and neuroblastoma[117].

The native TCR-mediated T cell activation is achieved via the association of two signals: the first being achieved through TCR engagement and activation and the second is achieved through CD28 activation via CD80 (B7-1) or CD86 (B7-2) engagement.[118] CD28 (Cluster of Differentiation 28) is a major co-stimulatory receptor constitutively expressed on naïve T cells and provides a potent co-stimulatory signal for activation, production of a range of cytokines, proliferation, and survival.[119–122] Lack of CD28 and B7 interaction and co-stimulation during the association of TCR and peptide-MHC results in T cell anergy.[110,123] Thus, it was reasoned the poor persistence[109], proliferation and premature anergy[110] of first-generation CAR T cells was a result of a lack of co-stimulatory signalling. Therefore, a co-stimulatory domain derived from the CD28 receptor was incorporated along with CD3ζ chain resulted in the creation of 'second generation' CARs. CAR T cells bearing the CD28 co-

stimulatory and CD3ζ signalling endodomain demonstrated enhanced interleukin-2 (IL-2) and interferon-γ (IFN-γ) secretion.[124]

A second-generation CAR composed of an extracellular PSMA targeting scFv antibody fragment, an intracellular CD28-CD3ζ co-stimulatory and signalling chain showed improved IL-2 secretion and proliferation against PSMA expressing tumour cells relative to a CAR lacking the CD28 co-stimulatory domain.[125] Additionally, the CD28-CD3ζ bearing anti-PSMA CAR T cells sustained expansion and multiple rounds of target cell killing.[125]

Furthermore, the use of second-generation CAR T cells against haematological malignancies has shown to be successful in the clinic. For example, Brentjens et al. reported the use of a second generation anti-CD19 CAR composed of a CD28 co-stimulatory and CD3ζ signalling chain to treat patients with relapsed B cell acute lymphoblastic leukemia (B-ALL). Upon CAR T cell infusion, all patients presenting morphological disease showed rapid tumour clearance as determined by PCR, with CAR T cell persistence measured 60 days post infusion. CAR T cell mediated toxicities such as cytokine release syndrome (CRS) was observed which required treatment with lymphotoxic steroids. However, B cell aplasia and elevated cytokine levels are suggestive of prolonged CAR T cell activation.[126]

In addition to the use of the CD28 endodomain, other co-stimulatory domains, such as 4-1BB and OX40 have also been incorporated into second-generation CARs.[127] 4-1BB, also known as CD137, belongs to the tumour necrosis factor receptor superfamily and its signalling is facilitated via the TNF Receptor Associated Factors (TRAF).[128] Activation of 4-1BB is linked to enhanced cytokine release, T cell proliferation and countering TGFβ related T cell suppression.[129–132] The use of a second generation anti-CD19 CAR composed of a 4-1BB-CD3ζ endodomain has been used to treat patients with refractory chronic lymphocytic leukemia (CLL). Upon CAR T cell infusion, patients showed tumour clearance within 28 days post infusion with CAR T cell persistence measured 6 months post infusion.[133]

Each subgroup of second-generation CAR T cells showed varying profiles of cytokines release, cytolytic degranulation, T cell amplification, and maturation downstream from CAR T cell activation due to differences in the intracellular domains. For example, CD28 co-stimulation tended to favour a potent effector response but led to T cell exhaustion, whereas 4-1BB co-stimulation favoured a central memory response, modest tumour depletion with greater CAR T cell persistence. Both independently providing T cell activation in the absence of co-stimulatory ligand on associated tumour.[134]

Incorporation of multiple co-stimulatory domains alongside the CD3ζ moiety are known as 'third-generation' CARs. Typically, third-generation CARs bear CD28-CD3ζ with the addition of either 4-1BB or OX40. So far, many reports have indicated the effector function of second-generation and third-generation CAR T cells remain comparable.[135–137]

A version of a second-generation or third-generation CAR modified to express an inducible therapeutic transgene of an anti-tumour payload were termed as 'fourth-generation' CARs or TRUCKs (T cells redirected for universal cytokine killing). These CAR T cells are used as vehicles to deliver transgenic anti-tumour cargos such as the pro-inflammatory cytokine IL-12 using an NFAT promoter, at the tumour site upon antigen exposure. Accumulation of pro-inflammatory cytokine in the tumour-microenvironment promotes T cell mediated inflammatory responses.[138]

1.4.5.2 CAR and TCR signalling

As previously mentioned, the CAR structure utilises TCR complex-derived signalling components, therefore we can deduce CAR T cells utilises a similar downstream signalling cascade. T cells express the multimeric TCR complex on its surface which is composed of the TCRα and β chains and the CD3 peptide complex. The TCRαβ dimer, generated via somatic VDJ recombination, is involved in the recognition of foreign antigenic peptide bound to the major histocompatibility complex (MHC) molecule. The CD3 complex, made up of epsilon (ε) chains, a gamma (γ) chain, a delta (δ) chain and zeta (ζ) chains, is involved in TCR signalling through the cytosolic domains which contain the immunoreceptor tyrosine-based activation motifs (ITAMs). TCR

and antigen-MHC engagement, mediated through the TCR CDR loops (CDR3α and CDR3β), triggers cytosolic phosphorylation of tyrosine residues within the ITAMS by a Src-family protein tyrosine kinase known as lymphocyte protein tyrosine kinase (Lck); a key event in early T cell activation. CD4 and CD8 co-receptors aid the recruitment of Lck to the TCR complex, enabling the phosphorylation of the ITAMs.[139,140] Evidence of constitutively active cytosolic Lck which phosphorylates the CD3 and ζ chains has also been reported.[141,142]

Lck-mediated double phosphorylation of tyrosine residues within the ITAMs in the CD3ζ chain results in an increased affinity for cytoplasmic zeta-chain-associated protein kinase 70 (ZAP-70) and thus its recruitment to the plasma membrane.[143] Zap-70 is a 70 kDa cytoplasmic tyrosine kinase is essential in the downstream T cell signal transduction. Zap-70 is a member of the Syk family of proteins and consists of tandem SH2 domains and a carboxy-terminal kinase domain; these are separated by a linker region called inter-domain A. Zap-70 owes its ability to become recruited to ITAMS on the ζ chain to its SH2 domains. These 100 amino-acid long domains are found in the structure of 111 human proteins and play an important role in protein-protein communication. An SH2 domain in a protein provides it with a strong affinity for phosphorylated tyrosine residues, such as the ones found on ITAMs on the CD3ζ chain. This gives proteins the ability to localise to specific compartments in the cell; here they can act as a scaffold to initiate further signalling. When two phosphorylation's have occurred, ITAMs recruit Zap-70 by binding to its tandem SH2 domains resulting in Zap-70 undergoing a conformational change from its native auto-inhibited state to that where its regulatory sites are exposed and susceptible to lck-mediated phosphorylation and are thus activated. Auto-phosphorylation and Lck-mediated phosphorylation of Zap70 ensures complete catalytic activity which then proceeds to phosphorylate several targets including LAT and SLP-76. These appear to act as docking sites for further protein signalling and T cell activation. Recruitment and activation of ZAP-70 therefore leads to the formation of multiple signalling complexes and triggering of downstream signalling cascades.[144,145]
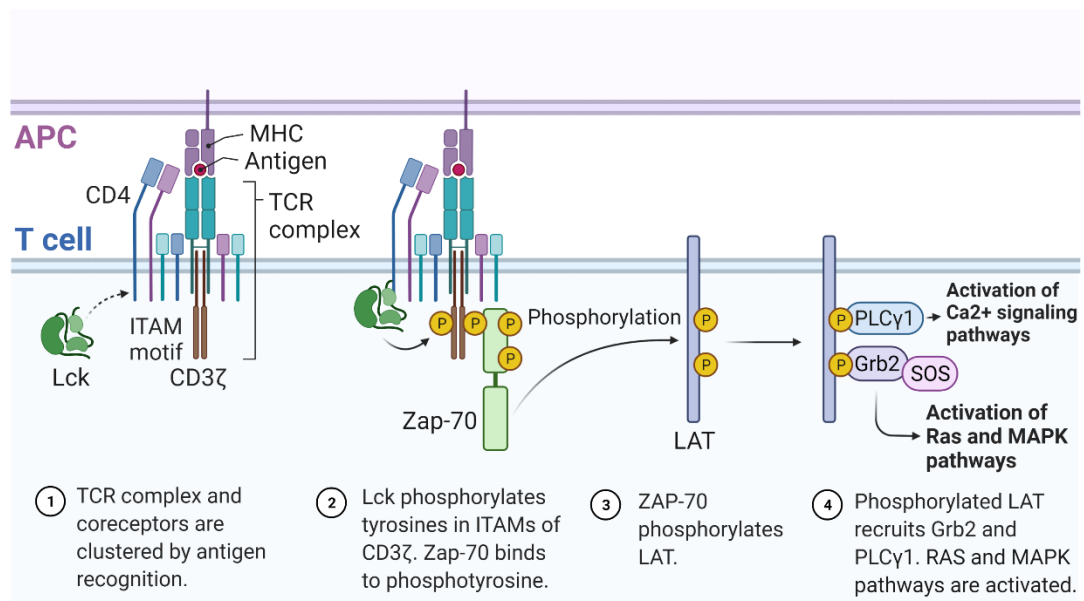
Figure 1.10. T cell receptor signalling.

The Src family kinases, Lck and ZAP-70, initiate the TCR signalling cascade. Lck activation phosphorylates ITAMs present on the intracellular tail of the TCR CD3ζ chains. Doubly phosphorylated ITAMs results in an increased affinity for ZAP-70. ITAMs proceed to recruit ZAP-70 to membrane ζ chains from the cytosol. Upon the phosphorylation of Tyr 315, Tyr 319, and Tyr 493 of ZAP-70 by Lck, ZAP-70 is fully activated from its native inactive state. ZAP-70 activation results in phosphorylation of two scaffold proteins, LAT and SLP-76, leading to the recruitment of downstream signalling proteins, Grb2 and PLCγ, which initiate a range of signalling cascades resulting in T cell activation.

1.4.5.3 CAR T cell therapy in the clinic

To date, three CAR T cell therapies have shown efficacy in a clinical setting and have successfully been granted FDA approval for the treatment of hematologic malignancies. The first approved CAR-T cell product, Kymriah (Novartis, CTL019), was approved in August 2017 and is constructed around a 4-1BB-CD3ζ endodomain based CD19 specific CAR for the treatment of refractory or later relapse acute lymphoblastic leukaemia (ALL) in paediatric and adult (up to 25-year-old) patients. Clinical trial data reports have indicated an overall remission rate of patients to be 81% within 3 months and 73% event-free survival after 6 months.[146] It was also noted the median persistence of

Kymriah was 163 days.[147] Kymriah has also been used in the treatment of Diffuse Large B-cell Lymphoma and has shown an overall survival rate in 90% of patients for more than a year. Additionally, long-term persistence and durable CAR T cell response up to 2 years post infusion was observed.[148]

The second CAR T cell approval, Yescarta (Kite Pharma), was approved in October 2017. Yescarta is constructed around a CD28-CD3ζ endodomain based CD19-specific CAR for the treatment of patients with relapsed or refractory diffuse large B-cell lymphoma (DLBCL). As of 2018, the objective response rate was reported as 82% with an 18-month overall survival rate of 52%.[149]

The third CAR T cell approval, Breyanzi (Juno Therapeutics, Bristol-Myers Squibb) was approved in February 2021. Breyanzi is a CD19 specific CAR bearing a 4-1BB-CD3ζ co-stimulatory domain for the treatment of adult relapsed or refractory large B-cell lymphoma, diffuse large B cell lymphoma (DLBCL), high-grade B-cell lymphoma, follicular lymphoma, and primary mediastinal large B-cell lymphoma. The independent review committee assessed the overall response rate (ORR) of Breyanzi in leukapheresed population to be 59%, with a complete response (CR) rate of 43% and a partial response (PR) rate of 15%.[150]

1.4.6 CAR T cell associated toxicities

1.4.6.1 CRS

The most significant adverse effect as a result of CAR T cell administration is the onset of a potentially life-threatening form of inflammatory response known as cytokine release syndrome (CRS).[151] CRS is characterised by elevated levels of serum cytokines such as interferon-gamma (IFN-γ), IL-10, IL-6 and granulocyte macrophage-colony stimulating factor (GM-CSF), and tumour necrosis factor-alpha (TNFα).[111,152] CRS is the most common toxicity brought on by CAR T cell therapy, with clinical presentation of CRS ranging from mild flu-like symptoms to severe life-threatening organ toxicity.[153] It has been shown that high disease burden in patients increases the chance of severe CRS upon CAR T cell infusion.[154,155] Patient prognosis is not associated with

the onset of severe CRS as patients have shown complete anti-tumour response in the absence of CRS-related toxicities. The appropriate intervention strategy to alleviate the physiological symptoms of CRS without eliminating the anti-tumour potential for CAR-T cells is essential in the successful application of adoptive T cell therapy. Administration of corticosteroid has been traditionally used to alleviate symptoms of CRS, although prolonged use of corticosteroids may result in clearance or dampening of the CAR-T cell population.[156,157] Currently, the favoured course of action to reverse CRS utilises the FDA-approved IL-6 receptor blocking antibody, tocilizumab.[153] However, the long-term consequences of this are poorly understood and the effects of IL-6 receptor blockade on CAR-T cell anti-tumour efficacy, proliferation and persistence is an area of intense research.

1.4.6.2 Neurotoxicity

Another life-threatening side effect of CAR T cell infusion is neurotoxicity also known as CAR T cell Related Encephalopathy Syndrome (CRES). Symptoms from CRES include hallucination, delirium, confusion, myoclonus, expressive aphasia and seizure and have been well documented in patients receiving anti-CD19 CAR T cell therapy.[15,152,159,155] For example, a clinical trial of a CD19 specific CAR T cell for the treatment of B-ALL was halted due to half of the participants developing severe neurotoxicity.[160] The exact mechanism leading to the neurological toxicities remains unknown, however neurological side effects have also been reported with the use of blinatumomab, a bispecific antibody targeting CD3 and tumour associated CD19, suggesting elevated cytokine levels may contribute to neurological sequelae.[161,162]

In cases of severe neurotoxicity, administration of corticosteroids such as dexamethasone is preferred over tocilizumab due to the fact of steroids being able to cross the blood-brain barrier.[153,163] Although effective in reducing the mortality rate, administration of corticosteroids leads to the abolition or dampening of the CAR T cell compartment resulting in disease relapse as shown during a trial carried out for the treatment of B-ALL using CD19-CAR T cells.[156]

More recently, Dasatinib, which is an FDA approved immunosuppressive chemotherapy drug, used in the treatment of chronic myelogenous leukemia (CML) and acute lymphoblastic leukemia (ALL) has shown promise in the management of CRS and neurotoxicity.[164] Dasatinib functions as a tyrosine kinase inhibitor which blocks adenosine triphosphate (ATP) binding sites of the tyrosine kinease, Lck. Therefore, inhibiting the CD3ζ-ITAM phosphorylation, recruitment of ZAP-70 and thus halting CAR-T cell signalling.[165] Both *in vitro* and *in vivo* models have shown dosed titration of dasatinib inhibits CAR T cell function in a dose-dependent manner with minimal abolition of CAR T cells. Furthermore, ceasing dasatinib administration restored anti-tumour activity, proliferation and cytokine secretion in CAR T cells.[166,166] Although dasatinib has the potential to provide reversible control of CAR T cell in the event of CRS and CRES, there are many reported adverse effects with the use of the drug. For example, the most common of the side effects reported have been secondary infections, bone marrow suppression, pleural effusion, dyspnea, swelling, fever, nausea and vomiting. Neutropenia and myelosuppression have also been reported as common toxic adverse events.

1.4.6.3 On-Target Off-tumour related toxicities

For CAR T cell therapy to function, it is essential for the antigen-binding domain to recognise and bind a tumour associated antigen(s) (TAAs). TAAs can be broadly categorised into five groups:[167] (i) antigens which bear mutations that are unique to tumour type such as the BCR-Abl antigen,[168] (ii) upregulated antigens on tumour cells compared to normal tissue, (iii) oncofetal antigens which are present in foetal tissue but not in adult tissue such as α-fetoprotein;[169] (iv) differentiation antigens such as CD19 expressed in B-ALL and (v) antigens expressed in testicular cancer but also expressed by spermatocytes such as melanoma-associated antigen.[170] Therefore, with the exception of a very small number of instances of viral antigens, only a select few mutated antigens are expressed exclusively on tumour cells.[111]

Pre-clinical studies using animal models may provide an understanding of the CAR T cell tissue selectivity, however the degree of on-target off-tumour toxicities in humans is difficult to predict. As a consequence, on-target off-tumour related toxicity which entails the recognition of the target antigen on normal tissues have been widely reported.[111]

In several instances, the use of CD19 specific CAR T cell therapy may result in the ablation of normal tissue such as the B-cell compartment expressing CD19. However, the on-target off-tumour toxicity can be offset with the use of immunoglobulin replacement therapy.

Where on-target off-tumour toxicities cannot be offset using replacement therapy, fatalities because of CAR T cell infusion have been reported. For example, in a clinical trial aiming to treat patients with colon cancer overexpressing the antigen *ERBB2,* a CAR expressing an anti-ERBB2 antigen-binding domain derived from the monoclonal antibody Trastuzumab and the CD28-4-1BB-CD3ζ co-stimulatory and signalling domains. Due to the low levels of antigen expression on lung epithelial tissue, all patients suffered from respiratory complications and CRS, followed by death within 5 days.[171] In another instance, a group of patients treated with a CAR T cell targeting the renal cell carcinoma antigen Carboxy-Anhydrase-IX (CAIX) developed unexpected treatment-related liver toxicity due to CAIX expression on the bile duct epithelium.[172]

These toxicities are very difficult to predict even with detailed animal studies or non-human primate work. Crucially, unlike small molecules and biologics, CAR T cells do not necessarily have a short half-life and one cannot cease administration and wait for the agent to breakdown or be excreted. CAR T cells are autonomous and can engraft and proliferate. Toxicity can therefore be progressive and fulminant. Suicide genes can be co-expressed in the CAR T cells the triggering of which results in the deletion of the CAR T cells permanently which not only destroys the anti-tumour activity of the therapy but can also pose an economic burden to re-administer the treatment.

1.4.7 Current Research in CAR-T cell Induced Toxicity Management

1.4.7.1 Clearance of CAR T cells using monoclonal antibodies

Due to the success of monoclonal antibodies (mAbs) in clinical trials, many mAbs have been FDA approved and are widely used in cancer therapy. As a result, suicide genes derived from the target epitopes of these clinically approved mAbs have been utilised in CAR T cell therapy. Examples include truncated EGFR which is recognized by the therapeutic antibody trastuzumab and RQR8 which contains dual epitopes for the anti-CD20 antibody rituximab separated by an epitope from the anti-CD34 antibody QBend10. Not only does RQR8 enable selection of transduced cells, but also selective deletion of CAR T cells using rituximab upon indications of CRS.[173] However, mAbs presents risks linked to the intrinsic toxicity of the antibody itself as well as the economic disadvantages of using mAbs in the clinic.[174] Additionally, such suicide genes may be inappropriate in settings in which the patient has been treated with the corresponding therapeutic antibody.

1.4.7.2 Induction of apoptosis for CAR T cell elimination

Remote control induction of apoptosis in CAR T cells has been explored with the use of a pro-apoptotic chimeric molecules which are able to dimerise and activate in the presence of a small molecule.[175,176] The chimeric inducible caspase-9 (iCasp9) made up of a truncated caspase-9 and a mutated FKPB12-binding domain can dimerize in the presence of rimiducid (AP1903) and initiate apoptosis to eliminate CAR T cell activity (Fig. 1.11). In addition, iCasp9 activity is independent of T cell anti-apoptotic factor upregulation. Apoptosis of CAR T cells against CD19 and CD20 has been shown using such a system. Further research in the field has utilised a rapamycin-induced caspase 9 suicide gene (rapaCasp9) in which the catalytic domains of caspase 9 are fused to FKBP12 and FRB and expressed in CAR T cells.[175–179] Although induction of apoptosis in CAR T cells acts as an efficient safety switch, such a mechanism is neither tuneable nor reversible.
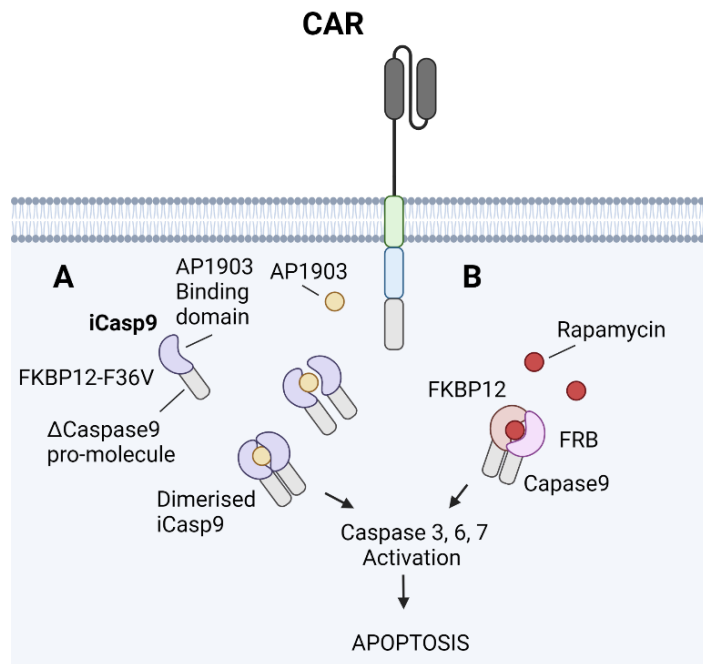
Figure 1.11. Chemically inducible caspase9/apoptosis in CAR T cells.

(A) Truncated caspase-9 pro-molecule fused to the F36V mutated FKBP12 fragment, and (B) the FKBP12 and FRB fused to the caspase 9 catalytic domain. Both systems induce the apoptotic cascade by dimerizing in the presence of rimiducid (AP1903) and rapamycin, respectively.

1.4.7.3 **Inducible ON-switch CAR activation using a dimerising small molecule**

Use of suicide genes results in obliteration of the CAR T cells permanently, therefore alternative mechanisms for improving CAR T cell safety have been developed. Several inducible CAR systems which can temporarily reduce or stop CAR T cell activity without permanently removing the CAR T cells have been described whereby the CAR T cell activation and effector function is remote-controlled through the presence of a small molecule dimerising drug. Such ON-switch systems rely on antigen engagement as well as the presence of a small molecule drug for CAR T cell activity.

For example, the inducible control and activation of CAR T cells has also been achieved through small-molecule mediated heterodimerization of the human FKBP12 binding protein to the mTOR FKBP-rapamycin T2089L mutant, FRB.

In most cases, the CAR structure is expressed as two separate polypeptides, the first chain is involved in antigen recognition and binding, whilst the second is responsible for T cell signalling and activation. By fusing the FKBP12 to the CAR antigen-binding domain and fusing FRB to the intracellular signalling domains bearing the CD3ζ chain, dosed administration of a rapamycin analogue, AP21967, results in the hybridisation of both components and subsequent CAR T cell activation in the presence of tumour antigen (Fig. 1.12).[180–182,183] Therefore, the immunoreactivity of CAR T cells is not only reliant on the presence of tumour antigen but also a small molecule drug, titration of which can be used to tune the CAR T cells effector activity. Several reports have utilised the FKBP12 and FRB proteins as the foundation of ON-switch CAR design in various iterations shown in Fig 1.19.[183–185] A key disadvantage of inducible ON-switch CAR designs is the requirement of prolonged administration of the small molecule drug to sustain CAR T cell efficacy for the duration of the therapy. The problem is further exacerbated in the case of using rapacycin, as it is an immunosuppressive drug which may be detrimental to the dampening the cytotoxic T cells.[186]
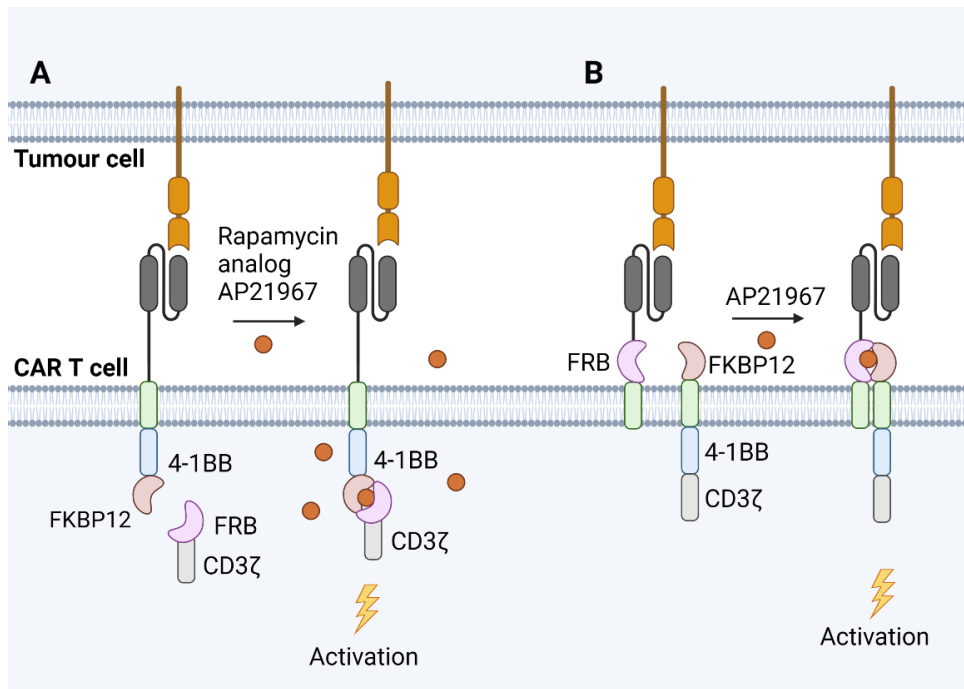
Figure 1.12. CAR activation capacity maintained upon dimerization of (A) intracellular and (B) extracellular anchored FKBP12 and FRB through the exogenous administration of the rapamycin analogue, AP21967.

1.4.7.4 Inducible OFF-switch CAR activation using a disrupting small molecule

More recently, inducible OFF-switch CARs which utilise a disrupting small molecule have also been developed.[187,188] One example describes a bi-partite CAR expressed as a separate antigen-binding polypeptide chain and a T cell signalling peptide chain. Each respective intracellular domain bears a protein domain known as a 'chemically disruptable heterodimer' which natively form into a heterodimer allowing for a functional CAR. Through the administration of an undisclosed drug, the heterodimer is disrupted thus preventing the CAR T cell activation independent of antigen engagement.[187]

An alternative OFF-switch CAR design functions via the small molecule drug mediated recruitment of a FKBP-SHP1 phosphatase chimeric protein to the CAR synapse. Therefore, resulting in dephosphorylation of the CAR CD3ζ signalling chain by the FKBP-SHP1, leading to the dampening of CAR-T cell signalling.[188]

Furthermore, the antibiotic drug tetracycline has also been used as a small molecule reversible safety switch for managing acute toxicity. The Tet-CAR system is also made up of a bi-partite CAR which is split into an antigen-binding chain and a signalling chain (Fig. 1.13). The enddomain of the former comprises of the tetracycline-binding TetRB proteins; the amino-terminus of the latter contains TIP, a peptide mimic of tetracycline. The CAR assembles via the docking of TIP with TetRB, resulting in functional CAR signal transduction. Tetracycline has a higher affinity for TetRB than TIP and upon its administration tetracycline disrupts TetRB interacting with TIP releasing the intracellular signalling domain from the CAR and inhibiting CAR activity. Once tetracycline is withdrawn, CAR-T cell activity is restored in a tuneable fashion. Although such a system shows tuneable and reversible CAR T cell activity with reduced cost of controlling acute toxicities, TebRb is a bacterial derived protein and therefore many safety concerns on potential immunogenicity in patients remains.[189]
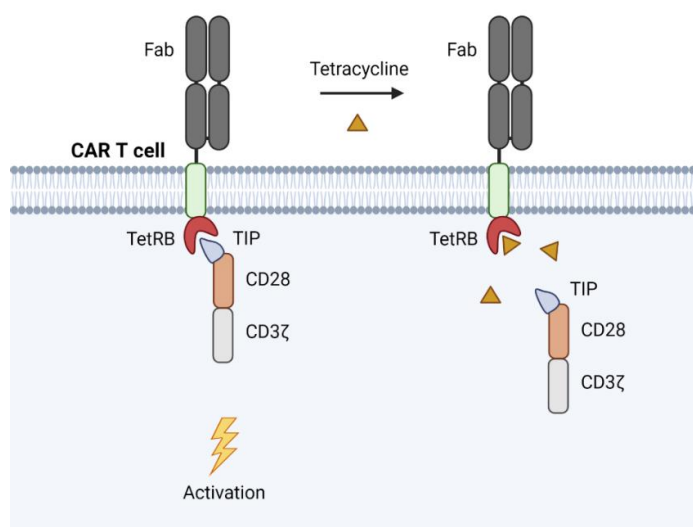
Figure 1.13. Schematic of the TetCAR system.

The antigen recognition component is the type I trans-membrane component comprising the scFv spacer, linker and TetRB. The second component of the bicistronic vector is TIP peptide fused to the co-stimulation domain CD28 and signalling chain CD3ζ. In the absence of tetracycline, a functional CAR signal transduction occurs. Addition of tetracycline displaces the displaces the TetRB

interaction with TIP, therefore inhibiting signaling capacity and effector function of the TetCAR transduction of the tet-CAR is inhibited.

1.4.7.5 Protease-based CAR inactivation system

Modulation of the CAR T cell activity through control of its degradation properties triggered through the presence of a small molecule has also been explored. The SWIFF-CAR system has a fused a protease target site, HCV NS3 protease and degradation moiety (degron) to the C-terminus end of a CAR architecture. Thus, upon cleavage of the protease target site, the protease target site-protease-degron component will be degraded whereas the CAR structure with a short 8-amino acid sequence of the CD3ζ domain will be expressed on the surface of T cells. Through the administration of an experimental drug candidate and protease inhibitor, Asunaprevir, this cleavage event cannot not take place resulting in the CAR structure fused to the degron which leads to CAR degradation through the T cell proteolytic pathways (Fig. 1.14).
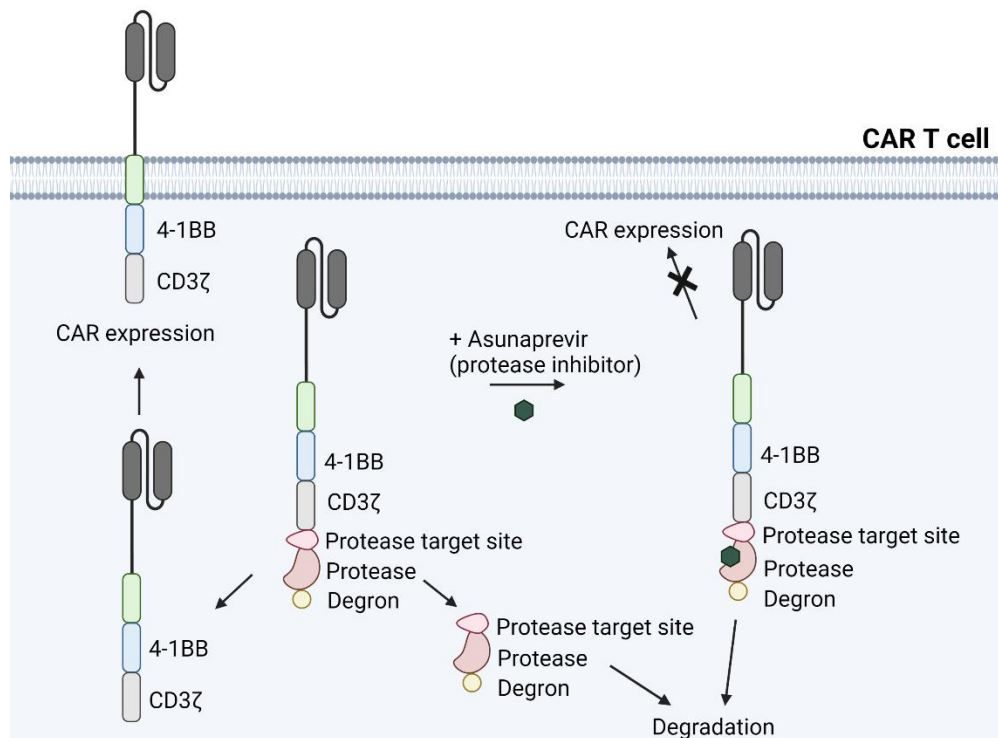
Figure 1.14. Schematic of the SWIFF-CAR system.

The SWIFF-CAR consists of a CAR architecture linked to a protease target site, a protease, and a degradation moiety (degron). In the absence of the protease inhibitory drug, Asunaprevir, cleavage takes place, and the CAR is liberated from the fused degron. The CAR is trafficked to the surface of a T cell to carry out cytolytic function ('ON'-state). In the presence of Asunaprevir, the cleavage event to liberate CAR from the degron is inhibited which leads to the degradation of the CAR via the cell's proteolytic pathways ('OFF'-state).

1.5 Project Aims

The principal aim of this research was to develop a remote-controllable OFF-switch split CAR architecture which utilises a small molecule-mediated protein-protein displacement system to act as a safety switch for CAR T cell inactivation in a dose-dependent, tuneable and reversible manner. Initially I aim to identify, using an immunised alpaca phage display library, a single-domain antibody (sdAb) which is capable of binding to minocycline with high affinity. Subsequently I intend to isolate, using a modified phage panning selection strategy, a cyclic peptide sequence capable of binding to the anti-minocycline sdAb but specifically displaced by minocycline. This will form the foundation of the protein-protein displacement platform. Finally, I aim to incorporate the anti-minocycline sdAb and displaceable peptide as a part of a split CAR architecture made up of a physically separated antigen-binding chain and signaling chain bearing each respective component. Via protein-protein interactions, functional heterodimerisation of each chain should result in a CAR T cell capable of activation, with transient suppression achieved through the administration of minocycline at therapeutic concentrations. Additionally, I aim to describe proof-of-concept applications using the displacement system by utilising the KDEL amino acid sequence, which retain proteins within the ER/Golgi apparatus, to tag the anti-minocycline sdAb. I hypothesise tagging IL-12 with one of the sdAb specific peptides will cause its retention and upon the addition of minocycline, the sdAb-peptide complex will dissociate enabling the secretion of IL-12.

2 MATERIAL & METHODS

2.1 MATERIALS

2.1.1 Material and Reagents

Table 2.1. Molecular biology reagents, chemicals, and kits

Reagent	Supplier	Catalogue Number/Code
Nuclease Free Water	Integrated DNA Technologies	11-05-01-04
TE buffer	Integrated DNA Technologies	11-05-01-05
Isopropanol	Thermo	10284250
Ethanol	Thermo	10644795
Buffer QG	Qiagen	19063
Buffer PE	Qiagen	19065
DNA Spin Columns with 2 ml Collection Tubes	Qiagen	27115
QIAquick PCR & Gel Clean up kit	Qiagen	28506
Stripette Controller	Drummond	N/A
Stripettes (5 ml)	VWR	734-1691
Stripettes (10 ml)	VWR	734-1693
Stripettes (5, 10, 25 ml)	VWR	734-1695
Scalpel	VWR	W261
0.2 ml PCR Tubes, 8 Strip with Cap	VWR	732-0546
Lint-free laboratory wipes	VWR	N/A
Bacterial Loop	VWR	612-9358
1.5 ml Centrifuge Tube	Star Labs	I1415-1002
L-shaped bacterial spreader	Star Labs	E1410-1025
Disposable Pipette Tips (10 µl)	Alpha Labs	FR1010-KIT
Disposable Pipette Tips (200 µl)	Alpha Labs	FR1200-KIT
Disposable Pipette Tips (1000 µl)	Alpha Labs	FR1250-KIT
Pipettes (P10, P100, P1000)	Thermo Fisher	F2
Round-bottom 12 ml Falcon tubes	Corning	352057
NucleoSpin® Plasmid EasyPure kit	Machery-Nagel	740727.250
Multichannel micropipette	Thermo Fisher	F2
NucleoBond® Xtra Combi Rack	Macherey Nagel	740415
50 ml centrifugation tubes (non-skirted)	Corning	430829/430921
Refrigerated centrifuge, ≥ 4,500xg	Thermo Fisher	X3R

Restriction endonuclease enzymes	New England Biolabs	See catalogue
Restriction endonuclease buffers, 10X	New England Biolabs	See catalogue
T4 Polynucleotide kinase (PNK)	New England Biolabs	M0201S
Phusion® High-Fidelity DNA Polymerase	New England Biolabs	M0530S
Phusion® HF Buffer	New England Biolabs	B0518S
Q5 High-Fidelity DNA Polymerase	New England Biolabs	M0491S
Q5 High-Fidelity 2X Master Mix	New England Biolabs	M0492S
Antarctic Phosphatase (AnP)	New England Biolabs	M0289
Antarctic Phosphatase Reaction Buffer, 10X	New England Biolabs	B0289
6x Gel loading buffer	New England Biolabs	B7024S
OneTaq® Quick-Load® 2X Master Mix with Standard Buffer	New England BioLabs	M0486
Quick-Load® Taq 2X Master Mix	New England Biolabs	M0271L
dNTP solution mix	New England BioLabs	N0447
Competent cells - NEB5alpha high-efficiency	New England Biolabs	C2987U
Competent cells - NEB5alpha subcloning efficiency	New England Biolabs	C2988J
SOC Media	New England Biolabs	N/A
NEBuilder® HiFi DNA Assembly Master Mix	New England BioLabs	E2621
M13KO7 helper phage	New England BioLabs	N03152
T4 DNA Ligase	Roche	10716359001
10X T4 DNA Ligase Buffer	Roche	11243292001
Invitrogen™ Anza™ T4 DNA Ligase Master Mix	Thermo Fisher	15535720
Hyper ladder 1 kb	Bioline	33026
Hyper ladder 100 bp	Bioline	33056
Agarose, Molecular grade	Bioline	BIO-41025

SYBR® Safe	Thermo Fisher	S33102
TG1 Electrocompetent Cells (manufactured by Lucigen, 24 reactions)	Cambridge Bioscience	60502-2
Expression Recovery Medium (lactose minus)	Cambridge Bioscience	80030-1
NucleoBond® Xtra Midi Kit, 100 reactions	Macherey Nagel	740410.100
Illustra RNAspin Mini RNA Isolation Kit	Sigma-Aldrich	25-0500-71
β-Mercaptoethanol, ≥ 99%	Sigma-Aldrich	M6250-10ML
RiboLock RNase Inhibitor 40 U/µl	Thermo Fisher	10859710
Superscript IV reverse transcriptase, 200 U/µl	Thermo Fisher	15307696
RNase H, 5 U/µl	Thermo Fisher	10334860
3 M Sodium Acetate Solution, pH 5.2	Thermo Fisher	10190890
SureClean Plus (containing pink co-precipitant)	Bioline	BIO-37047
KOD Xtreme™ Hot Start DNA Polymerase (EMD Millipore)	Sigma-Aldrich	71975-M
PfuUltra High-fidelity DNA Polymerase (2.5 U/µl)	Agilent	600380
Gene Pulser/MicroPulser Electroporation Cuvettes, 0.1 cm gap	BioRad	165-2089
Petri dishes, polystyrene, 150 mm × 15 mm	Sigma-Aldrich	P5981
Petri dishes, polystyrene, 24.5 x 24.5 cm	Corning	431272
Ampicillin stock 100 mg/ml	Sigma-Aldrich	C1613
Kanamycin stock 100 mg/ml	Sigma-Aldrich	K0129-20ml
50% (v/v) glycerol sterile	Sigma-Aldrich	91638
20% PEG 6000, 2.5M NaCl	Sigma-Aldrich	89510-1KG-F
20% Glucose stock sterile	Sigma-Aldrich	G8270-1KG
1x ROTI block, PBS	Sigma-Aldrich	70166-500G
Powdered milk (for milk 2% PBS)	Carl Roth GmbH	271-045-3
IPTG Stock 1 M	VWR Chemicals	437714-5x
Sequencing PCR Microplate	Axygen-Corning	PCR-96-AB-C
Sequencing Lids	Thermo	AB-0784
96-Deep well culture plate	4titude	4ti-0132
Aeration lids for deep well culture plates	4titude	4ti-0517/S5

Nunc Immunotubes	Thermo	341866
PBS + 0.1% Tween	Sigma-Aldrich	P2287-500ml
250 ml 0.22 μm vented baffled flask	Corning	431407
Minocycline Hydrochloride	Sigma-Aldrich	M9511
Doxycycline hyclate	Sigma-Aldrich	D9891
Methotrexate hydrate	Sigma-Aldrich	A6770
Tetracycline	Sigma-Aldrich	87128
Caffeine	Sigma-Aldrich	C0750
CPQWAMMFC peptide	GenScript Biotech	N/A
CPGWARAFC peptide	GenScript Biotech	N/A

Table 2.2. Tissue culture reagents and chemicals

Reagent	Supplier	Catalogue Number/Code
Sterile D-PBS	Sigma-Aldrich	D5773
Ficoll-Paque PLUS	GE Health Care	17-1440-02
RPMI 1640	Lonza	BE12-167F
IMDM	Lonza	BE12-726F
Sterile 0.5M EDTA	Fisher Scientific	10209454
Dimethyl sulfoxide anhydrous, ≥99.9%	Sigma-Aldrich	276855
Trypsin-EDTA	Sigma-Aldrich Life Science	T4049-100ML
Foetal Bovine Serum (FBS)	Labtech	FCS-SA
Glutamax 100X	Gibco	35050-061
Anti CD3 Pure (OKT3) (100 μg/ml)	Miltenyi	130-093-387
Anti CD28 Pure (15E8) (100 μg/ml)	Miltenyi	130-093-375
Human IL-2 (1 mg)	GenScript Biotech	200368
Retronectin	Takara	T100
Solution 18	Chemometec	910-3018
Cell Staining Buffer	BD	554656
GeneJuice® Transfection Reagent	Merc Millipore	70967
Antibiotic Antimycotic Solution (100x)	Sigma-Aldrich	A5955
BSA sterile solution (30%)	Sigma-Aldrich	A9576-50ML

Table 2.3. Tissue culture plasticware

Reagent	Supplier	Catalogue Number/Code
50 ml Falcon tubes	Corning	CLS430829
15 ml Falcon tubes	Corning	CLS430791
50 ml SepMate™ PBMC Isolation Tubes	StemCell	85450
Sterile Non-tissue culture grade 6 well culture dish	VWR	734-0948
Sterile Non-tissue culture grade 24 well culture dish	VWR	734-2779
Sterile Non-tissue culture 6 well culture dish	VWR	N/A
Sterile TC grade T175 Flasks	ThermoScientific	159910
Sterile TC grade T75 Flasks	ThermoScientific	156499
Sterile TC grade T25 Flasks	ThermoScientific	156367
Sterile TC grade 10 cm x 2 cm culture dish (50cm3)	Corning	430167
Sterile TC grade 15cm x 2.5 cm culture dish (148 cm^2)	Corning	430599
5 ml Stripette™ Paper/Plastic-Wrapped Sterile	Corning	10084450
10 ml Stripette™ Paper/Plastic-Wrapped Sterile	Corning	10084450
25 ml Stripette™ Paper/Plastic-Wrapped Sterile	Corning	10606151
50 ml Stripette™ Paper/Plastic-Wrapped Sterile	Corning	10636391
Nunc 96-Well Flat Bottom	ThermoScientific	167008
Nunc 96-Well U Bottom	ThermoScientific	163320
Sterile 50 ml reservoir	StarLab	E2310-1010
10 µl TipOne® RPT Graduated Filter Tip	StarLab	S1181-3810-C
20 µl TipOne® RPT Graduated Filter Tip	StarLab	S1180-1810-C
200 µl TipOne® RPT Graduated Filter Tip	StarLab	S1180-8810-C

1000 µl TipOne® RPT XL Graduated Filter Tip (sterile)	StarLab	S1182-1830-C
10 ml cryovials	Simport	T310-10A
1.8 ml Cryovial with External Thread, Self-Sealing Cap, Skirted (Sterile)	StarLab	E3090-6222
NC-Slide A8	Chemometec	942-0003

Table 2.4. Protein work reagents, chemicals and kits

Reagent	Supplier	Catalogue Number/Code
BioRad mini-protean TGX gels – 10 well	Biorad	4561093
BioRad mini-protean TGX gels – 15 well	Biorad	4561096
TGS 10X	Biorad	1610772
Precision Plus Protein™ All Blue Standards	Biorad	1610373
Precision Plus Protein™ Unstained Standards	Biorad	1610363
MeOH*	Any	
Acetic Acid*	Any	
Prometheus NT.48 Nano DSF Grade Capillaries Standard	Temper Technologies	PR-C002
Prometheus NT.48 Nano DSF Grade Capillaries High Sensitivity	Temper Technologies	PR-C006
0.5M NaOH*	Any	N/A
Distilled water*	Any	N/A
Sterile PBS	Sigma-Aldrich (Merck)	D8537-500ML
IgG elution buffer	ThermoFisher Scientific	21004
96 deep well plates	ThermoFisher Scientific	278605
Mab Select SURE 1 ml column	GE Healthcare	11003493
Amicon Ultra-15 10K Centrifugal Filter Devices	Merck	UFC901096

2.1.2 Solutions and Buffers

Table 2.5. Molecular biology media and buffers

Buffer	Composition
Luria-Bertani Broth (LB)	LB tablets purchased from MPBio LLC. Containing 10 grams of Tryptone, 5 grams of Yeast Extract and 10 grams of NaCl. pH range of 6.5 - 7.5. Dissolved in deionised H_2O.
2xYT Medium Broth	Add 16 grams of Tryptone, 10 grams of Yeast Extract, 5 grams of NaCl to deionised H_2O. Adjust to pH 7.0 using 5N NaOH. Adjust to 1 L using deionised H_2O. Sterilise using the autoclave.
Terrific Broth (TB)	Terrific broth powder purchased from Merck. TB per litre contained 12 grams of tryptone, 24 grams of yeast extract, 9.4 grams of dibasic potassium phosphate and 2.2 grams of monobasic potassium phosphate.
FACS buffer	PBS with 1% FBS
Tris/Borate/EDTA (TBE) buffer	1 litre of TBE buffer contained 9.3 grams of EDTA, 55 grams of Boric Acid and 108 grams of Tris-base. Adjusted to 1 litre of deionised H_2O.

Table 2.6. Tissue culture medium

Medium	Composition
Complete RPMI	10% FCS, 1% GlutaMAX
Complete IMDM	10% FCS, 1% GlutaMAX
Freezing media	FCS, 10% DMSO
PBMC maintenance medium	Complete RPMI supplemented with human IL-2 (100 I.U./ml)

2.1.3 Antibodies

Commercial antibodies used for flow cytometry, ELISA or functional assays are shown on Table 2.7.

Table 2.7. Antibody list

Antibody	Supplier	Catalogue Number/Code
Anti-M13-HRP	Sino Biologics	1197-mm05T-H
Anti-Myc-HRP	Genscript	A00863
CD3 PE-Cy7	Biolegend	317334
Human CD34 APC-conjugated Antibody	R&D system	FAB7227A
Human CD34 Alexa Fluor® 488-conjugated Antibody	R&D system	FAB7227G
Streptavidin PE	Biolegend	405204
APC anti-human EGFR Antibody	Biolegend	352905
Alexa Fluor® 488 anti-human EGFR Antibody	Biolegend	352907
PE anti-HA.11 Epitope Tag Antibody	Biolegend	901517
SYTOX™ Blue Dead Cell Stain	ThermoFisher	S10274

2.1.4 Cell lines

Table 2.8. Cell lines list

Cell line	Supplier	Catalogue Code	Details
Jurkat cells	ATCC®	TIB-152™	Human T lymphoblast derived from the peripheral blood of a fourteen-year-old boy with acute T cell leukaemia.
SUP-T1 cells	ATCC®	CRL-1942™	Human T lymphoblast derived from the malignant cells of an eight-year-old boy with T Cell Lymphoblastic Lymphoma. SupT1 cells were transduced to express EGFR and were used as a tumour model in this work.

293T cells	ATCC®	CRL-3216™	Derivative of the human embryonic kidney 293 cells is a highly transfectable and contains the SV40 T-antigen. Replicates vectors which carry the SV40 replicon. Was used to produce recombinant proteins, gene expression and high retroviral titres.
SKOV-3 cells	ATCC®	HTB-77™	Human hypodiploid epithelial-like cells derived from adenosarcoma. SKOV-3 cells natively express EGFR and were used in live-cell imaging by transducing cells to express mKate2.
ExpiCHO-S™ Cells	Thermo Fisher	A29127	Derived from CHO-S Chinese hamster ovary (CHO) cells. Using the ExpiCHO™ Expression System Kit high yields of recombinant antibodies were produced.

2.1.5 Equipment

Table 2.9. List of equipment

Equipment	Supplier
Azure 200	Azure Biosystems
MACSQuant®10 Flow Cytometer	Miltenyi Biotech
Nano differential scanning fluorimetry (nanoDSF)	Coriolis-Pharma
Mini-PROTEAN System vertical electrophoresis cell	Bio-Rad
NanoDrop™ 8000 Spectrophotometers	ThermoFisher
C1000 Touch Thermal Cycler	Bio-Rad
Automated ELISA Reader	ThermoFisher
Biacore™ T200	GE Healthcare Life Sciences
MicroCal PEAQ-ITC	Malvern Panalytical
Incucyte® ZOOM	Essen BioScience

2.1.6 Plasmids

Table 2.10. Plasmid reference table. Details of full list of plasmids cloned for use in this thesis

Vector plasmid	Details
RDF	RDF114
pEQ-Pam3-E	gag-pol expression plasmid
AbVec.aMinocycline_VHH_clone1-MuIgG2a	Murine IgG2a fused to anti-minocycline sdAb
AbVec.aMinocycline_VHH_clone4-MuIgG2a	Murine IgG2a fused to anti-minocycline sdAb
AbVec.aMinocycline_VHH_clone9-MuIgG2a	Murine IgG2a fused to anti-minocycline sdAb
AbVec.aMinocycline_VHH_clone14-MuIgG2a	Murine IgG2a fused to anti-minocycline sdAb
AbVec.aMinocycline_VHH_clone21-MuIgG2a	Murine IgG2a fused to anti-minocycline sdAb
AbVec.aMinocycline_VHH_clone22-MuIgG2a	Murine IgG2a fused to anti-minocycline sdAb
AbVec.aMinocycline_VHH_clone25-MuIgG2a	Murine IgG2a fused to anti-minocycline sdAb
AbVec.aMinocycline_VHH_clone26-MuIgG2a	Murine IgG2a fused to anti-minocycline sdAb
AbVec.aMinocycline_VHH_clone31-MuIgG2a	Murine IgG2a fused to anti-minocycline sdAb
AbVec.aMinocycline_VHH_clone32-MuIgG2a	Murine IgG2a fused to anti-minocycline sdAb
AbVec.aMinocycline_VHH_clone36-MuIgG2a	Murine IgG2a fused to anti-minocycline sdAb
AbVec.aMinocycline_VHH_clone37-MuIgG2a	Murine IgG2a fused to anti-minocycline sdAb
AbVec.aMinocycline_VHH_clone38-MuIgG2a	Murine IgG2a fused to anti-minocycline sdAb
AbVec.aMinocycline_VHH_clone40-MuIgG2a	Murine IgG2a fused to anti-minocycline sdAb
SFGmR.RQR8-2A-aMinoVHH_pan2c1-CD8STK-TM-41BBζ	Anti-minocycline VHH fused to CD8α spacer, 41BB and CD3ζ

SFGmR.RQR8-2A-aEGFRVHH-CD8STK-TM-41BBζ	Anti-EGFR VHH fused to CD8α spacer, 41BB and CD3ζ
AbVec.ACPGWARAFC-MuIgG2a	ACPGWARAFC fused to Murine IgG2a
AbVec.ACPHWAQAFC-MuIgG2a	ACPHWAQAFC fused to Murine IgG2a
AbVec.ACPQWAMMFC-MuIgG2a	CPQWAMMFC fused to Murine IgG2a
AbVec.ACPQWAYSFC-MuIgG2a	CPQWAYSFC fused to Murine IgG2a
AbVec.aMinocycline_VHH_clone1_G27A-MuIgG2a	sdAb alanine mutant fused to murine IgG2a
AbVec.aMinocycline_VHH_clone1_R28A-MuIgG2a	sdAb alanine mutant fused to murine IgG2a
AbVec.aMinocycline_VHH_clone1_T29A-MuIgG2a	sdAb alanine mutant fused to murine IgG2a
AbVec.aMinocycline_VHH_clone1_F30A-MuIgG2a	sdAb alanine mutant fused to murine IgG2a
AbVec.aMinocycline_VHH_clone1_S35A-MuIgG2a	sdAb alanine mutant fused to murine IgG2a
AbVec.aMinocycline_VHH_clone1_S36A-MuIgG2a	sdAb alanine mutant fused to murine IgG2a
AbVec.aMinocycline_VHH_clone1_ Y37A-MuIgG2a	sdAb alanine mutant fused to murine IgG2a
AbVec.aMinocycline_VHH_clone1_ N38A-MuIgG2a	sdAb alanine mutant fused to murine IgG2a
AbVec.aMinocycline_VHH_clone1_ I39A-MuIgG2a	sdAb alanine mutant fused to murine IgG2a
AbVec.aMinocycline_VHH_clone1_ G40A-MuIgG2a	sdAb alanine mutant fused to murine IgG2a
AbVec.aMinocycline_VHH_clone1_ A55S-MuIgG2a	sdAb alanine mutant fused to murine IgG2a
AbVec.aMinocycline_VHH_clone1_ I56A-MuIgG2a	sdAb alanine mutant fused to murine IgG2a
AbVec.aMinocycline_VHH_clone1_ S57A-MuIgG2a	sdAb alanine mutant fused to murine IgG2a
AbVec.aMinocycline_VHH_clone1_ W58A-MuIgG2a	sdAb alanine mutant fused to murine IgG2a
AbVec.aMinocycline_VHH_clone1_ S59A-MuIgG2a	sdAb alanine mutant fused to murine IgG2a
AbVec.aMinocycline_VHH_clone1_ G62A-MuIgG2a	sdAb alanine mutant fused to murine IgG2a

AbVec.aMinocycline_VHH_clone1_ A63S-MuIgG2a	sdAb alanine mutant fused to murine IgG2a
AbVec.aMinocycline_VHH_clone1_ R64A-MuIgG2a	sdAb alanine mutant fused to murine IgG2a
AbVec.aMinocycline_VHH_clone1_ T65A-MuIgG2a	sdAb alanine mutant fused to murine IgG2a
AbVec.aMinocycline_VHH_clone1_ Y66A-MuIgG2a	sdAb alanine mutant fused to murine IgG2a
AbVec.aMinocycline_VHH_clone1_ Y67A-MuIgG2a	sdAb alanine mutant fused to murine IgG2a
AbVec.aMinocycline_VHH_clone1_ A68S-MuIgG2a	sdAb alanine mutant fused to murine IgG2a
AbVec.aMinocycline_VHH_clone1_ D69A-MuIgG2a	sdAb alanine mutant fused to murine IgG2a
AbVec.aMinocycline_VHH_clone1_ S70A-MuIgG2a	sdAb alanine mutant fused to murine IgG2a
AbVec.aMinocycline_VHH_clone1_ V71A-MuIgG2a	sdAb alanine mutant fused to murine IgG2a
AbVec.aMinocycline_VHH_clone1_ K72A-MuIgG2a	sdAb alanine mutant fused to murine IgG2a
AbVec.aMinocycline_VHH_clone1_ G74A-MuIgG2a	sdAb alanine mutant fused to murine IgG2a
AbVec.aMinocycline_VHH_clone1_ G107A-MuIgG2a	sdAb alanine mutant fused to murine IgG2a
AbVec.aMinocycline_VHH_clone1_ R108A-MuIgG2a	sdAb alanine mutant fused to murine IgG2a
AbVec.aMinocycline_VHH_clone1_ G109A-MuIgG2a	sdAb alanine mutant fused to murine IgG2a
AbVec.aMinocycline_VHH_clone1_ W110A-MuIgG2a	sdAb alanine mutant fused to murine IgG2a
AbVec.aMinocycline_VHH_clone1_ G111A-MuIgG2a	sdAb alanine mutant fused to murine IgG2a
AbVec.aMinocycline_VHH_clone1_ E112A-MuIgG2a	sdAb alanine mutant fused to murine IgG2a
AbVec.aMinocycline_VHH_clone1_ A113S-MuIgG2a	sdAb alanine mutant fused to murine IgG2a
AbVec.aMinocycline_VHH_clone1_ I114A-MuIgG2a	sdAb alanine mutant fused to murine IgG2a
AbVec.aMinocycline_VHH_clone1_ L115A-MuIgG2a	sdAb alanine mutant fused to murine IgG2a
AbVec.aMinocycline_VHH_clone1_ D116A-MuIgG2a	sdAb alanine mutant fused to murine IgG2a

AbVec.aMinocycline_VHH_clone1_ Y117A-MuIgG2a	sdAb alanine mutant fused to murine IgG2a
SFG.EGFR	Epidermal growth factor receptor
SFGmR.RQR8-2A-aEGFRVHH_9G8-IgK-2A-aMinoVHH_pan2c1-CH1-CD28tm-CD28-2A-V5tag-GWARA-2xG4S-CD3epsilonEcto-CD3epsilonEndo	Chimeric GWARA fused to the TCR CD3ε chain expressed with the anti-minocycline and anti-EGFR sdAb fused to a CD28TM
SFGmR.RQR8-2a-V5tag-PWAYS-CD8STK_mono-CD28TM-CD28-41BBζ	V5-tagged PWAYS fused to CD8STK, a CD28TM, CD28-41BB-CD3ζ
SFGmR.RQR8-2a-V5tag-HWAQA-CD8STK_mono-CD28TM-CD28-41BBζ	V5-tagged HWAQA fused to CD8STK, a CD28TM, CD28-41BB-CD3ζ
SFGmR.RQR8-2a-V5tag-QWAMM-CD8STK_mono-CD28TM-CD28-41BBζ	V5-tagged QWAMM fused to CD8STK, a CD28TM, CD28-41BB-CD3ζ
SFGmR.RQR8-2a-V5tag-GWARA-CD8STK_mono-CD28TM-CD28-41BBζ	V5-tagged GWARA fused to CD8STK, a CD28TM, CD28-41BB-CD3ζ
SFGmR.RQR8-2a-V5tag-SG3S-CD8STK_mono-CD28TM-CD28-41BBζ	Ser-Gly(x3)-Ser fused to CD8STK, a CD28TM, CD28-41BB-CD3ζ
SFGmR.RQR8-2A-HAtag-aEGFRVHH_9G8-IgK-2A-aMinoVHH_pan2c1-CH1-CD28tm-RL-2A-V5tag-PWAYS-CD8STK_mono-CD28-41BBζ	Prototype split CAR bearing PWAYS peptide
SFGmR.RQR8-2A-HAtag-aEGFRVHH_9G8-IgK-2A-aMinoVHH_pan2c1-CH1-CD28tm-RL-2A-V5tag-HWAQGA-CD8STK_mono-CD28-41BBζ	PWAYS fused to CD8STK, CD28TM, CD28-41BB-CD3ζ. Expressed with anti-EGFR sdAb and anti-minocycline sdAb Fab spacer fused to a CD28TM
SFGmR.RQR8-2A-HAtag-aEGFRVHH_9G8-IgK-2A-aMinoVHH_pan2c1-CH1-CD28tm-RL-2A-V5tag-QWAMM-CD8STK_mono-CD28-41BBζ	QWAMM fused to CD8STK, CD28TM, CD28-41BB-CD3ζ. Expressed with anti-EGFR sdAb and anti-

	minocycline sdAb Fab spacer fused to a CD28TM
SFGmR.RQR8-2A-HAtag-aEGFRVHH_9G8-IgK-2A-aMinoVHH_pan2c1-CH1-CD28tm-RL-2A-V5tag-GWARA-CD8STK_mono-CD28-41BBζ	GWARA fused to CD8STK, CD28TM, CD28-41BB-CD3ζ. Expressed with anti-EGFR sdAb and anti-minocycline sdAb Fab spacer fused to a CD28TM
SFGmR.RQR8-2A-HAtag-aEGFRVHH_9G8-IgK-2A-aMinoVHH_pan2c1-CH1-CD28tm-RL-2A-V5tag-SG3S-CD8STK_mono-CD28-41BBζ	Ser-Gly(x3)-Ser fused to CD8STK, CD28TM, CD28-41BB-CD3ζ. Expressed with anti-EGFR sdAb and anti-minocycline sdAb Fab spacer fused to a CD28TM
SFGmR.RQR8-2A-HAtag-aEGFRVHH_9G8-IgK-2A-aMinoVHH_pan2c1-CH1-CD28-41BBζ	Monolithic CAR composed of anti-EGFR and anti-Minocycline sdAb Fab spacer, CD28TM-CD28-41BB-CD3ζ
SFGmR.RQR8-2A-HAtag-aEGFRVHH_9G8-IgK-2A-aMinoVHH_pan2c1-CH1-CD28tm-RL-2A-V5tag-GWARA-11aa-Linker-CD8STK_mono-CD28-41BBζ	GWARA 11aa Ser-Gly fused to CD8STK, CD28TM, CD28-41BB-CD3ζ. Expressed with aEGFR sdAb and aMino sdAb Fab spacer
SFGmR.RQR8-2A-HAtag-aEGFRVHH_9G8-IgK-2A-aMinoVHH_pan2c1-CH1-CD28tm-RL-2A-V5tag-GWARA-16aa-Linker-CD8STK_mono-CD28-41BBζ	GWARA 16aa Ser-Gly fused to CD8STK, CD28TM, CD28-41BB-CD3ζ. Expressed with aEGFR sdAb and aMino sdAb Fab spacer
SFGmR.RQR8-2A-HAtag-aEGFRVHH_9G8-IgK-2A-aMinoVHH_pan2c1-CH1-CD28tm-RL-2A-V5tag-GWARA-11aaLinker-GWARA-CD8STK_mono-CD28-41BBζ	GWARA 11aa Ser-Gly GWARA fused to CD8STK, CD28TM, CD28-41BB-CD3ζ. Expressed with aEGFR

	sdAb and aMino sdAb Fab spacer
SFGmR.RQR8-2A-HAtag-aEGFRVHH_9G8-IgK-2A-aMinoVHH_pan2c1-CH1-CD28tm-RL-2A-V5tag-GWARA-16aaLinker-GWARA-CD8STK_mono-CD28-41BBζ	GWARA 16aa Ser-Gly GWARA fused to CD8STK, CD28TM, CD28-41BB-CD3ζ. Expressed with aEGFR sdAb and aMino sdAb Fab spacer
SFGmR.RQR8-2A-HAtag-aEGFRVHH_9G8-GWARA-CD8stk-CD8TM-RL-2A-V5-aMinoVHH_pan2c1-monoCD8STK-CD8TM-CD28-41BBζ	aEGFR sdAb fused to a GWARA-CD8STK spacer, CD8TM. Expressed with aMino sdAb fused to a CD8STK, CD8TM, CD28-41BB-CD3ζ endodomain.
SFGmR.RQR8-2A-HAtag-aEGFRVHH_9G8-16AA_SG_L-GWARA-CD8stk-CD8TM-RL-2A-V5-aMinoVHH_pan2c1-monoCD8STK-CD8TM-CD28-41BBζ	aEGFR sdAb fused to a GWARA-CD8STK spacer, CD8TM. Expressed with aMino sdAb fused to a CD8STK, CD8TM, CD28-41BB-CD3ζ endodomain.
SFGmR.RQR8-2A-HAtag-aEGFRVHH_9G8-RL-GWARA-CD8stk-CD8TM-RL-2A-V5-aMinoVHH_pan2c1-monoCD8STK-CD8TM-CD28-41BBζ	aEGFR sdAb fused to a GWARA-CD8STK spacer, CD8TM. Expressed with aMino sdAb fused to a CD8STK, CD8TM, CD28-41BB-CD3ζ endodomain.
SFGmR.RQR8-2A-HAtag-aEGFRVHH_9G8-GWARA-CD8STK-CD8TM-CD28-41BBζ	aEGFR sdAb fused to a GWARA-CD8STK spacer, CD8TM, CD28-41BB-CD3ζ endodomain.
SFGmR.RQR8-2A-HAtag-aEGFRVHH_9G8-16AA_SG_L-GWARA-CD8STK-CD8TM-CD28-41BBζ	aEGFR sdAb fused to a GWARA-CD8STK spacer, CD8TM, CD28-41BB-CD3ζ endodomain.
SFGmR.RQR8-2A-HAtag-aEGFRVHH_9G8-RL-GWARA-CD8STK-CD8TM-CD28-41BBζ	aEGFR sdAb fused to a GWARA-CD8STK spacer, CD8TM, CD28-41BB-CD3ζ endodomain.

SFGmR.RQR8-2A-HAtag-aEGFRVHH_9G8-SG3S-CD8STK-CD8TM-RL-2A-V5-aMinoVHH_pan2c1-monoCD8stk-CD8TM-CD28-41BBζ	aEGFR sdAb fused to serine-glycine and a CD8STK spacer, CD8TM. Expressed with aMino sdAb fused to a CD8STK, CD8TM, CD28-41BB-CD3ζ endodomain.
SFGmR.RQR8-2A-HAtag-aEGFRVHH_9G8-IgK-2A-aMinoVHH_pan2c1-CH1-CD28TM-CD28-2A-V5tag-GWARA-CD8STK_mono-ζ	GWARA fused to a CD8STK, a CD28TM, CD3ζ. aEGFR sdAb and aMino sdAb Fab spacer fused to a CD28TM and CD28 endodomain.
SFGmR.RQR8-2A-HAtag-aEGFRVHH_9G8-IgK-2A-aMinoVHH_pan2c1-CH1-CD28TM-CD28-2A-V5tag-GWARA-CD8STK_mono-41BBζ	GWARA fused to CD8STK, CD28TM, 41BB-CD3ζ endodomain. aEGFR sdAb and aMino sdAb Fab spacer fused to a CD28TM and CD28 endodomain.
SFGmR.RQR8-2A-HAtag-aEGFRVHH_9G8-IgK-2A-aMinoVHH_pan2c1-CH1-CD28TM-CD28-2A-V5tag-GWARA-CD8STK_mono-CD28-41BBζ	V5-tagged GWARA fused to a CD8STK, a CD28TM, CD28-41BB-CD3ζ endodomain. aEGFR sdAb and aMino sdAb Fab spacer fused to a CD28TM and CD28 endodomain.
SFGmR.RQR8-2A-HAtag-aEGFRVHH_9G8-IgK-2A-aMinoVHH_pan2c1-CH1-CD28TM-CD28-41BB-2A-V5tag-GWARA-CD8STK_mono-CD28-41BBζ	GWARA fused to CD8STK, CD28TM, CD28-41BB-CD3ζ. Expressed with aEGFR sdAb and aMino sdAb Fab spacer fused to a CD28TM and CD28-41BB endodomain.
SFGmR.HA8-2A-fIL12	HA tag transduction marker. Flexi-IL-12 (p35-linker-p40 subunits)
SFGmR.HA8-2A-GWARA_fIL12	GWARA tagged flexi-IL-12 (p35-linker-p40 subunits)

SFGmR.HA8-2A-GWARA_fIl12-F2A-aMinosdAb	GWARA tagged flexi-IL-12 (p35-linker-p40 subunits). Expressed with anti-minocycline sdAb
SFGmR.HA8-2A-PWAYS_fIl12-F2A-aMinosdAb	PWAYS tagged flexi-IL-12 (p35-linker-p40 subunits). Expressed with anti-minocycline sdAb
SFGmR.HA8-2A-GWARA_fIl12-F2A-aMinosdAbKDEL	GWARA tagged flexi-IL-12 (p35-linker-p40 subunits). Expressed with anti-minocycline sdAb fused to KDEL
SFGmR.HA8-2A-PWAYS_fIl12-F2A-aMinosdAbKDEL	PWAYS tagged flexi-IL-12 (p35-linker-p40 subunits). Expressed with anti-minocycline sdAb fused to KDEL
AbVec.ACPGWARAFC_G4S_ ACPGWARAFC_G4S_ ACPGWARAFC_peptide-MuIgG2a	3xGWARA separated by serine-glycine(x4)-serine fused to a murineIgG2A-CH2_IgG2A-CH3
AbVec.ACPGWARAFC_ RL_ACPGWARAFC_RL_ ACPGWARAFC_peptide-MuIgG2a	3xGWARA separated by rigid linker fused to a murineIgG2A-CH2_IgG2A-CH3

2.1.7 Illustrations

Illustrations were created with BioRender.com.

2.2 METHODS

2.2.1 Molecular biology

2.2.1.1 Polymerase Chain Reaction

All primers were generated by Integrated DNA Technologies, Inc (IDT). Stock primers were stored at -20°C at a concentration of 100 μM in TE buffer and were diluted to a concentration of 10 μM prior to PCR set up. Template DNA plasmid was stored in a -20°C freezer at a concentration of 1000 ng/ml. PCR was carried out using the Q5® High-Fidelity DNA Polymerase kit according to manufacturer's protocol.

Assembly of PCR reaction was carried out on ice. Volume and corresponding concentration of each PCR component is indicated on Table 2.11. PCR reactions were placed in a thermocycler with appropriate thermocycling conditions indicated on Table 2.12.

Table 2.11. PCR master mix

Component	Volume used	Final Concentration
5X Q5 Reaction Buffer	10 ul	1X
Nuclease-free water	Up to 50 μl	
10 mM dNTPs	1 μl	200 μM
10 μM Forward Primer	2.5 μl	0.5 μM
10 μM Reverse Primer	2.5 μl	0.5 μM
Template DNA		<1 μg
Q5 High-Fidelity DNA Polymerase	0.5 μl	0.02 U/μl
5X Q5 High GC Enhancer	10 μl	1X

Table 2.12. Thermocycling Conditions for PCR reaction using Q5® High-Fidelity DNA Polymerase

Step	Temperature (°C)	Time
Initial Denaturation	98	30 sec
25-35 Cycles	98 50-72 72	5-10 sec 10-30 sec
Final Extension	72	20-30 sec/kb
Hold	4	

2.2.1.2 PCR fragment and DNA plasmid vector digestion using restriction endonucleases

Restriction digest of PCR products and DNA plasmid vector was performed in accordance with manufacturer's instructions (NEB) to create DNA fragments with respective exposed nucleotide bases for DNA ligation. For PCR fragments, samples collected from gel extraction were digested. For digestion of DNA plasmid vector or isolation of DNA fragments from the plasmid vector, 5ng of vector DNA was used in a total reaction volume of 40 µl. Based on the required restriction endonuclease, the appropriate buffer was selected in accordance with manufacturer's instructions. If buffers were incompatible for a double restriction digest, DNA was digested separately and purified using the Qiagen QIAquick clean-up kit prior to second digest. Table 2.13 shows restriction endonuclease DNA digestion reaction components and volumes.

Table 2.13. Restriction endonuclease master mix

Component	Volume
Vector DNA (1 µg/ml)/PCR product	5 µl/34 µl
H2O (nuclease free)	To 40 µl
Restriction endonuclease 1	1 µl
Restriction endonuclease 2	1 µl
Buffer	4 µl

2.2.1.3 DNA Dephosphorylation

Dephosphorylation of the 5´-ends of restriction digested DNA was carried out using Antarctic Phosphatase (NEB). 20µL reaction mix was prepared as shown on Table 2.14. Reaction mix was then incubated at 37°C for 30 minutes. Reaction was stopped by incubation at 80°C for 2 minutes.

Table 2.14. DNA Dephosphorylation using Antarctic Phosphatase

Component	Volume
DNA	1 pMol
Antarctic Phosphatase	2 µl
10X Buffer	5 units
Nuclease free water	To 20 µl

2.2.1.4 Gel electrophoresis

DNA fragments from the PCR or restriction digests for molecular cloning were visualised using agarose gel electrophoresis. Based on expected size of PCR products or DNA digest, 0.8-2% agarose gel was prepared by dissolving agarose powder in 1x TBE buffer using a microwave. 5 µl of SYBR Safe dye was added per 100 ml of 0.8-2% agarose gel to allow UV visualisation of the DNA product. Loading dye was added to a final concentration of 1x to DNA samples and loaded in the appropriate wells. Agarose gel was run in 1xTBE at 120V for 20-50 minutes until appropriate separation was determined using the loading dye marker. Hyperladder I and hyperladder II was used as a standard to determine DNA fragment size. DNA was visualised using the Azure c600 Gel Imaging System.

2.2.1.5 Gel extraction and DNA purification

Gel extraction and purification was carried out using the QIAquick Gel Extraction Kit. Using a scalpel, the desired DNA band was excised from the agarose gel, weighed, and transferred to a 2 ml Eppendorf tube. 3 gel volumes of Qiagen Buffer QG Solubilization buffer was added to the gel and dissolved by incubation at 50°C for 10 minutes. 1 gel volume of isopropanol was then added the tube and transferred to a QIAquick spin column placed in a 2 ml collection tube. QIAquick spin column was centrifuged at 17,900 xg for 60

seconds and the flow through was discarded. The column was washed using 750 µl of Buffer PE, followed by centrifugation at 17,900 xg for 60 seconds. Flow through was discarded and centrifuged again to remove residual Buffer PE. DNA was eluded by adding 35-50 µl of nuclease free water to the spin column and incubated for 1 minute at room temperature. The spin column was placed in a new 1.5 ml Eppendorf tube and centrifuged at 17,900 xg for 60 seconds to collect the DNA elution.

2.2.1.6 PCR purification

PCR purification was carried out using the QIAquick PCR Purification Kit in accordance with manufacturer's instructions. Binding Buffer PB (5X) was added to the PCR sample, transferred to a QIAquick spin column, and centrifuged at 17,900 xg for 1 minute. The flow through was discarded and washed using 750µL of PE buffer and centrifuged at 17,900 xg for 1 minute. Residual PE buffer was removed by centrifugation at 17,900 xg for 1 minute. DNA was then eluted by adding 35 µl nuclease free water to the QIAquick spin column and centrifuged at 17,900 xg for 1 minute.

2.2.1.7 DNA ligation

Ligation of digested vector DNA and PCR products were carried out using T4 Ligase in accordance with manufacturer's instructions. A vector to insert molar ratio of 1:3 was used. Ligation mix was incubated at 16°C for 1 hour. NEBioCalculator was used to calculate molar ratios.

Table 2.15. T4 DNA ligase reaction mix components

Component	Volume
T4 DNA Ligase	1 µl
H2O (nuclease free)	to 20 µl
Vector DNA	X
Insert DNA	X
Buffer (10X)	2 µl

2.2.1.8 Bacterial cultures

Bacteria cultures were grown in Luria-Bertani (LB) media supplemented with carbenicillin (100µg/ml) and cultured in a shaking incubator at 37°C with 220rpm agitation. LB agar plates supplemented with carbenicillin (100 µg/ml) were incubated at 37°C.

2.2.1.9 Bacterial transformation

50 µl NEB5alpha high efficiency *E. coli* cells (NEB) were thawed on ice prior to being transferred to 200 µl tubes. 2 µl of the ligation mixture was slowly added to NEB5alpha high efficiency *E. coli* cells and incubated on ice for 40 minutes. The *E. coli* cell and ligation mixture was heat shocked at 42°C for 35 seconds and placed on ice for an additional 5 minutes. A recovery step was carried by adding 200 µl of SOC media to the ligation mixture and incubated at 37°C with 220 rpm agitation for 45 minutes. Following the recovery step, the bacteria mixture was streaked on LB-agar plates supplemented with carbenicillin (100 µg/ml) and incubated overnight at 37°C.

2.2.1.10 Plasmids

In this work, the SFGmR plasmid vector was used for all γ-retroviral constructs. SFGmR vector is based on Moloney Murine Leukemia Virus (MoMLV), the transgene is positioned at the start codon site of a deleted envelope gene. Two or more transgenes were expressed as a single polypeptide chain and separated by the Thosea asigna virus 2A (T2A) self-cleavage peptide, resulting in equimolar expression levels of each transgene. Constructs indicated as SFGmR in Section 2.1.1 bear a scaffold attachment region which results in enhanced transgene expression. The AbVec plasmid vector was used for the generation of antibody fragments and pHEN1 plasmid vector was used as the phagemid vector for phage display.[190]

2.2.1.11 Plasmid DNA amplification and purification

For small scale DNA purification up to 20 µg of DNA, the QIAprep Spin Miniprep Kit was used in accordance with manufacturer's instructions. Briefly, 3-5 ml of bacterial culture (Section 2.2.1.8) was centrifuged at 17,900 xg for 5 minutes. Supernatant was discarded and bacterial pallet was resuspended in 150 µl of resuspension buffer P1. Bacterial cells were lysed using 250 µl of

lysis buffer P2, followed by incubation at room temperature for 2 minutes. The reaction was neutralised using 350 µl of neutralisation buffer N3. Samples were then centrifuged at 17,900 xg for 10 minutes to clear the lysate. Supernatant was then transferred to a QIAprep spin column and centrifuged at 17,900 xg for 1 minute. The spin column was washed using 250 µl of wash buffer PE. Residual wash buffer was removed by centrifugation, followed by elution using 35-50 µl of nuclease-free water or TE buffer.

For large scale DNA purification up to 400 µg of DNA, the NucleoBond™ Xtra MidiPrep kit was in accordance with manufacturer's instructions. Briefly, 50-100 ml of bacterial culture (Section 2.2.1.8) was centrifuged at 4,200 xg for 30 minutes at 4°C. Supernatant was discarded and bacterial pellet was resuspended in 8 ml of buffer RES supplemented with RNase A. Bacterial cells were lysed using 8 ml of buffer LYS followed by incubation at room temperature for 5 minutes. The reaction was neutralised using 12 ml of buffer NEU, followed by inverting 3 times. Samples were then loaded onto NucleoBond® Xtra Column Filter which had previously been equilibrated using 12 ml of buffer EQU. Once the lysate had passed through the column, the NucleoBond® Xtra Column Filter was washed using 5 ml of buffer EQU before being discarded. The column was then washed using 12 ml of buffer WASH. DNA was then eluted into a new falcon tube using 5 ml of buffer ELU. 3.5 ml of isopropanol was added and vortexed to precipitate the DNA. A centrifugation step at 4.5-15,000 xg for 30 minutes at 4°C was carried out to pellet the DNA. The DNA pellet was washed using 2 ml of 70% ethanol and centrifuged at 4.5-15,000 xg for 5 minutes. The 70% ethanol was discarded, and pellet was allowed to dry. DNA was reconstituted in appropriate volume of nuclease-free buffer or TE buffer.

2.2.1.12 DNA spectrophotometry

The Thermo Scientific™ NanoDrop™ 8000 Spectrophotometer was used to measure DNA concentration.

2.2.1.13 Golden Gate Assembly

Golden gate DNA assembly was designed using SnapGene Software.[191,192] Vector backbone and PCR products were digested using appropriate golden

gate restriction endonucleases (Esp3i, BsmBI, BbsI or BsaI), followed by DNA dephophorylation, DNA ligation and Bacterial transformation.

2.2.2 Phage display

2.2.2.1 Phage display library construction from immunised Alpacas

The engineered minocycline molecules used in the immunisation, panning and screening were carried out engineering a free sulfhydryl group on minocycline which was carried out by Dr. Eilitz (ChiroBlock), followed by conjugation of KLH and BSA to the engineered minocycline by GenScript.

The immunisation service provider, GenScript carried out the immunisation of Alpacas using minocycline conjugated to the immunogenic protein, keyhole limpet haemocyanin (KLH). Following six sub-cutaneous immunisations, sera was extracted and tested to confirm sera conversion of the animal. Lymphocytes were collected and preserved in RNAlater and shipped on dry ice to be used as the starting material for the construction of a phage display library.

Complementary DNA (cDNA) synthesis was carried out using primers designed to amplify, via polymerase chain reaction (PCR), the antibody heavy chain-coding region (VHH) from lymphocytes extending from the variable (V) region through to the constant heavy 2 domain (CH2) region. The camelid heavy chain antibody (HCAb) was isolated from classical antibody DNA by agarose gel electrophoresis and further amplified before cloning into the phage display vector pHEN1 by using unique primers containing SfiI and NotI restriction sites at the 5' and 3'ends, respectively (Table 2.16).

Table 2.16. Primer sequences utilised for the amplification of camelid heavy chain antibody (HCAb).

Primer name	Sequence
CALL001 primer	GTCCTGGCTGCTCTTCTACAAGG (leader sequence)
CALL002 primer	GGTACGTGCTGTTGAACTGTTCC (CH2 exon)
VHH Back primer	GATGTGCAGCTGCAGGAGTCTGGRGGAGG
PMCF primer	CTAGTGCGGCCGCTGAGGAGACGGTGACCTGGGT

The *E. coli* strain, ER2738, which has a tetracycline resistance gene linked to the F+ gene was transformed via electroporation by incubating ER2738 electrocompetent cells (Lucigen) with ligated DNA in chilled electroporation cuvettes (0.1 cm gap) prior to electroporation using the Bio-rad MicroPulser (EC1 cycle, time constant: 4.5-5.5 ms). 2 ml of warm Expression Recovery Medium (Lucigen) was used to wash out the cells from the cuvette and incubated in at 37°C, 250 rpm for 1 hour. After the incubation, cells were mixed thoroughly via pipetting to generate a homogeneous suspension. 100 µl of the transformed cells were used to make serial dilutions - $1:10^3$, $1:10^4$, $1:10^5$, and $1:10^6$ using sterile liquid $2 \times$ YT medium (16 g/L Tryptone, 10 g/l yeast extract, 5 g/L NaCl, pH 7.0). 100 µl were then plated separately onto 100mm agar plates (2×YT supplemented with 2 % Glucose, 100 µg/ml ampicillin and 0.02 g/ml agar) and incubated overnight at 37°C. The remainder of the transformed cells were divided and spread onto 15 – 20 large petri dishes (size 150 mm × 15 mm) each containing 50 ml of $2 \times$ YT supplemented with 2% Glucose, 100 µg/ml ampicillin and 0.02 g/ml agar. The number of colonies from the appropriate plated serial dilutions were counted to estimate the total number of clones in the library. The lawn of *E. coli* transformants on the large plates were scraped and collected with sterile 2×TY medium. Cells were centrifuged at 5,000 rpm for 20 minutes and the supernatant was removed. Cells were re-suspend using 10 ml filter-sterilised 2×YT media containing 50% Glycerol. Cell suspension was diluted to bring the OD600nm reading of 100–300 using sterile 2×TY media containing 50% Glycerol and frozen as 1 ml aliquots in individual cryovials at -80°C.

2.2.2.2 Phage Display Amplification and Precipitation

Amplification and precipitation of the phage library from bacterial glycerol stock must take place prior to downstream panning and selection. The pHEN1 phage vector is not sufficient for phage expression in *E. coli* cells strain ER2738 and therefore requires further 'superinfection' with a Helper Phage (M13K07) which provide the genetic material necessary for phage replication and release from cells.

Phage amplification was carried out by inoculating 50 µl of glycerol stock in 50 ml 2xTY media supplemented with 2% glucose and ampicillin (100 µg/mL) in

a 250 ml baffled flask. Helper Phage, M13K07 (N03152), was added at a concentration of 1 μl/ml once the inoculate reached OD600nm = 0.5. Bacterial culture was then incubated for 40 minutes without agitation prior to centrifugation at 3000 xg for 10 minutes. Cells were resuspended in 2xTY media supplemented with ampicillin only and incubated overnight at 30°C and agitated at 250 rpm.

For phage precipitation, cells were centrifuged at 6000xg, and supernatant was aspirated. Supernatant was resuspended in 5X 20% PEG-6000 and 2.5M NaCl and incubated on ice for 2 hours. Precipitated phage virions were pelleted by centrifugation at 15000xg for 20 minutes at 4°C and resuspended in 1 ml of PBS. Phage library was then proceeded to panning and selection.

2.2.2.3 Phage Display Library Panning and Selection

BSA conjugation to minocycline carried out by GenScript using minocycline which has been engineered with a free sulfhydryl group by Dr. Eilitz (ChiroBlock). Panning of the precipitated phage display library was carried out against BSA-conjugated minocycline. Specifically, BSA-conjugated minocycline was biotinylated and coupled to streptavidin-coated beads at a concentration of 1 μg/ml. Coated beads were washed using PBS 0.1% Tween and blocked for 1 hour using the blocking buffer made from 2% milk in PBS. Beads were washed using PBS 0.1% Tween twice before washing with PBS only. A 100-fold representation of the phage library from the phage stock was diluted in blocking buffer and added to minocycline-BSA coated beads and incubated at room temperature for 2 hours with agitation. Beads were washed 15 times with PBS 0.1% Tween, followed by 2 washes with PBS. Minocycline-BSA bound phage were eluted using pre-warmed (37°C) Trypsin-EDTA and rotated for 10 minutes at 37°C. ER2738 cells cultured to an OD600nm of 0.5 were infected and incubated at 37°C for 40 minutes. Cells were then plated on 21x21 mm 2xTY agar plates supplemented with ampicillin (100 μg/ml) and 2% glucose and incubated overnight at 30°C. Using 5 ml of 2xTY media, bacteria was gently scrapped off from the plate and proceeded to further amplification (following the amplification and precipitation procedure stated previously) by adding bacteria to 2xTY media (OD600nm of 0.1).

Remaining bacteria was stored as glycerol stocks in 50% (v/v) sterile glycerol in PBS at -80°C. This process was repeated for 2 rounds of selection, to which the phage library was screened by ELISA, first analysing enrichment of the whole library followed by single colony selection, screening and sequencing.

Single colonies from elution plates were picked into 500 µl of 2xTY media (+ampicillin/+2% glucose) in each well of a 96 deep-well culture plate and incubated overnight at 37°C and with agitation at 270 rpm. Overnight cultures were banked in 50% (v/v) sterile glycerol in PBS and stored at -80C. Stocks were diluted 1 in 100 in 500 µl of 2xTY media (+ampicillin/+2% glucose) and incubated at 37°C with agitation at 270 rpm until OD600nm of 0.5 was reached. For phage expression, 0.5 µl of M13KO7 helper phage were added per well and incubated at 37°C in 2TY media (+ampicillin) for 40 minutes. Supernatant was removed by centrifugation at 3000 xg, and pelleted cells re-suspended in 2xTY media (+ampicillin). Cultures were incubated overnight at 37°C and agitated at 270 rpm. Whole-phage anti-M13 ELISA screen was carried out. To generate soluble myc-tagged antibody, cells were resuspended in 500 µl of 2TY media supplemented with ampicillin and IPTG (200 µM) and incubated overnight at 30°C and 270 rpm. Secreted antibody in the supernatant and periplasmic bacterial extracts were collected for ELISA screening.

For ELISA screening, Nunc 96-well plates were coated with minocycline-BSA, minocycline-KLH or BSA only at 1 µg/ml. Plates were blocked with 2% milk in PBS for 1 hour. Whole-Phage, supernatant from soluble dAb and periplasmic extracted dAb was incubated in appropriate wells and incubated for 2 hours at room temperature. Anti-M13-HRP (0.5 µg/ml) was added for the whole phage ELISA and anti-Myc (0.5 µg/ml) was added for soluble protein ELISA and incubated for 1 hour at room temperature. TMB was then added for ELISA development and stopped using 2M NaOH. Plates were read 450nm using Varioskan Lux plate reader. Plates were washed 3 times with PBS 0.05% Tween between incubations. 50 µl volumes were used in all incubation with 200 µl volume for blocking.

2.2.2.4 Sequencing of positive clones

Analysis of positive ELISA binding data was used to select monoclonal phage for sequencing. PCR amplification of monoclonal phage DNA was performed using a colony PCR reaction. Using the 2x Master Mix OneTaq (M0486L) protocol (Table 2.17), PCR reactions containing 1 µl of bacteria from the phage containing supernatant as the template DNA were set up. Amplified DNA was sequenced using GATC sequencing.

Table 2.17. Colony PCR thermocycling conditions.

Step	Temperature	Time
Initial Denaturation	95°C	5 minutes
30 Cycles	95°C	30 seconds
	48°C	30 seconds
	68°C	45 seconds
Final Extension	68°C	5 minutes
Hold	4°C	

2.2.2.5 Panning of C7C Phage Display Peptide Library

To generate cysteine constrained 7mer (C7C) peptide sequences specific to an anti-minocycline single domain antibody, the ready to use Ph.D.™-C7C Phage Display Peptide Library Kit (E8120S) was used. This kit is composed of a combinatorial library consisting of randomised display peptides with a disulphide constrained loop (AC-XXXXXXX-CGGGS) fused to the pIII coat protein of the M13 phagemid. The library consists of approximately 1×10^9 unique sequences. Phagemid amplification, panning and selection was carried out as previously described with a few methical exceptions. To summarise, 3 rounds of panning and enrichment were carried out against biotinylated anti-minocycline single domain antibody clone 1 fused to streptavidin beads. Elution of bound phagemid was carried out using 1 µM minocycline.

2.2.3 Tissue Culture

2.2.3.1 Propagation of cell lines

2.2.3.1.1 Propagation of adherent cells lines

Adherent cell lines, HEK293T and SKOV-3 cells, were cultured in Iscove's Modified Dulbecco's Media (IMDM, Gibco) supplemented with 10% heat-inactivated foetal bovine serum (FBS, Biosera) and 1% L-Glutamine (GlutaMAX, Gibco) using T175 cm^2 tissue culture treated flasks and maintained at 37°C and 5% CO_2. Upon 90% observable confluency, cells were passaged by washing with 1x PBS and detaching from the flask at room temperature using 5 ml trypsin/EDTA. Detached cells were reseeded in fresh medium and cultured as above.

2.2.3.1.2 Propagation of non-adherent cells lines

ExpiCHO cell were maintained in ExpiCHO medium (Gibco) using Corning® Erlenmeyer shake flasks and maintained in a Kuhner shaker at 37°C and 8% CO_2, at 225 rpm. Cellular passage was carried out through resuspension of cells using fresh media to maintain culture density below 1x10^6/ml.

All other non-adherent cell lines were maintained in RPMI 1640 medium (Gibco) supplemented with 10% FBS (Biosera) and 1% L-Glutamine (GlutaMAX, Gibco) using T75 cm^2 tissue culture treated flasks and maintained at 37°C and 5% CO_2. Cellular passage carried out through resuspension of cells using fresh media to maintain culture density below 1x10^6/ml.

2.2.3.2 Cryopreservation of cell lines

Cell lines were cryopreserved by centrifuging cells at 400xg for 5 minutes and resuspending in chilled freezing media (FBS +10% DSMO) at 5x10^6 cells/ml. 5x10^6 cells were then aliquoted into cryovials and stored in CoolCell™ LX Cell Freezing Container (Corning®) at -80°C freezer for 24 hours. Cryovials were then placed in the liquid nitrogen.

2.2.3.3 Cryopreserved cell recovery

Cryopreserved cells were thawed using a 37°C water bath. As soon as cells were thawed, they were immediately resuspended in 50 ml of pre-warmed complete RPMI or IMDM media and centrifuged at 400xg for 5 minutes. The supernatant containing DMSO was removed, and cells were resuspended in

appropriate complete media. Cells were transferred to T75 tissue culture flask and incubated at 37°C and 5% CO_2.

2.2.4 Cell transfection

2.2.4.1 Transient 293T transfection

HEK293T cells were seeded at 3×10^6 total cells per plate in 10 cm plates, 6-well plates (minocycline mediated peptide-Fc dissociation cell assay) or 96-well plates (KDEL-IL-12 retention assay) to achieve confluency of 50-60% for next day transfection. Genejuice (EMD Millipore) was used as the transfection reagent. The quantities of DNA and volumes of IMDM media and GeneJuice used for transfection for each plate type is shown in Table 2.18.

Table 2.18. Well volume and mass requirements for the transient transfection of HEK293T cells in various plate formats.

Plate	Media (µl)	Genejuice (µl)	DNA (µg)
10cm	470	30	12.5
6-well	5	78	2
96-well	4.9	0.3	0.13

2.2.5 Transfection of ExpiCHO-S™ cells

Cells were split to a density of 3×10^6 viable cells/ml one day prior to transfection. 25 µg of plasmid DNA was diluted in 1 ml of OptiPRO™ medium, incubated with ExpiFectamine™ CHO reagent diluted in 1ml of OptoPRO™ medium for 5 minutes. The mixture was added to 25ml of cells at a final density of 6×10^6 viable cells/ml. 22 hours post transfection, 150 µl of ExpiFectamine™ CHO Enhancer and 6 ml ExpiCHO™ Feed were added to the transfected the cells. Supernatant was harvested 5 days post transfection.

2.2.5.1 Transfection of HEK293T cells for γ-retroviral supernatant production

2.5×10^6 HEK293T cells were seeded in 10 cm plates and allowed to adhere overnight at 37°C and 5% CO_2 to achieve 50%-60% confluency the following day. 30µl of GeneJuice and 470 µl of complete IMDM was incubated for 5 minutes at room temperature. 4.7µg of test DNA, 3.1 µg RD114 envelope and

4.7 μg gag/pol vector plasmids were added to the transfection mix and incubated for 15 minutes at room temperature. Transfection mix was then added dropwise to cells and incubated at 37°C and 5% CO_2. Supernatant was then harvested at 48 and 72 hours, pooled and stored frozen at -80°C until use.

2.2.6 Primary T cell work

2.2.6.1 Blood processing and Peripheral Blood Mononuclear Cell (PBMCs) isolation

Peripheral blood mononuclear cells (PBMCs) as Leukocytes cones were obtained from the National Health Service and Transplant (NHSBT; Colindale, UK). PBMCs were isolated using a Ficoll density gradient protocol: The contents of the leukocytes cone content were emptied into a 50 ml falcon tube, followed by diluting the blood with equal volumes of Phosphate Buffer Saline (PBS). 15 ml of Ficoll Paque Plus was pipetted into SepMate-50 tubes ensuring minimal bubbles. 25 ml of the blood-FBS mix was layered over the Ficoll Paque Plus media using the wall of the 50ml falcon to ensure minimal mixing taking place. A density gradient centrifugation step was carried out at 1200 xg for 20 minutes at room temperature with the acceleration and brakes set to 6. The PBMC layer was carefully collected using a Pasteur pipette and washed twice using RPMI media at 400 xg for 5 minutes at room temperature. Upon resuspension of cells in complete RPMI media, cells were counted using an automated cell counter (Automated Cell Analyzer NucleoCounter® NC-250™). Isolated PBMCs were cryopreserved by resuspending cells to a concentration of $50x10^6$ cells/ml in freezing media (10% DMS)/90% FCS) and aliquoted into 1ml cryovials (Corning). Cryovials were placed in a CoolCell™ LX Cell Freezing Container (Corning®), which provides a 1°C/min cooling rate and transferred to a -80C freezer. The following day, cryovials were transferred to liquid nitrogen until required.

2.2.6.2 Transduction of PBMCs using γRV Supernatant

PBMCs were resuspended to $1x10^6$/ml and stimulated using complete RPMI/10% FCS/1% L-Glutamine supplemented with 0.5 μg/mL of OKT3 (anti-CD3) and anti-CD28 antibodies in T175 TC-treated flasks for 24 hours. IL2

was then added to a concentration of 100 U/ml for a further 24 hours prior to retroviral transduction.

Non-Tissue culture-treated six-well plates were coated with Retronectin (Retronectin master mix was prepared by adding 8 µl of retronectin to every 1ml PBS) in accordance with manufacturer's instructions (Takara Bio) and incubated at 4°C for 24 hours prior to retroviral transduction or the T cells.

Viral supernatant was thawed using a water bath set to 37°C. Retronectin was removed from pre-coated plates. 3 ml of viral supernatant was plated prior to the addition of 1ml of activated T cells at a concentration of $1x10^6$ cells/ml, IL-2 was then added to a final concentration of 100 U/mL, and plates were centrifuged at 1000 xg for 40 minutes at room temperature. Plates were then incubated at 37°C and 5% CO_2 for 2-3 days.

2.2.6.3 Transduction of cell lines using γRV Supernatant

Non-Tissue culture-treated six-well plates were coated with Retronectin in accordance with manufacturer's instructions (Takara Bio) and incubated at 4°C for 24 hours prior to T cell transduction. 3ml of viral supernatant was plated prior to the addition of 1ml of chosen cell line at $1x10^6$ cells/ml. Plates were centrifuged at 1000 xg for 40 minutes at room temperature and incubated at 37°C and 5% CO_2 for 2-3 days.

2.2.7 Flow Cytometry

All Flow cytometry was carried out using the MACSQuant® Analyzer 10 or MACSQuant® X (Miltenyi Biotec). All flow cytometry data was analysed using FlowJo v.7.6.2 software (Tree Star Inc, Ashland, OR).

2.2.7.1 General flow cytometry analysis

Cells used for staining were counted, washed once using PBS and centrifuged at 400xg for 5 minutes at room temperature. $3x10^5$ cells were resuspended in 50µl of PBS containing the recommended concentration of antibodies and incubated at room temperature for 30 minutes. If secondary antibody was required, cells were washed with PBS and resuspended in 50 µl of PBS with the recommended concentration of secondary antibody. Cells were then washed with PBS and stained with appropriate viability dye such as SYTOX Blue or 7-AAD prior to Flow cytometric analysis.

2.2.7.2 T cells transduction efficiency analysis

$3\text{-}6\times10^5$ cells were transferred to each respective well of a U-bottom 96 well plate, centrifuged at 400 xg for 5 minutes at room temperature and the supernatant discarded. Following centrifugation cells were resuspended in a solution of antibodies diluted to the desired concentration in a final volume of 50 µl PBS and incubated for 15 minutes in the dark at room temperature. Cells were then washed with PBS and stained with appropriate viability dye prior to Flow cytometric analysis. 50 µl/well volume of antibody was used for the incubation step. Typically, transduction efficiency was determined by staining for the marker gene such as RQR8 or HA.

2.2.8 In vitro Functional Assays

2.2.8.1 Extracellular minocycline-CAR scaffold functionality assay

To test the minocycline-dependent control of CAR inactivation as a part of an extracellular scaffold. Nunc 96-Well Microplates (Thermo Scientific) were coated with Fc-tagged recombinant human EGFR protein (Sino biological, 10001-H02H) at 10 µg/ml for 2 hours at 37°C. Plates were then washed with PBS and 1×10^5 CAR T cells supplemented with minocycline at concentration of 0 µM, 1 µM and 10 µM were plated per well. 48 hours post culture, plates were centrifuged at 400 xg for 5 mins and supernatant collected for IFN-γ cytokine analysis by ELISA.

2.2.8.2 Tumour cell co-culture and flow cytometry-based cytotoxicity assay

To measure cytotoxicity, CAR T cells were co-cultured with target cells (SupT1-NT, SupT1-EGFR+, Nalm-6-EGFR+, SKOV3-mKate) cells at transduced effector cell to target ratios of 1:2 (25,000:50,000 cells), 1:4 (12,500:50,000 cells) and 1:8 (6,250:50,000 cells) in TC-treated flat bottom 96-well plates. In total, 200 µl of sample was present in each well. Where appropriate, minocycline was supplemented as a part of the culture conditions. Co-cultures were incubated for 24 or 72 hours at 37°C and 5% CO_2. After incubation, plates were centrifuged at 400 xg for 5 minutes, and the supernatant containing secreted cytokines was collected and stored at -20°C. Cells were stained with anti-hCD34-APC and anti-CD3-PeCy7 to differentiate effector T cells and target cells. Cells were incubated in the dark for 15 minutes

at room temperature then washed with 300µL of PBS and each sample was resuspended in 50 µl of PBS supplemented with SYTOX-blue viability dye in order to discriminate live from dead cells. Cytotoxicity readouts were acquired using the MACSQuant® Analyzer 10 flow cytometer (Miltenyi Biotec).

2.2.8.3 Reversibility and tuneability experiments using IncuCyte live cell imaging

For both reversibility and tuneablity experiments, EGFR+ SKOV3-mKate were seeded at 1.0×10^4 cells per well in a TC-treated flat bottom 96-well plate as target cells. For reversibility experiments, MinoCAR ON-OFF kinetics were tested by pre-activating CAR T cells by incubating cells for 2 hours on plates pre-coated with recombinant EGFR (10 µg/ml). CAR T cells were washed using 15 ml of PBS prior to co-culture. MinoCAR OFF-ON kinetics were tested by first inhibiting CAR T cells by incubating cells in RPMI supplemented with 10% FBS, 1% GlutaMAX and 10mM minocycline. Cells were then washed using 15 ml of PBS prior to co-culture. Untreated CAR T cells were used as a control and were directly preceded to co-culturing set. In each respective well, 0.5×10^4 transduced CAR T cells were co-cultured with EGFR+SKOV3-mKate target cells with and without minocycline (10 µM). The Incucyte® ZOOM Live-Cell Analysis System was used to carry out image capture at a rate of one image every 1hr for 150 hours. Tuneablity experiments were carried out co-culturing transduced PBMCs expressing the MinoCAR and EGFR-CAR (positive control) with target cells at an effector to target ratio of 1:2 and in the absence and presence of minocycline (0.625 µM, 1.25 µM, 2.5 µM, 5 µM, 10 µM). Image capture rate of each condition was set at 1 image per hour for 72 hours.

2.2.8.4 IFN-γ, IL-2 and IL-12 ELISA

IFN-γ, IL-2 and IL-12 secretion was measured by collecting supernatant from the respective cell-based assay and frozen at -20°C prior to analysis by ELISA. IFN-γ, IL-2 and IL-12 ELISAs were carried out using the Human IFN-γ ELISA MAX Deluxe kit, Human IL-2 ELISA MAX Deluxe kit and Human IL-12 (p70) ELISA MAX Deluxe kit in accordance with the manufacturer's instructions. Briefly, a Nunc 96-Well ELISA plate was incubated with capture antibody overnight at 4°C. Plate(s) were then washed and blocked using blocking

buffer. Plates were washed and test samples and standards were added to respective well and incubated for 2 hours at room temperature with 400 rotations per minute. Plates were washed and detection antibody was added, followed by incubation for 1 hour. Plates were washed again and incubated with avidin-horseradish peroxidase (HRP) for 30 minutes. Plates were washed a final time and incubated with substrate until the reaction was stopped through the addition of hydrogen peroxide stop solution. A Multiskan™ FC Microplate Photometer was used to measure the absorption at 450 nm. Cytokine concentration was determined by extrapolating from the standard curve.

2.2.8.5 Secretion of ER retained IL12 assay

HEK293T cells were seeded at 3×10^6 in 96-well plates to achieve confluency of 50-60% for next day transfection. A transfection master mix was made by adding 30 µl of GeneJuice transfection reagent to 470 µl plain IMDM and incubating for 5 minutes. For each well, 0.13 µg of plasmid DNA was then added to 5.2 µl of the IMDM-Genejuice master mix and incubated for 15 minutes. Transfection mix containing the GeneJuice-DNA complex was then added to the cells. All incubations were carried out at room temperature.

48 hours post transfection, sacrificial wells containing transfected cells were tested for transfection efficiency by staining cells using FITC anti-HA antibody (Biolegend, 901507). Upon confirmation of transfection, culture media was removed from cells and fresh media supplemented with minocycline at varying concentrations was added. 2 hours and 4 hours post minocycline addition supernatants were harvested and IL-12 ELISA was carried out following manufacturer's instructions (BioLegend, 431704).

2.2.8.6 General ELISA

High absorbent Nunc MaxiSorp 96-well plate clear flat bottom were coated with target antigen. Proteins were coated onto wells at 1 µg/ml in PBS, using 50 µl protein solution/well and incubated overnight at 4°C or 2h at RT on a rocker. Plates were washed 3 times with PBS 0.05% Tween20 using 200 µl per well. Wells were blocked using 200 µl of PBS supplemented with 2% BSA for 1 hour at room temperature on a rocker. Plates were washed with 200 µl

of PBS and incubated with primary antibody at the desired concentration diluted in PBS 0.5% BSA, using 50 µl/well (see note 5) for 1 hour at room temperature. Plates were then washed 3 times in PBS 0.05% Tween20 using 200 µl/well and incubated with the appropriate secondary antibody conjugated with HRP, diluted in PBS 0.5% BSA, using 50 µl/well. Plates were washed 3 times in PBS 0.05% Tween20 using 200 µl/well and developed by adding 45 µl of TMB substrate solution and incubated until signal appeared evident but before background started to raise. The chromogenic reaction was stopped with 45 µl of 2M H_2SO_4 and absorbance measured on a Varioscan Lux imaging unit selecting absorbance at 450 nm.

2.2.9 Protein work

2.2.9.1 SDS-PAGE

SDS-PAGE (Sodium Dodecyl Sulphate Polyacrylamide Gel Electrophoresis) was used to analyse purified protein samples by molecular weight (kDa) using an electric field applied across a polyacrylamide gel. Denatured proteins complexed with SDS allows a uniform negative charge which migrate in the direction of the positive anode when an electric field is applied. SDS-PAGE was used to confirm presence of correct protein size and determine protein purity.

Samples were prepared by diluting 1-5 µg of protein in 5X Invitrogen NuPAGE LDS loading buffer (non-reducing conditions) or loading buffer supplemented with β-mercaptoethanol (reducing conditions). The loading buffer consists of SDS, glycerol and bromophenol blue dye. SDS provides a homogeneous negative charge to the proteins permitting migration of the sample across the gel based on protein mass rather than the superficial charge of amino acid residues. Glycerol provides a higher sample density for ease of loading. Bromophenol blue provides visualisation of protein migration on the gel. For reducing conditions, β-mercaptoethanol (1 in 10 dilution) was added to reduce the disulphide bonds and resolve multimeric proteins.

Samples were incubated at 95°C for 5 minutes to denature the proteins. Pre-cast mini-protean 4-20% TGX gel and gel tank was prepared in accordance with manufacturer's instructions and tris-glycine SDS buffer was used to fill gel

tank cambers. 8 µl of sample was then loaded to each respective well alongside an appropriate Molecular Weight Marker. As the gel was analysed using UV excitation, the Precision Plus Protein™ All Blue Standards (250-10 kDa) and Precision Plus Protein™ Unstained Standards (1:1 ratio) were used as standards. The gel was then run at 200 V for 30-45 minutes based on protein marker migration before being removed and analysed under UV light at 320 nm using the Azure c600 Gel Imaging System.

2.2.9.2 Purification of proteins using Protein-A affinity chromatography

The ÄKTA pure Chromatography System was used to carry out protein purification. Prior to purification, buffer and system preparation was carried out. 0.5 M NaOH solution was prepared by dissolving 20 g of sodium hydroxide in 1 L of distilled water followed by filtering through a 0.22 µm filter. Protein samples were also filtered using a 0.22 mm filter. 0.5 M NaOH was used to perform a system clean of all lines (A1, A2, B1, B2, S1 and buffer line) to ensure removal of contaminants from the flow path. Designated line positions are indicated on Table 2.9. Pump wash of all lines was carried out using filtered distilled H_2O at a flow rate of 3 ml/min for 10 minutes. Flow rate was reduced to 1 ml/min prior to connecting the HiTrap MabSelect SURE 1 ml column. Pump wash of each line was carried out with respective solution at 3 ml/min. B1 was washed with IgG elution buffer whereas A1, S1 and buffer line with sterile PBS. After 10 minutes, the sample line was placed into the sample tube for purification set up.

Table 2.19. ÄKTA pure line positions.

Line	Component
A1	PBS
A2	NaOH
B1	Elution buffer
B2	dH$_2$O
Sample line S1	Sample
Buffer line	PBS
Sample line S7	NaOH

The mAb Select SURE 1ml with desalting column programme was used with respective line positions indicated in Table 2.19. The following programme set up was used: (i) Column equilibration from inlet A1 with 10 column volumes of PBS at 1 ml/min. (ii) Sample applied at 1 ml/min via sample inlet S1. (iii) Column wash via inlet A1 with 10 column volumes of PBS at 1 ml/min. (iv) Desalting column in-line step. (v) Sample elution via B1 with 3 column volumes of IgG elution buffer at 1 ml/min and fraction volume of 250 µl. (vi) Column washing via A1 using 10 column volumes of PBS at 1 ml/min. Fractions were collected using a 96-deep-well plate. Fractions were analysed using SDS-PAGE to confirm presence of appropriate size protein band and purify of protein sample.

2.2.9.3 Analysis of protein stability using NanoDSF

The Prometheus NT.48 NanoDSF instrument was used to characterise the thermal and chemical unfolding of single domain antibodies under native conditions and in the presence of minocycline. A dye-free protocol was used whereby the intrinsic fluorescence of tryptophan and tyrosine was measured by scanning samples at 330 nm and 350 nm to determine protein unfolding. Protein samples were normalised to 0.2-1 mg/ml and supplemented with minocycline at concentrations of 0.001 µM, 0.01 µM, 0.1 µM, 1 µM, 10 µM, 100 µM and 1000 µM. 15 µl of sample was then transferred to an Eppendorf tube. One end of the capillary tube was then carefully dipped into the sample until the capillary tube was filled via suction. Capillary tubes were then placed into the magnetic cover of the Prometheus NT.48 NanoDSF instrument. A discovery scan was carried out by adjusting the excitation power until the raw fluorescence was close to 10000 counts. Corresponding capillary slots were selected, and the melting scan was carried out by setting the run at 1°C/minute temperature increments from 20°C to 95°C.

2.2.9.4 Size Exclusion Chromatography

The ÄKTA pure Chromatography System was used to carry out size exclusion chromatography analysis. Antibody sample was concentrated using Amicon Ultra-15 10K Centrifugal Filter Devices (Merck). The Superdex 200 10/300 GL

was used as the size exclusion chromatography column. Purified protein sample was concentrated to 2.3 ml and slowly injected into 2ml loop using a 5 ml syringe with blunt needle via the injection valve, ensuring to remove air bubbles from the syringe before injection. The Superdex 200 10/300 GL was equilibrated using 1.5 column volumes of PBS (1.5 ml/min). The sample was applied (0.3 ml/min) using the capillary loop followed by column washing using 0.2 column volumes of PBS (0.3 ml/min). Sample was eluted using 0.5 column volumes of PBS (0.3 ml/min) using fraction collector and fixed fractionation volume of 0.25 ml. Column wash was carried out using 0.35 column volumes PBS (1.5 ml/min).

2.2.9.5 Surface Plasmon Resonance (SPR)

Surface plasmon resonance (SPR) affinity and kinetic analysis was carried out using the Biacore T200 instrument (GE Healthcare). Anti-minocyline antibodies were immobilised to a CM5 sensor chip at a density of 4300-4600 RU. Binding assays were carried out using 1x HBS-EP+ running buffer. Various concentrations (2.5 µM with 2-fold serial dilutions) of the analyte were injected for 150 second at 30 µl/min with 150 second dissociation time. Glycine-HCl (pH 2.0) was used as the regeneration buffer for the sensor chips. For the Alanine scanning experiments, the anti-minocycline antibody was captured on a Protein A series S sensor chip, to a density of 3000 RU. Minocycline was injected at a concentration of 5 µM with 2-fold serial dilutions, with 150 second contact time and 300 second dissociation at 30 µl/minute. Glycine-HCl pH 1.5 was used as regeneration buffer. In each case, flow cell 1 used for reference subtraction and a '0 concentration' sensogram of buffer alone was used as a double reference subtraction to factor for drift. Data analysis was carried out using the Biacore T200 Evaluation Software, version 3.0 and Biacore Insight evaluation software. The 1:1 Langmuir binding model was used to calculate the association (k_a) and dissociation (k_d) rate constants. The equilibrium dissociation constant (K_D) was calculated using the formula: koff/kon.

2.2.9.6 Isothermal Titration Calorimetry (ITC)

ITC measurements were performed using the PEAQ-ITC non-automated (MicroCal) at 25°C. Antibody sample was dialysed overnight using 5 L of PBS (20 mM Na_3PO_4, 150 mM NaCl, pH 7.4). Minocycline (Sigma-Aldrich) was dissolved in DMSO, followed by dilution in PBS such that the final DMSO concentration was 1%. The concentration of the anti-minocycline sdAb was determined using extinction coefficients $\varepsilon280nm= 31,065$ $M^{-1}cm^{-1}$ The single domain antibody (2 μM) in the cell was titrated with minocycline (50 μM) using 22 injections of 10 μl made at 120 second intervals with a stirring speed of 300 rpm. The binding isotherm plot was fitted by non-linear regression using the Origin software to a one set of sites 1:1 binding model to generate the thermodynamic parameters of the antibody-minocycline interaction.

2.2.10 Homology modelling

Homology model generation and antibody-ligand docking was carried out using Schrodinger BioLuminate software. Camelid single domain antibody templates were selected from the Protein Data Bank (PDB). The optimal template was selected as an appropriate template framework based on the composite scores, structural identities and PDB resolutions. In total, 10 predicted CDR loop were generated. The quality of the homology models and amino acid backbone conformations were assessed using Ramachandran plots. The Schrodinger Protein Preparation Wizard PrimeMini Package was utilised to reduce rigidity and optimise the homology model via energy minimisation.

Alanine scan mutagenesis of the CDR regions, as defined by the IMGT and Kabat numbering system, was carried out to generate 38 mutant anti-minocycline sdAbs independent alanine mutations or serine mutations where alanine was substituted. Critical hotspot residues were determined using Biacore SPR binding data to determine KD values for the interaction of minocycline or ELISA binding data to determine binding to GWARA peptide. Computational antibody-ligand docking was carried out by preparation of ligands using the LigPrep programme to convert 2D ligand (minocycline or GWARA) structures to produce corresponding low energy 3D structures. A receptor grid was placed on the anti-minocycline sdAb model for ligand

docking. The GlideScore function of the Schrodinger BioLuminate Glide programme was used to rank the docking models. In combination with experimental binding data from the alanine mutants, top poses were selected for analysis.

2.2.11 Statistical analyses

GraphPad Prism (GraphPad Software) was used to carry out statistical analyses and calculation (two-way ANOVA). Statistically significant differences were determined when the p values were <0.05.

3 GENERATION AND CHARACTERISATION OF MINOCYCLINE SPECIFIC SINGLE-DOMAIN ANTIBODIES

3.1 Introduction

Monoclonal antibodies have shown remarkable clinical success, with over 110 antibodies currently approved by the FDA. Besides conventional antibody formats for therapeutic applications, a new class of immunoglobulins is gaining momentum, comprising of the smallest naturally occurring intact antigen-binding fragment: the camelid IgG2 and IgG3 antibodies lacking the CH1 domain and light chains (VHH). Isolation and characterisation of camelid-derived single domain antibodies (sdAb) have produced a vast collection of high affinity sdAbs targeting protein antigens, haptens, small-molecule lipids and oligosaccharides with crystal structure analysis showing specific interaction of the sdAb-antigen complex. Remarkably, the V genes of the camelid sdAb bears high similarity to human VH3-23 subgroup family genes with approximately 80% homology, which may contribute to less immunogenicity.[193] In 2019, an anti-vWF sdAb for the treatment of acquired thrombotic thrombocytopenic purpura was the first sdAb approved by the FDA, with several other candidates currently in clinical evaluation.[194]

The primary interaction between classical antibodies and small molecular weight compounds (haptens) takes place at the binding interface of the VH and VL domains, specifically involving the residues of the CDRH3 and CDRL3 loops.[195,196] Likewise, classical antibodies also engage with short linear peptides within loops clustered between the H-chain and L-chain CDRs.[197] Whereas, sdAb-antigen interaction is achieved through an extended CDR3 domain loop structure, making them particularly suited to targeting cryptic epitopes with rapid tissue penetration.[198,199]

Generation and characterisation of high-affinity antibodies to low molecular weight compounds is far more challenging than to large immunogenic compounds and proteins. However, high affinity mAb targeting haptens have been generated from hybridomas and phage display technologies although inherent limitations of anti-hapten mAbs have been widely reported in the literature.[200–203]

Among the peculiar sdAb characteristics, the first is the small size (12-15 kDa), which is readily incorporated into a large complex DNA cassette compared to scFv, Fv or Fab antibody formats..[57] These sdAbs show an enhanced thermal stability, coupled with a higher hydrophilicity which results in an improved water solubility and lower aggregation propensity.[198,199] Recently, sdAbs have also been employed to functionalise CAR T cells with comparable functionality to the conventional scFv-based CAR architectures.[204–207]

Haptens are generally non-immunogenic, therefore, for high affinity antibodies to be generated against haptens, the hapten of choice must be conjugated to an immunogenic carrier protein to illicit an immune response in immunised animals. Such immunogenic proteins are typically haemocyanins, thyroglobulins, albumins and polylysine. Historically, antibodies generated against haptens have been used in immunoassays to detect hormones and drugs in environmental and biological samples but also for therapeutic applications in cancer therapy. The selection of anti-hapten antibodies is greatly influenced by the physio-chemical characteristics, spatial conformation, and conjugation protocol of the hapten as well as the antibody selection method.[208] Further issues of antibody cross-reactivity against structurally related compounds is also taken into consideration when screening for anti-hapten antibodies.[209]

SdAb-hapten complexes have been previously described and structural analysis of the interaction determined via crystallography.[210] SdAbs generated against protein-hapten conjugates have been widely reported in the literature. For example, sdAb against haptens such as the red azo-dye RR6 (728 Da), RR120 (1335 Da), methotrexate, the herbicide picloram, caffeine (194 Da), sulfonamide antibiotics, and the myotoxin 15-acetyldeoxynivalenol have been raised and characterised showing affinities in the nanomolar range.[200,211–215]

In this chapter, I describe the generation, using an alpaca phage display library, and the biophysical characterisation of sdAbs specific to minocycline, which is an inexpensive, well-tolerated, small molecule (457 Da) FDA-approved antibiotic drug. An anti-minocycline sdAb will be the central tool of an architecture of a minocycline-controlled protein-protein displacement

system, where binding to minocycline results in the displacement of a secondary protein interaction. Utilizing this controllable system, I aim to design and test a minocycline-controllable CAR T cell and a system for inducing secretion of an anti-tumour payload from T cells in response to minocycline dosing.

3.2 Aims

- To identify, using an immunised Alpaca phage display library, a range of single-domain antibody sequences which specifically bind to minocycline.

- To determine the affinity of the anti-minocycline antibodies binding to minocycline

- To test the stability and minocycline-binding capacity of the anti-minocycline antibody

3.3 Results

3.3.1 Generation of minocycline specific single domain antibodies using an immunised Alpaca phage display library

3.3.1.1 Chemical conjugation of minocycline to KLH and BSA

To generate a range of single domain antibody sequences specific for minocycline, a vaccination strategy was devised which involved the immunization of alpacas with minocycline. However, the low molecular weight, non-immunogenic nature of the minocycline antibiotic would not elicit an immune response in animals. Therefore, minocycline was separately conjugated to the inert carrier proteins, keyhole limpet hemocyanin (KLH) or bovine serum albumin (BSA) via maleimide linkage to an engineered free sulfhydryl group on minocycline (Fig. 3.1). Examination of the free -SH group content using Ellman's reagent showed 10-(6-Mercaptohexyl)-minocycline contains 40% free -SH group.

KLH, a large metalloprotein containing multiple immunogenic epitopes, was specifically used to stimulate a strong response from the immune system in order to generate antibodies against the minocycline-conjugated structure. BSA-conjugated minocycline was used for downstream screening applications. Engineering of the free sulfhydryl group on minocycline was carried out by Dr. Eilitz (ChiroBlock). KLH and BSA conjugation to minocycline was carried out by GenScript.
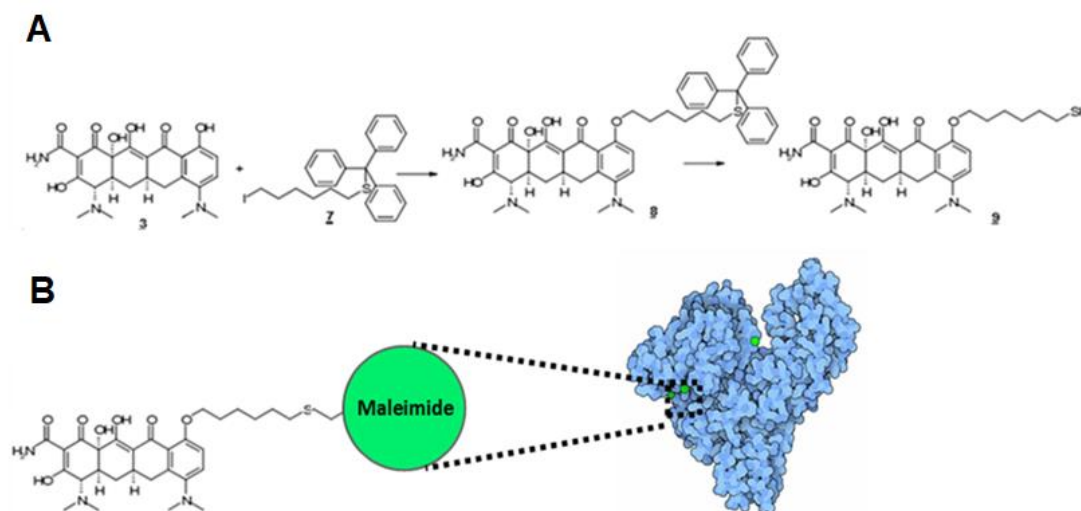
Figure 3.1. Chemical conjugation of minocycline to produce a phage display single domain antibody library through alpaca immunisation.

(A) Functionalisation of minocycline by addition of a free sulfhydryl group on a spacer arm (B) to enable maleimide conjugation to either (KLH) or (BSA) for immunisation and subsequent panning strategies, respectively.

3.3.1.2 Minocycline specific antibody response in immunised Alpaca serum

An alpaca was then immunised via subcutaneous injection of KLH-conjugated minocycline to generate an immune response against all regions of these molecules including the minocycline moiety. Briefly, the immunization schedule consisted of the alpaca receiving intramuscular injections at weekly intervals. Following six immunisations, 100 ml of sera was collected, and peripheral blood mononuclear cells (PBMCs) were extracted, and antibodies generated were screened against BSA-conjugated minocycline to select for antibodies specific to the minocycline rather than those generated against the KLH protein (Table 3.1).

Table 3.1. Minocycline-KLH immunization schedule for the immunization of alpaca. CFA – Complete Freund's adjuvant; IFA – Incomplete Freund's adjuvant

Day	Activity	Route	Dose	Adjuvant
Day 0	Pre-immune bleed and primary immunization	Intramuscular	200 µg KLH-10-(6-Mercathohexyl)-minocycline	CFA
Day 7	1st boost	Intramuscular	200 µg KLH-10-(6-Mercathohexyl)-minocycline	IFA
Day 14	2nd boost	Intramuscular	200 µg KLH-10-(6-Mercathohexyl)-minocycline	IFA
Day 28	3rd boost	Intramuscular	100 µg KLH-10-(6-Mercathohexyl)-minocycline	IFA
Day 33	1st test bleed (15 ml blood)			
Day 35	4th boost	Intramuscular	100 µg KLH-10-(6-Mercathohexyl)-minocycline	IFA
Day 40	1st bleed (100ml) and PBMCs prep.			
Day 42	5th boost	Intramuscular	100 µg KLH-10-(6-Mercathohexyl)-minocycline	PBS
Day 45	2nd test bleed (15 ml blood)			

Upon completion of the immunisation course, sera and isolated PBMCs were extracted to confirm that a specific immunological response to the drug was induced in the donor alpaca. Using a solid-phase ELISA, seroconversion was confirmed by screening test sera against immobilized BSA-conjugated minocycline relative to immobilized BSA only (Fig. 3.2). Bound anti-minocycline alpaca antibodies were detected using anti-alpaca-IgG1 antibody. The results indicate a strong IgG response generated specifically against minocycline over BSA only.

Alpaca seroconversion
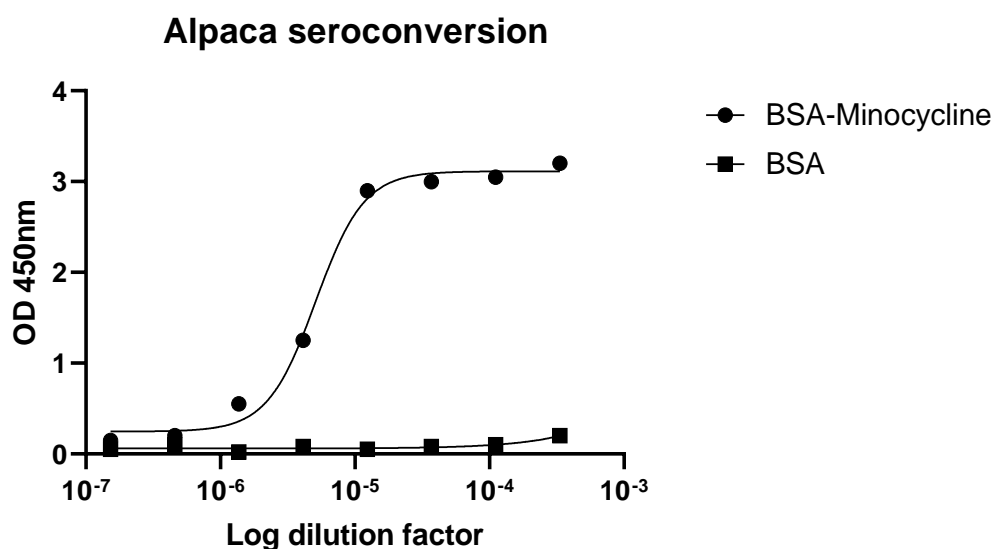
Figure 3.2. Immunised Alpaca serum showing specific antibody response to minocycline.

ELISA analysis of anti-minocycline conventional IgG and sdAb in alpaca serum. ELISA data confirming successful seroconversion of KLH-minocycline-immunised alpaca showing specific antibody response against immobilised BSA-minocycline, with wells coated with BSA alone as the negative control. BSA-minocycline and BSA were diluted in PBS to a concentration of 1 µg/ml. Subsequent blocking and serum dilutions were carried out in 1% BSA diluted in PBS. Alpaca serum was serially diluted from $3.3x10^{-4}$ to $1.5x10^{-7}$ and detected using anti-alpaca-IgG1 antibody conjugated to horseradish peroxidase (HRP). HRP activity was determined using TMB substrate and the absorbance readout was carried out at 450 nm.

3.3.1.3 Amplification of anti-minocycline sdAb repertoire

Upon confirmation of the presence of anti-minocycline antibodies, the sdAb repertoire of the immunised alpaca was amplified and construction of a comprehensive phage display library was undertaken. To determine the antigen-specific sdAbs in the library, determining the library diversity and size was essential. Lymphocytes from the immunised alpacas were used as the starting material to generate a sdAb library as they bear the minocycline specific sdAb encoding mRNA sequences. As detailed in the methods section, the extracted RNA was used in the complementary DNA (cDNA) synthesis.

Using primers designed to amplify, via polymerase chain reaction (PCR), the antibody heavy chain-coding region (VHH) repertoire extending from the variable (V) region through to the constant heavy 2 domain (CH2) region. Different primer sets were used to isolate the VHH from the classical VH antibody DNA. A further PCR was carried out with unique primers to amplify the VHH repertoire and to introduce restriction sites (SfiI and NotI).

The initial amplification resulted in two DNA products consisting of: a larger (~1000 bp) DNA coding sequence of the VH, CH1, hinge and a short sequence of the CH2 exon from a conventional camelid IgG1 antibody, and a smaller (~700 bp) DNA coding sequence of the VHH, hinge and a short sequence of the CH2 exons of non-conventional heavy chain antibodies (Fig. 3.3B). The smaller DNA product was used as the template for a nested PCR where primers were used to amplify only the VHH coding sequence (~400 bp) as well as introduce SfiI and NotI restriction sites at the 5' and 3'ends, respectively. This was crucial for downstream cloning into the phage display vector pHEN1 and subsequent library construction (Fig. 3.3C).
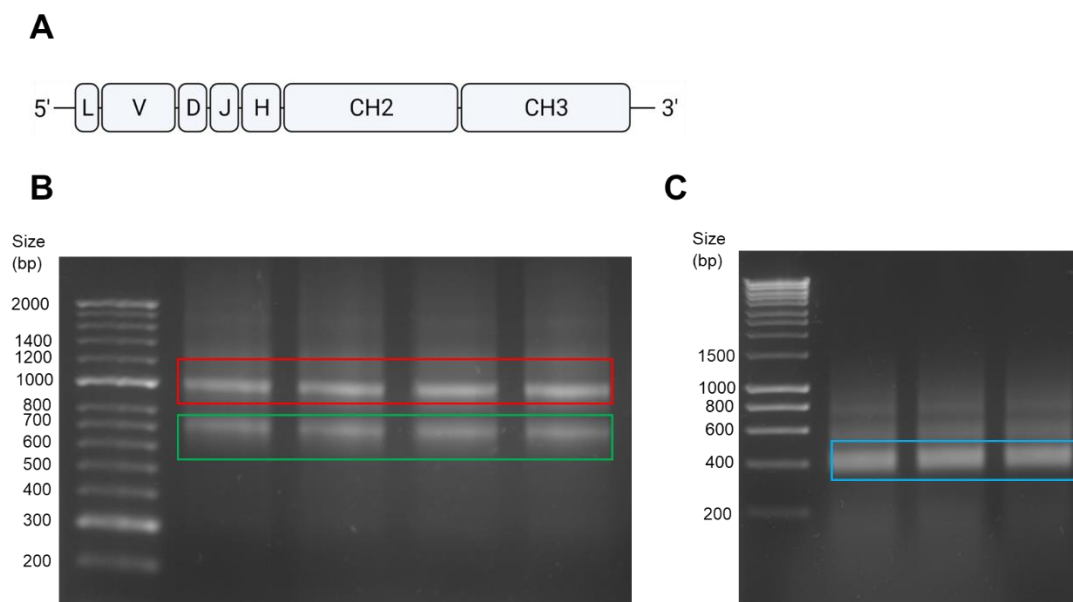
Figure 3.3. PCR amplification of isolated heavy chain antibody coding sequence from seroconverted Alpaca PBMCs.

(A) Schematic of PCR amplification region of V leader sequence to CH2 sequence of the heavy chain antibody coding sequence. (B) The ~850 bp DNA band (red) corresponds to the conventional camelid IgG1 antibody DNA

fragment (V, CH1, hinge and part of the CH2 region) and ~600 bp DNA band (green) corresponds to the non-conventional camelid single domain heavy chain IgG2 and IgG3 antibody (VHH, hinge and a part of CH2 region) DNA fragment. HyperLadder™ 50 bp was as the DNA molecular weight marker. (C) The single domain heavy chain antibody fragment (green) was further amplified using the V leader sequence and antisense JH primer. The corresponding ~400 bp DNA band (blue) encodes for the VHH region/VDJ region of non-conventional camelid single domain heavy chain IgG2 and IgG3 antibodies. The ~400 bp fragment was then purified and cloned into pHEN phage display vector for library generation. Each lane represents individual PCR reaction. HyperLadder™ 1 kb was as the DNA molecular weight marker. PCR fragments were separated on a 1.2% agarose gel for 45 minutes at 140 V.

3.3.1.4 Phage library construction and enrichment

To acquire a diverse phage display library for panning binders, the next stage of the process was to ligate the amplified sdAb sequences, using restriction enzymes SfiI and NotI into the phage display vector pHEN1 in frame with capsid protein gene-III (Fig 3.4). The *E. coli* (Escherichia coli) strain ER2738 (E4104, NEB), which has a tetracycline resistance gene linked to the F+ gene was transformed via electroporation. Incubation of ER2738 electrocompetent cells with ligated DNA in chilled electroporation cuvettes was used to generate a primary phage library. The estimated library size was determined by serially diluting (1:10^3, 1:10^4, 1:10^5, and 1:10^6) and plating the transformed cells. Counting of the colony forming units (cfu) showed the library yielding an estimated size of 5x10^8 unique sequences.

Ligation of the sdAb coding sequence within the pHEN1 vector results in an open reading frame through the addition of an N-terminal PelB leader sequence upstream of the isolated sdAb sequences. This directs the sdAb polypeptide chain into the bacterial periplasm for complete folding, disulphide bond formation and expression, allowing for the screening and characterisation of secreted sdAbs within the supernatant and periplasmic extract of the bacterial cultures. Moreover, a sdAb and capsid protein gene-III fusion at the C-terminal end is also achieved, with a stop codon (AMBER)

being situated between two components. Generally, stop codons halt translation; However, in the suppressor ER2738 *E. coli* strain, the AMBER stop codon is read-through by tRNA leading in the translation of a glutamine (instead of stopping translation) and forms a sdAb and gene-III fusion. Thus, resulting in the expression of the sdAb on the exterior of pIII phage particle.
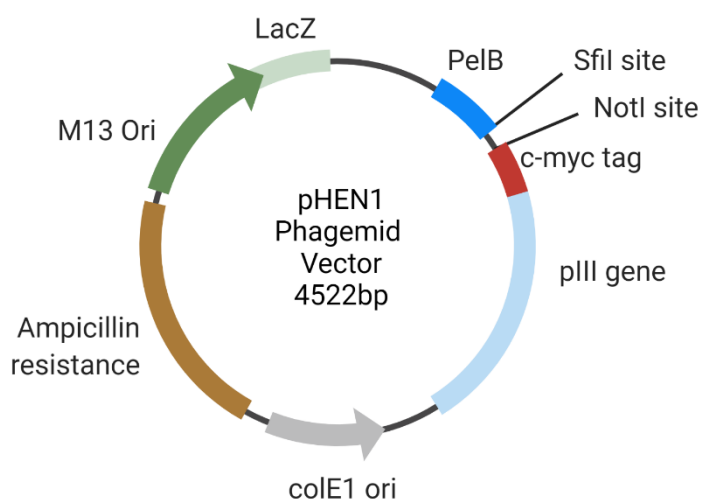
Figure 3.4. Schematic of the pHEN1 ligation sites and gene locus for the anti-minocycline sdAb sequence.

To remove KLH-specific antibodies generated during the immunisation strategy, phage panning was carried out against biotinylated BSA-minocycline conjugated to streptavidin-coated beads. Unbound phage was removed using PBS 0.1% Tween wash and minocycline-BSA bound phage was eluted using trypsin-EDTA. Phage panning was carried out by amplification and precipitation followed by a 100-fold to 1000-fold titration of the eluted library for subsequent re-infection of *E. coli* cells for the next panning and selection rounds.

After 2 rounds of panning, the resultant phage libraries were tested by ELISA against BSA-minocycline or unconjugated BSA to determine the degree of enrichment of minocycline-specific phage particles relative to the unpanned library (Fig. 3.5). Figure 3.5 indicates high levels of enrichment of minocycline-BSA-binding phage in pan 1 and pan 2 libraries compared to the unpanned library. Furthermore, phage from pan 1, pan 2 and unpanned libraries show

minimal background signal against unconjugated BSA-coated wells indicating that the observed enrichment is specific for the minocycline moiety.

A

**BSA-Minocycline
Phage enrichment**

B

**BSA only
Phage enrichment**
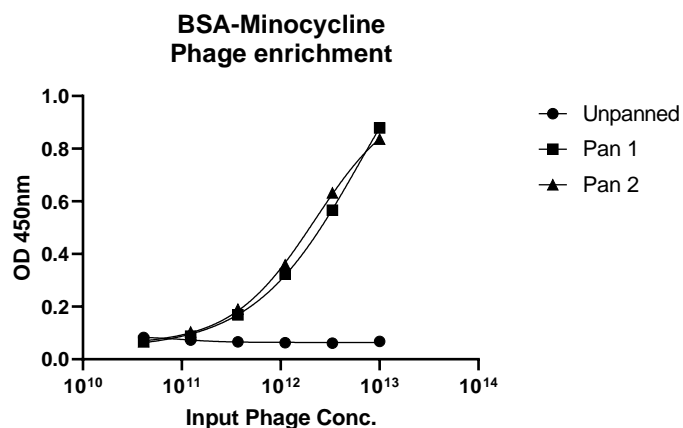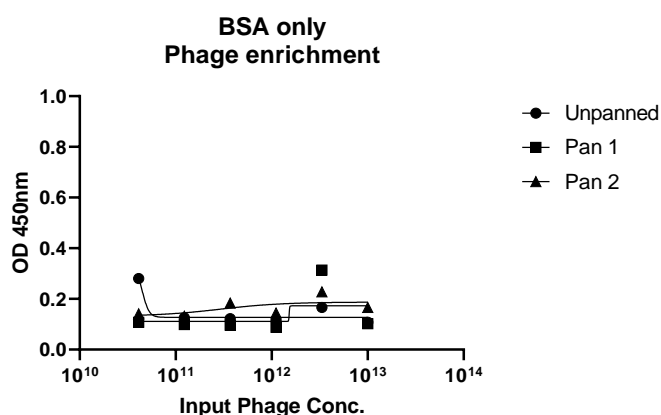
Figure 3.5. Minocycline specific phage enrichment ELISA.

Phage libraries eluted from pan 1 and pan 2 shows target-specific phage population enrichment as measured by a positive anti-M13 whole phage ELISA binding against minocycline-BSA relative to the unpanned library. (B) Unpanned, pan 1 and pan 2 phage library background binding against BSA only control. Input phage titration was carried out from $1x10^{13}$ to $1.37x10^{10}$

3.3.1.5 Selection of minocycline specific sdAb using ELISA

The resultant enriched panned libraries were evaluated for the frequencies of minocycline specific sdAbs. Following two rounds of panning, the phage library contained many potential minocycline-binding sdAb clones, therefore, to assess the enrichment, a whole phage ELISA was carried out. The whole phage ELISA is an invaluable tool to confirm the binding specificity of single clones against minocycline. It is particularly advantageous for expression of some sdAbs from bacterial cells, which may show low expression levels. Moreover, a whole phage ELISA is ideal in the early-stage screening due to the fact the ELISA signal detection is amplified because of multiple phage coat proteins (pVIII) present on the phage per binding partner.

In order to isolate individual monoclonal phage encoding the minocycline-binding antibodies on their exterior, individual bacterial colonies were picked, cultured and phage expression was screened using an anti-M13 whole phage ELISA. In brief, 95 single phage clones from pan 1 and 40 phage clones from pan 2 were screened for binding on wells coated with minocycline-BSA or unconjugated BSA as a negative control. Verification of results were determined by excluding phage showing signal against the negative control BSA only coated wells. Pan 1 and pan 2 libraries both contained minocycline-specific sdAbs with 17% and 35% of the screened phage showing binding to minocycline, respectively (Fig. 3.6). A greater proportion of minocycline-BSA-specific clones were identified in pan 2 compared to the pan 1 demonstrating a greater enrichment of this library. Although the results show the positive clones identified from pan 2 demonstrated higher levels of background binding to the negative control BSA only, the binding was greater against minocycline-BSA.

Due to the high sensitivity of a whole phage ELISA, it is susceptible to false positives, therefore a few variables were considered. Initially, it was paramount to reduce the unspecific phage binding to the ELISA plates, therefore a blocking solution of 2% milk in PBS was used for all coating and incubation steps. Most importantly, unspecific binding to carrier proteins of sdAbs raised against small molecules conjugated to carrier proteins such as KLH or BSA can take place. As described in Section 3.1.1.1, minocycline was conjugated

to KLH for the immunisation strategy. Therefore, in order to distinguish and select binder clones directed specifically towards minocycline over the carrier KLH, BSA was substituted as the carrier protein for all subsequent panning and screening.
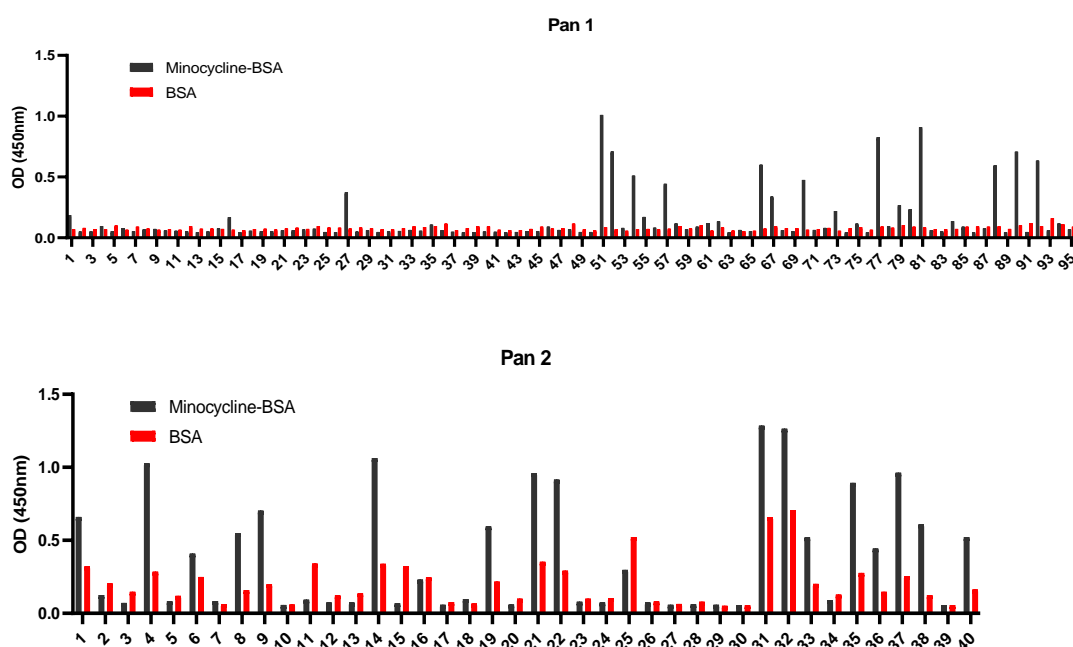
Figure 3.6. Anti-M13 whole phage ELISA analysis of minocycline specific sdAbs from pan 1 and pan 2.

Binding of single clone phage presenting individual sdAb clones on the exterior of phage particles measured at OD450 nm. (A) 95 individual clones from pan 1 screened against immobilised minocycline-BSA. (B) 40 individual clones from pan 2 screened against immobilised minocycline-BSA. Detection of bound phage was determined using anti-M13-HRP. Immobilized BSA only was used as a negative control.

Due to the enhanced signal achieved through the detection of multiple pVIII copies per phage particle, a whole-phage ELISA against immobilized antigen is a fast, convenient, sensitive, and a high-throughput method of confirming specific sdAb sequences. However, to further confirm that the phage-encoded sdAbs identified in the previous screen of the pan 2 library specifically bound to minocycline, screening was carried out on the isolated sdAbs themselves to increase the stringency of selection. Bacteria were infected with the phage clones from the pan 2 library and antibody expression was induced through

IPTG induction of the lac operon to express myc-tagged antibodies from the pan 2 library. Detection using an anti-myc-HRP antibody excludes the amplification of signal through whole phage detection and apply a more stringent selection criteria for assessing positive clones. Binding of secreted sdAb in the supernatant and from the periplasmic bacterial extract from 40 individual cultures showed 14 positive clones (threshold > 0.2 OD450 nm) binding to KLH- and BSA-conjugated minocycline but not to BSA alone (Fig. 3.7).
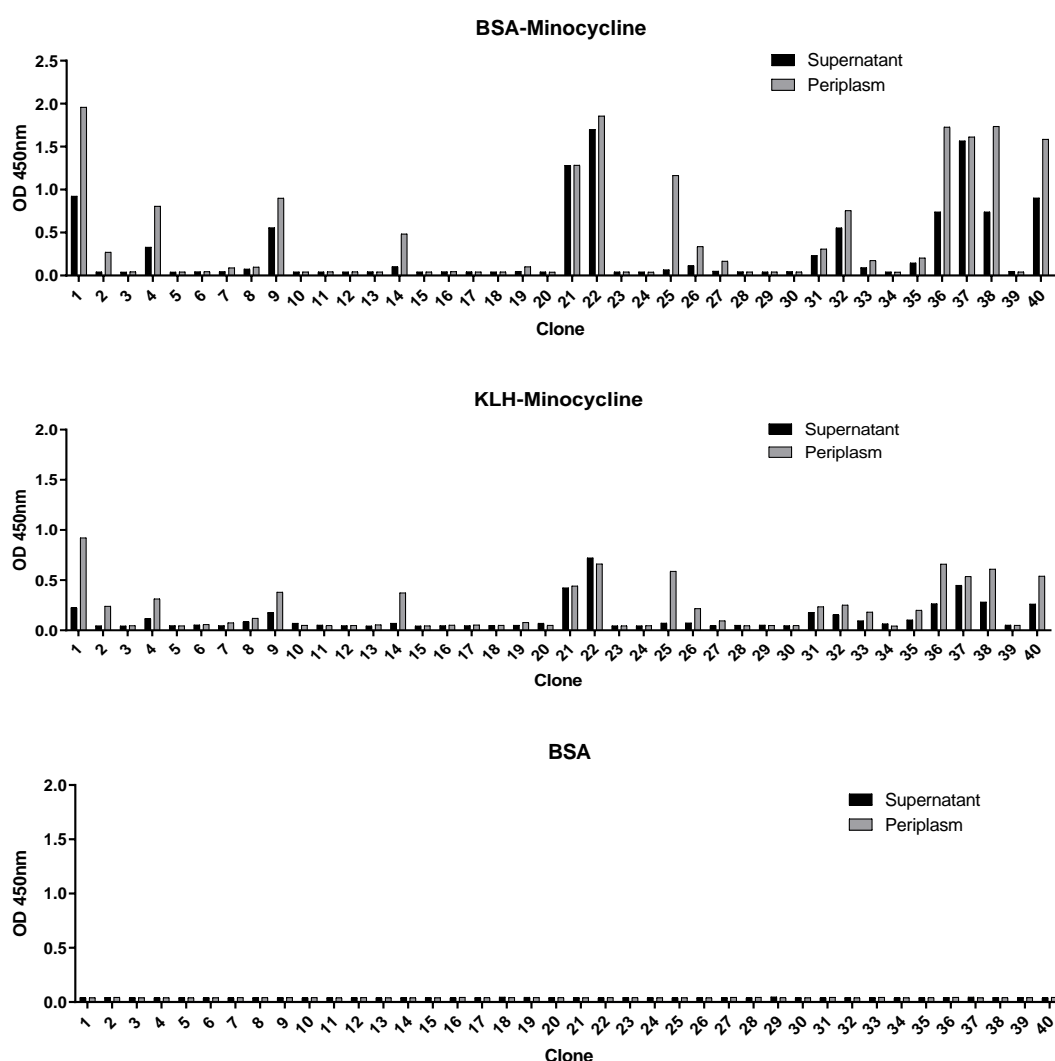
Figure 3.7. ELISA screen of monoclonal anti-minocycline sdAb clones. *Screening of supernatant and periplasmic extracted monoclonal* sdAb *was carried out against BSA-conjugated minocycline, KLH-conjugated minocycline and BSA only control. 17 clones showed positive binding to each minocycline conjugate and a lack of binding to BSA alone control.*

3.3.1.6 Sequence analysis of positively binding phage clones

Results from the ELISAs on whole phage clones and the respective expressed myc-tagged antibodies gave a clear indication of antigen specific sdAbs being present in the library. Based on the positive clones identified from anti-myc tagged antibody ELISA, I aimed to carry out further analysis of each clone. DNA from the 14 positive sdAb clones isolated from pan 2 (specifically clone #1, #4, #9, #14, #21, #22, #25, #26, #31, #32, #36, #37, #38 and #40) was used to carry out in depth analysis of the framework (FR) and complementarity-determining region (CDR) amino acid sequence. Table 3.2 shows the nucleotide sequence of the 14 selected clones and their alignment in accordance with the Kabat numbering system for the variable region. Remarkably, all sdAb clones sequence data shows distinctive hydrophilic amino acids being substituted in the framework-2 hallmark residues in place of hydrophobic residues which are typically found in VH domains (Positions 42, 49, 50, and 52).[216] Enrichment of extended CDR3 amino acid sequences is also characteristic feature of sdAbs resulting from compensation due to the lack of an interacting light chain.[65] Alongside extended CDR3s, the CDRs of sdAbs can also contain cysteine residues on top of conserved cysteines (22th and 98th amino acid position) that are involved in disulphide bond formation joining the framework-1 and framework-3 regions. These additional CDR3 cysteines can also form disulphides between different CDRs, within the CDR3 as well as provide additional binding scaffolds to stabilise the sdAb or antigen binding interaction.[217] From the sequencing results shown in Table 3.2, 13 out of the 14 clones bear an extended CDR3 (14 amino acids) although no cysteine residues in the CDRs were observed in any of the sequences. Sequence analysis showed in total nine unique sequences with random combinations of the FR and CDR enrichment. Clones with sequence homology were grouped and are shown in Table 3.2. To summarise: group 1 (clone 1), group 2 (clones 4 and 32), group 3 (clones 14 and 36), group 4 (clone 9), group 5 (clones 21 and 25), group 6 (clone 22), group 7 (clone 26), group 8 (clones 31) and group 9 (clones 37, 38 and 40). Such variations in the CDR3 region are a result of a different D gene segment used in the VDJ recombination event, with variations in the CDR1 and CDR2 region probably due to somatic hypermutation through the process of affinity maturation.

AMINO ACID SEQUENCE ALIGNMENT OF IDENTICAL SINGLE-DOMAIN ANTIBODY CLONES

GROUP 1

#1)
QVQLQESGGGLVQPGSSLRLSCAAS**GRTFSSYN**IGWFRQAPGKEREFVAA**ISWSGART**YYADSVKG
RFTISRDNAKNTVYLQMNSLKPEDTAVYSC**AAGRGWGTEAILDY**WGQGTQVTVSSAA

GROUP 2

#4)
QVQLQESGGGLVQPGGSLRLSCSAS**GRSLSSYV**MGWFRQAPGKEREFVAA**ISWSGART**YYADSVKG
RFTISRDNAKNTVYLQMNSLKPEDTAVYSC**AAGRGWGTEAILDY**WGQGTQVTVSSAA

#32)
QVQLQESGGGLVQPGGSLRLSCSAS**GRSLSSYV**MGWFRQAPGKEREFVAA**ISWSGART**YYADSVKG
RFTISRDNAKNTVYLQMNSLKPEDTAVYSC**AAGRGWGTEAILDY**WGQGTQVTVSSAA

GROUP 3

#14)
QVQLQESGGGLVQAGGSLRLSCAAS**GRTFSNYN**IGWFRQAPGKEREFVAA**INWSGGRT**YYADSVKG
RFTISRDNAKNTVYLQMNSLKPEDTAVYSC**AAGRGWGTEAILDY**WGQGTQVTVSSAA

#36)
QVQLQESGGGLVQAGGSLRLSCAAS**GRTFSNYN**MGWFRQAPGKREFLAA**INWSGGRT**YYVDSVKGR
FTISRDNAKNTVYLQMNSLKPEDTAVYRC**AAGRGWGTEAILDY**WGQGTQVTVSSAA

GROUP 4

#9)
QVQLQESGGGLVQAGGSLRLSCAAS**GRTFSSYN**IGWFRQAPGKEREFVAA**ISWSGART**YYADSVKG
RFTISRDNAKNTVYLQMNSLKPEDTAVYYC**VAGRGWGTEAILDY**WGQGTQVTVSSAA

GROUP 5

#21)
QVQLQESGGGLVQAGGSLRLSCAAS**GRTFSSYN**IGWFRQAPGKEREFVAA**ISWSGART**YYADSVKG
RFTISRDNAKNTVYLQMNSLKPEDTAVYSC**AAGRGWGTEAILDY**WGQGTQVTVSSAA

#25)
QVQLQESGGGLVQAGGSLRLSCAAS**GRTFSSYN**IGWFRQAPGKEREFVAA**ISWSGART**YYADSVKG
RFTISRDNAKNTVYLQMNSLKPEDTAVYSC**AAGRGWGTEAILDY**WGQGTQVTVSSAA

GROUP 6

#22)
QVQLQESGGGLVQAGGSLRLSCAAS**GRTFSRYN**IGWFRQAPGKEREFVAA**ISWSGART**YYADSVKG
RFTISRDNAKNTVYLQMNSLKPEDTAVYYC**AAGRGWGTEAILDY**WGQGTQVTVSSAA

GROUP 7

#26)
QVQLQESGGGLVQAGGSLRLSCAAS**GRTFSSYN**MGWFRQAPGKEREFVAA**ISRSGGIT**YYVDSVKG
RFTISRDNAKNTVYLQMNSLKPEDTAVYSC**AAGRGWGVEAILDY**WGQGTQVTVSSAA

GROUP 8

#31)
QVQLQESGGGLVQAGGSLRLACVAS**GNIGLVSV**MDWYRQVPGKERELVAT**ITGGGST**NYSDSVKGR
FTISMDYAKSTIYLQMNSLKPEDTAVYYC**RLVNNGRPF**WGQGTQVTVSSAA

GROUP 9

#37)
QVQLQESGGGLVAGGSLRLSCAAS**GRTFSSYN**IGWFRQAPGKEREFVAA**ISWSGART**YYADSVKGR
FTISRDNAKNTVYLQMNSLKPEDTAVYSC**AAGRGWGTEAILDY**WGQGTQVTVSSAA

Table 3.2. Amino acid sequence of isolated anti-minocycline sdAb clones of phage derived anti-minocycline sdAb antibodies.

Complementarity-determining region (CDR) amino acid residues highlighted in yellow, green, blue for CDR1, CDR2 and CDR3, respectively. CDRs defined using IMGT numbering.

3.3.2 Biophysical characterisation of the highest and lowest affinity anti-minocycline single domain antibodies

3.3.2.1 Expression and purification of antibody clones

In order to conduct biophysical characterisation of the single domain antibody clones showing specific binding to BSA-conjugated minocycline, isolated clones were sequenced and expressed as sdAb-murine-Fc conjugates (murine IgG2A-hinge, CH2 and CH3 regions) in Chinese Hamster Ovary (CHO) cells. Antibodies were then purified using protein-A affinity chromatography.

Plasmids encoding each clone were used to transfect exponentially growing ExpiCHO cell lines. Supernatant was filtered using a 0.22 µm filter and purified using MabSelect PrismA protein-A column. As representative examples, the purification steps of three anti-minocycline sdAb clones #1, #9 and #22 are shown (Fig. 3.8). Supernatant was loaded on the column using a sample pump at 1 ml per minute, followed by 20 column volume wash in PBS and an elution step in 0.1 M Glycine pH 2.8 (IgG Elution buffer) with in line buffer exchange through 10 ml HiTrap desalting columns. Eluted proteins were collected in 250 µl aliquots using an automated fraction collector.

A

Clone 1 sdAb-Fc
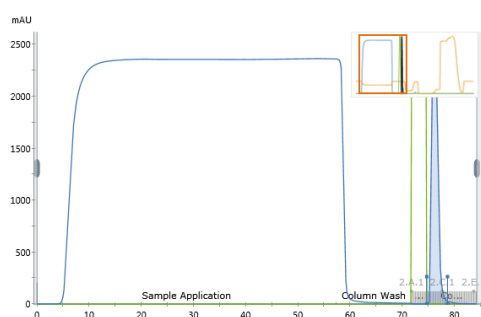
B
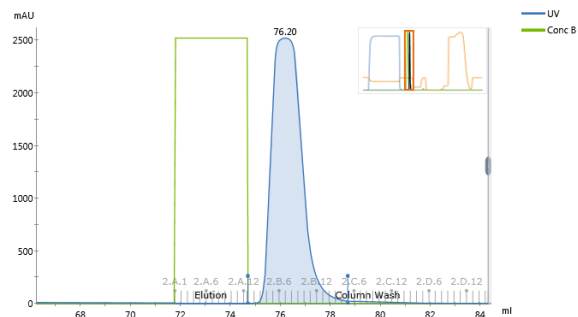
Clone 9 sdAb-Fc
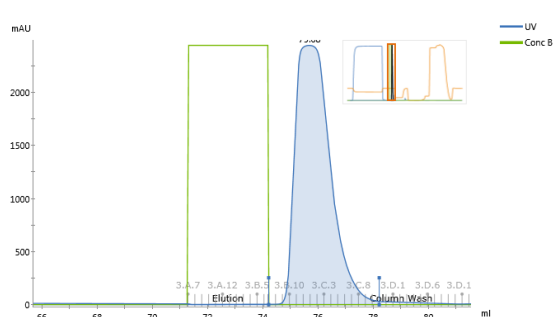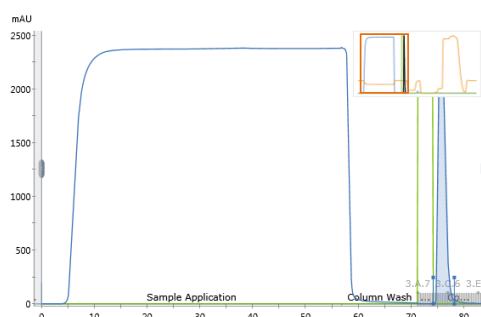
Clone 22-sdAb
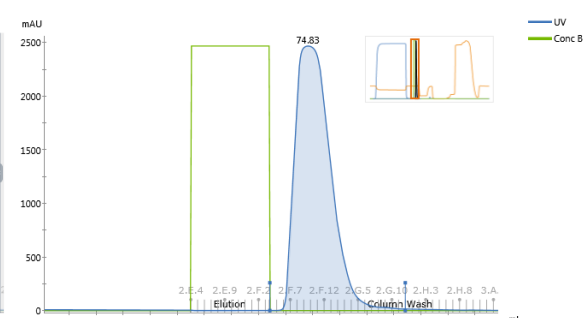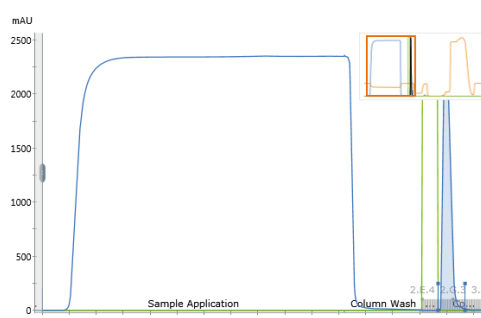
Figure 3.8. Soluble anti-minocycline sdAb purification using the AKTA Pure system.

Representative purification of anti-minocycline sdAb clone 1, clone 9 and clone 22 on MabSelect PrismA column. B) magnification of eluted peak. and mAbSelect SURE 1 ml column for affinity purification. Running conditions were as follows: PBS was used as the running buffer, 0.1 M glycine pH 2.8 (green line) was used as the elution buffer as a flow rate of 1 ml/min. 250 μl fractions were collected in a 96-well deep-well plate.

To assess the purity and size of the sdAb clones, 1 μg of purified antibody was loaded on a 4-20% miniProtean TGX gel in Nu-PAGE loading buffer with and without addition of 10 mM β-mercaptoethanol (reduced and non-reduced conditions, respectively). Samples were then run in Tris Glycine SDS buffer at 180 V. The presence of protein was determined by UV imaging at 302 nm in Azure C600 gel imager.

Under reducing conditions, the molecular weight was confirmed in accordance with the predicted molecular weight of a sdAb-murine-Fc homodimer (~40 kDa) and is revealed as single or closely collocated prominent protein bands of each overlapping monomer as expected upon reduction of the disulphide bond between the hinge region of each respective monomer. Under non-reducing conditions, the molecular weight is twice that of the monomeric chain displayed under reducing conditions, therefore confirming the full assembly of the antibody via disulphide bond formation between the interchain hinge regions. The molecular weight is consistent with the predicted molecular weight of a stable sdAb-murine-Fc antibody being expressed as a homodimer as a prominent band with a molecular weight of ~80 kDa (Fig. 3.9).
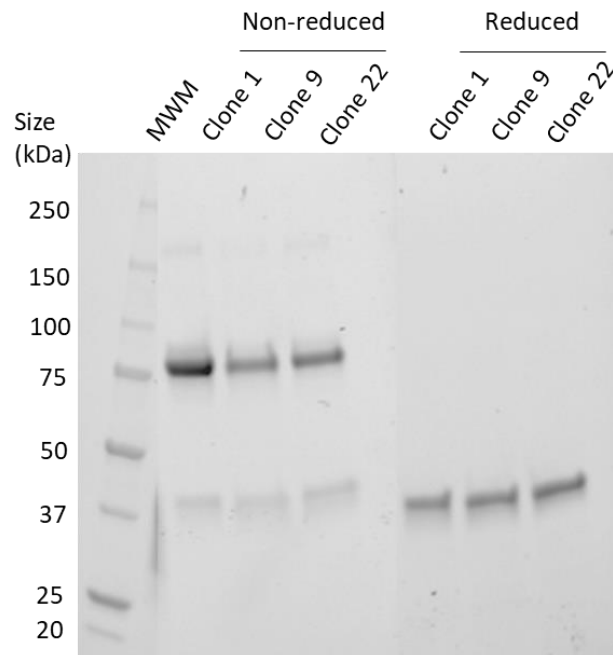
Figure 3.9. Expression and purification of sdAb-Fc conjugates in CHO cells.

Chinese hamster ovary cells (ExpiCHO) were transiently transfected with plasmid DNA coding for 3 different sdAb-Fc conjugates and expression carried out for 5 days. Proteins were purified by protein-A chromatography and desalting column. Samples were analysed by SDS-PAGE, each anti-minocycline sdAb was prepared and loaded (10 µg) using sample buffer consisting of 62.5 mM Tris-HCl, pH 6.8, 2% SDS, 25% (v/v) glycerol, 0.01% bromophenol blue (and 5% β-mercaptoethanol for reducing samples). Samples were then incubated at 95°C for 5 minutes prior to being loaded onto the gel. The mini-PROTEAN® TGX Stain-Free™ pre-cast 4-20% gradient gel was used to run samples. Running buffer consisted of 25 mM Tris, 192 mM glycine and 0.1% SDS. 180 V running voltage was used for 30-40 minutes. The Azure c600 Gel Imaging System by Azure Biosystems was used to image protein bands. Bio-Rad Precision Plus Protein Standards were used as reference protein ladder.

Size exclusion chromatography (SEC) was also carried out to determine the aggregation propensity or presence of breakdown products of each sdAb clone. SEC separates proteins and molecules based on differences in size. SEC resins are made up of a porous matrix of inert spherical particles which do not react/adsorb proteins. Upon sample injection, proteins larger than the size of the pores are unable to diffuse into the beads, therefore are eluted first. However, large aggregates may not transverse the column and prevent detection by SEC. Proteins which range in size between the very big and very small can penetrate the pores to varying degrees based on their size. The smallest molecules it will be able to enter the total pore volume and require the greatest distance to traverse before being eluted. Therefore, molecules which traverse the total pore volume are eluted last.

Figure 3.10 shows the presence of a single peak for clone 1 and clone 9 indicating each respective clones are stably expressed and do not form aggregates or lower order breakdown products. Clone 22 shows a broader peak with a lower OD280 indicative of antibody dimerisation (Fig. 3.10).
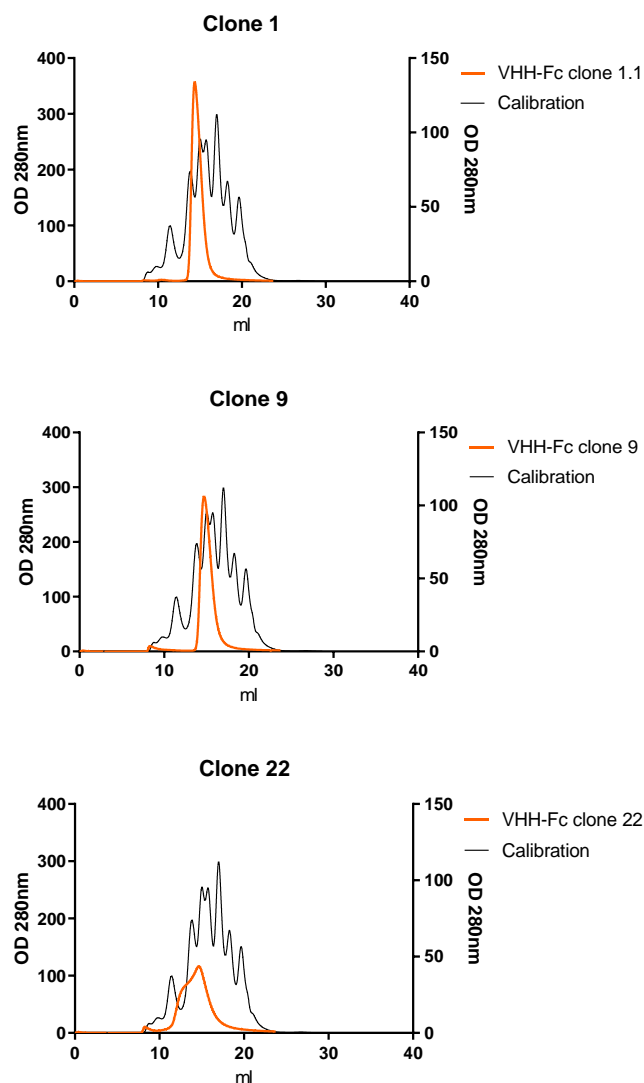
Figure 3.10. Size exclusion chromatography (SEC) of purified anti-minocycline single domain antibodies.

200 µl of purified antibodies was loaded into a Superdex 200 10/300 GL. The AKTA Pure system was used to carry out a loop injection at 0.3 ml/min and a flow rate of 0.4 ml/ml. PBS was used as the running buffer and protein was detected at OD 280 nm. Right axis indicates calibration run. Results show each representative clone formed a single peak by SEC.

3.3.2.2 Investigation of Binding Kinetics of the anti-minocycline antibody to minocycline

Antibody binding kinetic determination was carried out using surface plasmon resonance (SPR). Initially, affinity analysis using Biacore SPR was carried out by immobilising the sdAb-Fc conjugates on a CM5 Biacore chip. To confirm specificity of sdAb to minocycline over modified regions, unconjugated minocycline was injected as the analyte. Caffeine which has a similar molecular weight to minocycline but different molecular structure, was also injected as a negative binding control. To summarise, SPR analysis indicated that clone 1 and clone 22 showed the highest minocycline binding affinities of 31 nM and 67 nM, respectively (Fig. 3.11). The loss of affinity and 50% reduced response units of clone 22 may be attributed evidence of dimerisation observed using SEC (Fig. 3.10).

In contrast, clone 9 which showed positive binding to minocycline-BSA by ELISA did not show specific binding to minocycline using SPR. This result suggests low binding affinity to minocycline or that the specificity was directed towards modified regions or the maleimide linker sequence used to conjugate minocycline to the inert carrier protein, BSA, which would have been selected for during screening against minocycline-BSA (Fig. 3.11). An affinity of 31 nM, as measured for clone 1, lies within the nanomolar range of affinities previously described for a small molecule-based control system. Therefore, clone 1 was taken forward for further development and characterisation.
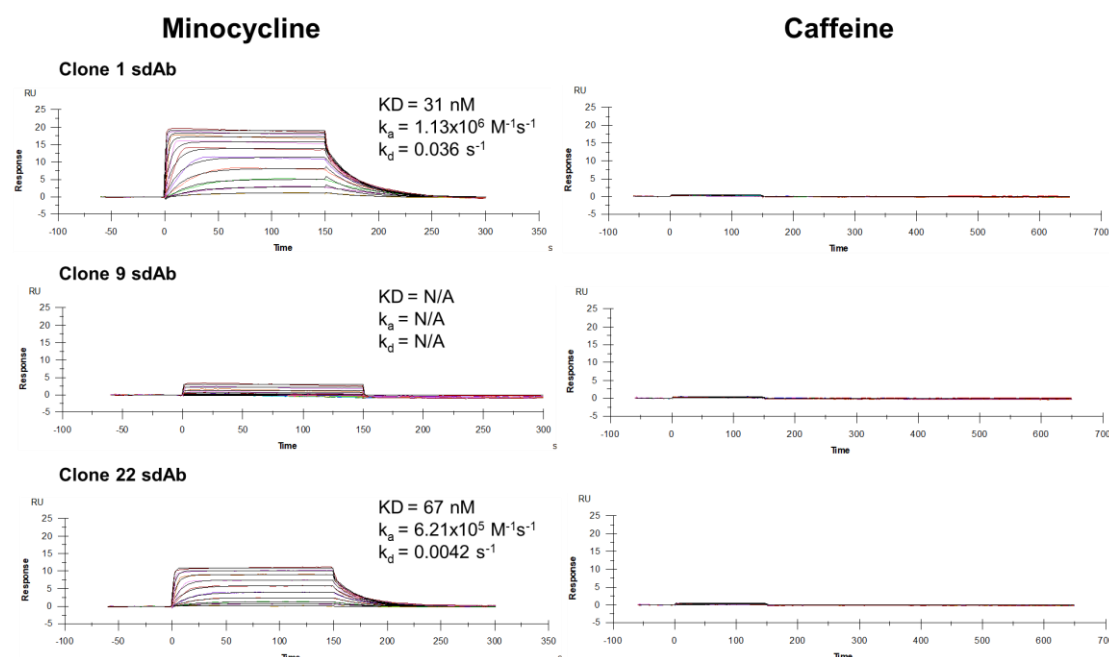
Clone	Target	k_a $M^{-1}s^{-1}$	k_d s^{-1}	KD (M)
1	Minocycline	1.13e06	3.6e-02	3.1e-08
	Caffeine	N/A	N/A	N/A
9	Minocycline	3.84e04	3.7e-02	9.74e-07
	Caffeine	N/A	N/A	N/A
22	Minocycline	6.21e05	4.2e-2	6.7e-08
	Caffeine	N/A	N/A	N/A

Figure 3.11. Surface plasmon resonance (SPR) of anti-minocycline sdAb-Fc clone 1, clone 9 and clone 22 binding to minocycline.

Anti-minocycline sdAb-Fc was immobilised by amine coupling to a CM5 chip, minocycline or caffeine were separately used as the analyte. Anti-minocycline sdAb clone 1 and clone 22 showed an affinity of 31 nM and 67 nM, respectively. In contrast, binding affinities of the anti-minocycline sdAb clone 9 were undetermined using Biacore SPR. Caffeine did not bind to sdAb-Fc conjugates.

Based on SPR, clone 1 presented the highest affinity interaction with minocycline. Therefore, in addition to SPR analysis, isothermal titration calorimetry (ITC) was used to study the thermodynamic parameters of antibody-minocycline interaction in solution and thus confirm the binding

affinity. Figure 3.12A shows a raw thermogram plot; Heat released during the initial ligand injections indicates the progression of an exothermic reaction as a result of antibody and minocycline binding. Upon successive ligand injections, release of heat is reduced (ΔH≈0) indicating sdAb-minocycline binding saturation. Figure 3.12B shows the binding isotherm plot which was generated by fitting the data points to a one set model in order to determine the binding kinetics of the reaction. The results confirm clone 1 sdAb to have an affinity of 25 nM (+/- 5.59 nM), which lies within the range indicated by SPR analysis.

A

B

c 1.1 (2uM) and minocycline (50uM) 201217
Model: One Set of Sites
[Cell] (M) = 2.00e-6
[Syr] (M) = 50.0e-6
N (sites) = 2.17 ± 2.0e-2
KD (M) = 24.9e-9 ± 5.59e-9
ΔH (kcal/mol) = -11.2 ± 0.252
Offset (kcal/mol) = -0.150 ± 0.156
ΔG (kcal/mol) = -10.4
-TΔS (kcal/mol) = 0.791
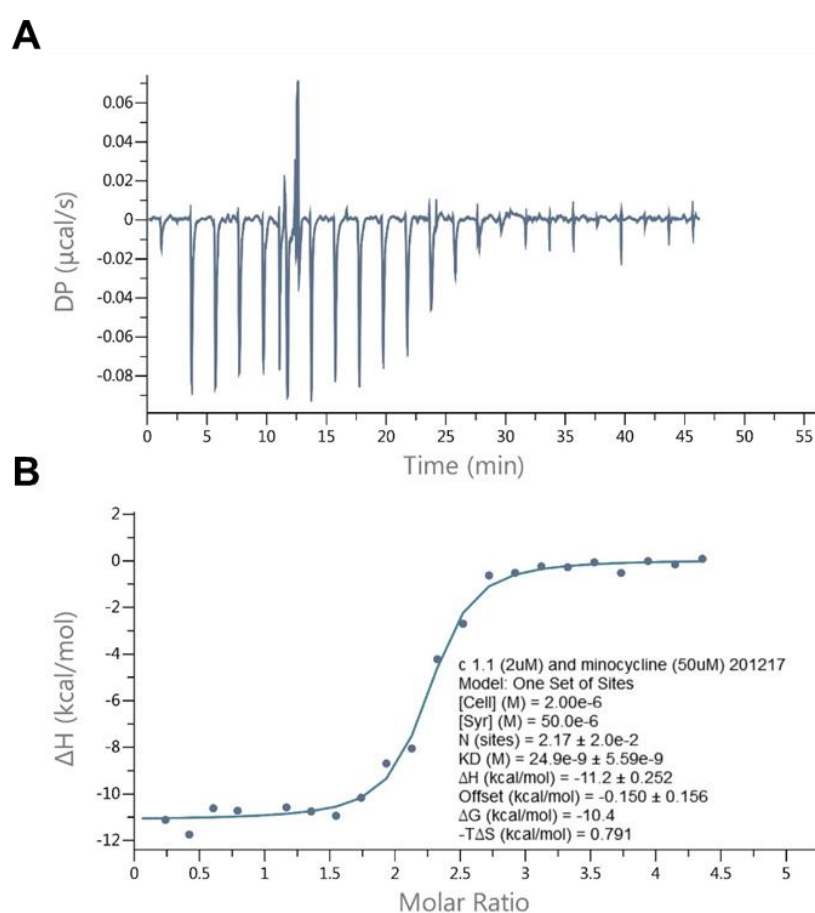
Figure 3.12. Isothermal titration calorimetry (ITC) thermogram of clone 1 sdAb binding to minocycline.

(A) Raw thermogram plot over time showing ligand injection and binding saturation; (B) Binding isotherm plot using the one set of sites (1:1) binding model (Origin's software) showing the molar ratio (of minocycline/anti-minocycline clone 1 sdAb) against the enthalpy change of the reaction which was used to deduce a KD value of 24.9 nM (± 5.59 nM).

3.4 Expression and purification of an unconjugated anti-minocycline sdAb

For downstream binding studies, an unconjugated anti-minocycline sdAb was required. Therefore, a construct expressing an untagged anti-minocycline sdAb sequence was used to transform NEB 5-alpha competent *E. coli* bacterial strain. Inoculum of transformed bacteria in 2TY media supplemented with Ampicillin and 0.1% glucose was used to generate the sdAb. The bacterial pellet (periplasmic extract) and culture supernatant was extracted and filtered using a 0.22 mm filter unit prior to PBS buffer exchange. A manual Protein-A Sepharose purification was carried out using the periplasmic and supernatant derived sdAb. Each fraction collected from the elution step of the protein-A affinity chromatography purification from the periplasmic and supernatant was analysed by sodium dodecyl sulphate (SDS) polyacrylamide gel electrophoresis (PAGE). SDS-PAGE analysis confirms the expected protein size of the unconjugated anti-minocycline sdAb of ~15 kDa as well as a predominant single band indicating successful purification (Fig. 3.13).
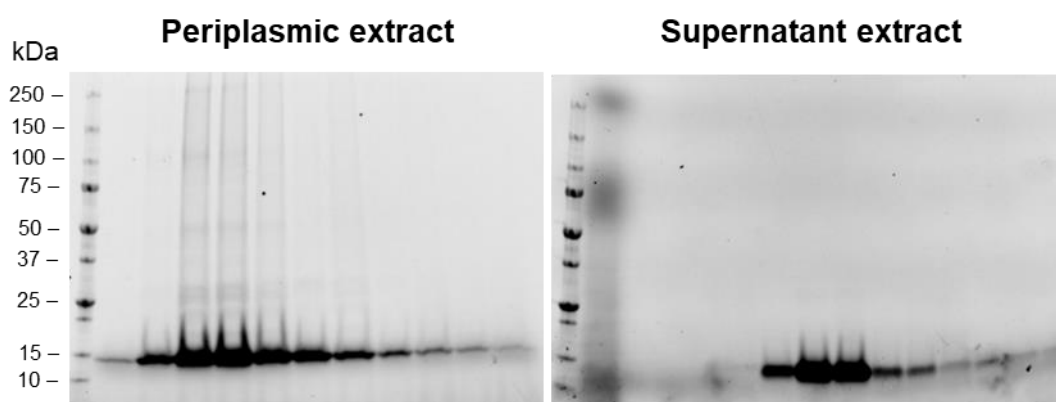
Figure 3.13. SDS page analysis of unconjugated anti-minocycline single-domain antibody fractions from periplasmic extract and supernatant extract.

Protein migration using SDS-PAGE. Each fraction collected from the protein-A affinity chromatography containing the unconjugated anti-minocycline sdAb clone 1 was prepared for loading using sample buffer consisting of 62.5 mM Tris-HCl, pH 6.8, 2% SDS, 25% (v/v) glycerol, 0.01% bromophenol blue. Each fraction sample was then incubated at 95°C for 5 minutes prior to being loaded to each lane of the gel. The mini-PROTEAN® TGX Stain-Free™ pre-cast 4-

20% gradient gel was used to run each fraction. Running buffer consisted of 25 mM Tris, 192 mM glycine and 0.1% SDS. 180V running voltage was used for 30-40 minutes. The Azure c600 Gel Imaging System by Azure Biosystems was used to image protein bands. Bio-Rad Precision Plus Protein Standards were used as reference protein ladder.

3.5 Investigation of conformational stability of the anti-minocycline antibody in the presence of binding partner

The conformational stability of the sdAb antibody in complex with various concentrations of minocycline were also investigated using nano differential scanning fluorimetry (nanoDSF). Through thermal unfolding transitions of the antibody's intrinsic fluorescence emission, predominately from the aromatic sidechains of tryptophan or tyrosine residues, assessment of the antibody unfolding and melting temperature (Tm) was carried out. Clone 1 sdAb showed a high first unfolding midpoint (Tm1) of 79.2ºC in the absence of minocycline. The presence of minocycline at a concentration of 0.001 μM, 0.01 μM, 0.1 μM, 1 μM, 10 μM, 100 μM and 1000 μM presented Tm1 values of 79ºC, 79.2ºC, 79.2ºC, 79.1ºC, 77.5ºC, 81.3ºC, 85.9ºC and 89.6ºC, respectively (Fig. 3.14). These results indicate clone 1 to be a highly stable sdAb antibody in the absence and presence of minocycline up to a concentration of 1000 μM.
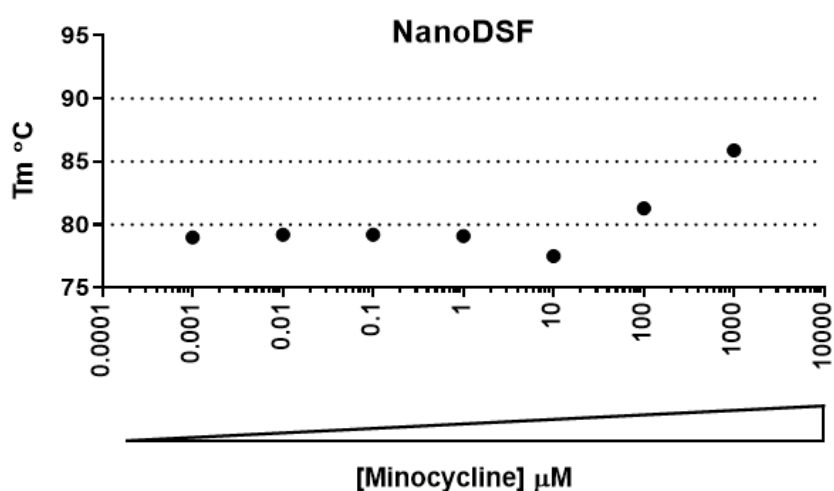
Figure 3.14. Analysis of sdAb stability by nanoDSF.

Thermal unfolding temperature (Tm) of anti-minocycline sdAb clone 1 in the presence of its binding partner at concentrations of 0.001 μM, 0.01 μM, 0.1 μM, 1 μM, 10 μM, 100 μM and 1000 μM Temperature gradient relationship to

F350/F330 fluorescence reading ratio. Protein concentration of 1 mg/ml suspended in PBS buffer solution (pH ~ 7.4).

3.6 Confirming stability and specificity of the anti-minocycline antibody fused to a cell-membrane

My intention was to use the isolated clone 1 sdAb to form the binding domain of a CAR structure which would be anchored to the cell surface. As the expression and stability of ScFv or sdAb antibody fragments as Fc-conjugates and as a membrane bound component of a CAR architecture do not necessarily correlate, it was imperative to test the expression levels and minocycline binding capacity of the anti-minocycline sdAb clone 1 in the context of a CAR before proceeding with generating peptides targeting the anti-minocycline sdAb clone 1. Therefore, the anti-minocycline sdAb clone 1 was incorporated into the extracellular portion of a CAR architecture by fusing the sdAb to the N-terminus of a CD8α spacer, CD8α transmembrane and a 4-1BB-CD3ζ co-stimulatory and signaling domains. RQR8 was used as a marker gene separated by the Thosea asigna virus 2A (T2A) self-cleavage peptide downstream of the CAR.

Expression of the anti-minocycline CAR was determined by staining cells using biotinylated BSA-conjugated minocycline, followed by streptavidin-PE. The anti-minocycline CAR T cells demonstrated significant binding to biotinylated-BSA-minocycline by means of fluorescently labelled avidin detection which was shown to be directly proportionate to that of the RQR8 marker gene (Fig. 3.15). Thus, indicating the anti-minocycline sdAb to be stable as a CAR architecture in the context of a cellular membrane and capable of binding minocycline when expressed on the surface of a cell, without risk of lower transgene expression, suboptimal sdAb transport to the cell membrane, or steric hindrance of sdAb binding.
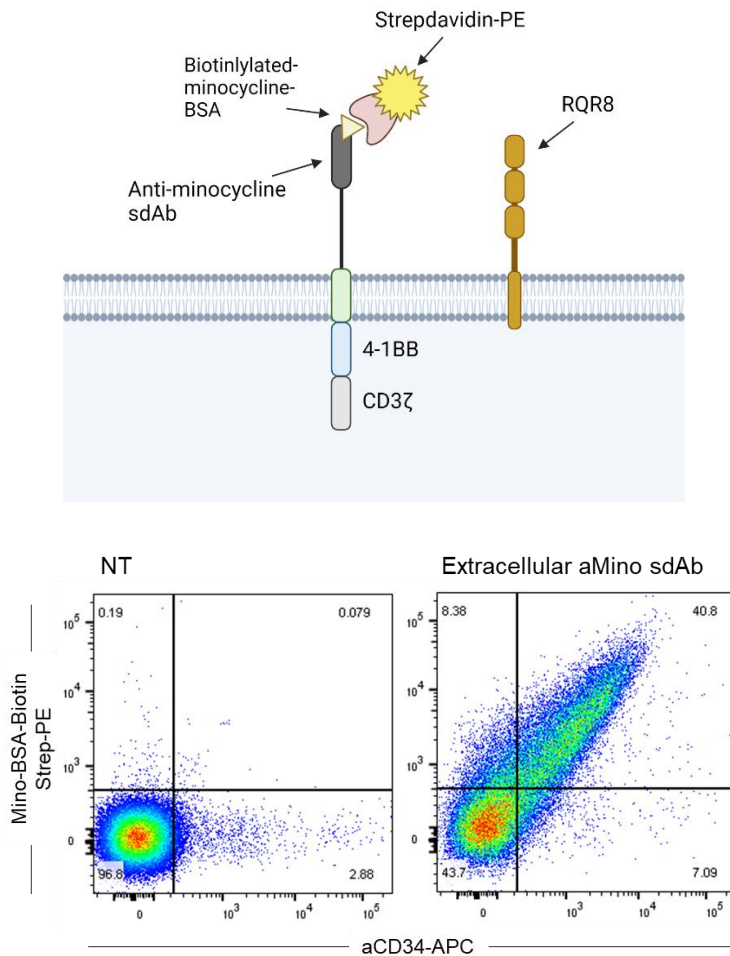
Figure 3.15. Extracellular expression of anti-minocycline sdAb clone 1 is stable in the context of a CAR scaffold.

293T were transfected to express anti-minocycline sdAb clone 1 CAR (sdAb/CD8α spacer/-transmembrane/4-1BB-CD3ζ) and a RQR8 cell surface marker. Expression levels of the CAR was tested by staining cells with minocycline-BSA-biotin followed by streptavidin-PE. RQR8 expression was tested using anti-CD34-APC.

3.7 Discussion

Antibodies are fundamental components of CAR T cell-based therapy in addition to other cellular therapies, diagnostics, and basic research applications. Conventional antibodies have shown a proven track record as powerful tools in cancer immunotherapy and CAR T cell applications. However, the continuous technological progress in the development of immunotherapies against solid tumours as well as the dynamic control of CAR T cells means additional protein components are needed. Here, the bulky protein structure and the limited real estate of the lentiviral or retroviral cassette for T cell based therapeutic applications means conventional antibodies are at a disadvantage.

Camelidae derived heavy chain antibodies (hcAbs) hold the potential to serve as an attractive alternative to conventional antibodies. HcAbs binding to antigens is achieved through a single domain known as VHHs (variable domain of heavy chain antibodies)/sdAbs (single-domain antibodies). SdAb display several desirable properties including extreme stability, improved tissue penetration, high levels of solubility and small size (~15 kDa).[218,219] Furthermore, reports have shown sdAbs are capable of binding cryptic epitopes inaccessible by conventional antibodies.[220]

To generate a comprehensive catalogue of anti-minocycline sdAb sequences through immunised alpacas, the alpaca must be capable of eliciting an immune response against the antigen. However, unsurprisingly many antigens (especially antibiotic drugs such as minocycline) are non-immunogenic, and the immune cells are incapable of eliciting an immune response, particularly against small and cryptic epitopes presented by small molecular weight compounds and peptides.[221] Therefore, such antigens have been historically injected in cocktail with an adjuvant in order to enhance the antigen immunogenicity.[222,223] Although adjuvants such as Freund's and Gerbu have been used to achieve this, many adverse effects such as severe inflammatory response have been linked to their use.

As the adjuvant only enhances the immune response rather than altering the immunogenicity of the antigen, non-immunogenic antigens must be coupled

to a large carrier protein to elicit an antigen specific immune response. To date, carrier proteins such as the keyhole limpet hemocyanin (KLH), ovalbumin (OVA) and bovine serum albumin (BSA) have been the most extensively used in research. The phylogenetic distance of KLH and mammalian proteins, as well as the presence of multiple amine groups allows for coupling with minocycline for a targeted immune response.[224] In this study, engineering of the free sulfhydryl group on minocycline was used to carry out maleimide linkage to KLH, which has been shown to maintain superior efficacy over other chemical conjugations such as glutaraldehyde linked KLH.[225] Most importantly, maleimide linked KLH conjugates have shown to possess superior antigen-specific antibody and T cell responses.[225] A positive serum screen confirmed KLH protein was sufficient in eliciting an immune response in the alpaca.

The structural interaction of conventional antibodies targeting low-molecular weight compounds have been investigated and well characterised.[226–228] These reports have shown hapten binding takes place primarily at VH and VL interface, specifically at each respective CDR3 converging loop structures. Despite the reduced binding interface of sdAbs due to lack of an interacting light chain, many sdAbs have been generated to haptens which bear affinities against target haptens comparable to conventional antibodies. For example, sdAb against haptens such as the myotoxin 15-acetyldeoxynivalenol, herbicide picloram, caffeine, red azo-dye RR6 and RR120, sulfonamide antibiotics and methotrexate have been characterised.[200,211–215] Many sdAb-antigen complexes have been described, however, for the vast majority of anti-hapten sdAbs there is minimal structural data revealing the mechanisms of hapten binding. Structural and biophysical data has shown sdAbs bind to haptens via many mechanisms, for example, through the precursory VH interface or via hapten induced sdAb homodimersation.[67,229,230]

In all, only five anti-hapten sdAbs in complex with each respective small molecule have been reported and available on the PDB database. These include, sdAb complexed with azo-dye RR6,[67] RR1,[229] methotrexate[195], triclocarban,[231] and cortisol.[232] The red azo-dyes have a much larger molecular

145

weight resulting in a large surface of interaction between the sdAb and the hapten. The mechanism of binding is like that of conventional antibodies, where the sdAb allows an efficient binding site involving all three CDRs. Specifically, the CDR1 imparts the greatest degree of interaction to the hapten via pair of histidine amino acid residues bound to the RR6-copper complex. In all this results in a dissociation constant of 22 nM.[67]

On the other hand, the molecular weight of methotrexate, triclocarban, and cortisol is 454.44 Da, 315.58 Da and 362.46 Da, respectively, therefore, comparable to the molecular weight of minocycline at 457.47 Da. X-ray crystallography of the four sdAb-hapten complexes show a unique mechanism of antigen binding. CDR1 was shown to be key to hapten binding over hapten interaction with the most variable region, CDR3. Despite the fact each CDR3 length and structure varied, each hapten appeared to show specific interaction with the CDR1 via their hydrophobic core. Interestingly, using structural analysis of the anti-methotrexate sdAb in complex with methotrexate, Fanning and Horn showed a novel mechanism of hapten binding. Firstly, substantial methotrexate surface burial was shown to be greater than levels found in conventional antibodies targeting small molecule ligands of less than 700 Da. This greater degree of penetration and surface interaction is likely to is key to gaining high affinity and specificity against the hapten. A non-hypervariable region outside of CDR1-3, termed as CDR4, residing within the framework region (FR)3 below CDR1 was found to interact with the hapten and drastically contributed to generating a high-affinity interaction with methotrexate. This, however, may not be completely unexpected as CDR4s have been used in affinity maturation and shown to significantly (up to 100-fold) increase the KD value of conventional Fab antibodies.[233] Fanning and Horn demonstrated mutating the CDR4 non-hypervariable loop of the anti-methotrexate sdAb improved binding affinity towards methotrexate from 6.7 µM to 5 nM.[195] Therefore, the CDR loop interaction outside of the CDR3 region may be significant when interacting with haptens.

Successfully isolating small molecule specific sdAbs is dependent on the generation of a large and highly diverse sdAb library composing of at least 10^5

clones.[218] Immunisation of animals to generate immune phage libraries is a viable approach for isolating specific sdAbs because a library size of 10^6 and 10^8 is typically generated.[234] Furthermore, selection of high affinity sdAbs is achieved through the exposure to the antigen and somatic hypermutation which leads to further improvements in binding affinity of each sdAb clone. Typically, a sdAb library is acquired by using peripheral blood mononuclear cells (PBMCs) as the genetic source to synthesise cDNA for library construction even though PBMCs are suboptimal in antigen specific sdAb enrichment. When using small rodents such as mice or rats as the donor for antibody production, the spleen or lymph node is extracted for cDNA synthesis since lymphocytes migrate and reside within the lymphoid organs rather than peripheral blood.[235] Nonetheless, there are many advantages with the use of PBMCs over spleen or lymph nodes as PBMCs can be screened many times through serum samples without the need to sacrifice the animal.[235] In addition, the library size may also be limited by factors such as number of B-cells isolated, mRNA yields and electroporation efficiency.[236] Through counting of the colony forming units (cfu) we showed the library generated an estimated size of 5×10^8 unique clones, which would be diverse enough to isolate high affinity antigen specific antibody clones.

To select minocycline specific sdAbs from the sdAb library, the phage display method was utilised. Phage display panning/selection consists of antigen coating, blocking, phage incubation and binding, washing and elusion. Over the past decade, many technical advancements have allowed for the optimal efficiency in high affinity antibody selection using a small molecule as the panning agent. Alongside the blocking buffer and rigorous washing steps, correct immobilisation of the antigen is essential. Generally, panning targets are passively immobilised to a solid surface such as magnetic beads[237], nitrocellulose[238] or polystyrol tubes/wells[45,239] without requiring chemical alteration of the target.[51] However, passive immobilisation may result in occultation of functional groups or may not be possible with small molecules.[240] Additionally, many antibodies have been reported in the literature to present weak binding affinities to free haptens.[237] Therefore, knowledge of organic chemistry is essential in immobilising small molecules

onto solid surfaces prior to panning. Such methods include direct chemical conjugation, self-assembling monolayer on a gold chip or biotinylation of the small molecule for streptavidin-coated beads.[241] As the vaccination strategy utilised minocycline conjugated to KLH, the selection of anti-minocycline antibodies was performed using an immobilised minocycline chemically coupled to BSA and coated on ELISA microplates thus, allowing for the selection of minocycline specific binders over the carrier protein. Furthermore, to exclude binders generated against the engineered free-SH group, SPR studies were carried out using unconjugated drug to show drug specific specificity only as well as excluding binding to structurally related molecule such as caffeine. The binding affinity and kinetic constants of clone 1 and clone 22 showed affinities of 31 nM and 67 nM, respectively. These results validate the affinity and kinetic profiles of isolated sdAbs being of high affinity and comparable to sdAb targeting protein antigens.[76,242]

The diversity generated through VH-VL pairing of conventional antibodies is lost in the case of sdAbs due to the lack of a VL domain. Therefore, to compensate for reduced diversity, *Camelidae* have evolved higher antibody somatic diversification processes such as gene conversion and somatic hypermutation.[64] With the latter being facilitated by hypermutation hotspots such as AGX and TAX motif (where X is C or T) to enhance the binding affinity of the VH/VHH repertoire.[72] Alpaca and dromedary IGHV genes reside within the same subgroup IGHV1 and make use of distinct sets of V genes encoding the VHH domain of HCAbs.[72] The tendency for a higher rate of somatic hypermutation was also observed in the sequences of the anti-minocycline sdAbs. Clones #1 and #4 have identical CDR3 sequence, but they differ in their CDR1 by three out of eight amino acid residues (37.5%). Furthermore, clone #1 and #32 have identical CDR3 sequence, but different in their CDR1 by four out of eight amino acid sequences (50%). In summary, out of the 14 positive clones, five CDR1, four CDR2 and four CDR3 unique sequences were generated. Such nuanced variations of the CDR sequences align with descriptions of somatic hypermutation hypervariability plots generated during VHH diversity generation.[72]

Alongside an increased somatic hypermutation rate, sdAb diversity is also generated through V-D-J recombination like that observed in conventional antibody diversity generation. These CDR1-3 sequence results show clone #1 and #9 having matching CDR1 and CDR2 but a different CDR3 sequence, this is likely a result of a different D segments being utilised during V-D-J recombination event with the CDR3 loop providing the key interaction with its target antigen.[65,220]

Although the VHH domain is composed of 4 framework regions (FR1-FR4) which rotate with 3 hypervariable regions (CDR1-3), like that of the VH domain structure, the CDR3 loop generated from the V-D-J junction typically bear an extended CDR3 length. Such an extended CDR3 region not only provides greater binding interface for interaction with cryptic epitopes but also provides greater structural diversity which allows access to epitopes inaccessible by VH domains of conventional antibodies.[64] As both heavy chain formats utilise the same D-J gene segments, the evolutionary selection of extended CDR3 structure is most likely attributed the use of two or more D segments during V-D-J recombination or via increased terminal deoxynucleotidyl transferase activity.[243] Evidence of elongated CDR3 structure was confirmed from sequencing data of the anti-minocycline sdAb clones which all possessed a CDR3 length of 14 amino acids.[64,244] Although the average CDR3 length of sdAbs is approximately 16 amino acids, each of the isolated clones showed greater CDR3 length compared to the average of 9-12 amino acids observed in conventional IgGs.[243] These CDR3 residues are potential candidates for direct interaction with minocycline but would require homology modelling and structural guided alanine scan mutagenesis or crystallography of the sdAb-minocycline complex.

The highest affinity sdAb isolated was clone #1, where the equilibrium dissociation constant (KD) of the sdAb-minocycline complex was measured at 31 nM as determined Biacore SPR spectroscopy and 25 nM as determined by ITC. The affinity values were comparable or improved to previously described KD values of other sdAb and low-molecular weight compounds; Such as sdAbs targeting PP6 dye (KD=2.5 nM),[245] picloram (KD=3-254 µM),[213] auxin

(KD=0.5-20 μM),[246] methotrexate (KD=29-515 nM),[212] 15-acetyl-deoxynivalenol/15-AcDON (KD=5 μM),[215] and triclocarban/TCC (KD= 0.98-1.37 nM).[247]

As the broader aim of the project was to develop a protein-protein interaction system for CAR T cell signaling or retention of an anti-tumour cargo. It was paramount for the interaction to be specific and long-lasting between the protein components of the system, of which the sdAb was one. With such applications, the minocycline is used to displace the interaction between the anti-minocycline sdAb and a sdAb specific peptide as the minocycline possesses a higher affinity for the sdAb than the peptide. Therefore, the affinity of the sdAb for minocycline must be in the high nanomolar range, to displace the sdAb-peptide interaction but also to allow for the affinity interaction between the sdAb and peptide to be high enough (also in the high nanomolar range) for the interaction to allow signal transduction in CAR T cells or to efficiently bind to the peptide conjugated to an anti-tumour cargo molecule.

An affinity of 31nM lies within the nanomolar range of affinities previously described for a small molecule-based control system. For example, work carried out by Hotblack et al. shows the development of an inducible OFF-switch CAR (TetCAR) which also utilised minocycline or tetracycline as a disrupting small molecule (Fig. 1.13).[187,188] In the TetCAR system, the antigen-binding chain of the CAR comprises of the tetracycline-binding TetRB protein which interacts with a peptide mimic of tetracycline known as TIP, fused to a CAR signalling endodomain. This interaction takes place with a KD of 640 nM.[248] This functional interaction is disrupted through the presence of tetracycline which interacts with TetRB with an KD of 2.8 nM.[249]

Furthermore, Greta Giordano-Attianese et al. also developed a synthetic inducible OFF-switch CAR where a small molecule drug disrupts the interaction between the antigen-binding and signaling chains. Bcl-XL protein (on the antigen-binding chain) interacts with a computationally designed LD3 protein (on the signalling chain) to form a functional heterodimeric CAR. Through the administration of a clinically unapproved drug, Bcl-XL and LD3

interaction is disrupted by binding to Bcl-XL as a result of having an affinity of <10 pM for Bcl protein.[187]

The conformational stability of clone 1 was tested using differential scanning calorimetry fluorimetry (NanoDSF). In addition, the conformational stability of clone 1 in complex with various concentrations of minocycline was also confirmed. NanoDSF is a method for determining the melting temperature (Tm) of antibodies by measuring protein unfolding via changes in fluorescence because of temperature. NanoDSF measures changes in intrinsic fluorescence emission as the antibody unfolds, predominately from the aromatic sidechains of tryptophan or tyrosine residues.[250]

Previous work has shown sdAbs to be more stable than conventional Abs, scFv and Fab. The high thermal stability of sdAbs is likely due to its unique structural features and small size. The longer CDR loops of sdAbs have been shown to bear constraining disulphide bonds to form binding sites and are thought to play a role in improving the thermal and confirmational stability of sdAbs as mutagenesis of these cysteine residues have shown to significantly reduce the Tm.[251–253] Other works have also shown to increase thermal stability as well as resistance to proteolysis and low pH conditions by introducing a non-canonical disulphide bond between FR2 and FR3 region.[254,255] A study looking into the relationship between sdAb thermal resistance and the number of disulphide bonds, showed while increasing the number of disulphide bonds increased the Tm, the sdAb half-life at 90°C was reduced.[256] It was also shown that substitution of cysteine residues with suitable amino acids can improve thermal resistance of a sdAb.

Interestingly, clone 1 did not bear constraining cystine residues within the CDR region, however 2 cysteine residues were present between the FR1 and FR3 region which is typical of most of the sdAb generated against small molecules (Table 3.2). From the literature, sdAbs generated against PP6 dye,[245,257] picloram,[213] auxin,[246] caffeine,[200] methotrexate,[212] 15-AcDON,[215] Ochratoxin-A,[258] TCC,[247] 2,2',4,4'-tetrabrominated diphenyl ether (BDE-47),[259]

tetrabromobisphenol A (TBBPA),[260] and aflatoxin-B1[261] all possessed a total of 2 cysteines within the FR1 and FR3 region.

With regards to binding to small molecules, van der Linden et al. first demonstrated sdAbs can maintain binding to small molecules up to 90°C, whilst conventional Abs cannot do so.[257] Most of the literature on the study of thermal stability of sdAb in presence of their small molecule binding partner has been carried out by assessing binding capacity or Tm measurements. Overall, these show sdAb have greatly increased thermal stability compared to the respective conventional Ab. For example, the sdAb generated against caffeine presented enhanced stability over the conventional murine Ab counterpart.[200] The anti-caffeine sdAb maintained the majority of its activity 20-minute post incubation at 90°C, whereas binding was completely abolished for commercial anti-caffeine mAb upon incubation at 70°C. However, not all functional sdAbs present high thermal stability, Franco et al. described an anti-caffeine sdAb which presented poor thermal stability with a Tm of only 56 °C.[262] Tabares-da Rosa et al. described the generation of 5 sdAbs targeting triclocarban (TCC), each showing enhanced stability and binding relative to a conventional rabbit Ab up to 85°C.[247] Similarly, the 2,2′4,4′-tetrabromodiphenyl ether (BDE47) targeting sdAb showed to maintain 50% of BDE47antigen compared to <5% binding activity of a conventional Ab after incubation at 95°C for 10 minutes.[259]

Although our proposed immunotherapy-based application was not temperature sensitive, we characterised the thermal stability and proper domain folding of the anti-minocycline clone 1 to confirm that the selected clone was highly stable and comparable to other sdAbs generated against small molecules such that future robust applications were available to explore. In doing so, we selected an optimally stable sdAb which was also stable in the presence of minocycline at a concentration up to 2500mM where the Tm1 ranged between values of 77.5ºC - 89.6ºC (Fig. 3.15).

Due to the previously mentioned advantages of sdAbs, many groups have aimed to develop CAR T cell therapies based on using sdAbs as the antigen-

binding domain. The first described use of sdAb as a part of a CAR structure utilised an anti-MUC1 sdAb fused to a human IgG3 hinge spacer region and a CD28-CD3ζ signaling domains. This CAR showed stable cell surface expression, MUC1+ target cell lysis, IL-2 secretion, and proliferation.[263] Based on encouraging results from the proof-of-concept work carried out using the anti-MUC1 CAR. CAR T cells bearing a sdAb targeting HER2[207] and TAG-72[264] were also developed. In total, five sdAbs were generated from a HER2 immunized camel, which were then fused to a hinge spacer, CD28 transmembrane and CD28-CD3ζ or CD28-OX40-CD3ζ signaling endodomains. Similarly, the anti-TAG-72 sdAb was also fused to an identical CAR structure. Since the initial reports of sdAb based CARs, many tumour targets have been explored and characterised for sdAb based CAR T cell therapy each possessing various spacer, transmembrane, co-stimulatory and signalling domains, showing stable cell-surface expression, IL-2 secretion, and cytotoxic activity upon target cell engagement. For example, anti-VEGFR2 and anti-PSMA sdAbs fused to a IgG1-Fc spacer, CD28TM and CD28-CD3ζ signaling domains; anti-PD-L1 and anti-EIIIB sdAbs fused to a CD8α spacer, CD8αTM and CD28-CD3ζ signaling domains; and an anti-CD38, anti-BCMA, anti-CD20 and anti-CD33 fused to a CD8α spacer, CD28TM and 4-1BB-CD3ζ signaling domains. Additionally, a bi-epitopic tandem anti-BCMA sdAb fused to a CD8α spacer, CD28TM and 4-1BB-CD3ζ signaling domains was also developed.

The monovalent anti-BCMA sdAb based CAR-T cell (PRG1801), bearing a 4-1BB-CD3ζ endodomains, has progressed to clinical studies with promising results.[265,266] Another anti-BCMA CAR T cell, developed by Nanjing Legend Biotech, utilises dual anti-BCMA sdAbs targeting independent epitopes within the BCMA antigen and also shown promising clinical outcomes.[204,267,268] With reports indicate clinical efficacy is comparable to the scFv based anti-BCMA CAR (bb2121) developed by Bluebird.[269]

As my aim was to use the isolated clone 1 sdAb to form the binding domain of a CAR structure, the anti-minocycline sdAb clone 1 was solely incorporated into the extracellular portion of a CAR architecture. In doing so I confirmed the

anti-minocycline sdAb clone 1 to be stable as a CAR architecture in the context of a cellular membrane and capable of binding minocycline when expressed on the surface of a cell (Fig. 3.16), thus, excluding potential risk of lower transgene expression, suboptimal sdAb transport to the cell membrane, or steric hindrance of sdAb-minocycline binding. However, further characterisation of CAR expression will be required once expressed in association with a tumour targeting sdAb (a dual sdAb CAR structure).

In this chapter, I have discovered and presented evidence of the isolation of single-domain antibodies derived from an immunised alpaca phage display library capable of binding minocycline. The highest affinity clone will be used as the foundation to develop a peptide capable of interacting with the sdAb but displaced in the presence of the drug. This forms the foundation of a protein-protein displacement system.

3.8 Conclusions

- Immunised alpaca produced specific antibody response to minocycline

- Phage display library successfully produced multiple unique sequences specific for minocycline

- Out of all tested anti-minocycline sdAb clones, the binding affinity of clone 1 showed to have the highest affinity for minocycline (KD= 31 nM by SPR and KD= 25 nM by ITC)

- Stability studies indicate the clone 1 sdAb is highly stable in solution with and without the presence of minocycline.

- The sdAb is stably expressed in the context of a cell-membrane and successfully detected by minocycline staining.

4 GENERATION OF A DISPLACEABLE CYCLIC PEPTIDE SPECIFIC TO THE ANTI-MINOCYCLINE SINGLE DOMAIN ANTIBODY

4.1 Introduction

Protein-protein interactions involving cyclic peptides have been shown to have many desired properties which would make them an ideal binding partner for the minocycline specific sdAb: cyclic peptides can be designed to bind to macromolecules with a high affinity as well as high degree of selectivity between similar amino acid residues folded in the same tertiary structure and showing high degree of sequence homology. As a result of flanking cysteine residues and subsequent formation of stabilising di-sulphide bonds, cyclic peptides are highly stable in comparison to linear peptides which are prone to degradation by protease activity. Furthermore, the low immunogenicity of cyclic peptides poses an attractive prospect for incorporating cyclic peptides as a part of an immunotherapy application.

Approximately 40 cyclic peptide-based drugs have been approved for use in the clinic for the treatment of a range of conditions such as cardiovascular diseases, infectious diseases and cancer.[270] Most of these cyclic peptides have been derived from microorganisms and animals in the form of the antibiotics such as vancomycin and daptomycin and hormones such as oxytocin and vasopressin. Historically, cyclic peptides have been isolated and purified from nature with a small percentage of cyclic peptides being generated de novo cyclization of natural linear peptides.

The advent of in vitro evolution technology, such as phage display, has enabled the generation of cyclic peptide binders against protein molecules with no natural binding ligands. The technology is based on displaying a cyclised peptide on the exterior of the phage particle through a disulphide bridge between flanking cysteine residues in reducing conditions, hence the term cysteine-constrained peptide. Since its discovery in 1985, the technique has been widely applied and proven to be highly robust with a catalogue of cyclic peptides having been characterised and reported in the literature. For example, the first phage library construction in the form of random cysteine

constrained peptides, XCXXXXXXCX-phage were shown to generate a diverse range of high-affinity peptides targeting the glycoprotein IIb/IIIa.[271] Cysteine constrained cyclic peptide library in the form of XCXXXXCX were also generated against streptavidin and the monoclonal antibody targeting β-endorphin.[272]

Since the success of these reports, many cyclic cysteine constrained peptides have been generated. With most of the consisting of the following format: XCXnCX where n=4−10aa. Which also includes the commercially available and widely used Ph.D.-C7C library from NEB of the following format: XCX7CX.[273] Conversely, phage display peptide libraries have also been shown to utilise a single cysteine residue which randomly forms a disulphide bond with a cysteine residue along the randomly occurring peptide sequence. Similarly, the use of fixed cysteines residues in three locations have also been used to generate peptide sequences circularised by two disulphide bonds.[274]

Naïve peptides can be fused to the exterior of the M13 phage major coat proteins (pVIII) or the minor coat protein (pIII) to achieve high or low valency interactions with their binding partner, respectively. The avidity effects of polyvalent peptide display on pVIII increases the binding interaction to target molecules compared to the intrinsic monovalent affinity of the peptide. In order to discriminate solely on the binding peptide characteristics over avidity effects, fusion of monovalent peptides to pIII is favoured. Low valency monovalent pIII fused peptide libraries allow rigorous selection of high-affinity peptide binders solely based on variance in either the peptide sequence, structure or interacting side chains. In addition, the affinity ranges of monovalent pIII fused peptide from phage particles correspond to the intrinsic affinity range of independently expressed peptides therefore allowing tolerance of the peptide expressed freely or on the cell-membrane. Identification of potent binding sequences by ELISA can facilitate detailed biophysical characterisation of these peptides to monitor and select only the highest affinity sequences capable of being displaced. Advances in methodologies and availability of large complex phage library kits with optimised protocols has allowed for the generation of high affinity peptides against targets such as novel single domain antibodies.

In this chapter, I aim to screen the Ph.D. XCX7CX-peptide library in order to identify peptides which bind to the anti-minocycline dAb clone 1 which can also be displaced by minocycline in order to form the envisaged two-component protein interaction system.

4.2 Aims

- Identify cyclic peptide sequences capable of binding to anti-minocycline sdAb clone 1

- Displace peptide from sdAb complex using minocycline

- Show peptide re-binding post minocycline displacement

4.3 Results

4.3.1 Phage selection and assessment of anti-minocycline sdAb binding peptide sequences using an M13-phage ELISA

The proposed strategy for the generation of disulphide linked cyclic peptides displayed on M13 bacteriophage is shown in Figure 4.1. The Ph.D.-7 Phage peptide (New England Biolabs) library is a combinatorial library which bears randomised heptapeptides on the exterior of the M13 phage minor coat protein, pIII.[275,276] The 7-mer polypeptide sequence is displayed at the N-terminus of pIII, fused to a G3S linker, followed by the pIII sequence.[273] To identify peptides capable of binding anti-minocycline sdAb clone 1 but displaceable in the presence of minocycline, an M13 phagemid library of cysteine-constrained 7mer peptides (CX7C) was utilised with a modified selection strategy. The CX7C peptide phagemid libraries were panned against biotinylated anti-minocycline sdAb that had been conjugated to streptavidin-coated beads. Rather than elute the bound phage using glycine-HCl as described previously in phage elution protocols, bound phage was eluted using 1 µM minocycline (Fig 4.1). In doing so, I anticipated the enrichment of phage populations specific for the anti-minocycline sdAb but showing lower affinities compared to minocycline and therefore displaceable by the drug. Following elution with 1 µM minocycline, the enriched phage library was recovered, amplified, and further incubated with the immobilised anti-minocycline sdAb for a total of three rounds of affinity selection.
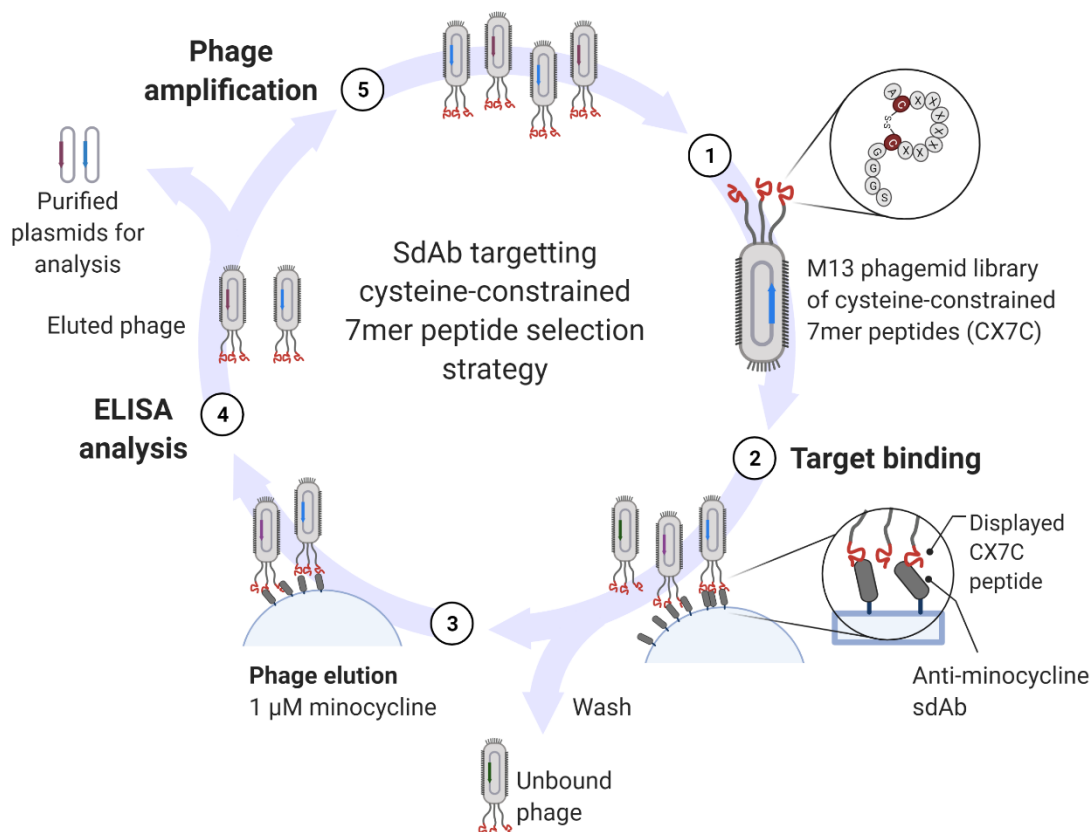
Figure 4.1. Panning and selection strategy for the isolation of minocycline displaceable cysteine constrained peptide sequences using a phagemid library.

(1) The Ph.D.-7 Phage peptide library contains the M13 phagemid combinatorial library which contains randomised cysteine-constrained heptapeptides (CX7C) on the exterior of the M13 phage minor coat protein, pIII. (2) The phage library was panned against biotinylated anti-minocycline sdAb conjugated to streptavidin-coated beads. (3) Bound phage was eluted using 1 µM minocycline. (4) Whole-M13 phage ELISA was carried out to determine binding to anti-minocycline sdAb. (5) Enriched phage library was amplified and a further three rounds of panning against immobilised anti-minocycline sab were carried out prior to analysis and isolation of peptide sequences.

Monovalent peptide display allows for the investigation of peptide affinity and displaceability whilst the peptide is still fused to the phage particle. By carrying out a competition whole phagemid anti-M13 ELISA, peptide candidates with desired characteristics can be rapidly identified for expression and

159

characterisation. Therefore, after three rounds of selection and panning, randomly selected monoclonal M13 phagemid clones were examined by ELISA to determine binding capacity against immobilised anti-minocycline sdAb. The phage bound to immobilized anti-minocycline sdAb were detected using anti-M13 antibody conjugated to horse radish peroxidase (HRP). Importantly, binding of phage particles was also carried out in the presence of 1 μM minocycline to confirm exclusive minocycline binding and peptide displacement, whether as a result of competition for the same binding epitope or induction of conformational changes to prevent peptide binding.

The anti-M13 phage ELISA showed 85% of selected monoclonal phage clones were positive for sdAb-Fc binding in the absence of minocycline, with a significant reduction of peptide-phage binding to the sdAb in competition with minocycline at 1 μM (Fig. 4.2). These results indicate that the sdAb shows preferential binding to minocycline over CX7C peptides. Non-selective binding was ruled out based on lack of binding to immobilized milk protein as a source of non-specific binding. Although the phage ELISA results do not quantitatively measure the binding constant because the exact phage concentration or peptide display levels on each phage is not known, the competition ELISA provides a binary determinate for binding and displacement of a multitude of potential peptide sequences for further isolation and characterisation.

Monoclonal CX7C Phage ELISA
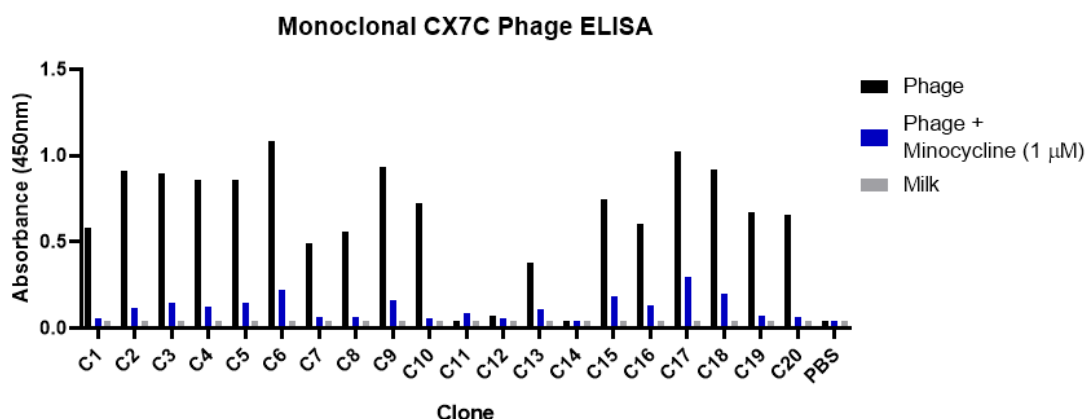
Figure 4.2. Anti-M13 ELISA of monoclonal whole phagemid clones (C1-C20) displaying CX7C-peptides binding to immobilised anti-minocycline sdAb in the absence and presence of minocycline (1 µM).

Plates were coated with anti-minocycline sdAb (1 µg/ml), monoclonal whole phage were incubated prior to detection with anti-M13-HRP.

4.3.2 Four unique cysteine-constrained peptide sequences bind to anti-minocycline sdAb

Upon sequencing the peptide coding region of the positively binding monoclonal phage, a total of 4 unique peptides sequences were determined out of 20 clones, with amino acid differences at positions CX_2, CX_5 and CX_6 (Table 4.1).

CX7C Scaffold Sequence	Peptide name
Ala-Cys-Pro-Gly-Trp-Ala-Arg-Ala-Phe-Cys / ACPGWARAFC	GWARA
Ala-Cys-Pro-Gln-Trp-Ala-Met-Met-Phe-Cys / ACPQWAMMFC	QWAMM
Ala-Cys-Pro-His-Trp-Ala-Gln-Ala-Phe-Cys / ACPHWAQAFC	HWAQA
Ala-Cys-Pro-Pro-Trp-Ala-Tyr-Ser-Phe-Cys / ACPPWAYSFC	PWAYS

Table 4.1. Anti-Minocycline sdAb binding peptides, abbreviated as GWARA, QWAMM, HWAQA and PWAYS, selected from a naïve CX7C phagemid library

All four CX7C peptides, were abbreviated as GWARA, QWAMM, HWAQA and PWAYS, based on the three amino acid differences between the cysteine residues. Peptide sequences were fused to the N-terminus of an IgG2a-Fc antibody structure and expressed in Chinese hamster ovarian (CHO) cells using transient transfection. The peptide-Fc complexes were then purified using protein-A affinity chromatography for subsequent biophysical characterisation. Firstly, the purified antibodies were analysed by sodium dodecyl sulphate (SDS) polyacrylamide gel electrophoresis (PAGE) analysis in reducing and non-reducing conditions to confirm predicted antibody size as well as the presence of a single predominant protein band. Under reducing conditions, the molecular weight of the peptide-Fc conjugates was confirmed in accordance with the predicted molecular weight (Fig. 4.3C) and was revealed as single or closely collocated prominent protein bands of each overlapping monomer as expected upon reduction of the disulphide bond between the hinge region of each respective monomer. The molecular weight of the peptide-Fc conjugates was shown as 33.0 kDa. Under non-reducing conditions, each peptide-Fc format showed twice the molecular weight to that of the monomeric chain displayed under reducing conditions. Therefore, confirming the full assembly of the peptide-Fc via disulphide bond formation between the interchain hinge regions. The molecular weight is confirmed in accordance with the predicted molecular weight of a stable peptide-Fc chimeric structure being expressed as a homodimer as a single band with a molecular weight of 65.9 kDa (Fig. 4.3B).

A CX$_7$C Peptide

MuFc region — C$_H$2 / C$_H$3

C Non-reduced / Reduced

Size (kDa): 250, 150, 100, 75, 50, 37, 25, 20, 15, 10

MWM, GWARA, QWAMM, HWAQA, PWAYS (Non-reduced) / GWARA, QWAMM, HWAQA, PWAYS (Reduced)

B

Protein	Monomer mass kDa/ Homodimer mass kDa
Peptide-Fc	33.0/65.9
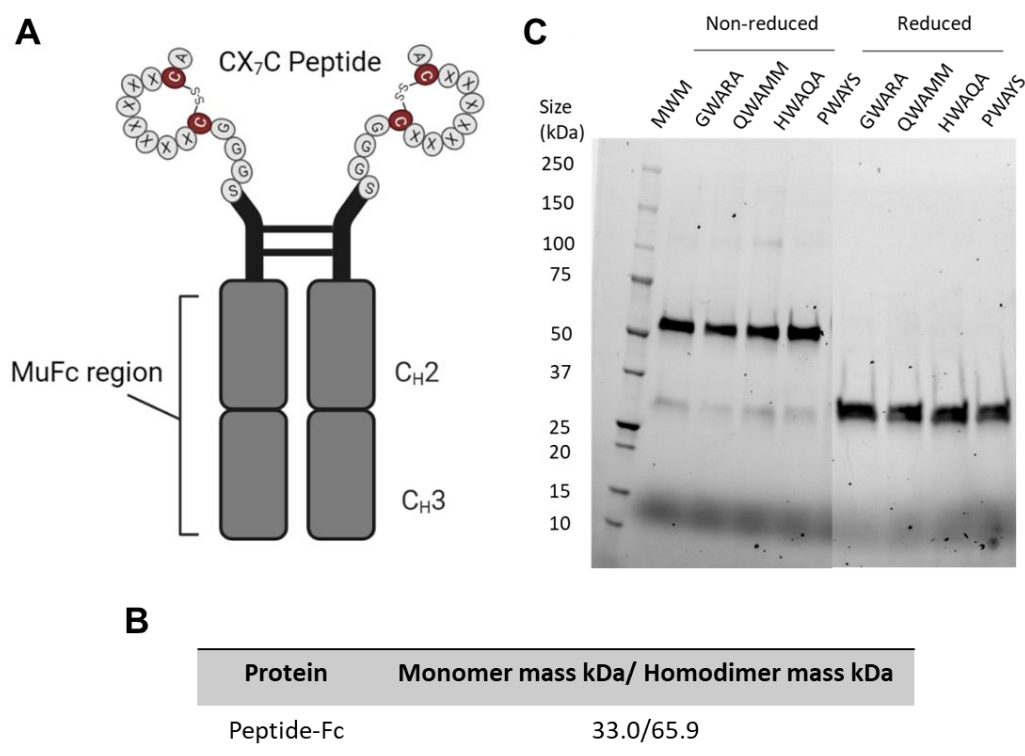
Figure 4.3. SDS page analysis of GWARA, HWAQA, PWAYS and QWAMM murine Fc conjugates.

(A) Illustration of Peptide (GWARA, QWAMM, HWAQA and PWAYS) fused mIgG2A-Fc homodimeric construct used in the biophysical characterisation of anti-minocycline sdAb specific peptides. (B) Predicted molar masses (kDa) of peptide-Fc antibodies determined through protein bioinformatics software ExPasy ProtPara from the amino acid sequences. The native state is expressed as a homodimer, monomer molar mass also indicated. (C) Protein migration using SDS-PAGE. 5µg of each peptide-Fc conjugate was prepared for loading using sample buffer consisting of 62.5 mM Tris-HCl, pH 6.8, 2% SDS, 25% (v/v) glycerol, 0.01% bromophenol blue (and 5% β-mercaptoethanol for reducing samples). Samples were then incubated at 95°C for 5 minutes prior to being loaded onto the gel. The mini-PROTEAN® TGX Stain-Free™ pre-cast 4-20% gradient gel was used to run samples. Running buffer consisted of 25 mM Tris, 192 mM glycine and 0.1% SDS. 180 V running voltage was used for 30-40 minutes. The Azure c600 Gel Imaging System by Azure Biosystems was used to image protein bands. Bio-Rad Precision Plus Protein Standards were used as reference protein ladder.

4.3.3 Investigation of CX7C-Peptide Binding Kinetics

CX7C peptide binding kinetics were determined using the Biacore SPR analysis. Peptide-IgG2a-Fc conjugates were immobilised to Series S CM5 Biacore chip and unconjugated anti-minocycline sdAb was injected as an analyte. An anti-methotrexate sbAb was also injected as the analyte and used as the negative control. The measured affinities (equilibrium constant KD) of the GWARA, HWAQA, PWAYS and QWAMM were 111 nM, 328 nM, 283 nM and 209 nM, respectively (Fig 4.4). Moreover, the component kinetics exhibited varying profiles between the four peptides. The association rate constant (ka) was measured at 1.55×10^5, 1.78×10^4, 1.98×10^4 and 2.07×10^4 M^{-1}s^{-1} and the dissociation rate constant (kd) was measured as 0.017, 0.0058, 0.0056 and 0.0043 s^{-1} for GWARA, HWAQA, PWAYS and QWAMM, respectively. GWARA showed the highest affinity of 111 nM and ideal component kinetics with the fastest on-rate and slowest off-rate compared to HWAQA, PWAYS and QWAMM (Fig. 4.5). The component kinetics of GWARA will occupy the antibody binding pocket for a longer time before being disassociated or outcompeted by minocycline. A summary of the affinity measurements and component kinetics of each peptide is shown on Table 4.2. As expected, each peptide did not show binding affinity to the negative control, anti-methotrexate sdAb.
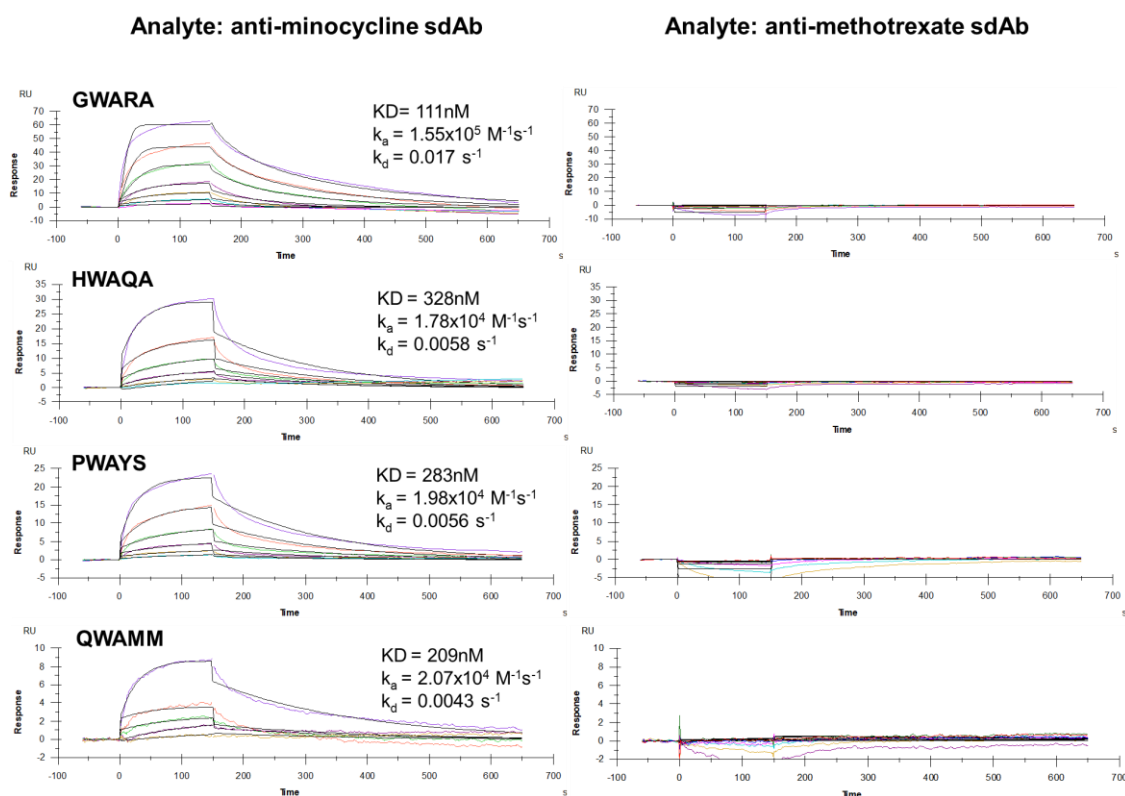
Figure 4.4. Biacore sensorgram of aMinocycline sdAb binding to CX7C-peptide-antibody complexes.

Each sensorgram shows binding shown with increasing concentrations of aMinocycline sdAb (0 nM to 1500 nM) to 4 CX7C-peptide-IgG2a-Fc antibody complexes (GWARA, HWAQA, PWAYS and QWAMM) immobilized to Series 5 CM5 Biacore chip. A non-specific sdAb was used as a negative control. Kinetic data points fitted using 1:1 Langmuir binding model and analysis of kinetic data performed using the BIAevaluation software.

Peptide	ka (1/Ms)	kd (1/s)	KD (M)	Affinity
ACPGWARAFC	*1.55E+5*	*0.017*	*1.11E-7*	*111nM*
ACPHWAQAFC	*1.78E+4*	*0.0058*	*3.28E-7*	*328nM*
ACPPWAYSFC	*1.98E+4*	*0.0056*	*2.83E-7*	*283nM*
ACPQWAMMFC	*2.07E+4*	*0.0043*	*2.09E-7*	*209nM*

Table 4.2. CX7C peptide-Fc affinity data for anti-minocycline sdAb clone 1. Affinity and component kinetic data were generated by Biacore SPR. CX7C peptide-Fc conjugates were immobilised to a CM5 chip and anti-minocycline sdAb was injected as an analyte.
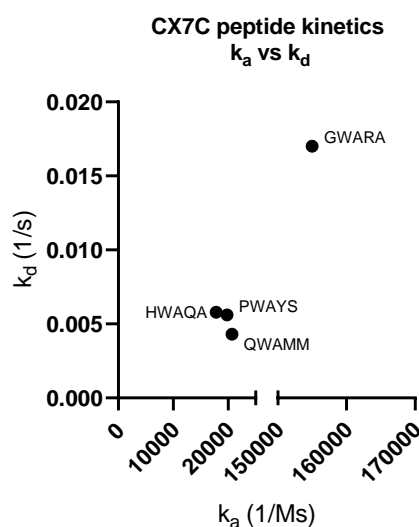
Figure 4.5. Component kinetics of the CX7C peptide-Fc conjugates.

4 CX7C-peptide-IgG2a-Fc antibody complexes (GWARA, HWAQA, PWAYS and QWAMM) were immobilized to Series 5 CM5 Biacore chip and unconjugated anti-minocycline sdAb clone 1 was used as analyte. Kinetic data points fitted using 1:1 Langmuir binding model and analysis of kinetic data performed using the BIAevaluation software.

4.3.4 Peptide displacement from sdAb is achieved through the presence of minocycline

To ensure each of the unique peptides bound the specifically to anti-minocycline clone 1 sdAb and not to an unrelated sdAb a further ELISA was carried out against immobilised clone 1 and clone 31, a sdAb isolated from the initial phage display library which is incapable of binding to minocycline, in the absence and presence of minocycline at a concentration of 1 µM (Fig. 4.6). All four CX7C peptides, GWARA, QWAMM, HWAQA and PWAYS, displayed binding to clone 1 but not clone 31. Additionally, in the presence of minocycline, a significant drop in binding to clone 1 was observed confirming the displacement of these peptides by the antibiotic (Fig. 4.6).

aMino sdAb Clone	CDR 1	CDR 2	CDR 3
1	GRTFSSYN	ISWSGART	AAGRGWGTEAILDY
31	GNIGLVSV	ITGGGST	RLVNNGRPF
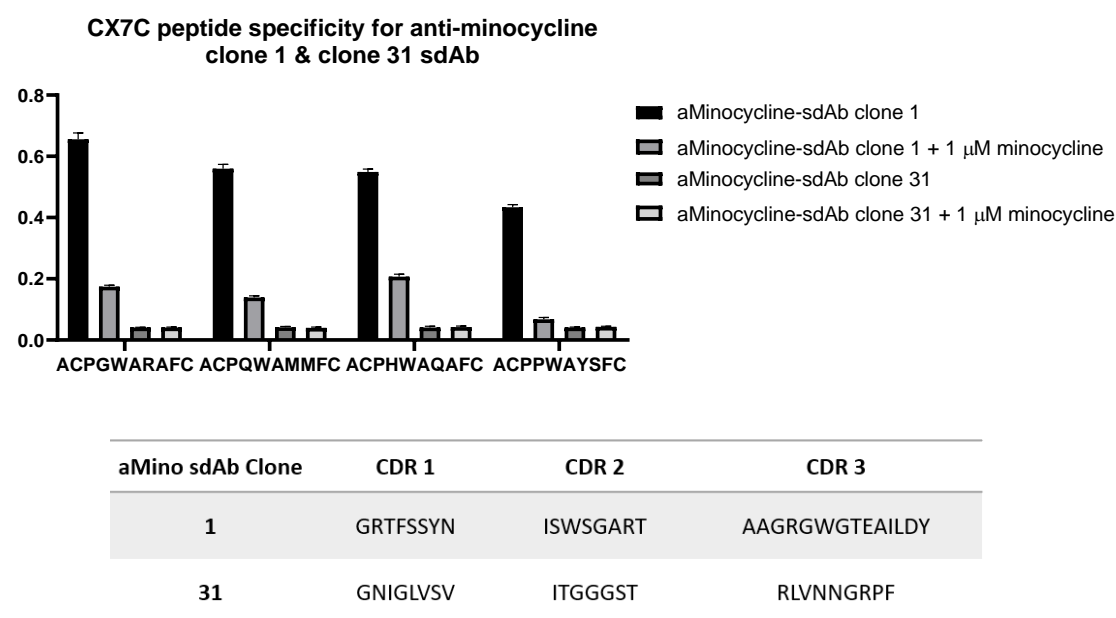
Figure 4.6. CX7C peptide-Fc conjugates bind specifically to anti-minocycline sdAb clone 1 and is disassociated in the presence of minocycline.

Four CX7C peptides showing unique sequences with three amino acid difference were isolated and tested for sdAb binding as CX7C-peptide-IgG2a-Fc antibody conjugates (Peptide-Fc). Plates were coated with anti-minocycline sdAb clone 1 and clone 31 (1 µg/ml). Peptide-Fc (10 µg/ml) were produced from CHO cell transfections, purified using protein-A affinity chromatography and tested by ELISA to show specific binding to anti-minocycline sdAb clone 1 with reduced binding observed in the presence of 1 µM minocycline.

4.3.5 In vitro Peptide-Fc displacement from extracellular anti-minocycline sdAb CAR

So far, I characterised this system successfully via protein-protein interactions on artificial surfaces. Here I demonstrate the dose-dependent capacity of minocycline to dissociate bound peptide-Fc (GWARA, QWAMM, HWAQA, PWAYS) from an anti-minocycline-sdAb in the context of an extracellular CAR scaffold composed of an anti-minocycline sdAb or an anti-EGFR sdAb fused to a CD8α spacer, CD28-4-1BB-CD3ζ. 293T cells were transfected to express the extracellular anti-minocycline-sdAb CAR construct (Fig. 4.7A) or an anti-EGFR-sdAb CAR construct (Fig. 4.7B). These cells were then incubated with peptide-Fc targeting the anti-minocycline sdAb CAR, upon which minocycline was spiked at varying concentrations of 0, 1 μM, 10 μM & 100 μM. Peptide binding was measured by the mean fluorescence intensity (MFI) of detectable peptide-Fc bound to the surface of the cells at various concentrations of minocycline.

Peptide-Fc shows binding to the anti-minocycline-sdAb CAR in the absence of minocycline. Upon the addition of minocycline, peptide-Fc binding was reduced with increasing concentrations of minocycline suggesting the peptide-Fc was dissociated in a dose dependent manner (Fig. 4.7). Against the anti-EGFR-sdAb CAR, peptide-Fc showed no binding and minocycline addition at the highest experimental concentration of 100 μM did not alter level of peptide binding.

A
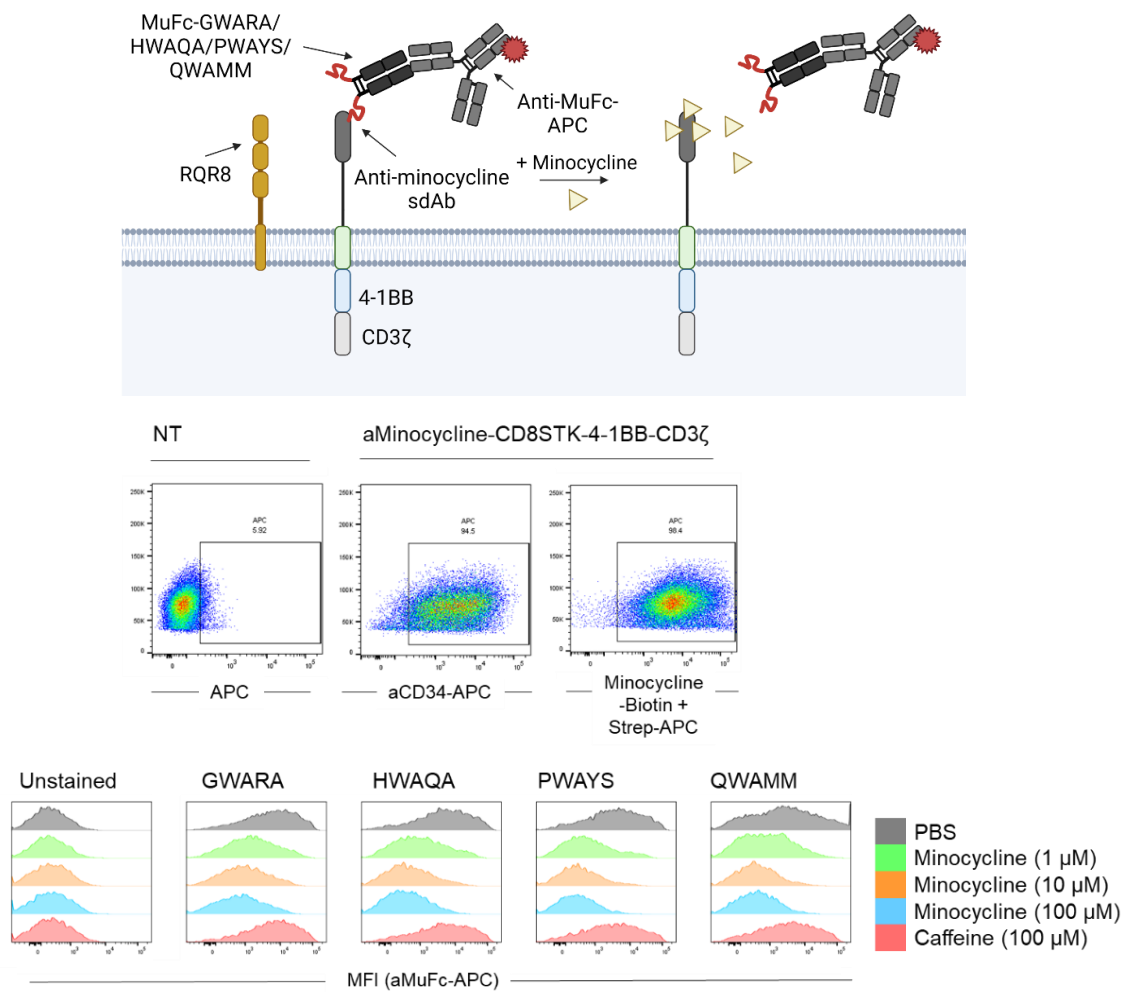
B
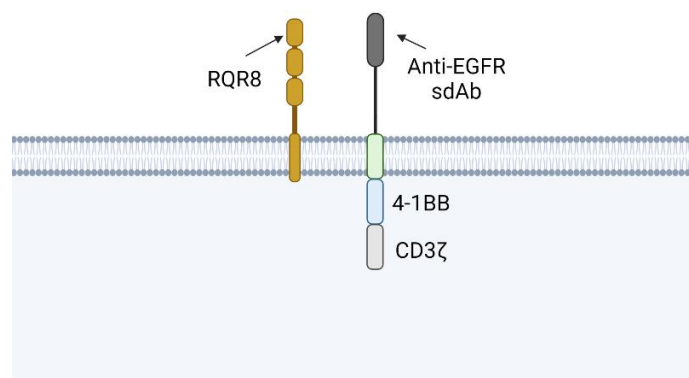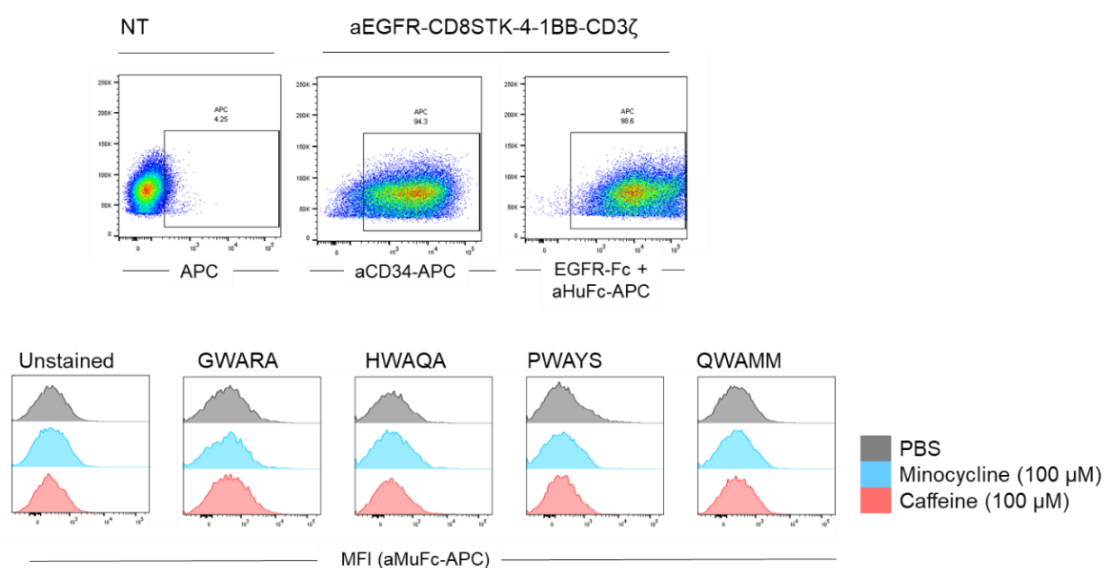
Figure 4.7. Minocycline mediated peptide-Fc dissociation from extracellular anti-minocycline-sdAb CAR.

293T cells transfected to express either (A) an extracellular anti-minocycline-sdAb-CAR, co-expressed with the marker gene RQR8, consisting of the anti-minocycline sdAb as an extracellular binder, a CD8 stalk spacer and CD28 transmembrane region or (B) negative control consisting of an RQR8-tagged anti-EGFR-sdAb-CAR comprised of an anti-EGFR sdAb as an extracellular binder, a CD8 stalk spacer and CD28 transmembrane region. Cells expressing either construct were stained for expression of the RQR8 marker gene, using aCD34-APC antibody, to measure overall transduction or assessed for their ability to bind minocycline or EGFR. Wild-type 293T cell (NT) were incubated with each antibody to determine gating. Cells were incubated with murine-Fc tagged anti-minocycline-sdAb specific CX7C peptides for 30 minutes prior to the addition of minocycline at 1 µM, 10 µM, 100 µM, a no-drug control (black) and a non-specific drug control (Caffeine; red) for 15 minutes. Peptide-Fc (GWARA, HWAQA, PWAYS, QWAMM) binding was determined using anti-murine-APC antibody. Increasing concentrations of minocycline results in dose-dependent dissociation of peptide-Fc. RQR8 expression was shown on both anti-minocycline and anti-EGFR sdAb CARs. Anti-minocycline-sdAb expression was determined using minocycline-biotin (0.5 µg/ml) followed by streptavidin-APC. Anti-EGFR-sdAb expression determined using human-Fc-EGFR (0.5 µg/ml) followed by anti-human-Fc-APC.

4.3.6 Investigation of CX7C-peptide re-challenge post minocycline displacement using SPR analysis

To determine the capacity of the CX7C peptides and anti-minocycline sdAb interaction to be reformed after multiple minocycline-mediated displacement events, a Biacore SPR protocol was designed to show sequential binding and displacement of the peptide upon multiple injections of minocycline.

As individual peptides (analyte) were injected, these soluble peptides bound to immobilized anti-minocycline sdAb resulting in an increase in refractive index in real time, presented as response units (RUs) against time in seconds. Once the association phase was halted, a fall in RUs relative to the baseline value was observed indicating natural dissociation rate of peptide from sdAb complex (dissociation phase). Minocycline (1 µM) injection resulted in a sudden decrease in RU relative to baseline RU indicating complete displacement of the peptide from the ligand. Minocycline was washed from the system and peptide re-injected allowing subsequent binding of peptide-Fc to the anti-minocycline sdAb to take place. This indicated the structural integrity of the clone 1 anti-minocycline sdAb binding pocket or resulting conformational change is robust for multiple re-binding events to take place and suggests the utilisation of these components would result in an interaction being reversible.

Further evidence for the specific displacement of peptide binding by minocycline was achieved through the injection of a molecule with a similar molecular weight to minocycline such as caffeine. Results indicate that upon the injection of caffeine the dissociation rate of peptide was unaltered and comparable to injection of PBS during the wash phase; hence, confirming lack of peptide displacement by a non-specific small molecule. Additionally, the baseline RU increased after each round of peptide injection due to lack of peptide displacement by caffeine and sequential saturation of the anti-minocycline sdAb (Fig 4.8).
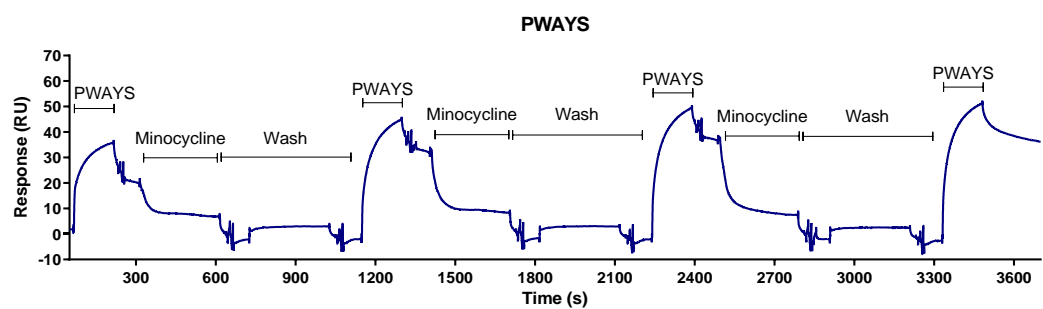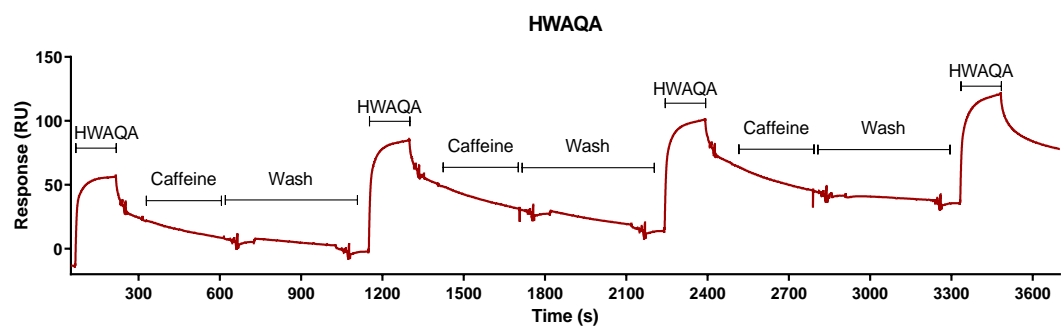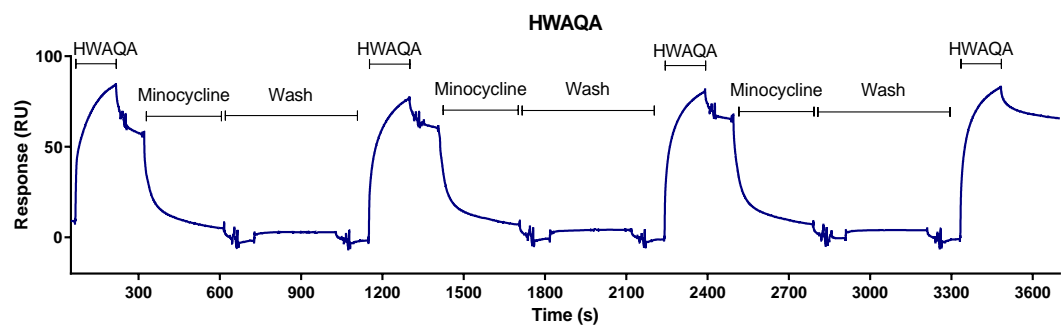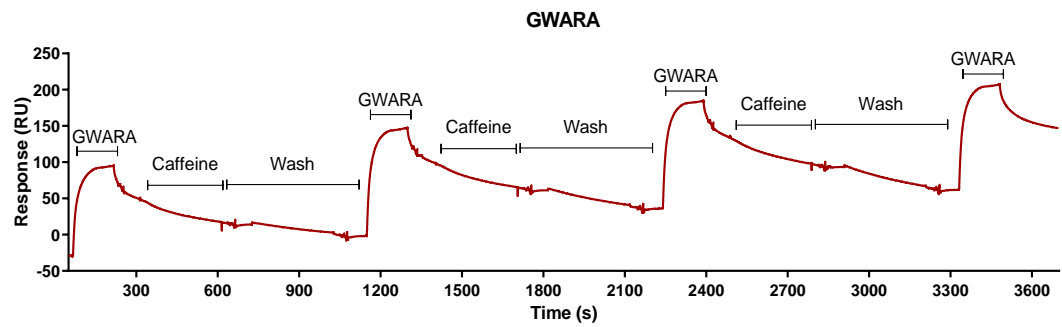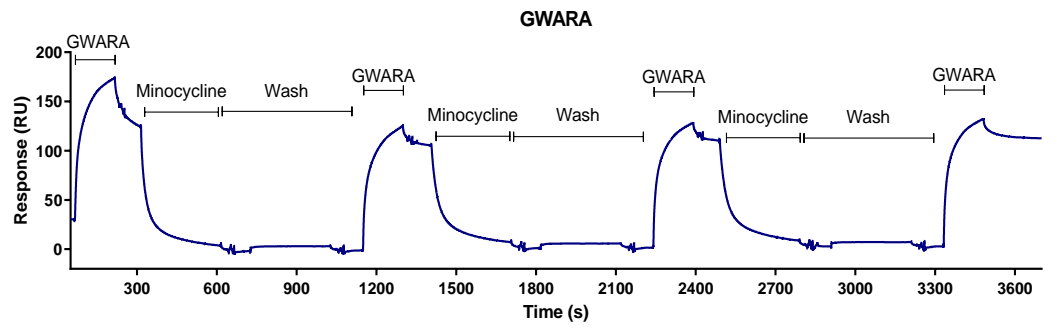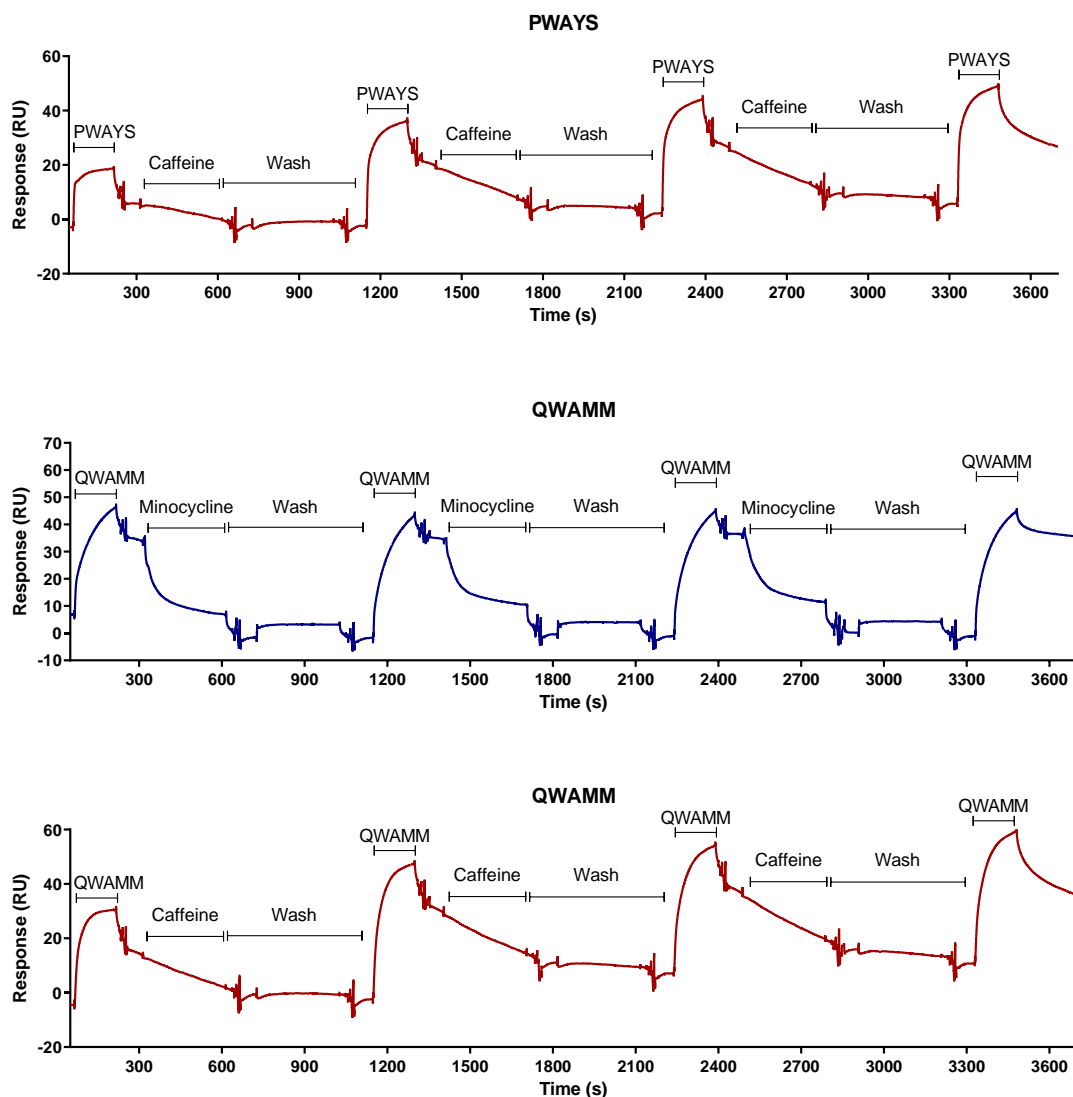
Figure 4.8. Biophysical characterisation and sequential binding studies of anti-minocycline sdAb clone 1 specific peptides.

Anti-minocycline sdAb clone 1 was immobilised on a Biacore chip and CX7C peptide-Fc conjugates (GWARA, HWAQA, PWAYS and QWAMM) were injected as the analyte. Following the injection of peptide-Fc, minocycline at 1 mM (blue) was injected to dissociate the peptide-Fc from the peptide-sdAb complex. The system was then washed prior to re-challenge with peptide-Fc and the cycle repeated. Caffeine at 1 mM (red) was injected separately as the negative control.

4.4 Discussion

Here I show the screening of combinatorial phagemid library of cysteine-constrained peptides against the previously characterised minocycline specific sdAb clone 1; To generate peptide sequences with an affinity less than 31 nM and therefore capable of being displaced from the sdAb in the presence of minocycline. This screening and selection process generated a homologous consensus motif (Pro-Gly/Gln/His-Trp-Ala-Arg/Met/Gln-Ala/Met/Ala-Phe). One of these peptides, ACPGWARAFC, bound the sdAb with an equilibrium dissociation constant (KD) in the low-nanomolar range. The peptide-sdAb complex was also shown to be specifically disrupted by minocycline over other low molecular weight drugs. Moreover, with the use of SPR analysis, these cyclic peptides were shown to rebind the sdAb upon multiple rounds of displacement in which minocycline was added and subsequently washed away. These results will allow for a novel protein/peptide displacement model that has potential utility in controlled drug release, gene-expression, cytokine receptor activation and immunotherapy safety switches.

In this chapter, we show the successful use of the commercial Ph.D.-7 Phage Display Peptide Library to select disulphide bridged peptide binders against the previously isolated minocycline-specific sdAb clone 1. Using this library, we were able to probe the combinatorial library of genetically arbitrary cyclic amino acid sequences which were constrained by a highly stable disulphide bond. The phage selection employed a seven-residue cyclic peptide library constrained with a flanking cystine residues forming a disulphide bond. With a library size of 1×10^9 unique nucleotide sequences, I believed that I achieved adequate coverage of the possible peptide sequences.

The system described here may not be suitable for intracellular applications due to the use of cysteine constrained peptides. In mammalian cells, disulphide bond formation between cysteine residues takes place during the folding of peptides entering the secretory pathway (ER lumen) through the process of covalent linkage catalysed by the protein disulphide isomerase family of enzymes. To drive disulphide bond formation, protein disulphide isomerase enzymes must be oxidized. However, these enzymes can be reduced by thiol glutathione, which is significantly more oxidised within the

174

lumen of the ER than in the cytosol. As a result of its reducing cytosolic environment, correct disulphide bonds do not form within the cytosol. The isolation and use of linear peptides targeting the sdAb is attractive due to the lack of reliance on reducing conditions for functional epitope formation, whereas use of cysteine constrained peptides is limited in their intracellular use due to the reliance on disulphide bond formation. However, above all, high affinity sdAb interaction of the isolating peptide binders was essential in the process of developing a protein-protein displacement system for the interaction to induce potent signalling in the context of CAR-T cells. Many reports have shown the dissociation constants of cystine constrained cyclic peptides generated through phage display, to lie within the millimolar to picomolar range, with most peptides isolated against protein targets falling within the micromolar range. Such affinity ranges have generally been shown to be substantially greater than linear peptide binders.[277–279] An example of phage-derived CX7C peptides was described by Duncan et al. and targeted the Phosphorylation-Dependent Peptidyl-Prolyl Cis/Trans Isomerase PIN1 overexpressed on various cancers. The binding affinity of the peptide sequence CRYPEVEIC as cyclic and linear peptide structures were tested to show the cyclic peptide had an 85-fold greater binding affinity relative its linear peptide counterpart.[280]

Moreover, bioactive peptides in the form of linear and cyclic peptides have been explored in the treatment of cancer and other disease. These mimic the key epitope and activity of endogenous proteins to form low molecular weight therapeutic peptides, which can act as antagonists to prevent downstream cellular signaling and mitigate cancer proliferation. Zilberberg et al. tested the binding affinity of the VEGF derived linear peptide sequence DFPQIMRIKPHQGQHIGE and the cyclic variant (cyclo-VEGI) to the kinase receptor domain of VEGF receptors. It was demonstrated that that cyclo-VEGI displaced I-VEGF from VEGFR-1 and VEGFR-2 with IC_{50} values of 1.3 and 0.7 µM, respectively, whereas the linear peptide did not. Additionally, cyclo-VEGI eliminated VEGF-induced migration of VEGTR+ BAE cells and showed anti-angiogenic activity on the chorioallantoic membrane of the chick embryo, whereas the linear peptide did not eliminate cell migration and showed no

difference to the expression of micro-vessels in chick chorioallantoic membranes relative to the control. Thus, showing the cyclic analogue of the peptide successfully inhibited VEGF activity due to increased affinity as a result of peptide cyclization.[281]

In addition to enhanced affinity of cyclic peptides, linear peptides are prone to proteolytic degradation. Researchers have shown enhancing peptide stability can be achieved through peptide cyclisation, use of D-amino acids and blocking at the N-terminus and C-terminus.[282,283]

Although the development of an anti-idiotype antibody targeting the anti-minocycline sdAb was considered, the use of small ligands has been shown to possess improved pharmacokinetic properties due to their small size (<2 kDa).[284] Generally showing enhanced tissue penetration, showing minimal non-specific uptake and immunogenicity, and occupying negligible real-estate within a vector construct.

Use of immunized animals as a source of diversity against the anti-minocycline sdAb would have been attractive in generating a library of binders. Primarily as an immunised library is biased toward the immunised sdAb, thus generating high-affinity binders which would have gone through the natural process of affinity maturation where the antibody response to antigens in animals results in improvements in the affinity of circulating antibodies through of B-lymphocyte antibody gene hypermutation. However, a single large naïve or synthetic library was preferred due to the nature of the selection being undertaken.[50,285–287] In addition to these libraries being shown to generate high affinity peptide binders to a diverse group of targets. The strategy was based on selecting for binders by applying the candidates against the immobilised sdAb, followed by elution in the presence of minocycline/competitor which binds to the potential epitope. This competitor will displace phage particle-bound bioactive epitope or prevent binding altogether, whilst allowing non-displaceable/higher affinity peptide candidates to remain bound. The displaced/unbound phage can then be panned against the sdAb for enrichment. Therefore, with the use of a synthetic library, such a modified selection strategy can enable the discovery of candidates with unique

specificity and affinities which would not be possible with the use of an immunised animal phage library.

With the goal of developing protein-protein displacement system for use in immunotherapy applications in patients, it was essential each component had the potential to be used in a clinical setting. Previous work on cysteine-constrained cyclised peptide development has been shown to have successful use in the clinic. For example, phage display was used in the development and isolation of a disulphide bond-constrained peptide of 20 amino acid mimicking the EPO molecule.[288] EPO which usually dimerises the EPO receptor and controls the proliferation and differentiation of immature erythroid cells was a target for anaemia treatment. The cyclic peptide, which was conjugated to poly(ethylene glycol) (PEG), showed therapeutic efficacy in the clinic for the treatment of anaemia and maintenance of haemoglobin.[288]

An essential characteristic of the phage display method is the capacity to select library of binders directed towards an epitope of interest and deplete binders directed to epitopes which do not serve this function. With the use of a competitor molecule or compound which occupy the epitope of interest with a higher affinity, phage selection can be modified to enrich for binder candidates being outcompeted for. For example, in the generation of binders targeting the active site of the matrix metalloproteinase 14 (MMP-14) protein, selection was carried out in the presence of its natural ligand which allowed for the selection of phage particles competing for the functional active site and eliminating binders to non-specific regions by permitting these to remain bound.[289]

In this case, subsequent selection in the absence of the natural ligand was used to isolate highly specific peptides to act as competitive inhibitors to the natural ligand.[290] In this case, the opposite outcome was the primary aim, in that the selection was to identify peptides which bound the minocycline sdAb with a lower affinity than minocycline and in the correct position to be displaced by minocycline itself. Minocycline was used in each of the three selection rounds to enrich displaceable binders.

Cysteine constrained peptides which act as mimotopes for antibodies have previously been described and utilised as a safety switch in immunotherapy. RQR8 receptor is one such example which is composed of two 7-mer cyclic peptides, Rp15-C and Rp13-C.[291] These two CD20 mimotopes, alongside a CD34 epitope, fused to the cell membrane via a CD8a stalk can be targeted by the FDA-approved anti-CD20 antibody, rituximab, for the positive selection of cells during the manufacturing process or targeted depletion.[173,292,293]

In total, 4 unique peptide sequences were isolated, the consensus sequence showed each containing a Pro in the second position, Trp in the fourth, Ala in the fifth position, and Phe in the eighth position: CPXWAXXFC. Most cyclic peptides previously described have shown binding affinities to lie within the micromolar range.[277–279] In recent years, high affinity cyclic peptides within the nanomolar range have also been described.[294,295] For example, cyclic peptides which mimic and bear the CDRH3 sequence of an anti-influenza-haemagglutinin (HA) antibody showed to bind HA with an affinity of <100 nM and directly comparable to parental IgGs.[295]

Another protein-protein interaction system which utilises an antibiotic drug, tetracycline, to displace the protein interaction is based on the phage-library derived Tip peptide and tetracycline-binding TetRB protein. Here, the ~200-fold higher binding affinity of tetracycline (2.8 nM), over the binding affinity of Tip peptide (640 nM) for TetRB results in the efficient displacement of the TetRB-Tip interaction.[248,296] Therefore, in order for the peptide and anti-minocycline-sdAb interaction to be displaceable by minocycline, SPR analysis of the binding affinity was carried out to confirm each isolated peptide fit the criteria of presenting a binding affinity less than that of 31 nM (the affinity of the sdAb for minocycline). Overall, each isolated peptide presented nanomolar affinities for the sdAb, with values ranging from 111-328 nM. The peptide sequence ACPGWARAFC showed the highest of all four peptides (KD: 111 nM) (Fig. 4.4).

As mentioned in Section 3.7, the protein-protein interaction of the TetCAR system induces functional signal transduction and was sufficient for a therapeutic output through the 640 nM interaction between TetRB protein and

Tip peptide (Fig. 1.13).[187,188,248] Thus, I believe, an affinity of 111 nM between GWARA and sdAb will be sufficient for signal transfer in the context of a split CAR module. Furthermore, the displacement of TetRB protein and Tip peptide took place in the presence of tetracycline as tetracycline had a greater affinity for TetRB (KD: 2.8 nM).[248,249] Likewise, I present evidence showing all four isolated peptides are displaced in direct competition with minocycline as shown using ELISA. In addition, displacement of peptide is also achieved once peptides have bound to the sdAb in the absence of the drug using a cell-based flow cytometric assay.

If required in future development, the generation of binders with an affinity closer to 31 nM could be achieved by reducing the stringency of elution using minocycline, either through elusion using lower concentrations of minocycline or avoiding minocycline mediated elution in the later rounds of panning. Furthermore, In vitro affinity maturation techniques can also be used to mimic the natural affinity maturation process and evolve high-affinity peptides by increasing selection stringency through the gradual reduction in anti-minocycline sdAb concentration during the panning stage thus only selecting the highest affinity peptide.[297]

With the use of customised SPR protocol (Fig. 4.9), each cyclic peptide was shown to rebind the sdAb upon multiple rounds of displacement in which minocycline was added and washed away, indicating the structural integrity of the sdAb binding pocket is undisrupted or refolded upon subsequent displacement events. Therefore, suggesting that this protein-protein displacement system is robust enough for multiple re-binding events to take place and providing evidence that this interaction has the potential to be used as a reversible system. Further evidence for peptide binding and specific displacement by minocycline was achieved through the injection of a non-displacing molecule with a similar molecular weight to minocycline such as caffeine. The results indicate that upon the injection of caffeine the disassociation rate of peptide was unaltered and comparable to injection of PBS during the wash phase; hence, confirming lack of peptide displacement by minocycline over a non-specific small molecule such as caffeine. Additionally, the baseline RU increased after each round of peptide injection

due to lack of peptide displacement by caffeine and increasing peptide binding to the anti-minocycline sdAb (Fig 4.8).

4.5 Conclusions

- A 7-amino acid cyclic peptide, ACPGWARAFC (termed GWARA) was isolated using the commercial Ph.D.-7 Phage Display Peptide Library

- GWARA showed significant ability to bind the anti-minocycline single domain antibody with an affinity of 111 nM

- Due to the phage panning selection strategy, GWARA was specifically displaced by minocycline

- Displacement of GWARA from the anti-minocycline single domain antibody was reversible with multiple re-binding events taking place post displacement

- Using a cell binding assay, fusion of the GWARA sequence as an antibody structure showed dose dependent displaceability

5 PREDICTING THE BINDING INTERFACE OF THE ANTI-MINOCYCLINE SINGLE-DOMAIN ANTIBODY WITH MINOCYCLINE & GWARA PEPTIDE

5.1 Introduction

Protein-protein and protein-ligand interactions are fundamental to biological processes. Several reports have underlined that the nature of residue interactions at the binding interface between antibodies and proteins/ligands are responsible for conferring specificity and stability of the bound complex. Such interactions are highly specific in relation to the protein sequence and the three-dimensional structure in complex. Antibody-ligand interactions are generally transient whereby the association and disassociation rates differ drastically. The transient binding nature of antibody-ligand interactions means a high affinity interaction must be maintained, such that the interfacial residues which influence a significant energy of stabilization between binding partners are known as hotspots and mutations in such regions result in a substantial drop in binding affinity. [298,299]

An area of progress in the field of antibody engineering and drug development is the in-depth understanding of the binding interface between CDRs and their respective antigen.[300] Previously, the collection of CDR-epitope structural interaction data has been relatively limited mainly because techniques such as NMR spectroscopy and X-ray crystallography are time-consuming, labour-intensive, expensive, and often require highly trained technicians to perform.[301–303]

An emergent strategy for identifying and characterizing antibody-ligand epitopes involves computational modelling and complementary experimental evidence.[304]

The use of computational-based amino acid prediction and design has generated many successful protein engineering applications which have been powerful enough to alter protein function such as the introduction of zinc-finger motifs to protein structures which self-fold without the presence of co-factors as well as producing novel enzymes which lack natural catalysts.[305,306] The use of computational protein design has also guided protein engineers to

increase the stability and binding affinity of proteins with experimentally validated single mutations.[307,308]

Computational prediction of the antibody-ligand structural interaction is essential in the design of novel ligands for applications in immunotherapy as well as further developing our understanding into the nature of competing molecules and peptides. As the variable region, specifically the complementarity-determining-regions (CDRs) impart most, if not all the antigen binding specificity, research into homology modelling has been centred around predictions based on the CDR region.

Relying solely on computational methods for epitope prediction are rapid and economical although, as it stands, not sufficiently accurate to be used on its own.[300,309] Although the computational scoring method generates accurate antibody binding models, the sole use of such scores cannot be used to identify the most precise structure. Nonetheless, the use of experimental data in conjunction can be used to validate the computational models generated. Previous work has shown that binding assays of computationally-derived antibodies can be used to validate or discard the homology docking model, thus determining the overall binding residues.[304] Combining computational models and experimental data can accurately identify epitope residues responsible for antigen binding. For instance, methods reported by Hua et al. described the generation of an antibody homology model based on screening the sequence of the unknown antibody structure to a bank of previously solved antibody crystal structures. The subsequent homology model was then docked with target antigens based on experimental binding assays on antibody variants generated through mutagenesis of CDR amino acids to assess the accuracy of the antibody homology model which uses available solved antibody crystal structures to computationally guide the folding of an unrelated antibody sequence.[304]

In this chapter, Schrodinger BioLuminate software will be used to generate a full homology model of the anti-minocycline sdAb structure, which will then be used to carry out molecular docking studies to determine the binding interface and decipher the key residues of the antibody involved in the minocycline and

GWARA peptide binding. The homology model will be validated with the aid of functional readouts using a range of mutant anti-minocycline sdAbs generated through alanine scanning-mutagenesis. This will provide valuable information to understand the mechanism of binding utilised by minocycline and GWARA and the basis of GWARA peptide displacement by minocycline. This may aid in the future development of additional protein-protein displacement systems.

5.2 Aims

- To construct a homology model for the anti-minocycline single-domain antibody.

- Identifying the critical residues within the antibody/minocycline and antibody/GWARA binding interface using functional experiments on a range of sdAb mutants generated through alanine scanning mutagenesis.

- Based on experimental binding data, validate the computational sdAb-minocycline and sdAb-peptide docking to visually identify the sdAb engagement with minocycline and GWARA to determine mode of interaction.

5.3 Results

5.3.1 Single-domain antibody sequence homology search and model construction

5.3.1.1 Homology search

In order to define the interaction of the sdAb with minocycline or the GWARA peptide, a sdAb structural homology model was first constructed with the aim to dock this predicted structural model with the respective ligands and validate the docking models using functional data from a range of sdAbs bearing alanine mutations within the CDR residues. The homology search was used to assess the framework identity against a catalogue of experimentally derived Camelid heavy chain antibody crystal structures which showed the framework identity and similarity being greater than 0.90.

In the case of this study, I utilised methods within Schrodinger BioLuminate software to generate the structural model of the anti-minocycline sdAb which were subsequently used to generate docking models via the CDR-ligand docking algorithm.[310] Generation of a predicted three-dimensional structural model of the anti-minocycline sdAb using BioLuminate was achieved by identifying a heavy chain framework region to act as a template by scanning the anti-minocycline sdAb primary sequence against an antibody structural database. The VHH domain EgA1 antibody (PDB ID 4KRN, resolution: 1.55 Å) was selected as an appropriate template framework based on the composite scores, structural identities and PDB resolutions. Specifically, 4KRN presented a composite score of 0.95, framework similarity of 0.95 and framework identity of 0.93.[311,312] The IMGT unique numbering system was used to determine the framework regions and the CDRs of the sdAb.[309,310] Furthermore, carrying out sequence alignment of the sdAb and template antibody sequence, it was observed with the exception of 1-3 residues, the CDR1 and CDR2 amino acid sequence of the anti-minocycline sdAb was highly homologous to 4KRN. In comparison, the predicted CDR3 of the anti-minocycline sdAb shows minimal sequence similarity with the respective regions of 4KRN (Fig. 5.1).

```
Framework alignment

4KRN    1    QVQLQESGGGLVQPGGSLRLSCAASGRTFSSYAMGWFRQAPGKQREFVAAIRWSGGYTYY    60
             QVQLQESGGGLVQPG SLRLSCAASGRTFSSY  GWFRQAPGK REFVAAI WSG  TYY
aMino   1    QVQLQESGGGLVQPGSSLRLSCAAS<mark style="background:yellow">GRTFSSYN</mark>IGWFRQAPGKEREFVAA<mark style="background:lime">ISWSGART</mark>YY    60

4KRN   61    TDSVKGRFTISRDNAKTTVYLQMNSLKPEDTAVYYCAATYLSSDYSRYALPQRPLDYDYW   120
              DSVKGRFTISRDNAK TVYLQMNSLKPEDTAVY CAA           A       DYW
aMino  61    ADSVKGRFTISRDNAKNTVYLQMNSLKPEDTAVYSC<mark style="background:cyan">AA---GRGWGTEAI------LDY</mark>W   111

4KRN  121    GQGTQVTVSS   130
             GQGTQVTVSS
aMino 112    GQGTQVTVSS   121
```

Figure 5.1. Sequence alignment of anti-minocycline sdAb and its homology template, the VHH domain EgA1 antibody (PDB ID 4KRN).

Heavy chain framework search identified two template frameworks to act as the basis of the single-domain antibody structural prediction. The VHH domain EgA1 antibody (PDB ID 4KRN) was selected as the framework template based on the composite score, framework similarity and framework identity. Complementarity-determining region (CDR) amino acid residues are highlighted in yellow, green, blue for CDR1, CDR2 and CDR3, respectively.

5.3.1.2 Model generation and selection

Using the X-ray solved structural template (PDB: 4KRN), ten loop models for the anti-minocycline sdAb were generated (Fig. 5.2) and the quality of homology model was assessed using Ramachandran plots. The Ramachandran plot is a two-dimensional representation of the φ–ψ torsion angles of an antibody template which provides a minimal representation of protein conformation. The φ–ψ torsion angles group into distinctive areas in the Ramachandran plot which corresponds to a specific secondary structure. In Ramachandran plots shown in Figure. 5.3, each sdAb residue is positioned in either energetically or conformationally favourable positions (red), in constrained but acceptable regions (yellow) or in outlier regions (white) relative to the template antibody. Based on the majority of sdAb residues being within the favoured and acceptable regions of the Ramachandran plots, model 10 was selected as the sdAb homology model.

As the modelling was based on a rigid crystal structure, the Schrodinger PrimeMini Package was utilised to reduce rigidity and optimise the homology model via energy minimisation to enhance in-silico proteins prediction for

ligand binding. Figure 5.4A shows a visual representation of the homology model generated post energy minimisation where the framework regions (FR) are indicated by the purple ribbons, the Veriner zone indicated by the blue ribbons and the CDR regions are shown in maroon.[7] Additionally, the Protein Preparation Wizard was used to assign bond order, add hydrogens and create disulphide bonds prior to ligand docking simulations (Fig. 5.4B).
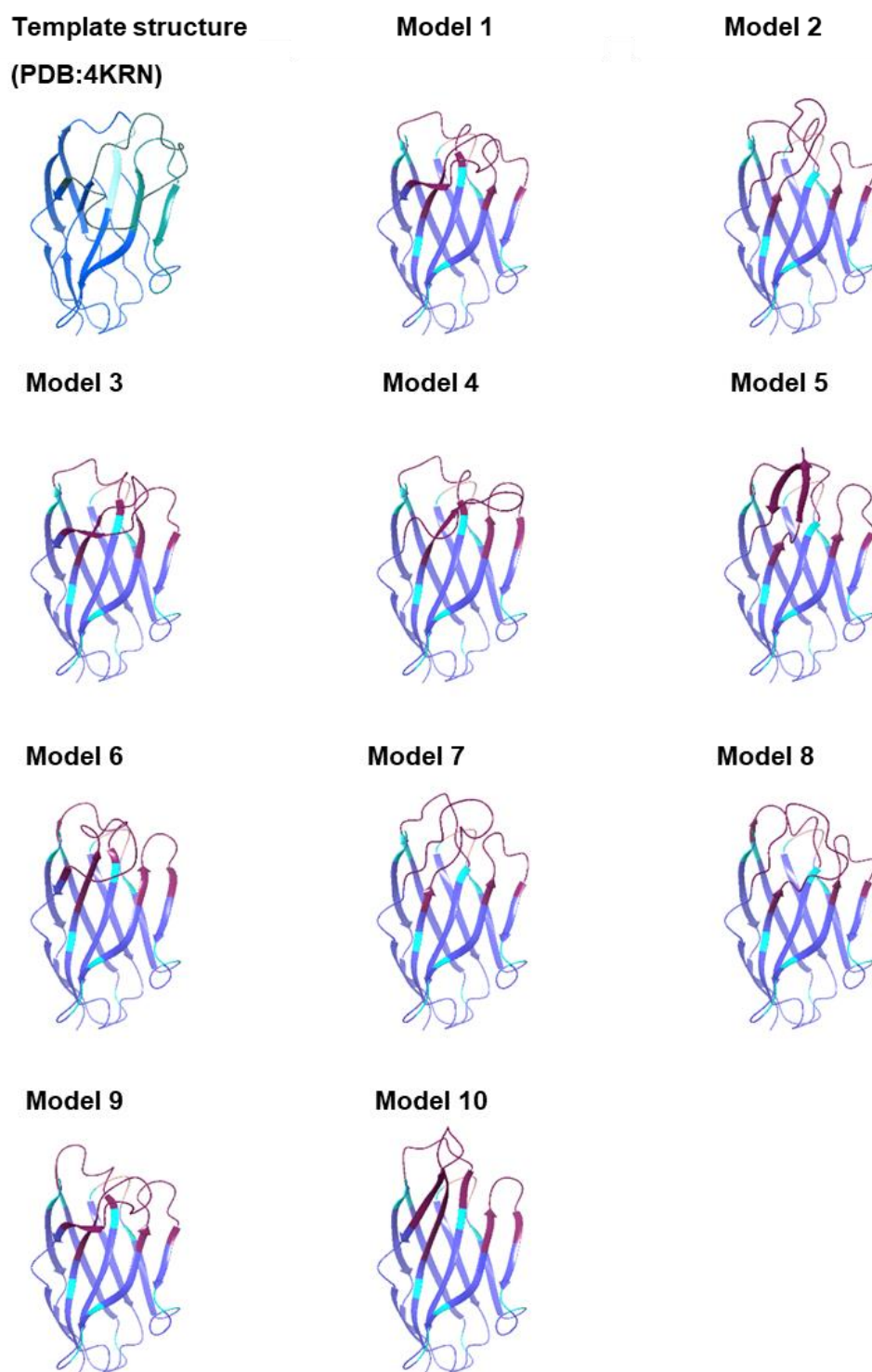
Figure 5.2.   Anti-minocycline sdAb CDR loop models using template framework (PDB ID 4KRN).

The VHH domain EgA1 antibody (PDB ID 4KRN) was used as the homology template which generated ten CDR loop models of the anti-minocycline sdAb. Antibody framework regions are shown in purple, Vernier zone is shown in blue and the CDRs are shown in maroon.
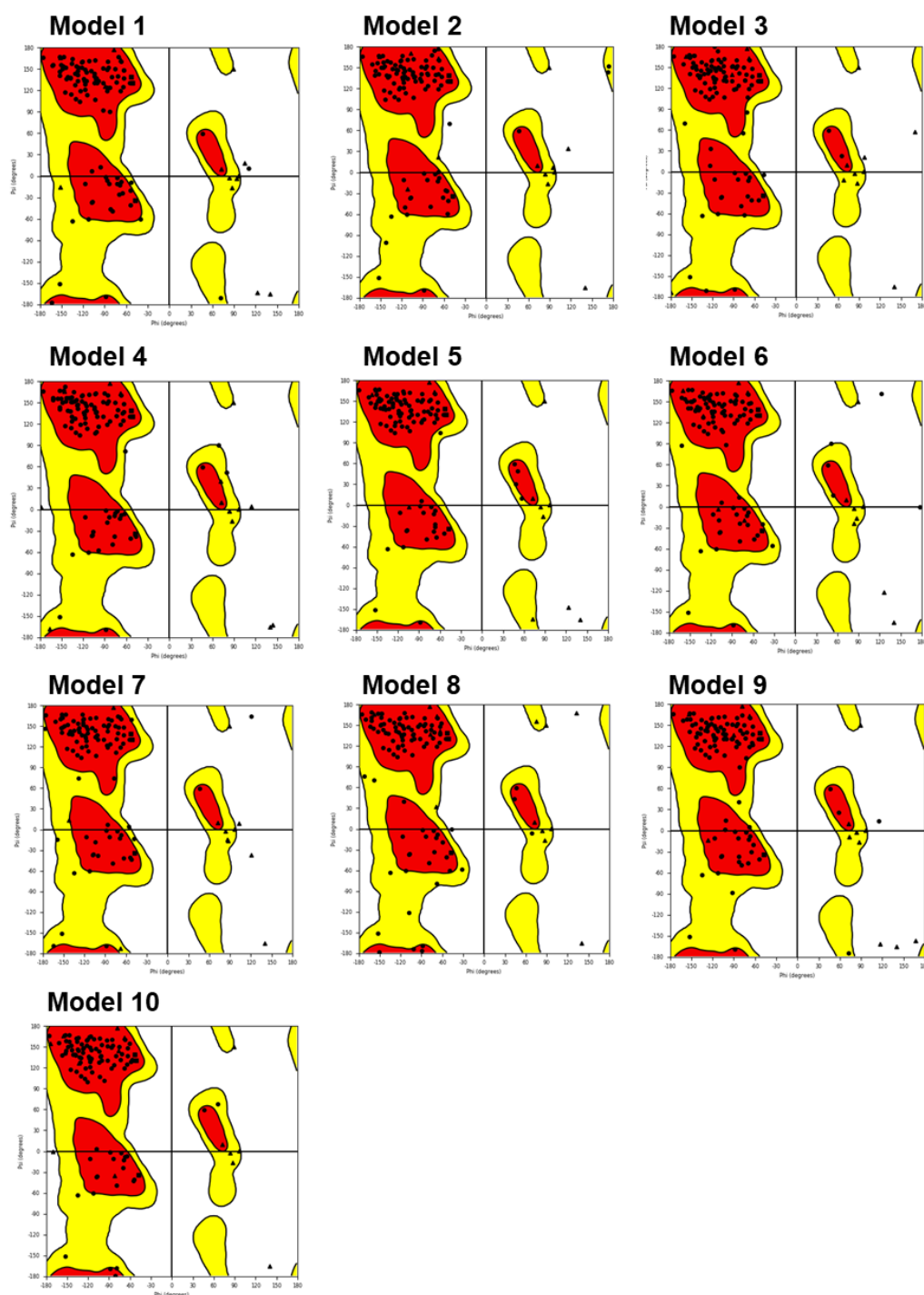
Figure 5.3. Ramachandran plots of anti-minocycline sdAb sequence.

Model 10 was selected as the highest quality model based on the positioning of the anti-minocycline sdAb residues in either energetically or conformationally favourable positions relative to the template. Glycine residues shown as triangles, Proline shown as as squares and all other residues shown as circles. Red area: allowed conformations without steric clashes. Yellow area; Allowed regions with short van der Waals radius.
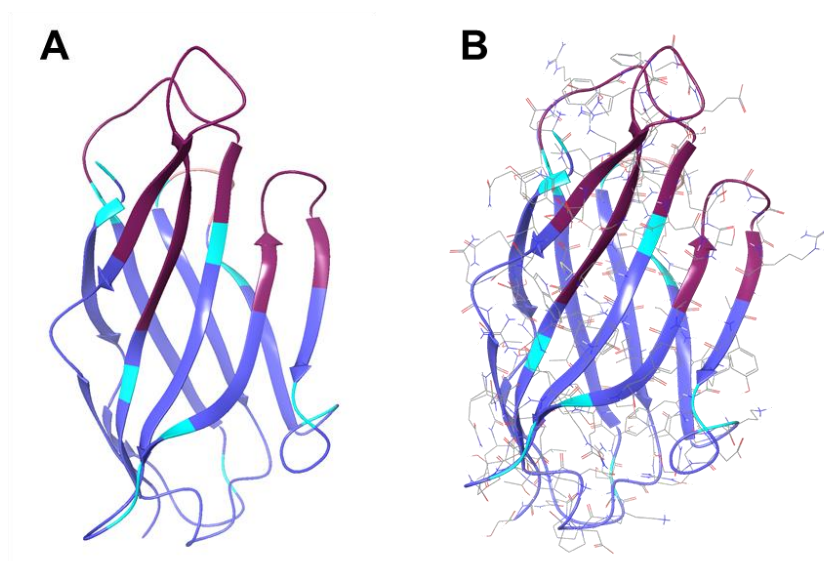
Figure 5.4. Homology model of the anti-minocycline sdAb.

(A) The highest quality predicted anti-minocycline antibody structure generated using the template heavy chain framework VHH domain EgA1 antibody (PDB ID: 4KRN) shown in three-dimensional orientation. Antibody framework regions are shown in purple, Vernier zone is shown in blue and the CDRs are shown in maroon. (B) The Schrodinger Protein Preparation Wizard was used to assign bond order, add hydrogens and create disulphide bonds at pH 7.0 +- 2.0.

5.3.2 Experimental identification of critical sdAb and minocycline binding residues

To aid in validating the future binding interface predictions made by computational docking of sdAb-minocycline/GWARA peptide, experimentally derived binding data was essential. Therefore, to reveal the critical hotspots involved in anti-minocycline sdAb binding to minocycline and GWARA, empirical alanine scanning mutagenesis of residues within all three sdAb CDR region was carried out. CDR regions were identified using the IMGT and Kabat numbering system to consider the broadest defined CDRs involved in binding. Once the CDR residues (38 in total) were defined, the functional significance of each residue was tested experimentally by measuring the binding of minocycline against a panel of recombinantly expressed anti-minocycline sdAb constructs bearing alanine substituting mutations at 38 independent

residue positions or serine substitutions where alanine was being mutated. Biacore SPR was used to determine KD values for the interaction of minocycline with each alanine mutant. The critical residues were determined as those which showed a 10-fold reduction in binding affinity (KD) relative to the wild-type sdAb.[315]

To summarise, upon introducing alanine substitution mutations to each hotspot residue position, each construct was expressed with the addition of an Fc-region at the C-terminus and purified using protein-A affinity chromatography. Binding was then tested by immobilising each sdAb mutant to a Protein-A Biacore chip and binding kinetics against minocycline was measured relative to the wild-type sdAb (Table 5.1). Table 5.1 shows significant reduction in minocycline binding in one of the mutants (A55S) with binding completely abolished in the case of 7 mutants (N38A, W110A, G111A, E112A, L115A, D116A and Y117A). Additionally, I observed an approximate 2-fold reduction in binding affinity (KD) for a further 7 mutants (Y37A, I56A, S57A, S59A, G109A, A113S, I114A).

Mutation	ka (1/Ms)	kd (1/s)	KD (M)	Ratio (WT/mutant)
WT	5.29E-02	3.32E-08	3.61E-08	1.00
G27A	2.10E+06	8.57E-02	4.08E-08	0.88
R28A	2.64E+06	7.49E-02	2.83E-08	1.28
T29A	1.83E+06	4.49E-02	2.45E-08	1.47
F30A	5.55E+06	1.45E-01	2.61E-08	1.38
S35A	1.97E+06	7.36E-02	3.73E-08	0.97
S36A	1.71E+06	6.34E-02	3.70E-08	0.98
Y37A	5.09E+05	4.04E-02	7.93E-08	0.46
N38A	N/A	N/A	1.00E-06	0.04
I39A	3.17E+06	8.47E-02	2.67E-08	1.35
G40A	1.73E+06	3.66E-02	2.12E-08	1.70
A55S	5.63E+05	1.46E-01	2.59E-07	0.14
I56A	4.30E+05	3.27E-02	7.62E-08	0.47
S57A	2.01E+06	1.51E-01	7.51E-08	0.48
W58A	2.23E+06	7.58E-02	3.40E-08	1.06
S59A	1.72E+06	1.13E-01	6.60E-08	0.55
G62A	2.96E+06	7.68E-02	2.60E-08	1.39
A63S	1.38E+06	6.43E-02	4.67E-08	0.77
R64A	5.19E+06	1.62E-01	3.13E-08	1.15
T65A	3.86E+06	2.15E-01	5.57E-08	0.65
Y66A	4.48E+06	6.55E-02	1.46E-08	2.47
Y67A	1.85E+06	7.19E-02	3.88E-08	0.93
A68S	2.03E+06	8.52E-02	4.21E-08	0.86
D69A	4.99E+05	3.02E-02	6.06E-08	0.60
S70A	1.60E+06	7.36E-02	4.61E-08	0.78
V71A	2.07E+06	5.93E-02	2.87E-08	1.26
K72A	2.61E+06	9.72E-02	3.72E-08	0.97
G74A	1.67E+06	5.54E-02	3.32E-08	1.09
G107A	4.42E+06	1.72E-01	3.89E-08	0.93
R108A	1.05E+07	4.29E-01	4.10E-08	0.88
G109A	5.07E+05	4.43E-02	8.74E-08	0.41
W110A	N/A	N/A	1.00E-06	0.04
G111A	N/A	N/A	1.00E-06	0.04
E112A	N/A	N/A	1.00E-06	0.04
A113S	2.23E+06	1.41E-01	6.31E-08	0.57
I114A	1.37E+06	1.20E-01	8.77E-08	0.41
L115A	1.41E+05	1.61E-01	1.14E-06	0.03
D116A	N/A	N/A	1.00E-06	0.04
Y117A	N/A	N/A	1.00E-06	0.04

Table 5.1. Kinetic constants ka (1/Ms), kd (1/s) and KD (M) of the wild-type anti-minocycline sdAb and alanine scan mutagenesis based anti-minocycline sdAb clones binding to minocycline.

Ratio of alanine scan mutagenesis based sdAb KD (M) against WT KD (M) also presented to show abolishment of binding (red) and increase in binding affinity relative to WT sdAb (green).

5.3.3 Confirmation of thermal stability of alanine sdAb mutants

To exclude the elimination of binding as a result of protein instability and domain unfolding, assessment of the antibody unfolding and melting temperature (Tm) of the of wild-type anti-minocycline sdAb and each mutant sdAb was determined using nano differential scanning fluorimetry (nanoDSF). High first unfolding midpoint (Tm) of ~80-70°C was measured for all mutant sdAbs, except for G62A, which presented a Tm value of 57.7°C. Although a Tm value of 57.7°C was lower than the majority of sdAb, it does not suggest G62A was unstable (Fig. 5.5).
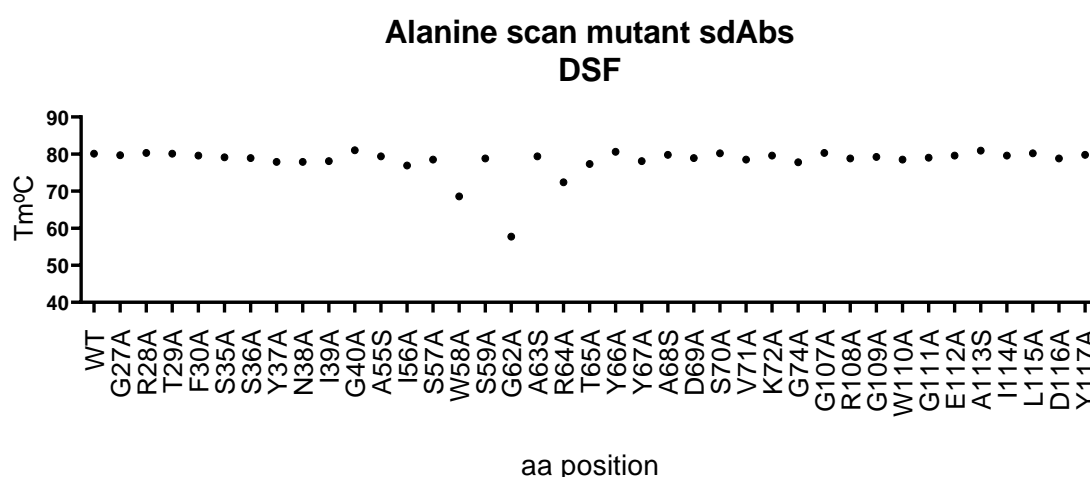
Figure 5.5. Thermal stability of alanine mutant sdAbs by nanoDSF.
Melting temperature (Tm) of wild-type anti-minocycline sdAb and each mutant sdAb. Temperature gradient relationship to F350 nm/F330 nm fluorescence reading ratio.

5.3.4 Experimental identification of critical sdAb GWARA binding residues

Next, I set out to determine the critical residues involved in GWARA peptide binding by carrying out an ELISA using each of the recombinantly expressed 38 alanine-scan sdAb mutants. Binding (OD450) was tested by immobilising ACPGWARAFC peptide to the respective wells of an ELISA plate, followed by incubation with wild-type anti-minocycline sdAb and the full range of mutated sdAbs. The functional significance of each mutation was then judged by measuring binding of that mutant compared to wild-type sdAb. With the

information gathered, I set out to assess the degree of binding site overlap by comparing the functional binding data generated though GWARA binding to that previously indicated to be binding hotspots involved in minocycline binding.

Figure 5.6 shows that multiple alanine sdAb mutants demonstrated a significant reduction in binding to GWARA. The greatest obliteration in GWARA binding was observed in the following mutants: R28, S35, G40, S58, A63, R64, and R108.
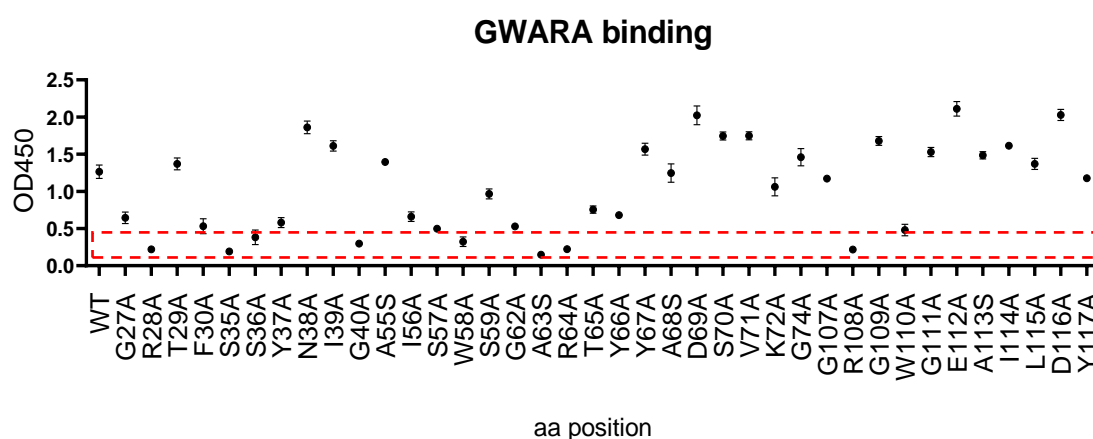
Figure 5.6. ELISA binding of GWARA peptide against a panel of recombinantly expressed anti-minocycline sdAb constructs bearing alanine substituting mutations at 38 independent CDR residue positions. *Binding of wild-type sdAb and alanine-scan sdAb clones to ACPGWARAFC peptide was determined using a sandwich ELISA. ACPGWARAFC peptide was immobilized to respective wells at a concentration of 1 μg/ml. Wild-type sdAb and alanine-scan sdAb variants, expressed as fusions to a murine-Fc-region at the C-terminus and purified using protein-A affinity chromatography, was then incubated as the secondary antibody. Anti-murine-HRP conjugate was then used as the detection antibody. Readouts were taken using the Multiskan™ FC Microplate Photometer at a wavelength of 450 nm.*

5.3.5 Computational protein–ligand docking to predict sdAb-minocycline/GWARA peptide residue interaction and binding interface

5.3.5.1 Preparation of ligands

Before carrying out further computational studies such as the Schrodinger's antibody-ligand docking program, preparation of ligands using the LigPrep programme was carried out to convert the 2D ligand (minocycline or GWARA) structures to produce corresponding low energy 3D structures in either an SD or Maestro format. With the option to expand each input structure by generating variations on the ionization state, tautomers, stereochemistry and ring conformations (Fig. 5.7). Schrodinger's Epik tool was also used to generate chemically favourable states at pH 7.0 ± 2.0. The most energetically favourable states of the 3D ligand as a measure of kcal/mol were selected for downstream computational docking studies with the previously generated sdAb homology model.

A

2D minocycline structure
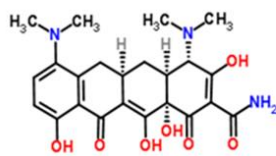
3D minocycline structures generated using LigPrep
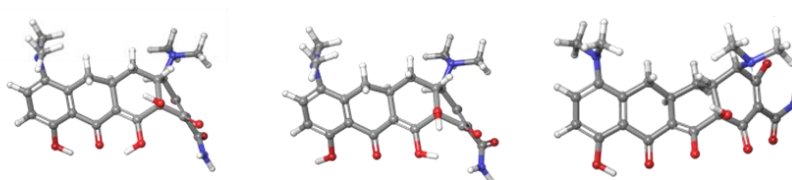
Overlay of 3D structures
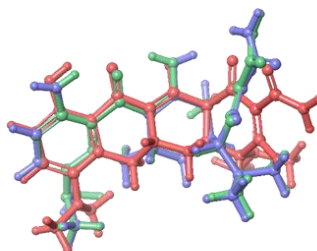
B

2D ACPGWARAFC peptide structure
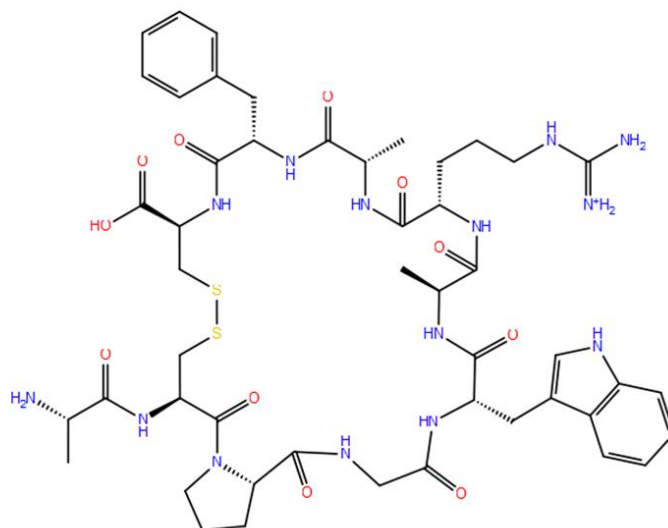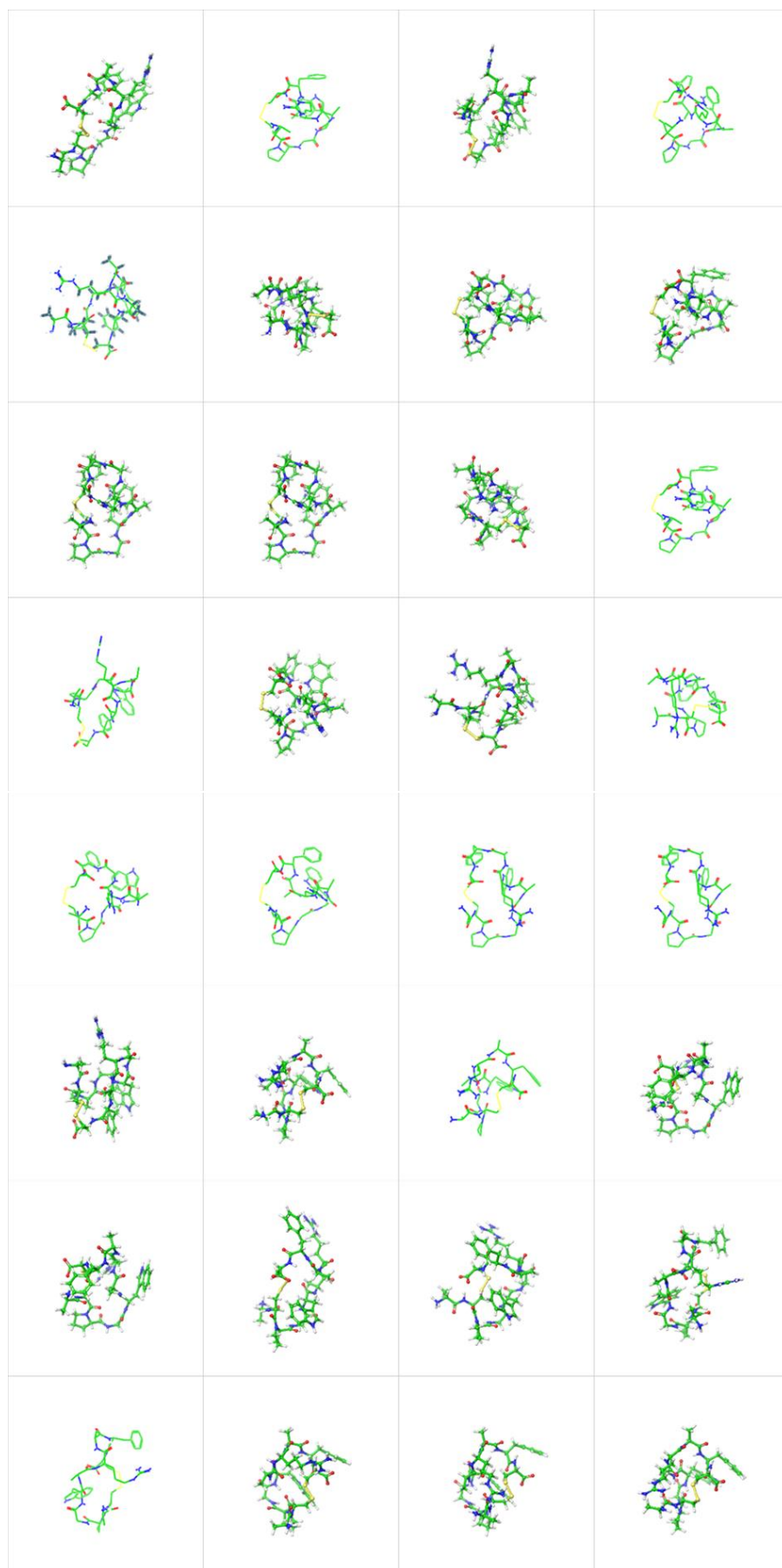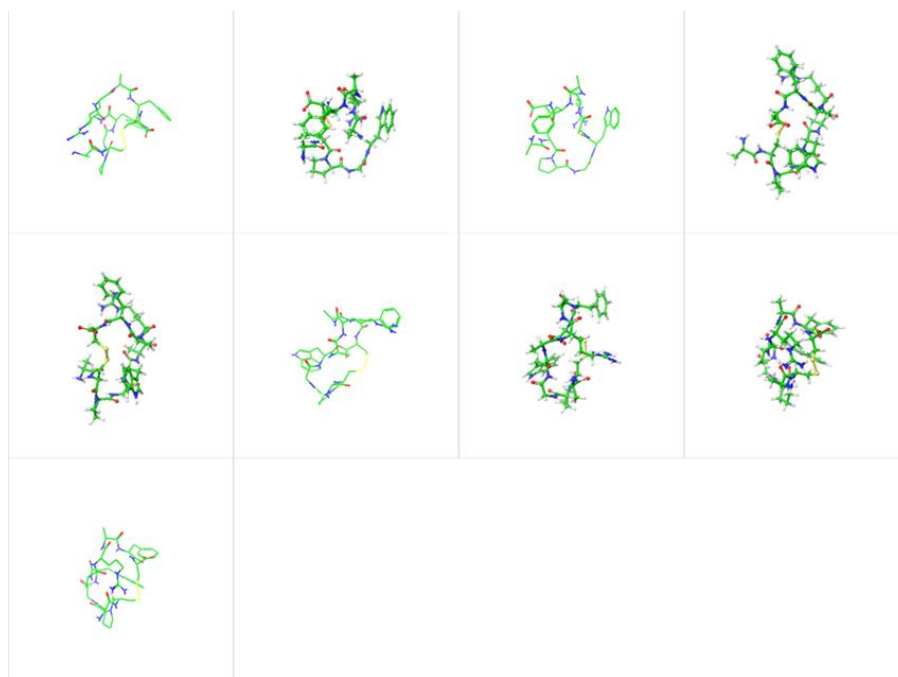
Figure 5.7. Minocycline and GWARA peptide were converted from 2D structures to produce corresponding low energy 3D structures using LigPrep Wizard for subsequent ligand-sdAb docking studies.

(A) 2D Minocycline structure generated three 3D-ligand structures and (B) 2D structure of GWARA peptide generated 41 corresponding 3D structures. Schrodinger's Epik tool was used to generate chemically favourable states at pH 7.0 ± 2.0 and the energetically favourable states of the 3D ligand as a measure of kcal/mol were selected.

5.3.5.2 Computational protein–ligand docking to predict sdAb structure and minocycline/GWARA peptide interaction

Prior to carrying out docking of the prepared 3D minocycline and GWARA structures with the sdAb homology model, a receptor grid was placed on model 10 (energy minimised) to restrict the Ab:ligand interface (Fig. 5.8). The receptor grid generated was relatively broad at approximately 10 Å in each direction (X, Y and Z planes) from the geometric centre of the three CDRs.
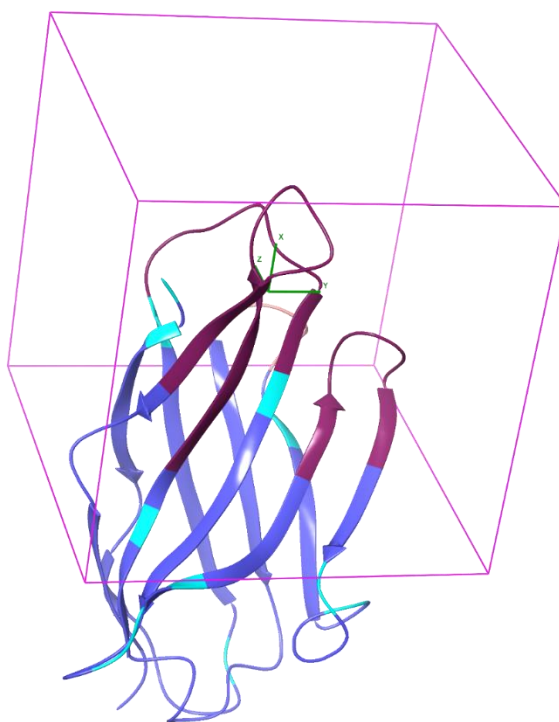
Figure 5.8. Receptor grid generation defined for protein-ligand docking optimisation.

Ligand interaction was programmed to be restrained to residues within the CDR to be included as a part of the binding interface (10 Å X,Y,Z span).

5.3.5.3 Identification of the anti-minocycline dAb and minocycline binding interface

Once the CDR receptor grid was imposed on and the conversion of 2D ligands to 3D structures had been generated, the Schrodinger BioLuminate software was used to perform a rigid body CDR-ligand docking optimisation resulting in several poses, each of which were ranked based the Glide docking methodologies.[316,317] Glide utilises a series of hierarchical filters to seek regions of the ligand which interacts with the CDR. The structure and properties of the CDR region are characterized via different sets of fields which offer increasingly more accurate scoring of the antibody-ligand pose. Comprehensive ligand conformations are refined in torsional space in the antibody. A number of poses are then minimised upon receptor docking with full ligand flexibility (post-docking minimization). Glide uses the GlideScore

function, which is an empirical scoring function intended to rank strongly binding compounds with high binding affinity from weak to no binding.[317] As with empirical scoring function, the physics of a binding interaction such as electrostatic forces, lipophilic-lipophilic interactions, hydrogen bond formation, salt bridge formation, and van der Waals bond conditions taking place between the antibody and ligand are considered.

Based on the high/optimal glide score in conjunction with functional SPR binding data generated from minocycline binding to a panel of sdAb bearing alanine mutations within the CDR regions, 3 docking poses were selected which were likely to resemble the true binding interface (Fig. 5.9A). Figure 5.9A shows the top ranked poses of the minocycline/sdAb binding interface generated using 4KRN as the template framework in various binding orientations with each top ranked pose presenting a glide score of -4.060, -3.265 and -2.726, respectively, with pose_1 showing the highest score of -4.060. Higher resolution images of the amino acid residues within the sdAb CDR loops directly interacting with the functional groups of minocycline are shown in Figure 5.9B and indicate key predicted hotspot residues. Pose_1 predicted S36, N38 and E112 contribute to minocycline binding, pose_2 predicted S36, G107 and E112 to contribute to minocycline binding and pose_3 predicted N38 to directly interact with minocycline.

A

Pose_1 (Glide score: -4.060)
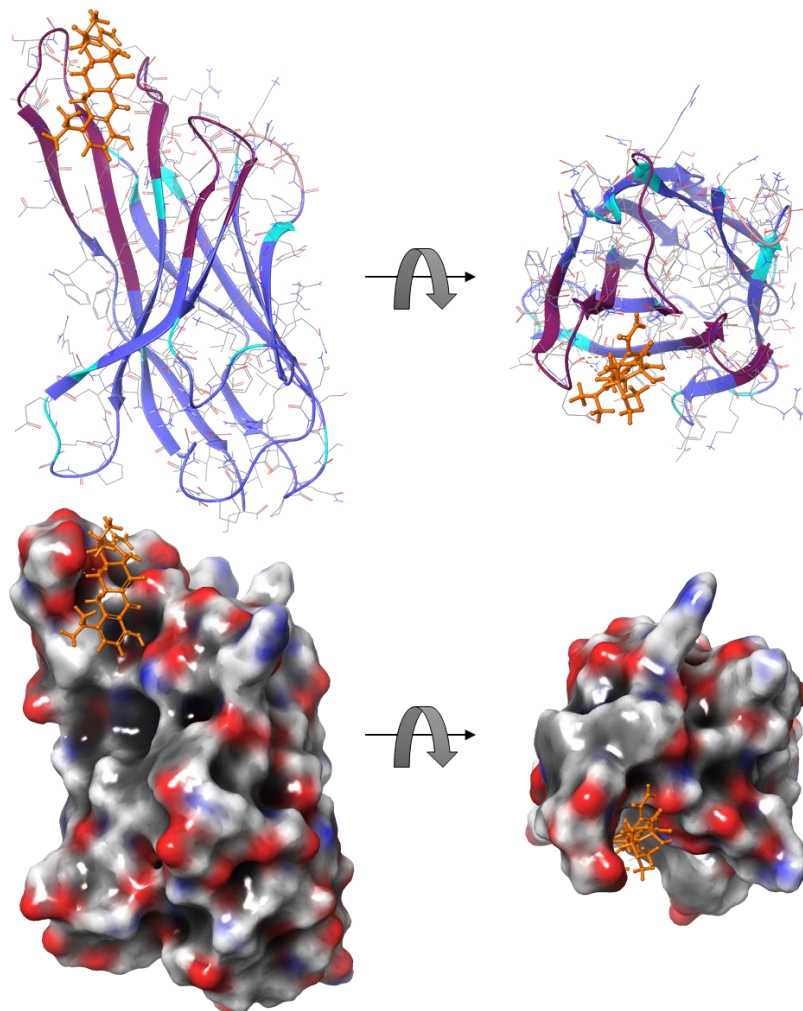
B
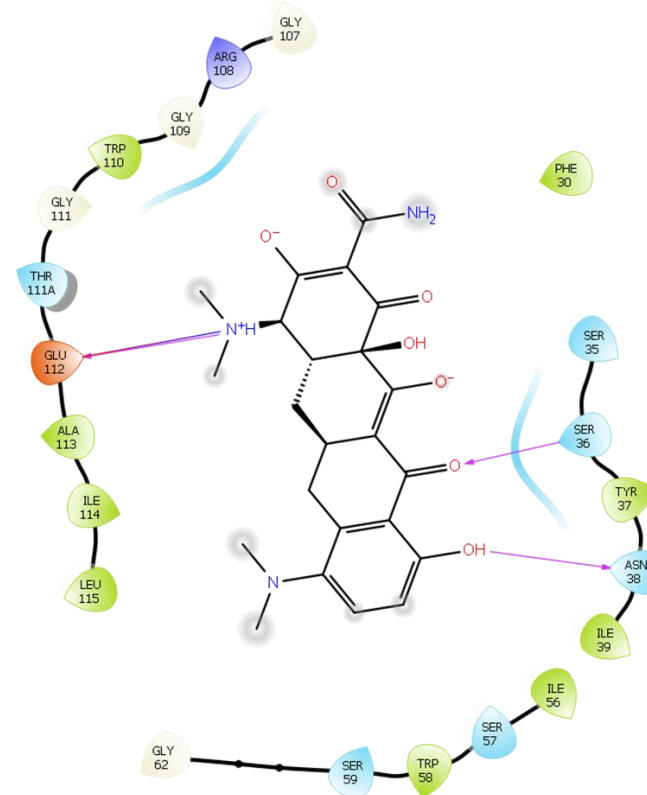
A

Pose_2 (Glide score: -3.265)
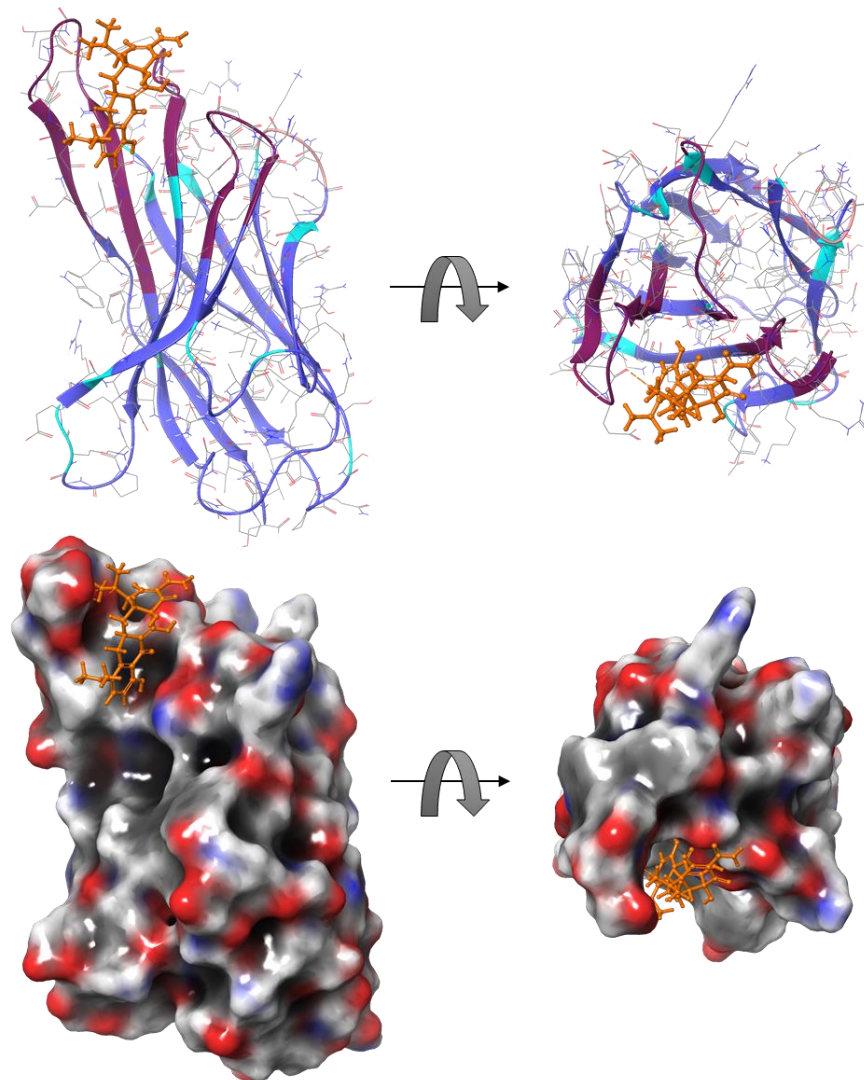
B
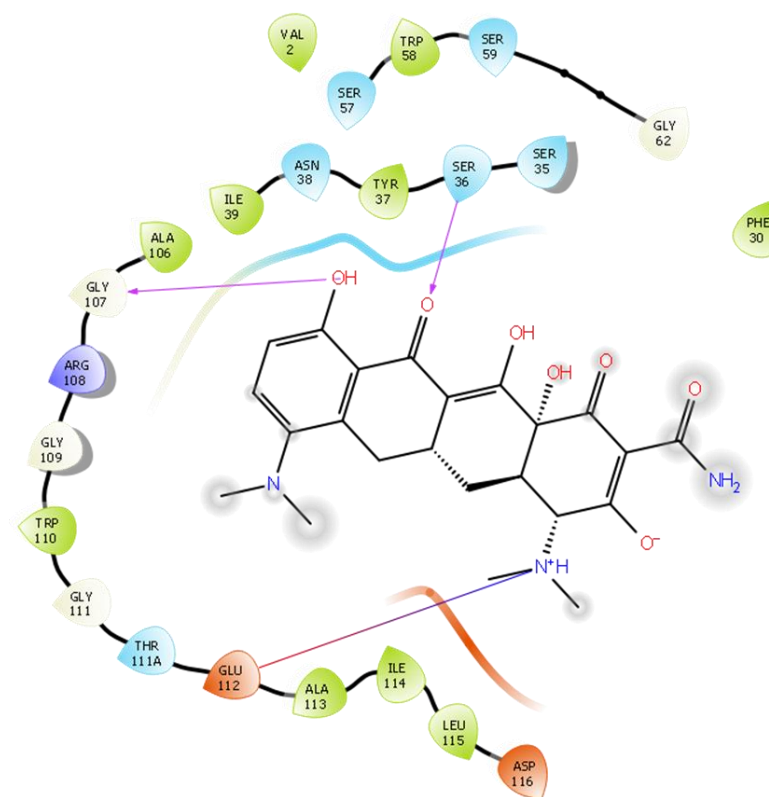
A

Pose_3 (Glid score: -2.726)
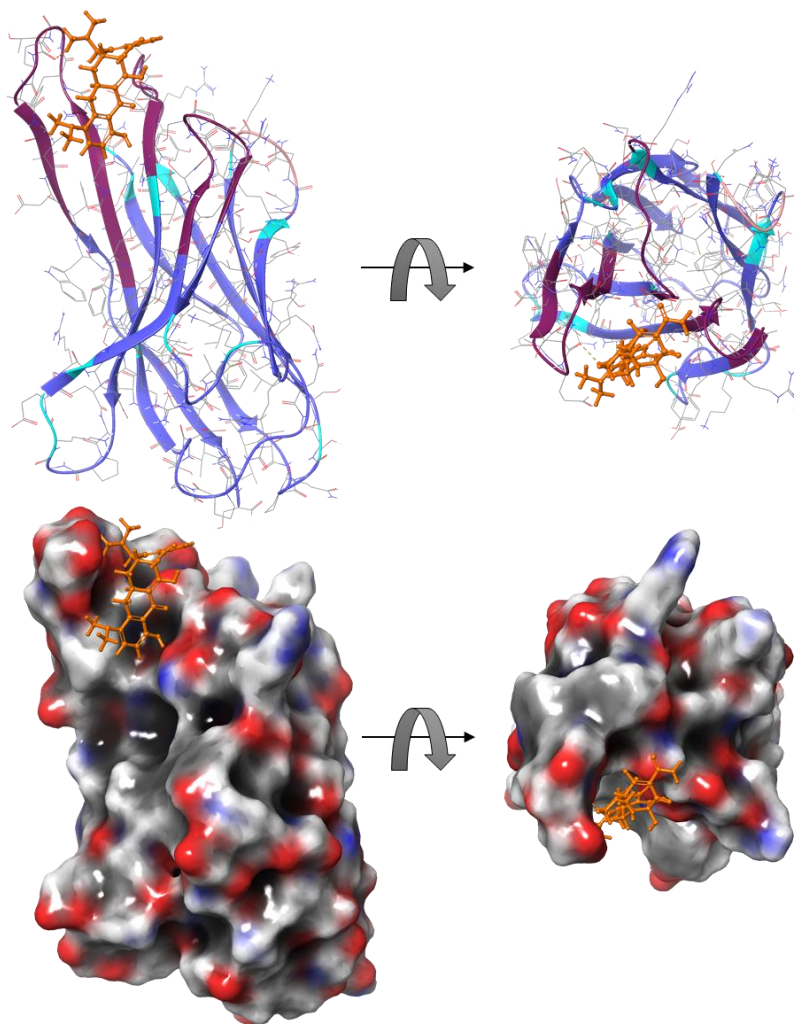
B
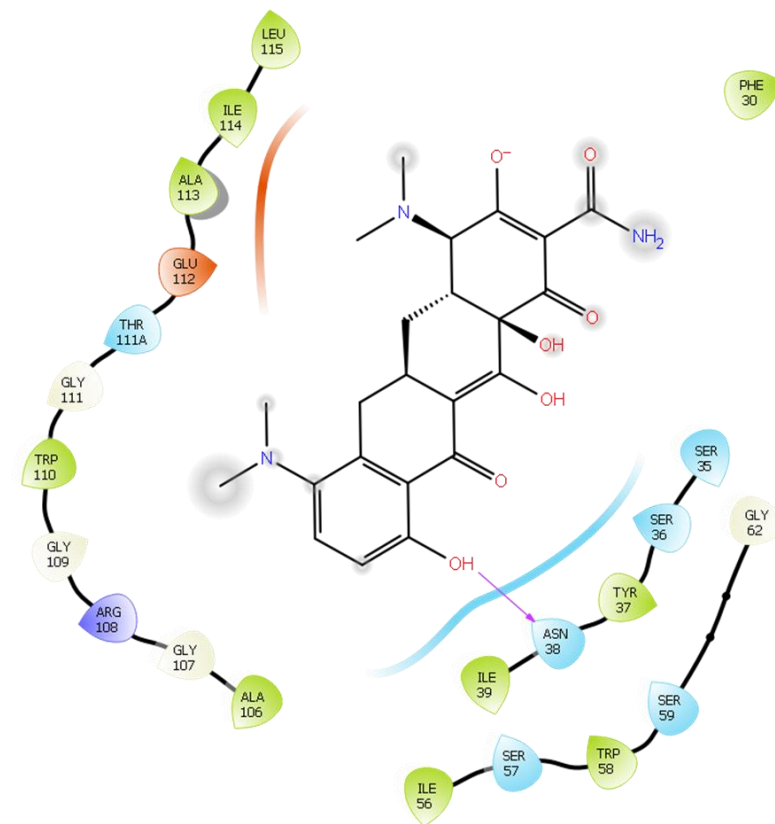
Figure 5.9. Computational antibody-ligand docking of sdAb-minocycline binding.

(A) The top three ranked antibody-minocycline docking models generated by Schrodinger BioLuminate based on the Glide score. Each sdAb-minocycline binding interface is shown in three-dimensional orientations (zy-plane and xy-plane) and the orientation is constant for each pose. (B) Docking images are accompanied by ligand interaction diagram showing the 2D ligand molecule and all sdAb aa within a 6 Å distance (including aa from CDR1-3 and framework residues). Hydrogen bond: violet arrow line; salt bridge: direct connectine line red to blue.

5.3.5.4 Identification of the anti-minocycline sdAb and GWARA peptide binding interface

Using an identical sdAb CDR receptor grid definition for protein-ligand docking, GWARA peptide docking was carried out on the sdAb homology model previously generated. In addition to the glide score, the experimental binding data from the library of the sdAb alanine scan mutagenesis was also taken in consideration to select models from all the possible binding conformations. Experimental data showed GWARA binding was significantly reduced in sdAb clones bearing alanine mutations at positions: R28, S36, G40, S57, A63, R64, R108 and W110. Figure 5.10 shows the top ten ranked poses of the GWARA/sdAb binding interface in various binding orientations.

In addition, the direct interaction with the CDR residues, weak interactions with proximal CDR residues which have the potential to directly interact or be crucial in forming binding hotspots through the formation of the CDR structure were indicated (Fig. 5.10). To summarise, pose 1 predicted specific bond formation interaction with R64 and E112, pose 2 and 3 both predicted interactions with S57 and E112, pose 4 predicted interactions with R64 and E112, pose 5 and 7 both predicted interactions with D116 and W118, pose 6 and 9 predicted interactions with only E112, pose 8 showed interactions with N38 and E112, whilst pose 10 predicted interactions with S59 and E112 (Fig. 5.10)

A
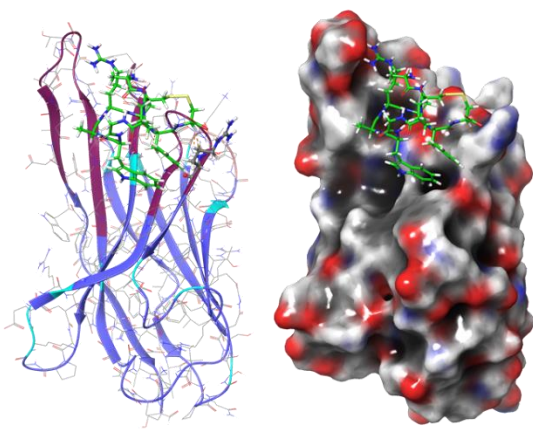
Pose_1 (glide score: -6.014) Pose_2 (glide score -5.871) Pose_3 (glide score -5.843)
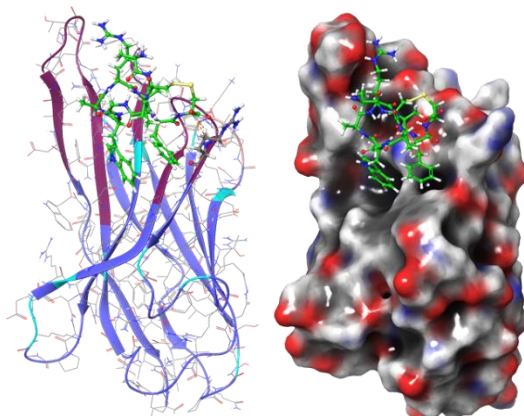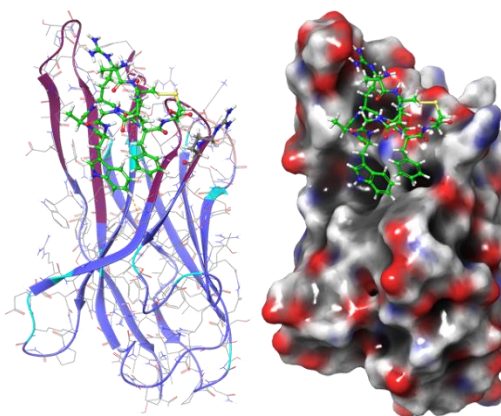
Pose_4 (glide score -5.725) Pose_5 (glide score -5.69) Pose_6 (glide score -5.631)
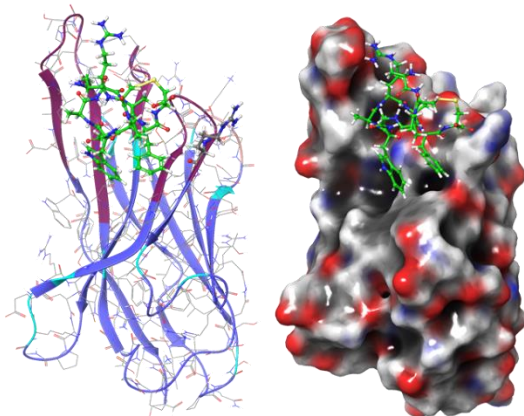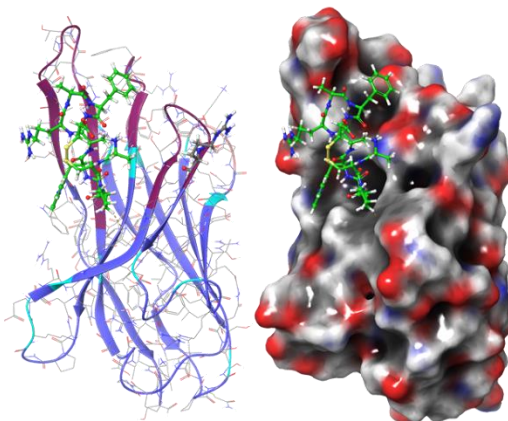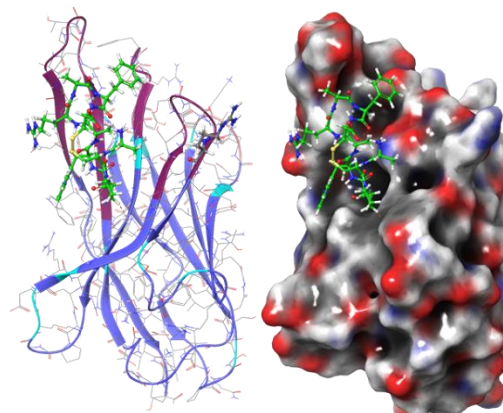
Pose_7 (glide score: -5.542)
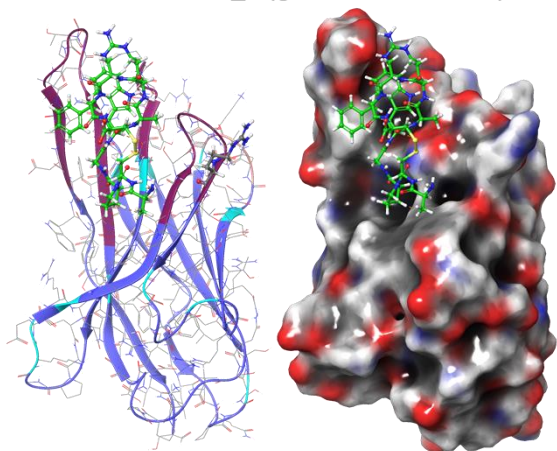
Pose_8 (glide score -5.488)
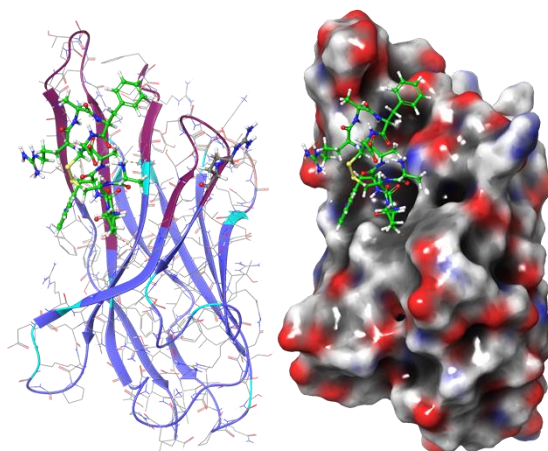
Pose_9 (glide score -5.474)
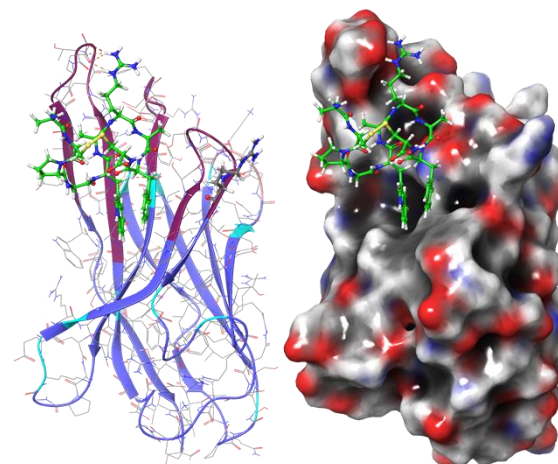
Pose_10 (glide score -5.446)

B

Pose_1 (glide score: -6.014)

Pose_2 (glide score -5.871)

207

Pose_3 (glide score -5.843)

Pose_4 (glide score -5.725)

208

Pose_5 (glide score -5.69)

Pose_6 (glide score -5.631)

Pose_7 (glide score: -5.542)

Pose_8 (glide score -5.488)

210

Pose_9 (glide score -5.474)   **Pose_10 (glide score -5.446)**
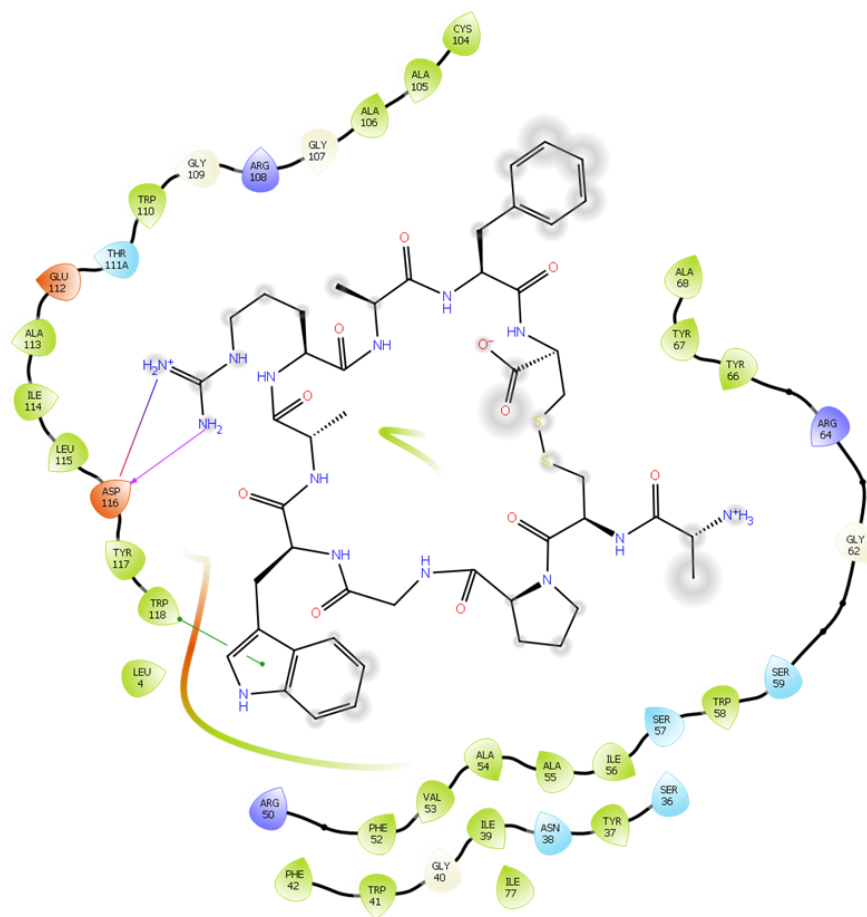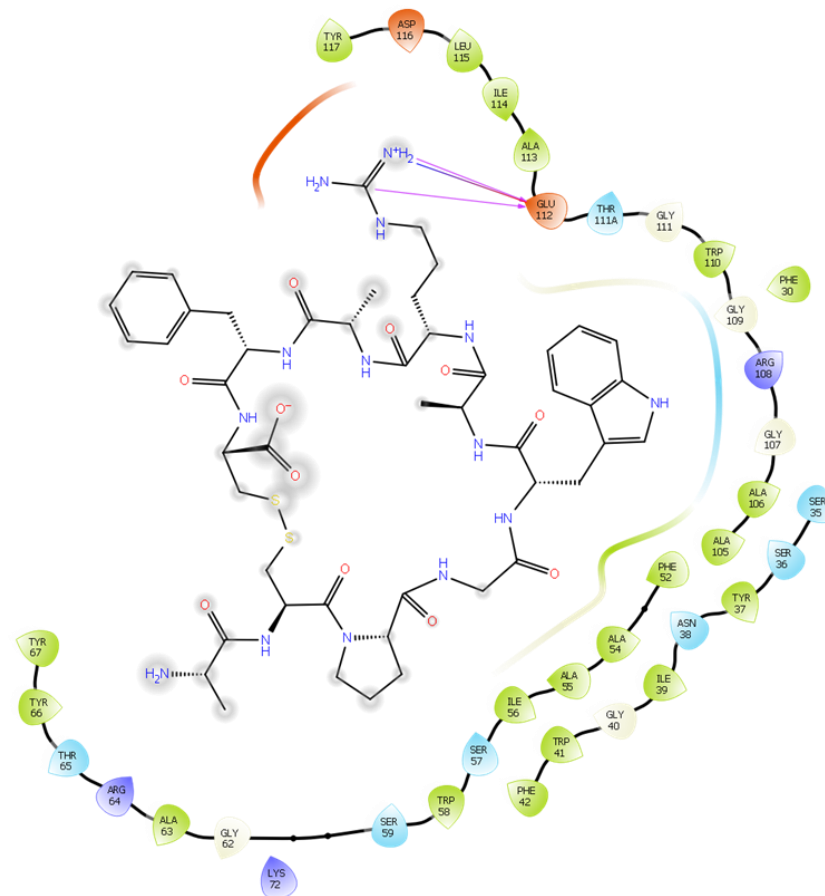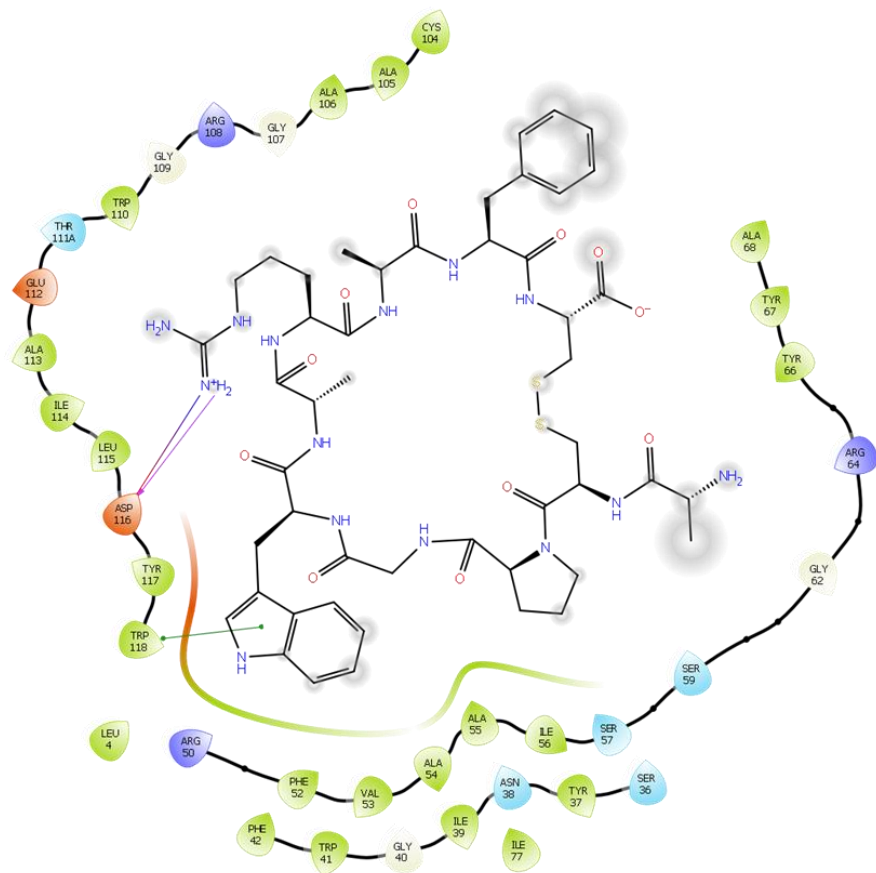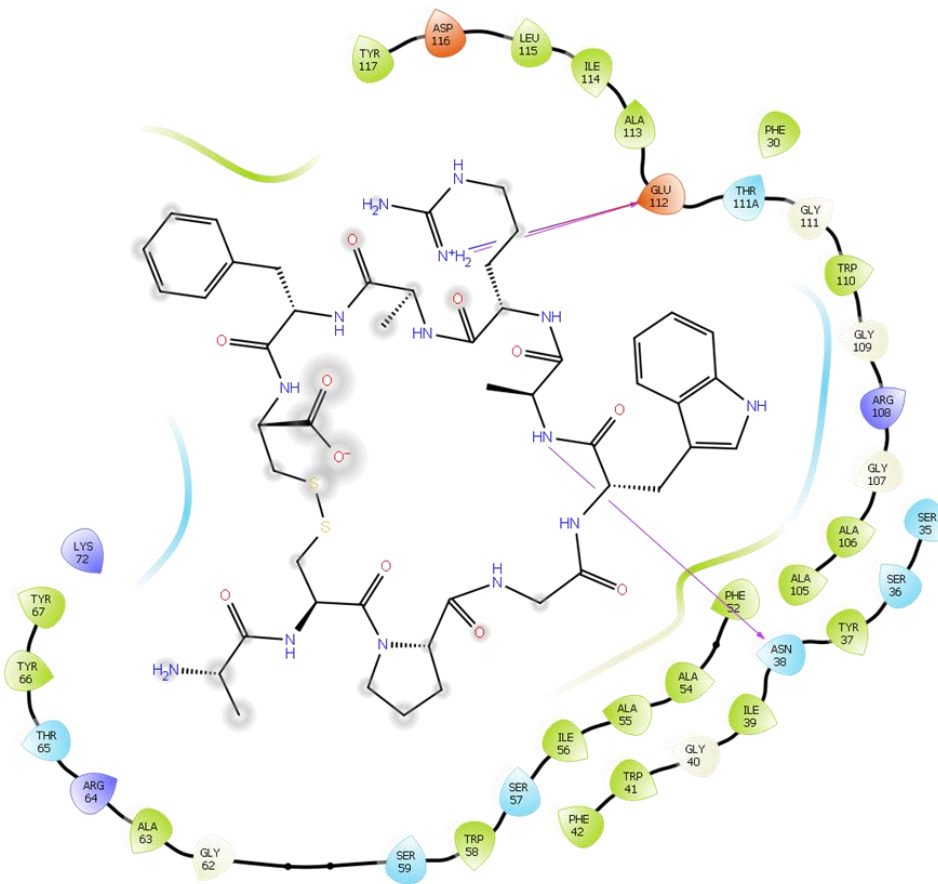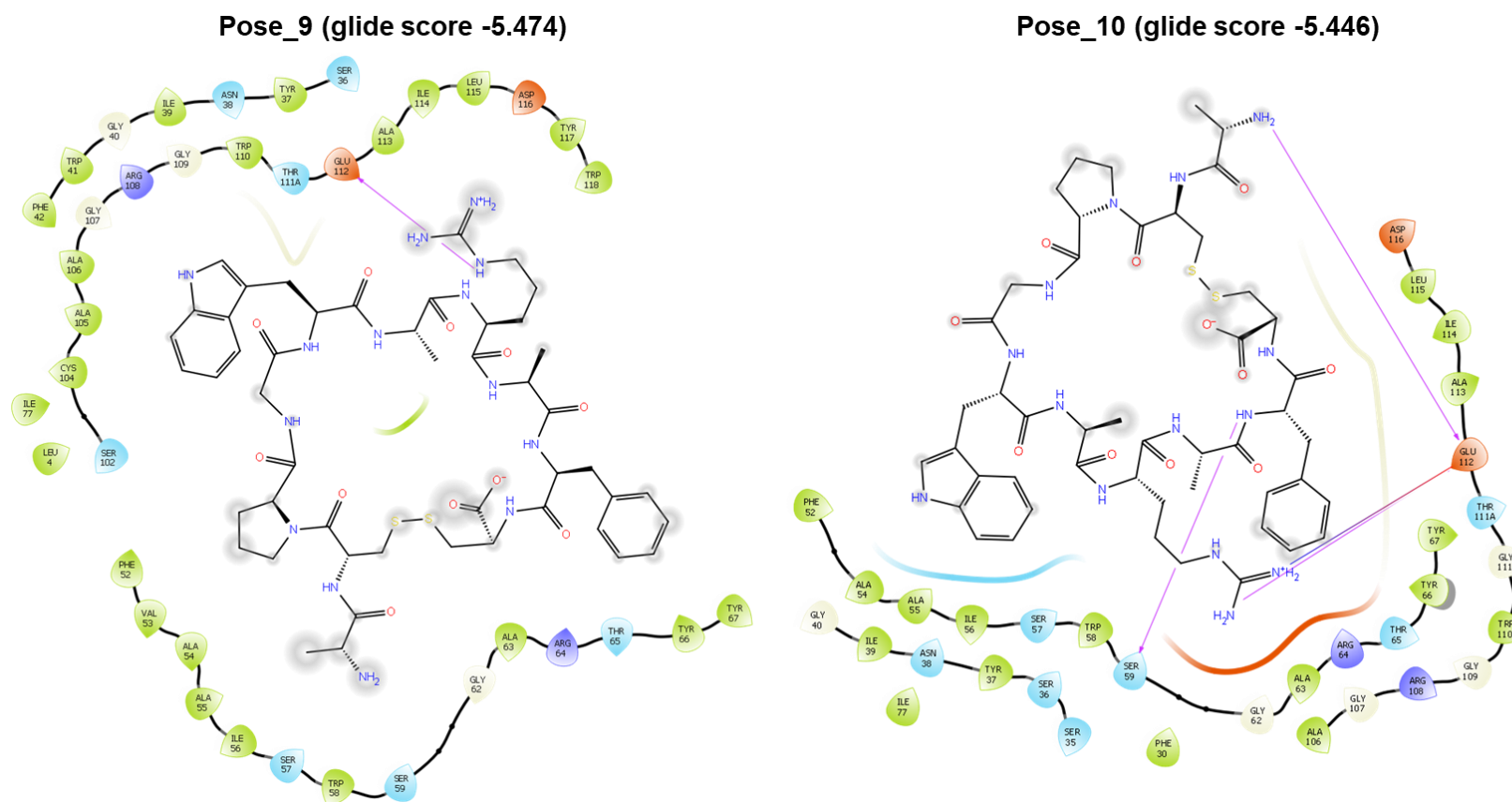
Figure 5.10. Computational antibody-ligand docking of sdAb-GWARA binding.

(A) The top ranked antibody-peptide docking models generated by Schrodinger BioLuminate based on the Glide score. Each sdAb-GWARA binding interface is shown in three-dimensional orientations (zy-plane and xy-plane) and the orientation is constant for each

pose. (B) The docking visualisations are accompanied by higher resolution ligand interaction diagrams showing the 2D peptide structure and all sdAb aa within 6 Å distance (including residues from CDR1-3 and framework regions). Hydrogen bond: violet arrow line; salt bridge: direct connecting line red to blue; pi-pi: green line.

5.4 Discussion

In this chapter, I utilised Schrodinger BioLuminate computational homology protein modelling to generate a 3D model of the anti-minocycline sdAb using an experimentally validated crystal structure of a homologous sdAb. As the number of available antibody and sdAb crystal structures expands, antibody homology models generated are consistently reaching high resolution (1.5-3.5 Å) accuracy for the FR and CDRH1/H2, excluding the CDRH3.[318] With an Ab homology modelling generally considered to be of high quality with <2 Å root-mean-square deviation (RMSD) from native structure for all regions with the HC-CDR3 region having 6 Å RMSD.[319,320] I selected a template framework which showed high level of structural identity, similarity and resolution which I believe to contribute to a successful docking model (PDB ID 4KRN, resolution: 1.55 Å) as single domain antibodies derived from camelids specifically containing long CDRH3s are generally considered to be trickier to model. The EgA1 (4KRN) sdAb is known to be an inhibitory antibody binding with high affinity to the extracellular region of epidermal growth factor receptor (EGFR) near the domain II/III junction.[311] Upon carrying out loop optimisations of homology models, model 10 was selected based on the Ramachandran plots showing the lowest percentage of amino acids being positioned in outlier regions relative to the template antibody. Although the quality of the Ramachandran plots generated were high, in the future, the performance of the homology model generated will improve with greater number of solved crystal structures of Camelid derived sdAbs. Typically, the approach used here utilises human derived conventional antibodies bearing structures which are constrained and possess a greater repertoire of homologs which generate high-quality docking model. In my selections, it was important to choose homology models using templates from crystal structures over homology models as higher quality docking models have been reported using this approach.[304,321]

Selection of a panel of paratope residues to undergo alanine-scanning was broadly determined as CDR residues using IMGT and Kabat numbering.

However, it cannot be ruled out that our selection criteria were too restrictive and may have prevented paratope residues within the FR impacting both specificity to the binding interface via direct contact or indirect conformational changes of the sdAb binding pocket. Although mutating the CDRs was the most logical step for initial alanine scanning, previously solved crystal structure of sdAb-hapten complexes show CDR1 to be key in hapten binding over CDR3. As the N38A mutation resides within the CDR1 region and shows a significant reduction in the affinity for minocycline this may also be true for minocycline binding. On the other hand, structural analysis of the anti-methotrexate sdAb in complex with methotrexate showed framework region (FR)3, which is upstream of CDR3, was found to interact with the hapten and drastically contributed to generating a high-affinity interaction with methotrexate.[233] Therefore, the CDR loop interaction outside of the CDR3 region may be significant when interacting with haptens. Although the database of solved structures of sdAb-haptens complexes are very limited, a large library of alanine mutagenesis of the FR residues may be required for model refinement.

Whilst selecting the CDR residues to mutate, the aim was to disrupt paratope-epitope binding whilst maintaining antibody stability and expression. Although controlling the balance of functional binding and stability is unpredictable, I sought a more favourable setup of completely disrupting the interaction/affinity, rather than improving the affinity. Similarly, I sought to maintain antibody expression and stability by focusing on solvent exposed residues for alanine scan mutagenesis, as these are generally less prone to influence the overall structure of the antibody.

Analysis of the top ranked sdAb-minocycline and sdAb-GWARA binding interface showed the top two poses of each docking models to be both energetically favourable interactions with the sdAb and reliable with respective experimental data, except for S36 shown to be a hotspot residue for minocycline binding and E112 shown to be interacting in GWARA binding in all top ranked poses. The most significant predicted commonalities in sdAb-minocycline ligand binding were shown to be S36, N38 and E112. These were

all indicated in pose_1. This validated the experimental data which indicated mutations at positions N38, W110, G111, E112, L115, D116 and Y117 to abolish minocycline binding. On the other hand, the most energetically favourable docking model suggested R64 and E112 to form hotspot resides for GWARA binding. Experimental data showed GWARA binding was significantly reduced in sdAb clones bearing alanine mutations at positions: R28, S35, G40, S58, A63, R64, and R108. However, although experimental data corroborates R64 to abolish binding to GWARA, mutation of E112 (which was predicted to interact in all 10 poses) did not abolish binding to GWARA. Therefore, the in-silico data is only partially in agreement with experimental data. Additionally, experimental binding data shows minimal overlap between hotspot residues for minocycline and GWARA binding. Superimposing the two top ranked poses, provides the basis of a possible explanation for the displacement/completion between the two ligands, potentially a result of competition for the same binding pocket within the sdAb rather than targeting mutually binding amino acid residues (Fig. 5.11). Figure 5.11 shows both minocycline and GWARA interact for the same region within the antibody.
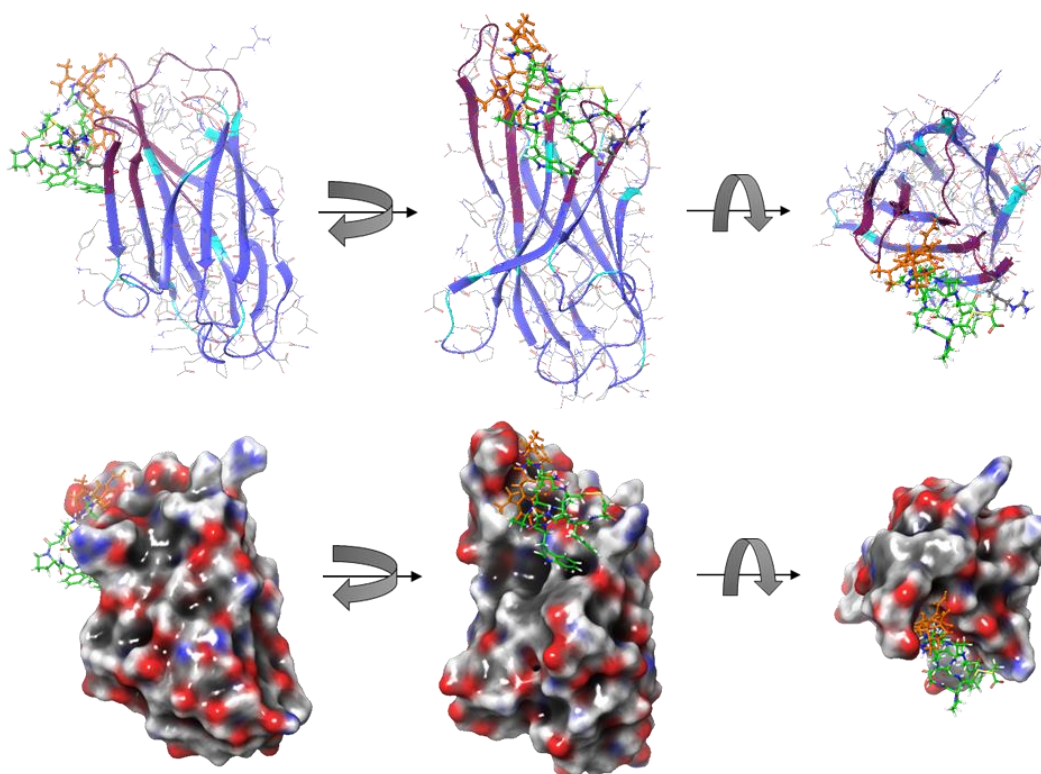
Figure 5.11. Overlay of top scoring poses for docking interface of anti-minocycline sdAb-minocycline (orange) and anti-minocycline sdAb-GWARA (green) generated by Schrodinger BioLuminate based on the Glide score. Each overlay binding interface is shown in three-dimensional orientations.

Improvements in the docking models could be achieved through the use of new homology modelling using multiple other scaffold antibodies and assessing the predicted poses with experimental data. Additionally, molecular dynamics simulation could be performed which would allow greater flexibility to accommodate the sdAb in an optimal conformation. Finally, improving attempts at solving x-ray structural data by improving stable crystal structure formation will conclusively provide accurate structural characterization of antibody-drug and antibody-peptide complexes. Nevertheless, although conclusive evidence of the binding mechanism could not be drawn from these limited models, we have previously shown (Chapter 3 and Chapter 4) several pieces of evidence confirming engagement of the sdAb with minocycline and GWARA.

The computational model described in this chapter has many limitations: for example, the docking is based on an antibody model structure, therefore inaccuracies at the early stage of model generation are exaggerated once a docking programme is applied. Ideally, a solved x-ray crystallography structure would provide a more accurate basis for carrying out in-silico ligand docking. Moreover, docking poses do not fully recapitulate the experimental data which may be result of incorrect suggested poses. Furthermore, the abolished binding observed in the panel of sdAb alanine mutants may be caused by alteration of the CDR loop folding rather than direct interactions. Additional in-silico work to evaluate the fidelity of the model may be done by running in-silico alanine scanning and evaluating predicted delta affinity values.

5.5 Conclusions

- Homology models of the anti-minocycline sdAb were determined, which were used to carry out with computational sdAb-minocycline and sdAb-peptide docking

- Using a range of mutated anti-minocycline sdAbs generated through alanine scanning-mutagenesis of the CDRs, key hotspot residues in minocycline binding (N38, W110, G111, E112, L115, D116 and Y117) and GWARA binding (R28, S35, S36, G40, W58, R64 and R108) were determined

- Using the docking model in conjugation with experimental data, the data show that minocycline and GWARA most likely compete for the same antibody pocket rather than shared residues.

6 DEVELOPMENT AND IN-VITRO TESTING OF A NOVEL MINOCYCLINE MEDIATED OFF-SWITCH CAR T CELL

6.1 Introduction

In previous chapters I presented work on the generation and characterisation of a single domain antibody targeting minocycline (anti-minocycline sdAb) which also showed specificity towards a cyclic peptide, GWARA within a high nanomolar interaction range. Additionally, I presented evidence showing the presence of the drug minocycline inhibits or displaces this sdAb-peptide interaction, which forms the basis of a protein-protein displacement system. While this system has potential applications in protein purification and protein displacement-based assays, the greater promise was in an immunotherapeutic based application. In this chapter, the development and optimisation of a minocycline-based OFF-switch split CAR will be described.

As previously detailed, the development and use of cellular therapies has shown great potential in the treatment of conditions such as autoimmune diseases and cancer.[322–324] Whereas, unlike the use of small molecule drugs and biologics, cellular therapies can be programmed to carry out an output function based on external inputs to fulfil a set of well-coordinated and complex actions.[325,326] In recent times, the use of CAR T cells, which are T cells expressing an artificial receptor structure composed of an tumour-associated antigen binding domain (ScFv or sdAb) and an intracellular TCR signaling and co-stimulatory domains, have been widely reported to achieve robust and potent responses against a host of chronic and acute B cell leukaemia's.[327–329] Data from clinical trials have shown successful outcomes with the use of anti-CD19 CAR T cells against relapsed or refractory B-cell malignancies.[330–332] CAR T cells achieve tumour cell clearance through engagement with the tumour-associated antigen(s) leading to direct cytotoxicity and secretion of anti-tumour cytokines resulting in cytotoxic killing of tumour cells and proliferation of the CAR T cells in vivo. Such exponential proliferation results in the subsequent amplified effector function and thus tumour clearance within weeks of administration.[323]

Despite the efficacy demonstrated with the use of CAR T cell therapy, the treatment carries potential risks of significant toxicities. On-target off-tumour related toxicity entails the recognition of the target antigen on normal tissues resulting in the killing of healthy tissue, this is due to the fact only a select few antigens are expressed exclusively on tumour cells.[111] Even with ideal antigen selection and targeting, with no on-target off-tumour related toxicities observed, the most substantial adverse effect resulting from the CAR T cell activity and increased levels of cytokines is the onset of a potentially life-threatening forms of inflammatory responses such as cytokine release syndrome (CRS) and neurotoxicity.[151] Early trials using 'first-generation' CARs, which lacked costimulatory domains, showed poor cytokine production, T cell activation, proliferation and anti-tumour activity.[111–113] With the development of 'second-generation' CARs, these limitations were overcome to show vastly improved anti-tumour responses against hematologic malignancies. Although, this potent anti-tumour response was paired with the potential onset of CRS.[330,333]

The key challenge facing the field of adoptive T cell therapy in response to the diagnosis of CRS, is determining the appropriate intervention strategy to alleviate the physiological symptoms of CRS without eliminating the anti-tumour potential for CAR T cells. Traditionally, corticosteroid have been administered to reverse symptoms of CRS, however, prolonged use of corticosteroids can inhibit CAR T cell function.[157,330] The use of the IL-6 receptor blocking antibody, tocilizumab, is the favoured option to reduce CRS, however, both are show limited effectiveness in treating immune effector cell associated neurotoxicity syndrome (ICANS).[336,337] The large degree of variation in patient responses and toxicity risk means the CAR T cell dosing can also be difficult to determine.[338] CAR T cells against solid tumours have also faced many hurdles in their clinical development, although the latest generation of CAR T cells have provided much hope of efficacy against solid tumour targets. In fact, the mechanisms such as the upregulation of metabolic and physical obstacles, by which the solid tumour microenvironment evades cellular therapies in addition to the mechanism of CAR T cell effector function impairment and exhaustion is well researched.[339] A vast array of technologies,

such as expression of artificial cytokine receptors, cytokines, chemokines, and stimulatory molecules in conjugation with CARs have been engineered and extensively researched to overcome such difficulties with the use of adoptive T cell therapy for solid tumours with promising preclinical data.[339–341] As a result of such potent modifications, the risk of on-target off-tumour toxicity is further magnified by the lack of tumour exclusive antigens found in solid malignancies and has proven to be a profound obstacle to progressing new solid tumour specific technologies the clinic.[171] With the development of highly potent CAR T cell therapies targeting solid-tumours intensifying, the repercussions of uncontrolled T cell activation mean the stakes of adverse toxicities are significantly burdensome. Therefore, engineering novel regulatory mechanisms for precisely and remotely controlling T cell function could not only improve safety of adoptive T cell therapies but also fast-track the route to clinical trials.

Subsequently, many CAR T cell control safety modules have been developed. As detailed in Section 1.4.7, these include the use of suicide switches using pro-apoptotic chimeric molecules which can dimerise and activate in the presence of a small molecule thus initiating apoptosis and the elimination of CAR T cells.[175–179] Although suicide switches act as efficient safety switches by ablation of CAR T cells permanently, this approach may require re-administration of the treatment to control disease. Successive developments have focused on modulating CAR T cell activity in a tuneable and reversible manner. The use of ON-switch CARs which temporarily induce CAR T cell activation in the presence of a small-molecule drug via dimerization of a physically separated antigen-binding domain and signalling domain have been described.[185,342,343] Consequently, ceasing to administer the dimerising small-molecule drug results in CAR deactivation, However, persistent dosing and reliance on the drug may inconvenient for the patient as well as issues related to the short half-life and bio-distribution of the drug is problematic. On the other hand, OFF-switch split CARs provide a more convenient mode of control where a small-molecule drug disrupts the heterodimer made up of an antigen-binding domain and a signaling domain to deactivate the CAR T cell.[187,189] Although small molecule-based ON-switch systems have shown promise in

pre-clinical studies, such approaches have many limitations and concerns. Such as the use of experimental small-molecule drugs which may limit clinical approval or the use of potentially immunogenic, bacterial derived proteins as the dimerising component. .[187,189]

With increasing safety concerns surrounding the potential toxicity associated with immunotherapy largely attributed to the absence of a specific mechanism for controlling the CAR T cell function post infusion, remote control activation of CAR T cells through the exogenous administration of minocycline is desirable. So far, I have described and characterised a novel sdAb against the antibiotic drug minocycline with an affinity of ~31 nM and a cyclic peptide which interacts with the anti-minocycline sdAb with an affinity of ~111 nM. I have also provided evidence of the interaction between the sdAb and the cyclic peptide being displaced in the presence of minocycline. The aim of this chapter is design, develop and test CAR structures, centred around the principle of protein-protein displacement, as the basis of a tuneable 'OFF'-switch CAR which enables transient suppression in T cell activity, as opposed to abolishing the CAR T cells via the administration and removal of a small molecule, minocycline. An FDA approved drug which is widely available, easily/orally administered and well tolerated drug with good tissue penetration and a long half-life – properties which are ideal for immunotherapy applications. With the principle aim of systemically administering minocycline at a range of doses to achieve optimum therapeutic results.

6.2 Aims

- To confirm and evaluate maximal T cell activation achieved via the signaling chain
- To evaluate the effector function of the bipartite CAR architecture
- To optimise the minoCAR effector function through architecture refinement
- To validate the tunability and reversibility of the minoCAR and evaluate the kinetics of CAR cytotoxicity

6.3 Results

Previously, engineering T cell activation and other cellular responses using a small-molecule based dimerization module has been explored and well characterised.[176] My aim was to develop a novel negative regulating CAR architecture, where a small-molecule induced disruption was essential for the deactivation of T cell effector function. I aimed to design and optimise various bipartite receptor architectures which presented potent antigen-induced effector function, comparable to that of a conventional CAR architecture but also one which was capable of being disrupted in the presence of therapeutic concentrations of minocycline.

6.3.1 Generation of EGFR+ SupT1 cell line

As the tumour antigen-targeting sdAb utilised during the development of a tuneable CAR T cell architecture was against the epidermal growth factor receptor (EGFR), the human T cell lymphoblastic lymphoma derived SupT1 cells were engineered to express EGFR (SupT1-EGFR+) and were used as a tumour target cell line for subsequent in vitro co-culturing assays. Figure 6.1 shows the expression profile of SupT1-EGFR+ relative to non-transduced SupT1 cells (SupT1-NT) which was tested using anti-EGFR antibody conjugated to Alexa-Fluor-647 (Anti-EGFR-APC).
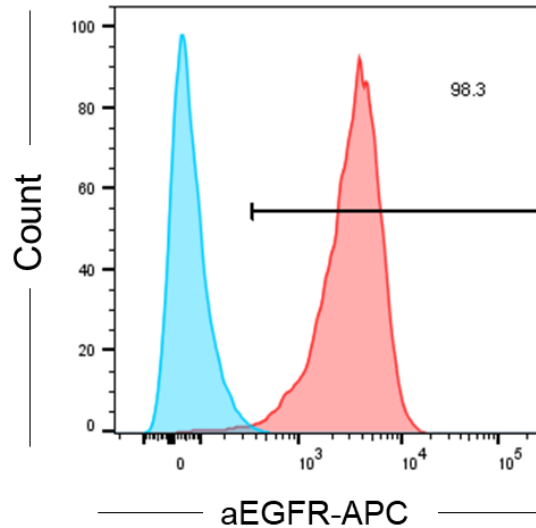
Figure 6.1. Generation and characterisation of SupT1-EGFR+ target cells. *The human T cell lymphoblastic lymphoma derived SupT1 cells were transduced with a retroviral vector expressing the EGFR tumour antigen (red histogram). 7 days post transduction, cells were stained with anti-EGFR-APC to confirm expression of EGFR relative to non-transduced SupT1 cells (SupT1-NT) (blue histogram).*

6.3.2 Chimeric TCR-incorporated MinoCAR T cell lack stability to induce heterodimerisation and cytotoxic function

Initially, a strategy was conceptualised which was centred around the use of a chimeric structure which aimed to incorporate the signaling capacity and the effector function of the TCR complex to enhance T cell activation and tumour directed cytotoxicity. T cells natively express the heterodimeric TCR complex on its surface and is composed of the TCRα and β chains, which are linked via hydrophobic interactions, and the CD3 peptide complex. The TCRαβ dimer, generated via somatic VDJ recombination, is involved in the recognition of foreign antigenic peptide bound to the major histocompatibility complex (MHC) molecule. The CD3 complex, made up of ε, γ and δ chains, is involved in TCR signaling through the cytosolic domains which contain the immunoreceptor tyrosine-based activation motifs (ITAMs) and are made up of tandem repeats of the sequence, YXXL/I. TCR and antigen-MHC engagement, mediated through the TCR CDR3a and CDR3b, triggers

223

cytosolic phosphorylation of ITAMs tyrosine residues by lymphocyte protein tyrosine kinase (Lck); A key event in early T cell activation. Additionally, phosphorylation and activation of Lck and other Src-family protein tyrosine kinases (PTKs) is regulated through CD45 tyrosine phosphatase. Lck-mediated double phosphorylation of ITAMs in the CD3ζ chain results in an increased affinity for cytoplasmic zeta-chain-associated protein kinase 70 (ZAP-70) and thus recruitment to the plasma membrane and formation of multiple signaling complexes and triggering of downstream signaling cascades and activation.

My aim was to enhance the T cell signaling and effector function using the native TCR-mediated signal transduction with the use of an artificial antigen binding subunit. Specifically, a chimeric TCR was designed by fusing the GWARA peptide to the N-terminus of the TCR CD3ε chain and served the purpose of signal transduction upon antigen engagement. The antigen recognition domain was physically separated by a 2A self-cleavage peptide sequence and consisted of a Fab antibody heterodimerization domain made up of N-terminal sdAb targeting epidermal growth factor receptor (EGFR) fused to Ig-Kappa-CL and the anti-minocycline sdAb fused to CH1 and anchored to the membrane via a CD28 transmembrane domain (CD28TM) (Fig 6.2A). The rationale behind this design was as follows: in the absence of minocycline (ON-state), dimerization between the anti-minocycline sdAb of the antigen recognition domain and the chimeric GWARA-CD3ε chain, which is incorporated into the TCR, leads to an antigen initiated signaling and cytotoxic response in T cells upon encounter of this chimeric complex with tumour-cell expressed EGFR. I hypothesized that enhanced signaling of the full CD3 complex would result in cytokine production and cytotoxic killing of tumour target cells.

72 hours post transduction, flow cytometry was used to determine the expression on transduced T cells of the chimeric CD3ε subunit fused to an N-terminal V5-tagged GWARA peptide and the HA-tagged anti-EGFR and anti-minocycline sdAb binding chain or the conventional HA-tagged anti-EGFR CAR (Fig. 6.2A). Expression of RQR8 confirmed transduction of the T cells. Analysis showed successful expression of the antigen-binding chain as a

measure of a positive HA-tag signal, whereas the lack of V5 tag expression suggested that the chimeric GWARA_CD3ε subunit was not expressed. HA expression indicated complete expression of the conventional EGFR CAR (Fig 6.2A).

The cytotoxicity of incorporating the naïve TCR signaling compartment through the interaction with the antigen-binding domain and chimeric CD3ε was tested by co-culturing the T cells with non-transduced SupT1 cells (SupT1-NT) and EGFR+ SupT1 cells (SupT1-EGFR) at an effector to target ratio of 1:2. Additionally, minocycline was also supplemented at concentrations of 1 µM and 10 µM. 72 hours post initiation, the co-culture was stained using anti-CD3-PeCy7 to differentiate effector T cells from SupT1 target cells and the CAR T cell cytotoxicity was measured by counting the number of live target cells using flow cytometry. Killing of target cells was normalised to killing mediated via presence of non-transduced PBMCs. The results show, as expected the conventional EGFR CAR showed a complete cytotoxic response against SupT1-EGFR cells irrespective of minocycline concentration, with minimal background cytotoxicity against SupT1-NT cells. In contrast, the chimeric GWARA_CD3ε variant showed no cytotoxic response against SupT1-EGFR cells. This was likely due to the fact the chimeric GWARA_CD3ε was undetectable on the surface of T cells, suggesting the chimeric GWARA_CD3ε receptor was not folded correctly, not stable on the T cell surface or not properly transported to the T cells surface preventing interaction with the antigen-binding chain.

A

aEGFR-CD28-4-1BB-CD3ζ — RQR8 | T2A | HA | aEGFR | CK | T2A | aMino | CH1 | CD28TM | CD28 | 4-1BB | CD3ζ

aEGFR + GWARA-2xG4S-CD3ζ — RQR8 | T2A | HA | aEGFR | CK | T2A | aMino | CH1 | CD28TM | T2A | V5 | GWARA | CD3ε

aEGFR-CD28-4-1BB-CD3ζ

RQR8
aEGFR sdAb
aMinocycline sdAb
Cκ
CH1
CD28
4-1BB
CD3ζ

aEGFR + GWARA-2xG4S-CD3ζ

aMinocycline sdAb
aEGFR sdAb
GWARA-CD3ε
TCR
RQR8
Cκ
CH1
CD3 complex
ζ

B

NT | aEGFR-CD28-4-1BB-CD3ζ | aEGFR + GWARA-2xG4S-CD3ε

Anti-V5-APC (y-axis)
Anti-HA-PE (x-axis)

NT: 0.70, 0.070, 98.8, 0.39
aEGFR-CD28-4-1BB-CD3ζ: 0.52, 3.06, 27.6, 68.8
aEGFR + GWARA-2xG4S-CD3ε: 1.18, 1.99, 63.1, 33.7

C

Figure 6.2. Chimeric TCR-incorporated MinoCAR T cell lack stability to induce heterodimerisation and cytotoxic function.

(A) Construct design and schematic illustration of a conventional anti-EGFR CAR made up of an anti-EGFR sdAb fused to Ig-Kappa and the anti-minocycline sdAb fused to CH1, CD28TM and CD28-4-1BB-CD3ζ signaling and co-stimulatory domains (aEGFR-CD28-4-1BB-CD3ζ); and the TCR integrated MinoCAR which is composed of a GWARA expressed on the N-terminus of the TCR CD3ε subunit which interacts with the physically separated Fab antibody heterodimerization binding subunit composed of a N-terminus anti-EGFR sdAb fused to Ig-Kappa and the anti-minocycline sdAb fused to CH1 and anchored to the membrane via a CD28 transmembrane domain (aEGFR + GWARA-2xG4S-CD3ζ). Each construct expressed the transduction marker, RQR8. (B) Expression profile of TCR integrated CAR structure in PBMCs. PBMCs were stained using anti-HA-PE and anti-V5-APC to test for expression of the anti-EGFR binding chain and GWARA-CD3ε chimeric subunits respectively. Anti-huCD34-AF488 was used to detect the transduction marker, RQR8. Flow cytometry-based analysis was used assess the expression profile and efficiency of each component. Based on RQR8 expression, transduction efficiency was normalised to 30% prior to co-culturing

with tumour cell line. Gating strategy was as follow: Singlets (FSH/FS)>Live cells (SYTOX-Blue)>anti-HA-PE/anti-V5-APC/Anti-CD34-AF488. One donor is shown as a representative example. (C) Flow cytometry-based cytotoxicity assay of TCR-integrated MinoCAR. Conventional EGFR CAR and the TCR-integrated MinoCAR T cells were co-cultured with 50,000 SupT1-NT or SupT1-EGFR in the absence and presence of minocycline at concentrations on of 1 μM and 10 μM, at an E:T ratio of 1:2 for 72hr. Cytotoxicity was determined by staining cells with anti-CD3-PeCy7 to differentiate T cells from SupT1 target cell lines and analysed by flow cytometry. The gating strategy was as follows: Singlets (FSH/FCA)>Live cells (SYTOX blue)>anti-CD3-PeCy7. In total 3 donors were tested (n=3). Percentage target cell survival was normalised to NT T cells. TCR integrated CAR failed to express the signaling chain (GWARA-CD3ε chimeric subunit) and thus failed to kill SupT1-EGFR cells. Conventional EGFR CAR presented total target cell killing.

6.3.3 Design of an OFF-switch minocycline-controlled CAR T cell (MinoCAR)

To design an 'OFF'-switch CAR architecture which solely required antigen for signal transduction and activation, with inactivation achieved through the presence of minocycline, two approaches of a bi-partite receptor module were designed and investigated: the dual-sdAb Fab structure (prototype MinoCAR) and the peptide-spacer structure (peptide-spacer MinoCAR).

I initially developed the MinoCAR constructs targeting the human EGFR antigen for comparison with a well-established conventional CAR architecture. The anti-EGFR MinoCAR bipartite CAR (MinoCAR) architectures were designed consisting of a physically separate antigen-binding subunit and a T cell activation/signaling subunit. In fact, heterodimerisation of split modules of antigen-binding from signaling motifs on distinctively separate polypeptide chains/receptors being essential for a functional receptor complex is widely reported feature of the innate and adaptive arms of the immune system, as it allows signal transduction to be maintained whilst the time-consuming events of gene rearrangement and encoding of the antigen-binding receptor can

diversify.[344,345] Such multiple polypeptide chain dimerisation offers a great opportunity to engineer chimeric antigen receptor control via a disrupting small-molecule.

6.3.4 Structure of the prototype MinoCAR

The architecture for the 'OFF'-switch MinoCAR (prototype MinoCAR) consists of (i) an antigen binding chain and (ii) a signaling chain (Fig. 6.3). The antigen-binding chain utilised a Fab antibody heterodimerization domain made up of an N-terminus sdAb targeting epidermal growth factor receptor (EGFR), an antigen that is often mutated and overexpressed in various forms of human cancers, fused to Ig-Kappa. The antigen-binding chain also expresses the anti-minocycline sdAb fused to CH1 and anchored to the membrane via a CD28 transmembrane (CD28TM). The physically separated T cell activation/signaling chain contains an N-terminal cognate high affinity CX7C peptide, GWARA or QWAMM, or a non sdAb specific serine-glycine-glycine-glycine-serine (SG3S) amino-acid repeats (negative control) fused to a human CD8α spacer (CD8STK), CD28TM, CD28 and 4-1BB costimulatory domains (CD28-4-1BB) and a CD3ζ intracellular signaling domain.[345] In the absence of minocycline ('ON'-state), functional heterodimerization of each subunit takes place through the interaction between the anti-minocycline sdAb and GWARA expressed on the N-terminus of each chain to form an antigen initiated signaling response in T cells. The ITAM motifs of the signaling chain are phosphorylated upon signaling chain activation which leads subsequent Src homology 2 (SH2) domain ZAP70 recruitment and downstream T cell activation cascade. Each component bearing heterodimerization domains interact in the absence of a disrupting small molecule.[346] Through the dosed administration of minocycline ('OFF'-state), the greater affinity (31 nM vs 111 nM) of the sdAb for minocycline results in the displacement and disruption of the heterodimerization between the antigen-binding chain and signaling chains, thus halting T cell activation signal transduction and CAR T cell effector function. A third-generation anti-EGFR CAR composed of an identical sdAbs, Fab spacer, CD28TM domain and CD28-4-1BB-CD3ζ co-stimulatory and signaling domains was used as a positive control. For retroviral expression, the safety switch and transduction surrogate RQR8 and the two

functional components are separated by the Thosea asigna virus 2A (T2A) self-cleavage peptide. The cassette was placed under the Moloney Murine Leukemia Virus (MMLV) retrovirus packaging signal and enhancer.

Figure 6.3. Illustration of a prototype minocycline-mediated tuneable CAR structure.

6.3.5 Investigation of the MinoCAR CX7C-peptide signaling chain mediated activation in Jurkat cells

In the previous section, it was shown the introduction of a N-terminal GWARA peptide sequence to form a chimeric CD3ε structure was not readily expressed on the cell surface. Therefore, to begin with, it was paramount to determine the stable cellular expression as well as the T cell activation capacity of the signaling chain component of the prototype CAR architecture. Consequently, the candidate signaling chain receptor was screened to determine activation levels and minocycline mediated inactivation in human CD4+ Jurkat cells. A plate bound T cell activation assay was set up to assess T cell activation as a measure of the expression profile of the early activation marker, CD69, and IL-2 release.

The signaling chain was composed of a V5-tagged anti-minocycline specific cyclic peptide (either QWAMM or GWARA, or a non-specific serine-glycine-glycine-glycine-serine (SG3S) amino-acid repeats) fused to the CD28-4-1BB-CD3ζ intracellular co-stimulatory and signaling domains via a human CD8α spacer and expressed in Jurkat cells (Fig. 6.4A - QWAMM, GWARA, SG3S). Transduced Jurkat cells were then labelled using anti-V5-APC antibody to confirm stability of cyclic peptide once fused to the signaling domain of a CAR. Jurkat cells were also labelled with anti-human CD34 antibody conjugated to AF488 (QBend10-AF488) to confirm expression of RQR8 which was used as a transduction marker (Fig. 6.4B). Seven days post transduction stable expression of the signalling domains was detected on the surface of Jurkat cells with V5+RQR8+ expression levels of QWAMM, GWARA and SG3S showing 86.6% 86.8% and 89.0%, respectively (Fig. 6.4B).

A
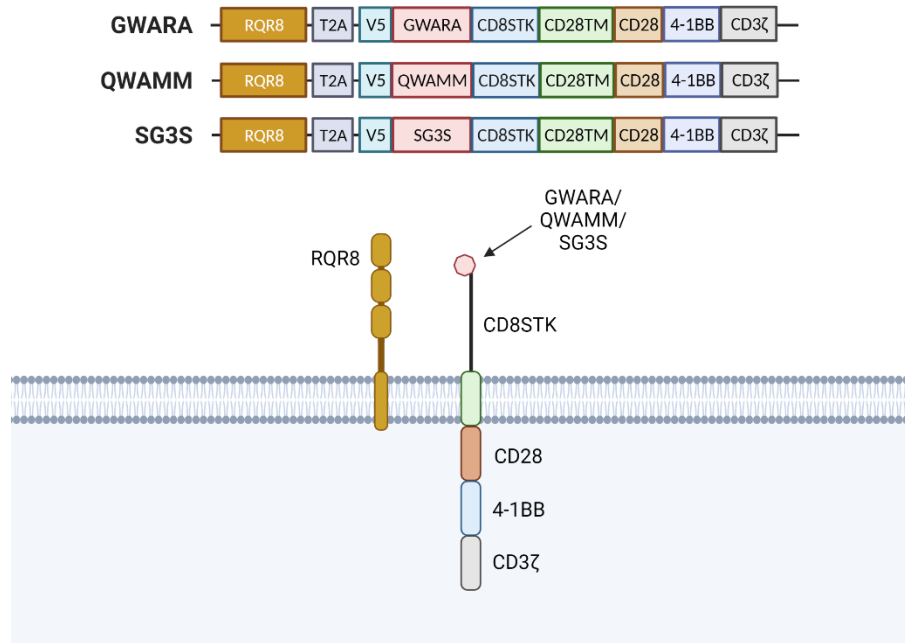
B
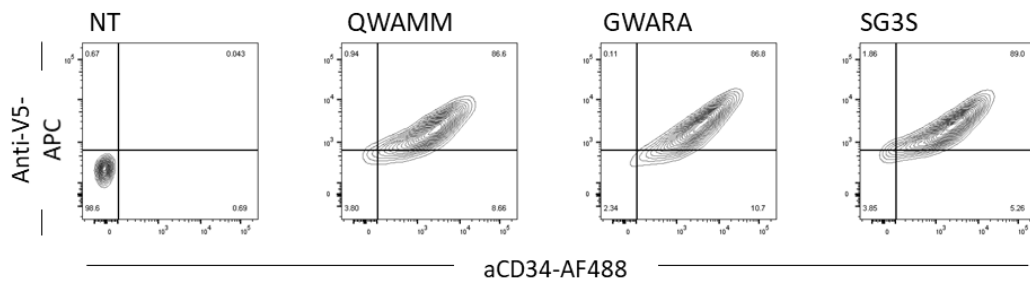
Figure 6.4. Construct design and transduction profile of the prototype MinoCAR signaling subunit in Jurkat cells.

(A) Jurkat cells were transduced to express V5-tagged peptides (QWAMM, GWARA, SG3S) fused to a human CD8α stalk spacer (CD8STK), a CD28 transmembrane domain (CD28TM), CD28-41BB costimulatory domains and a CD3ζ intracellular signaling domain. (B) Transduction profile and efficiency was determined by staining all Jurkat cells using anti-V5-APC and an anti-Human CD34 antibody conjugated to AF488 (aCD34-AF488) to detect V5 and the marker gene RQR8, respectively. Gating strategy: Singlets>Live cells (SYTOX Blue)>Anti-V5-APC/Anti-CD34-AF488. Gating is based on non-transduced Jurkat cells.

The maximal activation capacity of the signaling subunit was achieved in two ways: through the aggregation and activation via a plate-bound commercial anti-V5-antibody, which reflects the maximum subunit signaling capacity achievable through a high-affinity interaction. The second method involved activation through binding to plate-bound minocycline sdAb, this would mimic the activation mediated through the binding chain of the complete bipartite CAR structure upon strong association with antigen. In both cases the activation was carried out in the presence of increasing concentrations of minocycline (0.1 µM, 1 µM and 10 µM).

Analysis of both the CD69 expression and IL-2 secretion from either V5 or anti-Minocycline sdAb activation confirmed that, in the absence of minocycline, activation of the signaling subunit was achieved to comparable levels regardless of method of activation used. However, with increasing concentrations of minocycline from 0.1 µM to 10 µM, the QWAMM or GWARA peptides were unable to interact with the immobilised minocycline-sdAb and hence activation of the cells is reduced in a dose dependant manner as shown by reduced levels of CD69 expression and IL-2 secretion. Furthermore, minocycline did not appear to impair cell activation through the V5 tag. (Fig. 6.5 & Fig. 6.6).

A
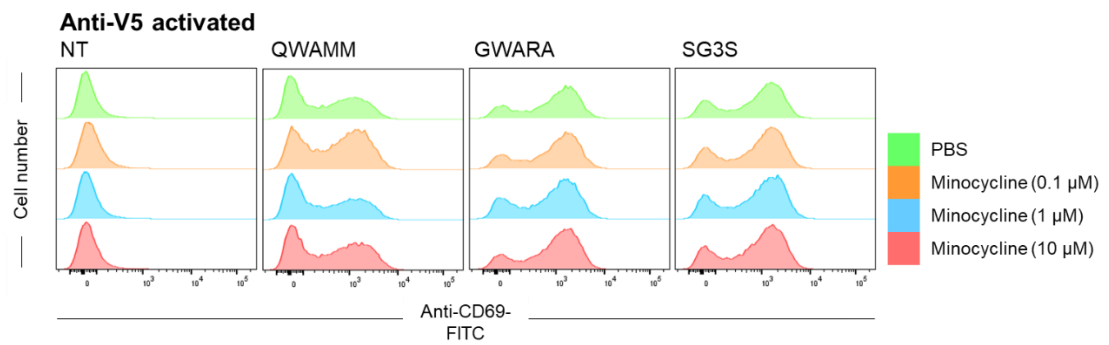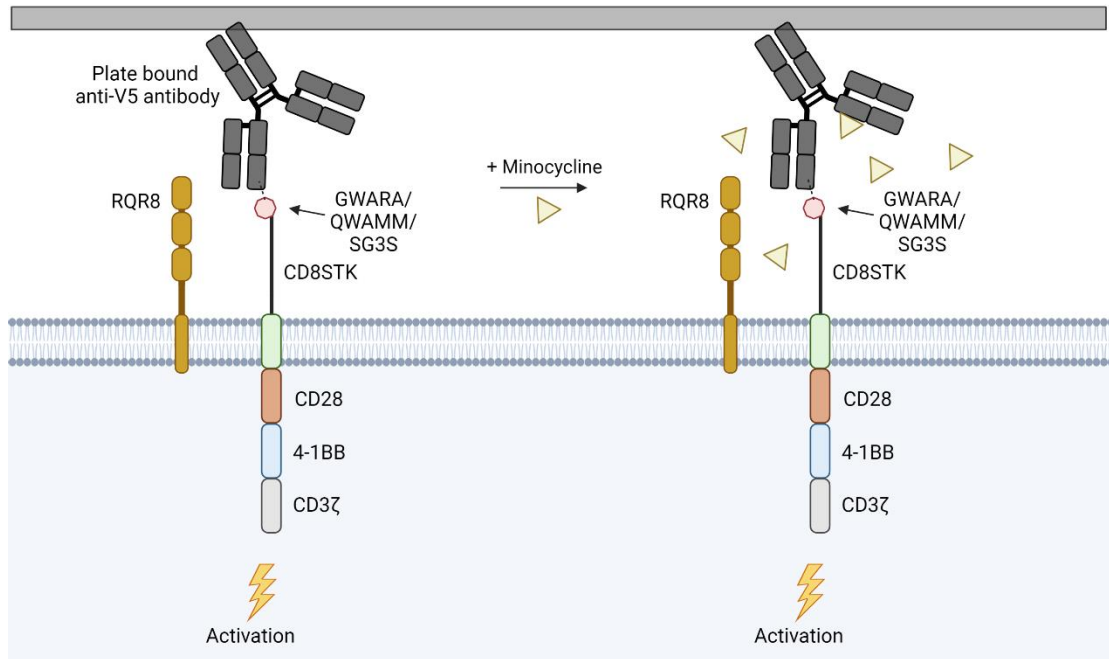
B
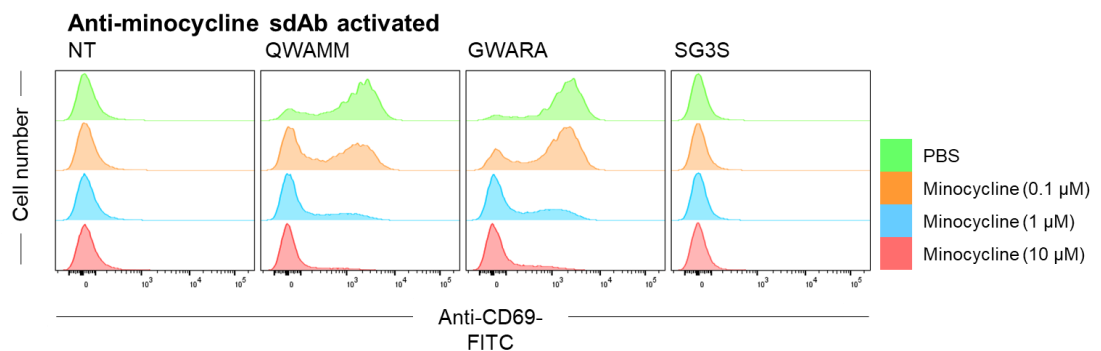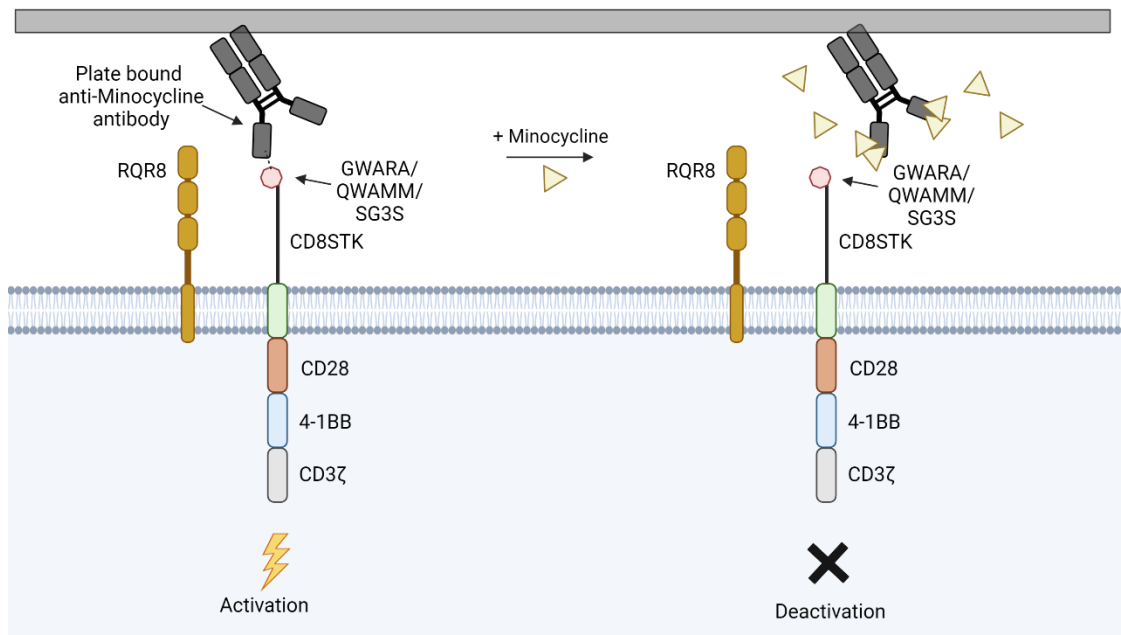
Figure 6.5. The early T cell activation marker, CD69, is expressed through stimulation of the prototype MinoCAR signaling chain expressed alone in Jurkat cells.

Jurkat cells were activated by incubating 50,000 transduced Jurkat cells on plates coated with 10 µg/ml of anti-V5 antibody or the anti-minocycline clone 1 sdAb, separately. Minocycline at concentrations of 0.1 µM, 1 µM, 10 µM was also spiked into each culture condition where indicated. Expression of the early activation marker, CD69, was determined by staining cells using anti-CD69-FITC, 24 hours post incubation.

Effect of minocycline on anti-V5 activation
IL-2 ELISA

Effect of minocycline on aMino-sdAb activation
IL-2 ELISA
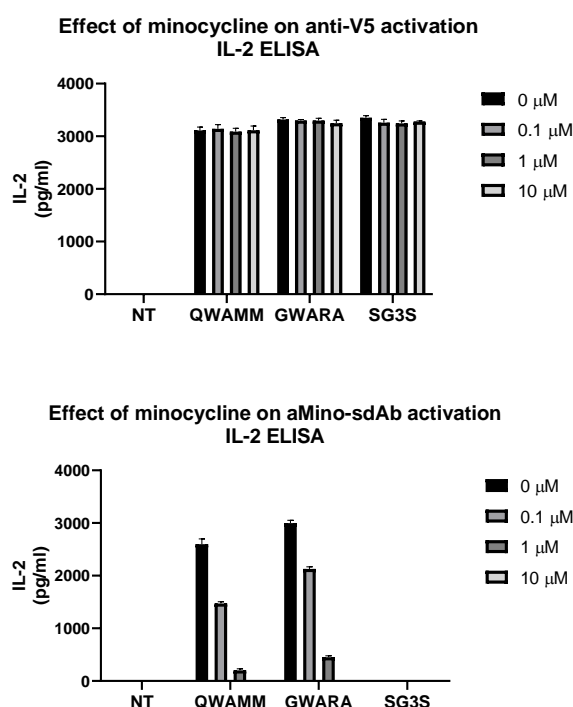
Figure 6.6. T cell activation is achieved through stimulation of the MinoCAR signaling chain expressed alone in Jurkat cells.

Jurkat cells were activated by incubating 50,000 transduced Jurkat cells on plates pre-coated with 10 µg/ml of anti-V5 antibody and the anti-minocycline clone 1 sdAb, separately. Minocycline at concentrations of 0.1 µM, 1 µM, 10 µM was spiked into each culture condition where indicated. 24 hours post incubation, supernatant was also collected for subsequent IL-2 ELISA.

6.3.6 Investigation of the MinoCAR CX7C-peptide signaling chain mediated activation in T cells

Once I had confirmed the stable expression and activation of the CX7C-peptide signaling chain in Jurkat cells I set out to assess the stable expression and activation in primary T cells prior to characterisation of the fully bipartite prototype MinoCAR structure in primary T cells. Therefore, T cells were transduced to express each of the V5-tagged peptide (QWAMM, GWARA, SG3S) fused signalling chains and a plate-bound activation assay was set up using immobilised anti-V5 antibody or the anti-Minocycline sdAb antibody with and without the presence of minocycline (0.1 µM, 1 µM and 10 µM). In the absence of minocycline, activation as a measure of IL-2 secretion from either

anti-V5 or anti-minocycline sdAb-induced activation of the signaling subunit were comparable between method of activation.

Increasing concentration of minocycline from 0.1 µM to 10 µM in assays in which T cells were activated by anti-minocycline sdAb reduced levels of IL-2 for QWAMM- and GWARA-bearing signaling chains indicating that displacement of peptide from the dAb was achieved in a manner dependent on the dose of minocycline. As SG3S bearing signaling chain does not interact with the anti-minocycline sdAb, IL-2 was not detected under any condition. Additionally, minocycline did not appear to impair cell activation using anti-V5 antibody mediated activation. (Fig. 6.7).

A
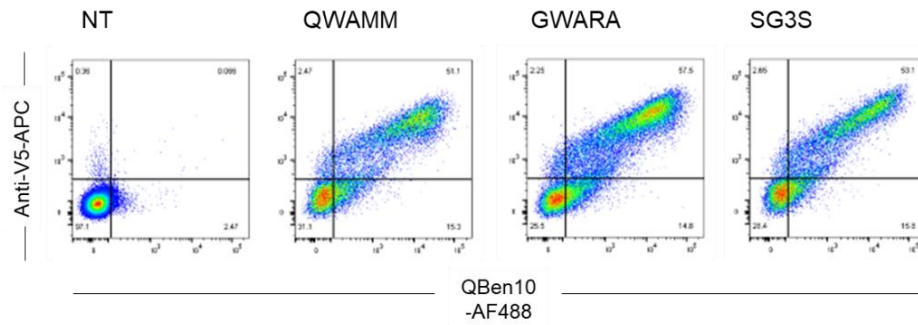
B
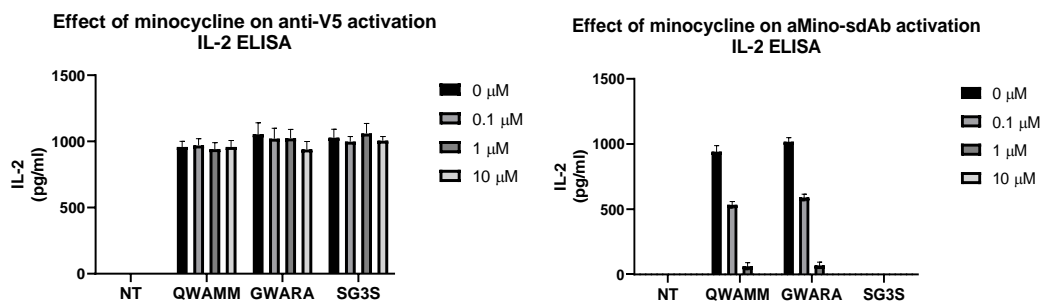
Figure 6.7. T-cell activation is achieved through stimulation of the prototype MinoCAR signaling chain expressed alone in primary T cells.

(A) Expression of the MinoCAR signalling chain (V5-tagged peptides fused to a CD8STK, a CD28TM, CD28-41BB costimulatory domains and a CD3ζ intracellular signaling domain) on primary T cells was determined by staining all T cells using anti-V5-APC and an anti-Human CD34 antibody conjugated to AF488 (QBen10-AF488) to detect V5 and the marker gene RQR8, respectively. Gating strategy: Singlets>Live cells (SYTOX Blue)>Anti-V5-APC/QBen10-AF488. Gating is based on non-transduced T cells. (B) T cells were activated by incubating 50,000 transduced T cells on plates pre-coated with 10 μg/ml of anti-V5 antibody or the anti-minocycline clone 1 sdAb. Minocycline at concentrations of 0.1 μM, 1 μM, 10 μM were spiked into each culture condition at the beginning of the activation period. 24 hours post incubation, supernatant was collected for subsequent ELISA to detect IL2.

6.3.7 Characterisation of a prototype bipartite "OFF"-switch CAR structure in primary T cells

6.3.7.1 Expression profile of T cells expressing the bipartite MinoCAR and lone signaling chain

Following confirmation that the signalling domain of the proposed bi-partite minoCAR structure could activate T cells upon interaction with immobilised anti-minocycline sdAb experiments were undertaken to assess the function of the complete MinoCAR in T cells. Initially, T cells were transduced with the conventional aEGFR-CAR, prototype aEGFR-MinoCAR (MinoCAR), and signaling chain alone. The structure of these constructs is outlined in Fig 6.8, all include RQR8 linked to the CAR components by a viral 2A sequence which serves as an independent marker of transduction. To determine the cell surface expression profile of each MinoCAR component in transduced PBMCs, cells were stained with anti-V5-APC for the detection of the V5-tagged anti-minocycline specific cyclic peptide fused to a human CD8α spacer (CD8STK), CD28TM, CD28-4-1BB costimulatory domains and the CD3ζ signaling domain (CD28-4-1BB-CD3ζ). An anti-HA-PE antibody was used for the detection of the HA-tagged anti-EGFR sdAb as a part of the Fab binding component (consisting also of the anti-minocycline sdAb) fused to a CD28TM. An anti-Human CD34 antibody conjugated to AF488 (QBen10-AF488) was also used to detect the RQR8 transduction marker. Cells were analysed by flow cytometry and gating was based on singlets and live cells using the viability dye SYTOX-Blue, with non-transduced T cells included as a negative control. As expected, PBMCs expressing the signaling chain of the MinoCAR expressed V5 and RQR8, whereas the bipartite MinoCAR constructs expressed V5, HA and RQR8 to comparable levels. Upon confirmation of transduction and corresponding MinoCAR subunit expression of the transgene, T cells were normalised to 30-40% CAR expression based on RQR8 expression readouts. Subsequent experiments were then carried out.
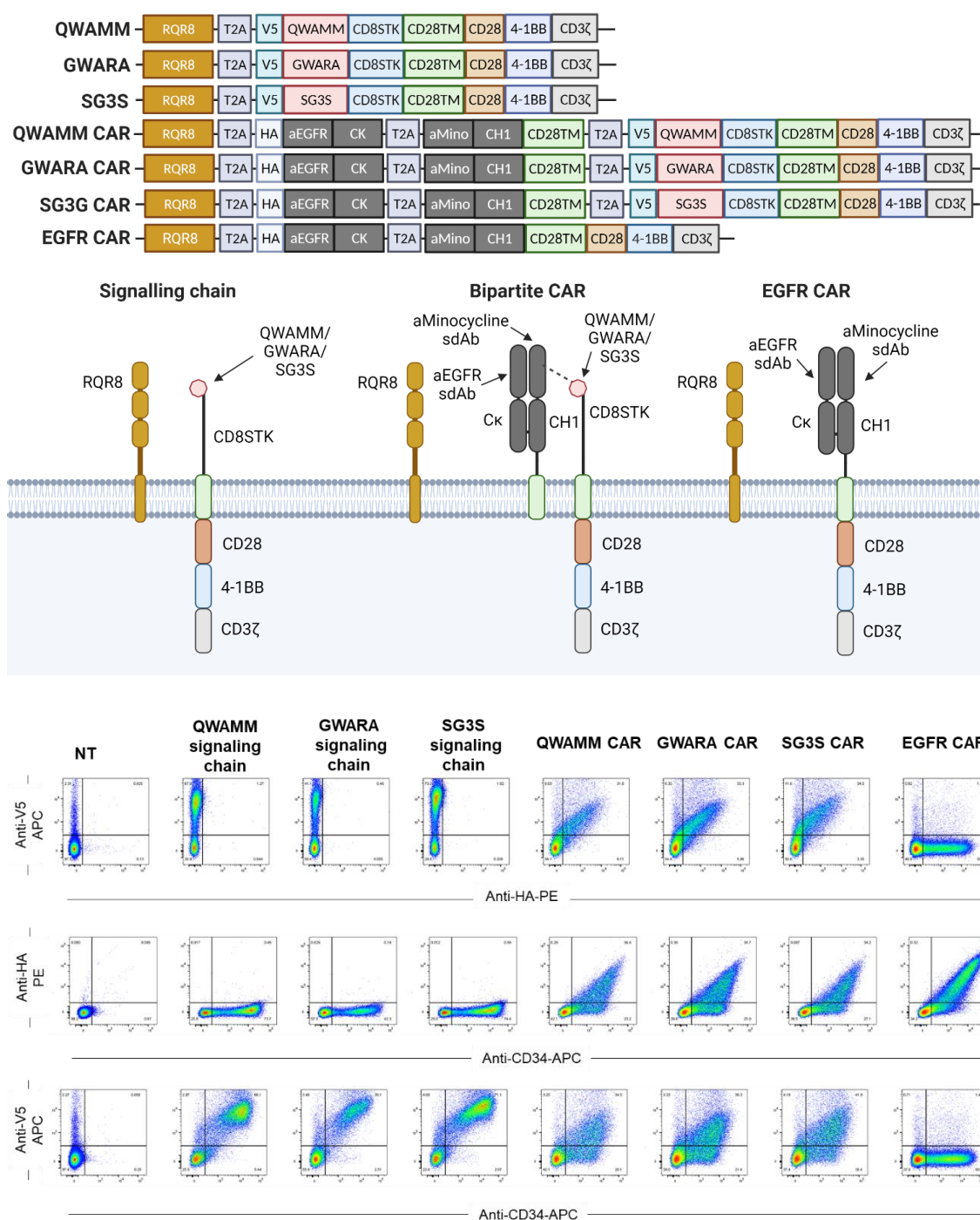
Figure 6.8. Prototype MinoCAR subunit expression profile in PBMCs.

All PBMCs were stained using anti-HA-PE and anti-V5-APC to determine expression profile of the MinoCAR binding chain and signaling chain, respectively. PBMCs were also stained for the transduction marker, RQR8, using an anti-Human CD34 antibody conjugated to AF488 (anti-CD34-AF488). Gating strategy: Singlets>Live cells (SYTOX Blue)>aV5-APC/aHA-PE/aCD34-AF488. Gating is based on non-transduced PBMCs. One donor is shown as a representative example out of four donors.

240

6.3.7.2 Prototype MinoCAR T cell plate-bound activation assay

MinoCAR was expressed as a tri-cistronic construct separated via a 2A self-cleavage peptide sequence. I hypothesized the interaction between the extracellular anti-minocycline sdAb and peptide fused to the CD8α spacer will form an active CAR capable of signaling in the absence of minocycline. Upon the addition of minocycline, the peptide-CD8STK-4-1BB-CD3ζ should dissociate and therefore render the CAR inactive. T cells were transduced with the complete MinoCAR variants (QWAMM CAR, GWARA CAR, SG3S CAR – non-interacting CAR), with the signaling chains alone (QWAMM signaling chain, GWARA signaling chain, SG3S signaling chain), and a monolithic conventional EGFR-CAR as a positive control. These cells were activated by incubation on plates separately pre-coated with the anti-V5 antibody, the anti-minocycline sdAb or the tumour target (recombinant EGFR). As this was the initial screening process to demonstrate proof-of-concept, activation of the CAR was assessed by measuring IFN-γ release, which has a lower threshold of secretion compared to IL-2.[347,348]

The results indicate the maximal signaling potential upon activation through plate bound anti-V5 antibody showed comparable levels of IFN-γ secretion between the fully bipartite CAR and 'signaling chain' only (Fig. 6.9A). In the absence of minocycline, when the cells are activated through immobilised anti-minocycline sdAb, the GWARA-signaling chain and QWAMM-signaling chain expressing cells show an approximately 2-fold greater levels of in IFN-γ secretion than the bipartite CARs, with a relative reduction in IFN-γ release with increased concentration of minocycline (Fig. 6.9B). This 2-fold reduction in activation of the fully bipartite CAR expressing cells is most likely due to peptide (on the signaling chain) engagement with anti-minocycline sdAb (on the binding chain) co-expressed on the T cell membrane, therefore the occupation of QWAMM-signaling chain and GWARA-signaling chain results in less aggregation to plate bound anti-minocycline-sdAb antibody and thus reduced signaling and activation. In the presence of minocycline, dose-dependent reduction in T cell activation and IFN-γ release was observed. With levels of IFN-γ levels similar to those observed from the negative controls, SG3S signalling chain and SG3S CAR. Therefore, if suboptimal activation in

subsequent characterisation experiments is observed, this will unlikely be attributed to the signaling capacity through the peptide-signaling subunit. Importantly, inhibitory effects of minocycline up to 10 µM on T cell activation were not observed.

Testing the bipartite CARs against tumour antigen binding (EGFR) showed activation in the absence of minocycline. Increasing concentrations of minocycline results in dissociation of the peptide-signaling subunit and therefore dose-dependent inactivation as a measure of supernatant IFN-γ concentrations. Minocycline addition (0.1 µM, 1 µM and 10 µM) did not have an effect in IFN-γ secretion in the conventional monolithic EGFR-CAR (Fig. 6.9C). The levels of IFN-γ secretion through plate-bound recombinant EGFR activation were approximately 20-fold greater in the EGFR-CAR control compared to the bipartite CARs. Although, assessing IFN-γ secretion in the context of plate-bound antigen proves to be an efficient screening tool, CAR function may not translate against tumour models.
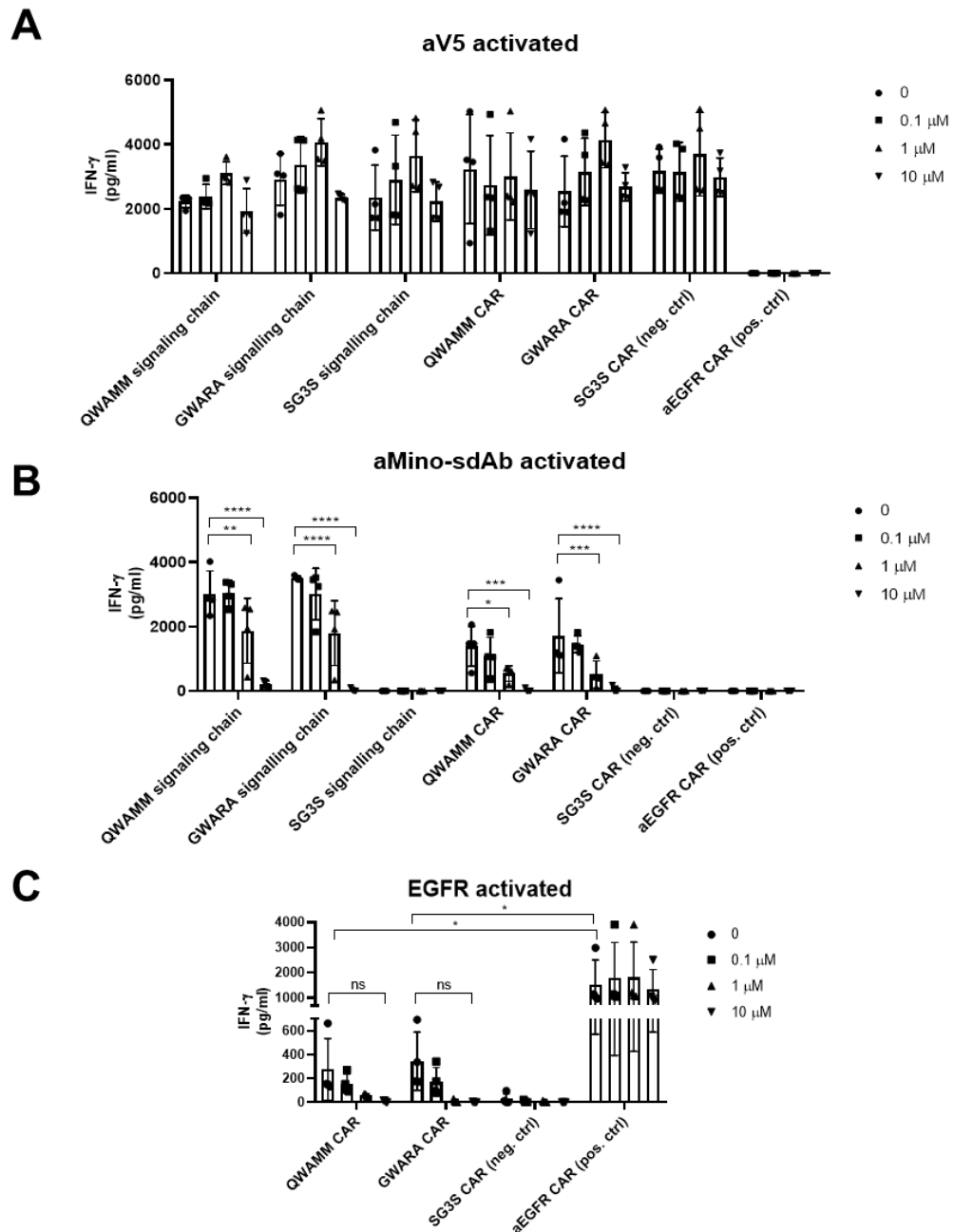
Figure 6.9. Prototype MinoCAR signaling chain and bi-partite MinoCAR plate bound antigen activation assay.

(A) Lymphocytes were retrovirally transduced with the following constructs: Signaling chain only, V5-tagged-X/CD8α spacer/CD28TM/CD28-4-1BB-CD3ζ, where X is the anti-minocycline sdAb specific peptide, QWAMM or GWARA or a nonspecific peptide, SG3S, acting as a negative control. The functional bipartite MinoCAR constructs, where HA-tagged-aEGFR sdAb

(Kappa chain)/aMino sdAb clone 1 (Heavy chain)/CD28-transmembrane acts as the binding domain and the V5-tagged-X/CD8α spacer/CD28TM/CD28-4-1BB-CD3ζ acts as the signaling domain (QWAMM CAR, GWARA CAR, SG3S CAR). A dual sdAb CAR made up of a HA-tagged anti-EGFR and anti-minocycline sdAb fused directly to CD28-4-1BB-CD3ζ, acting as the positive control (EGFR-CAR). 3 days post transduction, expression of markers, HA and V5, were determined by staining with anti-HA-PE and anti-V5-APC, respectively. Following transduction, 50,000 transduced cells were plated on non-TC treated flat bottom 96 well plates previously coated with (A) anti-V5 antibody. (B) anti-minocycline sdAb and (C) EGFR-Fc a concentration of 10 µg/ml. Varying concentrations of minocycline (0, 0.1 µM, 1 µM and 10 µM) were also spiked in the culture media. Supernatant was collected 48 hours post culture and an IFN-γ ELISA readout was carried out. (B) Data represented as mean ± SD, n=4, **** p<0.0001, *** p<0.0005, ** p<0.005, * p<0.05, two-way ANOVA (Dunnet's multiple comparisons test).

6.3.8 Development and optimisation of a minocycline-mediated tuneable dose dependent 'OFF'-switch CAR T cell

6.3.8.1 Prototype 'OFF'-switch MinoCAR T cells show cytotoxic killing of tumour cells with dose-dependent CAR inactivation

Whilst the MinoCAR structure could be activated by plate bound antigen the magnitude of activation, as assessed by IFN-γ secretion, was substantially less than for a more conventional, monolithic CAR structure. In order to understand how this affected the MinoCAR function experiments were carried out to test the cytotoxicity and cytokine secretion of T cells expressing the minocycline-controlled anti-EGFR MinoCAR T cell (prototype MinoCAR) and compared to the effector function of a conventional anti-EGFR CAR architecture in response to tumour cells expressing EGFR. Targeted killing of tumour cells is a key feature of CAR T cell function, with the principal objective of CAR T cells to develop anti-tumour immunity through the redirecting of pre-programmed CD8+ T cell killing against a specific antigen expressed on tumour cells. The first stage of assessing the CAR effector function is to assess the T cell mediated apoptosis of tumour cells, followed by cytokine

secretion and proliferation. This is because the onset of cytotoxicity of tumour cells occurs with a lower threshold and within hours of co-culture, whereas the cytokine secretion and proliferation require a longer time scale and greater threshold for initiation.[347,348] Therefore, I carried out analysis using the prototype MinoCAR expressing primary T cells to determine (i) if a cytotoxic killing of EGFR+ tumour cell lines was achievable and (ii) if minocycline disrupted the interaction between the two chains of the MinoCAR and prevented cytotoxic killing.

PBMCs were transduced with retroviral vectors expressing the prototype MinoCARs (QWAMM CAR and GWARA CAR), conventional EGFR-CAR or the negative control CAR lacking anti-minocycline specific peptide (SG3S CAR). Cell surface receptor expression was confirmed by staining transduced PBMCs with anti-V5-APC, anti-HA-PE and anti-CD34-AF488 (aCD34-AF488) to detect each MinoCAR antigen-binding chain, signaling chain and RQR8 transduction marker, respectively (Fig. 6.10).

To assess the prototype MinoCAR cytotoxicity against antigen expressing cells relative to the conventional EGFR-CAR T cells, transduced T cells were co-cultured with SupT1-NT and SupT1-EGFR+ cells at an effector to target ratio (E:T) of 1:2 for 24 hours, in the absence and presence of minocycline (0.1 µM, 1 µM and 10 µM). 24 hours post co-culture, a flow cytometry-based cytotoxicity assay was used to determine the cytotoxic capacity of the conventional EGFR-CAR and prototype MinoCAR T cells as a measure of the levels of target cells present amongst all viable cells. An anti-CD3 antibody conjugated to the fluorophore PeCy7 (anti-CD3-PeCy7) was used to differentiate effector cells from target cells (Fig. 6.11).

In the absence of minocycline, effective cytotoxic killing was observed with the MinoCAR showing equivalent levels of cytotoxicity towards EGFR-SupT1 as the conventional EGFR-CAR, relative to the negative control. Increasing concentration of minocycline resulted in a progressive ablation of cytotoxicity by the MinoCAR with improved SupT1-EGFR+ target cell survival, indicating minocycline displacement of the bipartite CAR subunits showing a dose dependent reduction in CAR T cell effector function whilst the conventional

EGFR CAR remained unaffected (p<0.0001). Non-specific killing of target cells lacking antigen (SupT1-NT) was not observed for either CAR. From these results, I can confirm that the level of antigen specific T cell mediated cytotoxic killing, in the absence of the disrupting minocycline molecule, was directly comparable to a conventional CAR architecture. Furthermore, killing of cognate target cell was halted in a dose-dependent manner with increasing concentration of minocycline. Therefore, confirming the prototype 'OFF'-switch MinoCAR permits titratable control of tumour cell lysis (Fig. 6.11).
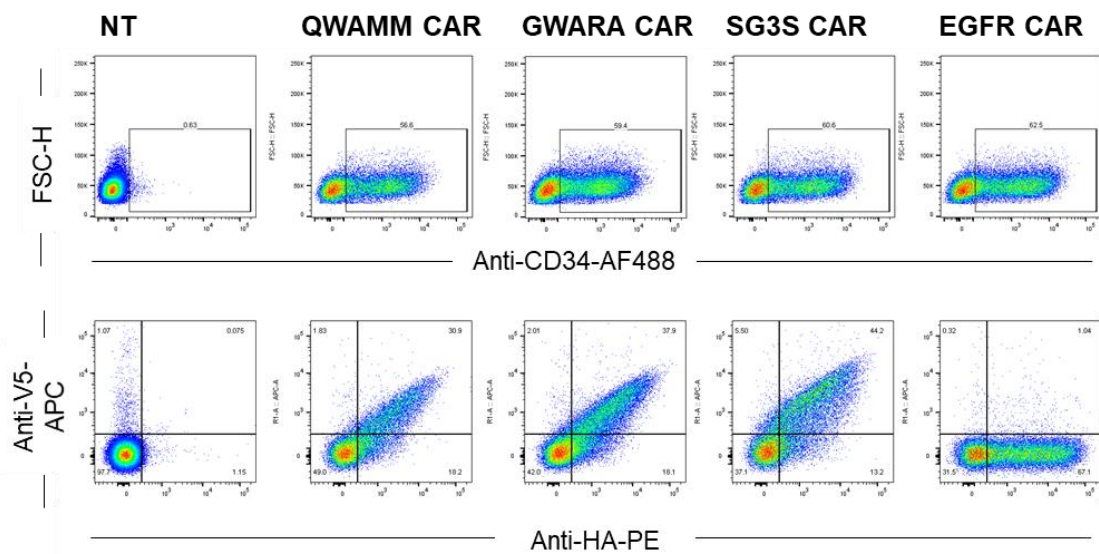
Figure 6.10. T cell transduction of the prototype bi-partite minocycline mediated tuneable CAR.

Flow cytometry of the transduction efficiency analysis showing the expression profiles of the MinoCAR binding chain (HA-tagged) and signaling chain (V5-tagged) on primary human T cells using anti-HA-PE and anti-V5-APC antibodies. Anti-CD34-AF488 was used to detect the transduction marker, RQR8.Gating was carried out using non-transduced PBMCs. One donor is shown as a representative example out of four donors.

A
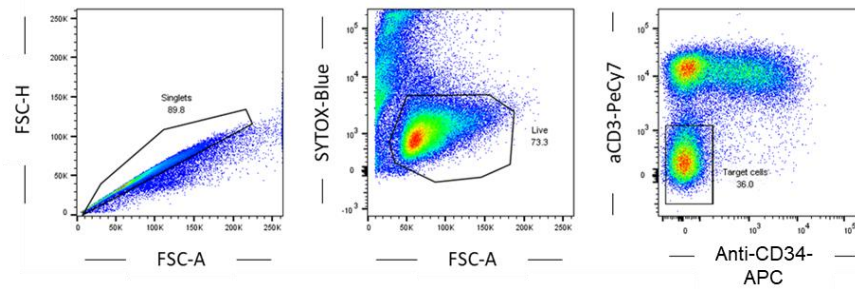
B
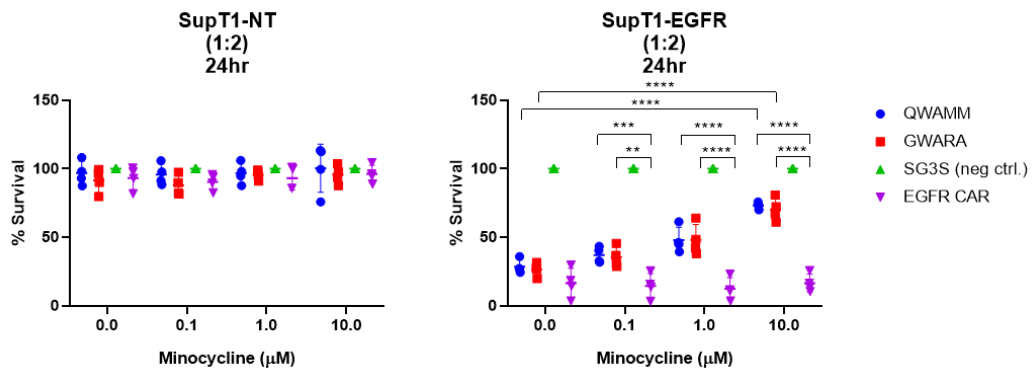
Figure 6.11. Cytotoxicity of a prototype minocycline-controlled MinoCAR T cells showing SupT1-EGFR+ cell killing and dose-dependent minocycline-mediated OFF control.

(A) Gating strategy was as follows: Singlets (FSH/FSA)>Live cells (SYTOX blue)>Anti-CD3-PeCy7. (B) Flow cytometry-based cytotoxicity assay of PBMCs transduced with a prototype bipartite MinoCAR expressing an antigen-binding chain and two high affinity peptides on the signaling chain (QWAMM CAR and GWARA CAR), a non-binding serine-glycine peptide sequence on the signaling chain negative control (SG3S CAR) and a conventional anti-EGFR dual sdAb CAR positive control (EGFR-CAR). Non-transduced Sup-T1 cells (SupT1-NT) and Sup-T1 cells expressing EGFR (SupT1-EGFR+) were used as target cells. Effector cells were co-cultured with target cells at a ratio of 1:2 with increasing concentrations of minocycline (0.1 µM, 1 µM and 10 µM) for 24 hours. The percent of live tumour cells was determined using the MACSQuant X Flowcytometry Analyzer and normalised to the faulty SG3S negative control CAR (n=4). Data represented as mean ± SD, n=4, **** p<0.0001, *** p=0.0005, ** p=0.0012, two-way ANOVA (Dunnet's multiple comparisons test).

Previously, several reports have shown that the use of split CAR architectures in which the antigen-binding domain and the signalling domain are separated onto distinct polypeptide chains which require association through protein-protein interaction domains to form a functional CAR result in decreases in the level of cytokine release and have thus required optimisation and engineering of the split module structure.[189,342] Therefore, the levels of secreted IFN-γ and IL-2 levels in the supernatant from previous co-culture experiments was assessed. The EGFR-CAR T cell when co-cultured with SupT1-EGFR+ showed to produce ~6000 pg/ml and ~1000 pg/ml levels of IFN-γ and IL-2, respectively which remained unaffected by the presence of minocycline. In comparison, the prototype MinoCAR T cells in the absence of minocycline produced a significantly lower levels of IFN-γ release and undetectable levels of IL-2 in co-culture with SupT1-EGFR+ cells (Fig. 6.12). Neither the EGFR-CAR nor the MinoCAR T cells showed detectable levels of IFN-γ and IL-2 production when co-cultured with SupT1-NT (data not shown).
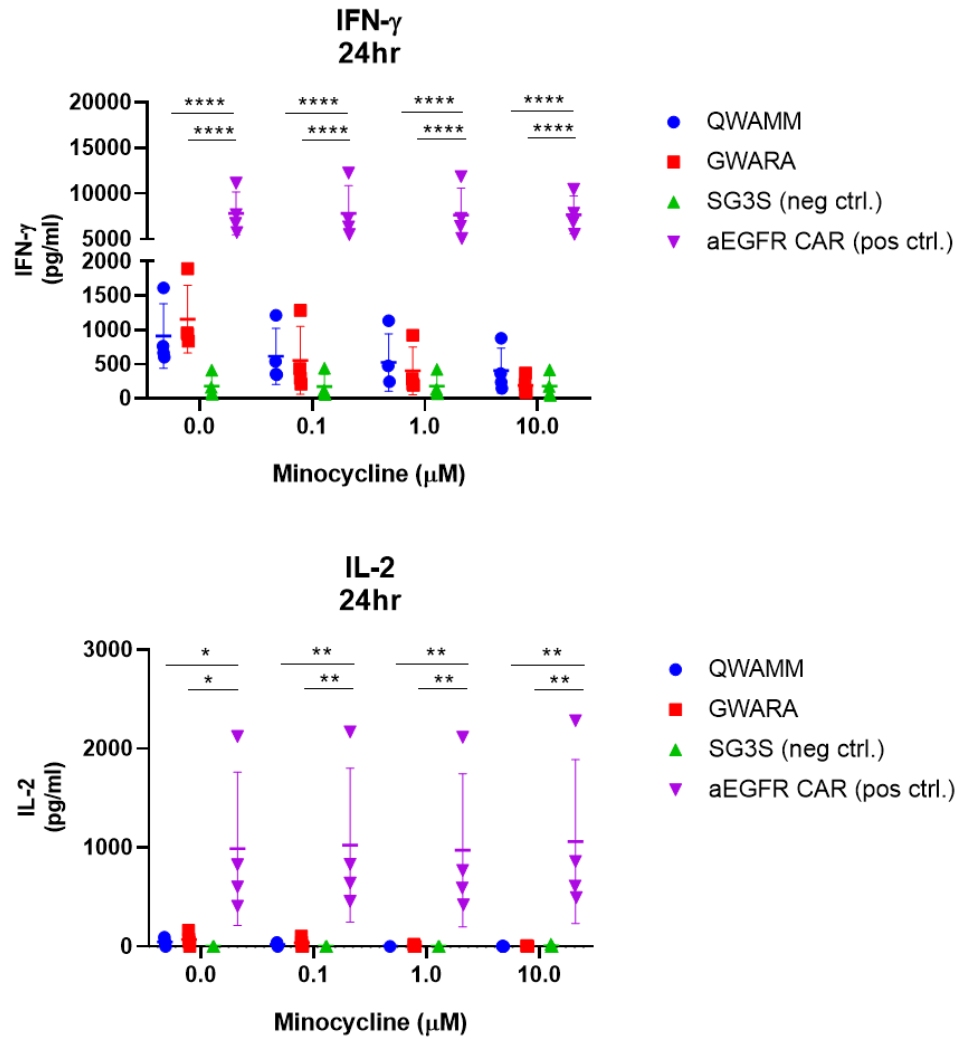
Figure 6.12. Cytokine secretion (IFN-γ and IL-2) of a prototype minocycline-controlled OFF-switch MinoCAR T cells.

*Supernatant was collected from the co-culture for cytokine analysis by IFN-γ and IL-2-specific ELISA. Co-culture of T cells which expressed the bipartite MinoCAR structure bearing the antigen-binding chain and two high affinity peptides on the signaling chain (QWAMM CAR, GWARA CAR), a non-binding serine-glycine peptide sequence on the signaling chain negative control (SG3S CAR) and a conventional anti-EGFR dual sdAb CAR positive control (EGFR-CAR). Non-transduced Sup-T1 cells (SupT1-NT) and Sup-T1 cells expressing EGFR (SupT1-EGFR+) were used as target cells. Effector cells were co-cultured with target cells at a 1:2 ratio with varying concentrations of minocycline (0.1 µM, 1 µM and 10 µM) for 24 hours. Data represented as mean ± SD, n=4, * p<0.02, ** p<0.01, **** p<0.0001, two-way ANOVA (Dunnetts's multiple comparisons test).*

6.3.9 Investigating MinoCAR T cell effector function through the addition of a flexible linker and multiple GWARA

So far in this work, the affinity characterisation of the sdAb and peptide interaction has been achieved through Biacore SPR and ITC which rely on free ligand interactions in solution. However, experiments in primary T cells demonstrate that the prototype MinoCAR fails to fulfil the essential criteria of efficient IFN-γ and IL-2 secretion comparable to that of the conventional CAR, despite sufficient binding chain and signaling chain expression in primary human T cells (Fig. 6.10). One explanation for this is that although the affinity of interaction between the signalling and antigen binding chains was sufficient for cytotoxic killing and comparable to other split-module CARs, the interaction between the anti-minocycline sdAb and GWARA was not optimal for inducing cytokine secretion possibly due to steric hindrances or sub-optimal positioning of the two interacting elements with respect to each other which do not give the GWARA peptide adequate distancing from the membrane to bind to the anti-minocycline sdAb. One potential method to overcome this problem is introduction of added length and flexibility, through the use of a flexible serine-glycine linker between the GWARA and CD8α spacer region of the signaling chain, in doing so improving the efficiency and dynamics of interaction and thus induce potent signaling. The increased flexibility and mobility of the peptide expressed on the cell membrane could mimic the high affinity interaction seen using a solution phase sdAb/peptide, reducing the entropic burden of membrane restricted anti-minocycline sdAb and GWARA binding, thus improving the interaction and resulting in an improvement in signaling chain activation upon antigen aggregation through the binding chain. Additionally, increasing the avidity interaction using multiple peptide sequences was also explored. To this end signalling domains with dual GWARA peptides separated by various serine glycine flexible linkers were incorporated into the MinoCAR with the aim to increase the avidity interaction with the antigen-binding chain which may prolong the interaction between the two MinoCAR components thus increasing the strength of the activatory CAR signal sufficient to increase cytokine secretion.

6.3.9.1 Design of a MinoCAR structure bearing a signaling chain with a flexible linker and dual GWARA peptides

To test the impact of a flexible linker between the N-terminal GWARA peptide and human CD8α spacer (CD8STK) of the signaling chain, two retroviral constructs were designed and cloned. The GWARA peptide was fused to the CD8α stalk by an 11aa serine-glycine linker with a CD28-41BB-CD3ζ endodomain and a second identical construct in which the serine-glycine linker was extended to 16aa. For assessing the functional impact of multiple sequential GWARA sequences on the signaling chain, two additional retroviral constructs were designed and cloned. Here two GWARA peptides separated by 11aa serine-glycine linker were fused to a CD28-41BB-CD3ζ endodomain. A second identical construct in which the two GWARA peptides were separated by a 16aa serine-glycine linker. These signaling chains were expressed with the antigen binding chain (Fab antibody heterodimerization domain an of an EGFR-sdAb-Ig-Kappa and anti-minocycline-sdAb-CH1-CD28TM) as a single polypeptide chain separated by a 2A self-cleavage peptide. RQR8 was also used as a transduction marker (Fig 6.13).

Figure 6.13. Construct design of flexible linker bearing GWARA and dual GWARA bearing prototype MinoCAR variants.

Construct design of the bipartite MinoCAR structures with modifications to the signaling chain subunit. Constructs showing the addition of a flexible serine-glycine linker between the N-terminal GWARA peptide and human CD8α spacer (CD8STK): (i) V5-tag-GWARA-(SGGGGSGGGGS)-CD8STK-CD28TM-CD28-4-1BB-CD3ζ and (ii) V5-tag-GWARA-(SGGGGSGGGGSGGGGS)-CD8STK-CD28TM-CD28-4-1BB-CD3ζ.

Constructs showing the addition of a second GWARA peptide sequence separated by a flexible serine-glycine linker: (iii) V5-GWARA-

(SGGGGSGGGGS)-GWARA-GGGS-CD8STK-CD28TM-CD28-4-1BB-CD3ζ
and (iv) V5-GWARA-(SGGGGSGGGGSGGGGS)-GWARA-GGGS-CD8STK-
CD28TM-CD28-4-1BB-CD3ζ. These signaling chains were expressed with the
antigen binding chain (Fab antibody heterodimerization domain an of an
EGFR-sdAb-Ig-Kappa and anti-minocycline sdAb-CH1-CD28TM) as a single
polypeptide chain separated by a 2A self-cleavage peptide. RQR8 was also
used as a transduction marker.

6.3.9.2 Introduction of flexible linkers and dual GWARA sequences to the signalling subunit of the prototype MinoCAR does not improves effector function

To test improvements in effector function of each MinoCAR variant bearing a flexible and dual-GWARA, transduced T cells were co-cultured with SupT1-NT and SupT1-EGFR+ cells at an effector to target ratio (E:T) of 1:2, 1:4 and 1:8 for 24 hours, in the absence and presence of minocycline (1 µM and 10 µM). Secreted IFN-γ and IL-2 levels in the supernatant from co-culture was removed for concentration analysis using ELISA. From the results shown on Fig. 6.14, in the absence of minocycline, these modified MinoCAR constructs produced significantly lower levels of IFN-γ and IL-2 in co-culture with SupT1-EGFR+ cells compared to the conventional EGFR CAR. Neither the EGFR-CAR nor the MinoCAR T cells showed detectable levels of IFN-γ and IL-2 production when co-cultured with SupT1-NT (data not shown). Based on these results, the introduction of a flexible serine-glycine linker between the GWARA and the CD8α spacer region or the addition of a dual-GWARA sequence on the signaling chain, did not improve IFN-γ and IL-2 secretion that was observed in the original MinoCAR architecture.
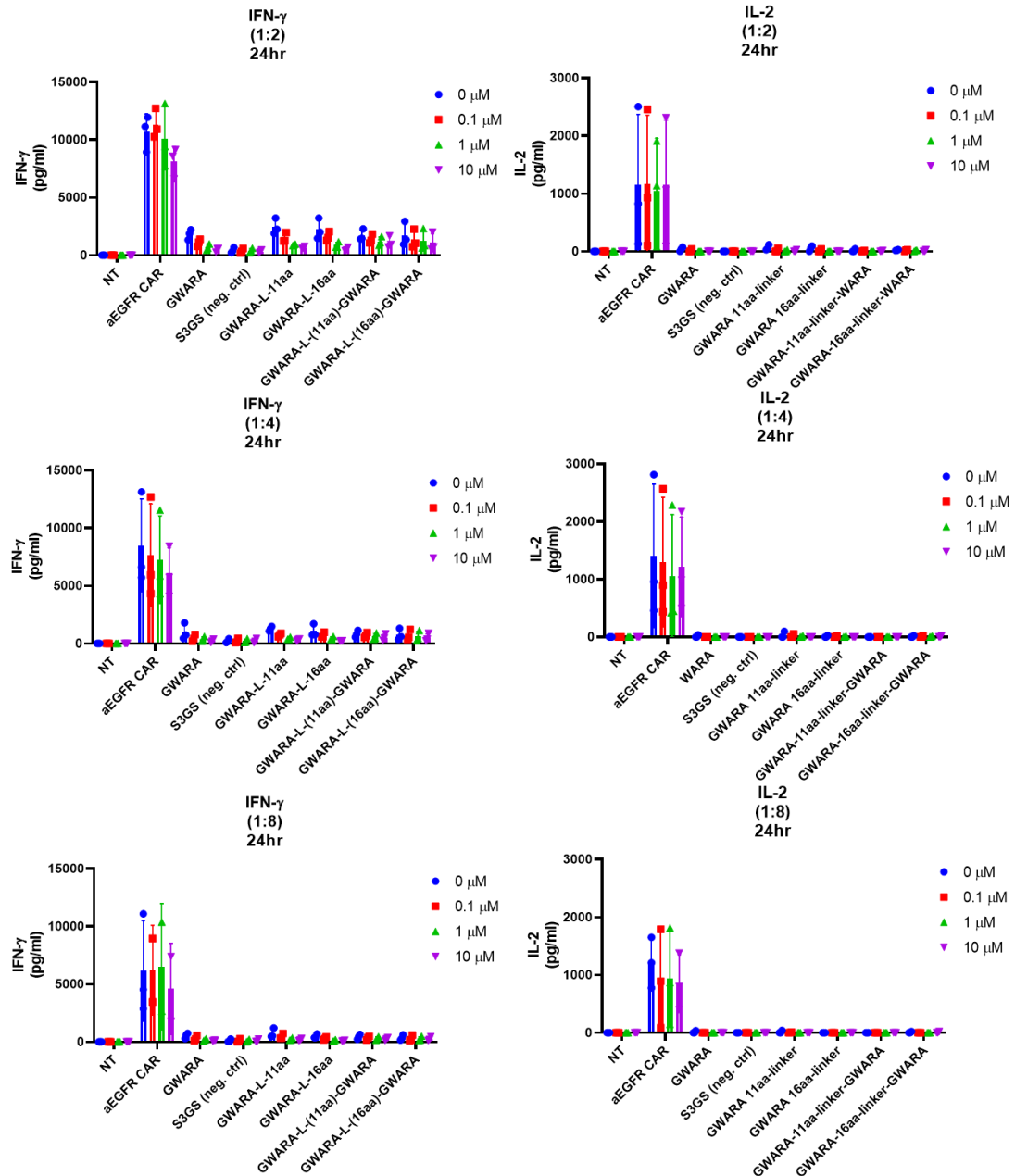
Figure 6.14. Cytokine release profile of prototype MinoCAR T cells bearing flexible linkers and dual GWARA on the signaling chain.

Supernatants were removed 72 hours post co-culture to assess the concentration of IFN-γ and IL-2 secreted by CAR T cells in the absence and presence of minocycline at concentrations of 1 μM and 10 μM. Co-cultures were set up at an effector to target ratio (E:T) of 1:2, 1:4 and 1:8 against SupT1-NT and SupT1-EGFR target cells. 3 donors were tested (n=3).

6.3.9.3 Use of multiple sequential GWARA peptide sequences does not improve binding to the anti-minocycline sdAb

Having demonstrated that structures of dual peptides or peptides flanked by various linkers do not show functional improvements in cytotoxic killing of tumour cells and cytokine (IFN-γ and IL2) secretion in CAR format. I aimed to characterise the binding kinetics of multiple peptides as free molecules in solution using ELISA and SPR analysis. In doing so, I aimed to establish whether multiple GWARA peptides displayed a higher avidity for the anti-minocycline sdAb than a single peptide. In doing so, I set out to exclude the possibility of increasing the avidity interaction via the use of multiple peptides in the context of bipartite CARs and explore alternative methods for improving the effector function. Therefore, 2 constructs were designed and cloned which were expressed soluble Fc-conjugates, these were composed of triple GWARA peptides sequences separated by a serine-glycine-serine flexible linker (GWARA-SG4S(x3)-Fc) or a rigid linker (GWARA-RL-Fc) (Fig. 6.15A).

To confirm stable peptide-Fc-conjugate expression and assess the molecular mass of each structure, transient transfection of each peptide-Fc encoding vector was carried out using Chinese hamster ovarian (CHO) cells which yielded concentrations of 1.3, 1.4 and 1.1 mg/ml for GWARA-Fc, GWARA-SG4S(x3)-Fc and GWARA-RL-Fc, respectively. Purification was carried out using protein-A affinity chromatography and analysed by sodium dodecyl sulphate (SDS) polyacrylamide gel electrophoresis (PAGE) analysis in both reducing and non-reducing conditions. Under reducing conditions, the molecular weight was in accordance with the predicted molecular weight (Fig. 6.13A) and is detected as single or closely collocated prominent protein band of each overlapping monomer upon reduction of the disulphide bond between the hinge region of each respective monomer. The molecular weight of GWARA-Fc, GWARA-G4S-(x3)-Fc and GWARA-RL-(x3)-Fc was shown as 33.0 kDa, 36.7 kDa and 44.3 kDa, respectively. Under non-reducing conditions, each antibody format showed a molecular weight of twice that of the monomeric chain displayed under reducing conditions, confirming the full assembly of the Fc-conjugates via the disulphide bond formation between the interchain hinge regions. The molecular weight was consistent with the

predicted molecular weight of a stable peptide-antibody chimeric structure being expressed as a homodimer with GWARA-Fc, GWARA-G4S-(x3)-Fc and GWARA-RL-(x3)-Fc shown as a single prominent band with the molecular weight of 65.9 kDa, 73.4 kDa and 88.7 kDa, respectively (Fig. 6.15B). Upon confirmation of the size and stability of peptide-Fc conjugates, ELISA was carried out to determine binding EC50. ELISA binding of GWARA-Fc, GWARA-SG4S(x3)-Fc and GWARA-RL-Fc to aMino-sdAb produced EC50 values of 0.1164, 0.5835 and 4.667 respectively (Fig. 6.15C).
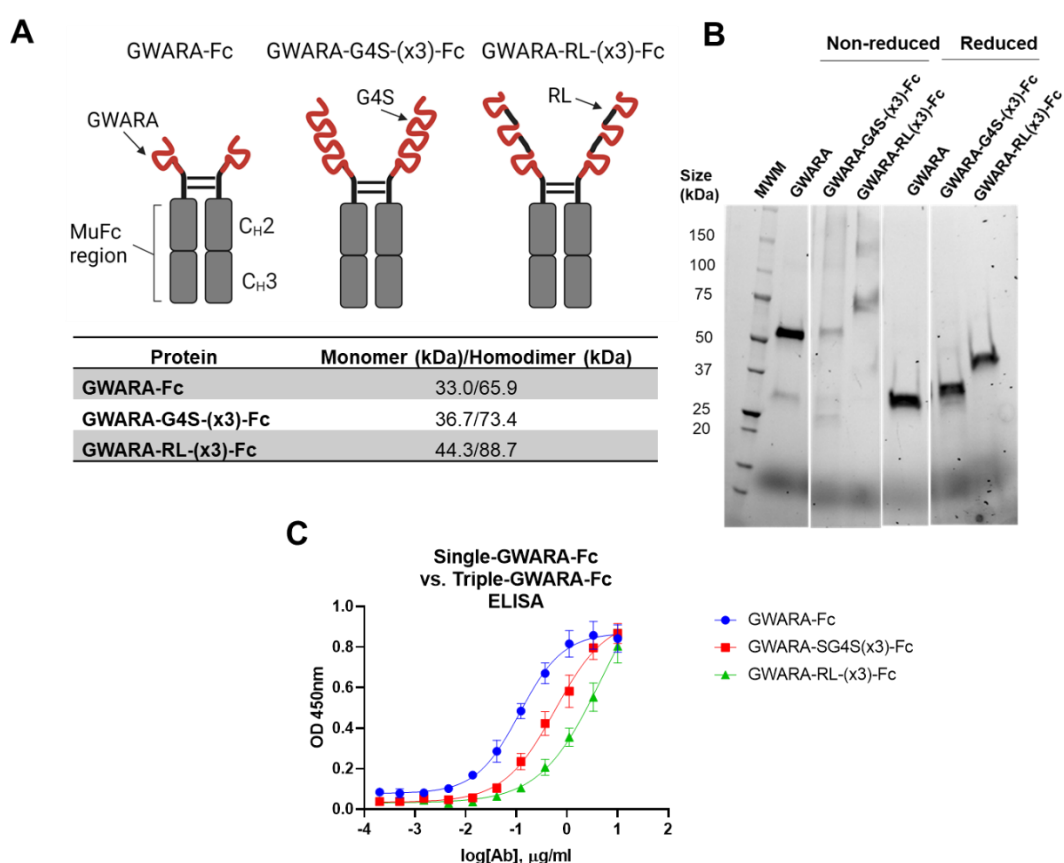
Figure 6.15. Multiple sequential GWARA peptide sequences do not improve binding to the anti-minocycline sdAb.

(A) Illustration and corresponding molecular weight of single and multiple (3x) GWARA peptide conjugated to murine-Fc. GWARA bearing Fc-conjugates used for the biophysical characterisation of single and multiple GWARA constructs and each respective CMV-SP6-mIgG2AFc vector. Downstream of the GWARA peptide sequences are the gene segments encoding the mIgG2A-hinge region, the CH2 and CH3 regions. Three constructs are shown and have the following structure: (i) A single GWARA peptide expressing

antibody conjugate was expressed as a control with the following structure: GWARA_serine-glycine(x4)-serine_MurineIgG2A-Hinge_IgG2A-CH2_IgG2A-CH3 (Fc tag), (ii) GWARA_serine-glycine(x4)-serine_GWARA_serine-glycine(x4)-serine_GWARA_serine-glycine(x4)-serine_MurineIgG2A-Hinge_ IgG2A-CH2_IgG2A-CH3 and (ii) GWARA _RL_GWARA_RL_GWARA_RL_ MurineIgG2A-Hinge_IgG2A-CH2_IgG2A-CH3 (Fc tag), where RL is the rigid linker amino acid sequence of LEAEAAAKEAAAKEAAAKEAAAKALE. (B) Predicted molar masses (kDa) of Peptide-Fc-conjugates determined through protein bioinformatics software ExPasy ProtPara from the amino acid sequences. The native state is expressed as a homodimer, monomer molar mass also indicted. The expression vector contains and is driven through the human CMV enhancer and promoter backbone, with the simian virus SV40 origin of replication (ori), SV40 poly(A) signal and F1 phage ori. AgeI+BamHI restriction sites are upstream of the mouse IgG2A-CH2-CH3 coding region for N-terminal peptide insertion. (B) SDS page analysis of GWARA, GWARA-G4S(x3) and GWARA-RL(x3) murine Fc conjugated antibodies. 5 µg of GWARA, 3xGWARA-G4S (and 3xGWARA-RL Fc conjugates were prepared for loading using sample buffer consisting of 62.5 mM Tris-HCl, pH 6.8, 2% SDS, 25% (v/v) glycerol, 0.01% bromophenol blue (and 5% β-mercaptoethanol for reducing samples). Samples for then incubated at 95C for 5 minutes prior to being loaded onto the gel. The mini-PROTEAN® TGX Stain-Free™ pre-cast 4-20% gradient gel was used to run samples. Running buffer consisted of 25 mM Tris, 192 mM glycine and 0.1% SDS. 180 V running voltage was used for 30-40 minutes. The Azure c600 Gel Imaging System by Azure Biosystems was used to image protein bands. Bio-Rad Precision Plus Protein Standards were used as reference protein ladder. (C) Investigating binding capacity of single-GWARA-Fc and triple–GWARA-Fc using ELISA. Peptide-Fc conjugates (GWARA-Fc, GWARA-SG4S(x3)-Fc and GWARA-RL-Fc) were produced via the transient transfection of CHO cells and purified using protein-A affinity chromatography. aMino-sdAb was immobilised, at a concentration of concentration of 1 µg/ml, to ELISA plates, which were subsequently blocked (1% BSA diluted in PBS) and peptide-Fc conjugates were bound to the immobilised anti-mino sdAb (starting concentration of 10 µg/ml followed by 1/3 dilution). Binding was then detected using anti-muFc-

HRP and activity was determined using TMB substrate. Read out was carried out at 450 nm. Binding of GWARA-Fc, GWARA-SG4S(x3)-Fc and GWARA-RL-Fc to aMino-sdAb produced EC50 values of 0.1164, 0.5835 and 4.667 respectively. Technical repeats n=3.

6.3.10 Investigating MinoCAR T cell effector function via incorporating the GWARA peptide within the spacer region of the antigen-binding subunit (peptide-spacer MinoCAR)

An alternative bipartite CAR structure was also designed and tested to assess its ability to function as a tunable CAR which was responsive to minocycline. The structure was composed of an antigen binding subunit harbouring an anti-EGFR-sdAb and and having the GWARA peptide integrated into the spacer region which connects the sdAb to the membrane. This was paired with a separate signaling subunit bearing the anti-minocycline sdAb connected to the intracellular T cell activation domains. The antigen-binding chain was specifically composed of an N-terminal anti-EGFR-sdAb fused to the GWARA peptide sequence (flanked by a range of serine-glycine/rigid linkers), CD8α spacer stalk (CD8STK) and CD8 transmembrane (CD8TM). Whereas, the signaling subunit was composed of the anti-minocycline sdAb fused to a wobbled CD8STK, CD8TM, CD28-4-1BB costimulatory domains and a CD3ζ intracellular signaling domain.[345] A negative control was also designed in which the GWARA peptide was substituted with a SG3S peptide incapable of interacting with the anti-mino sdAb. Two variants on this basic design were also constructed in which the distance between the GWARA peptide and the aEGFR sdAb was increased through the use of either a rigid linker or a 16 amino acid Ser-Gly linker to account for the possibility that the GWARA peptide, being cysteine-constrained, may cause steric hindrances which prevent the sdAb binding to EGFR. Three positive control constructs composed of an N-terminus anti-EGFR-sdAb fused to the GWARA peptide sequence (flanked by a range of serine-glycine/rigid linkers), CD8STK-TM and CD28-4-1BB-CD3ζ intracellular domains were also designed (Fig. 6.16).
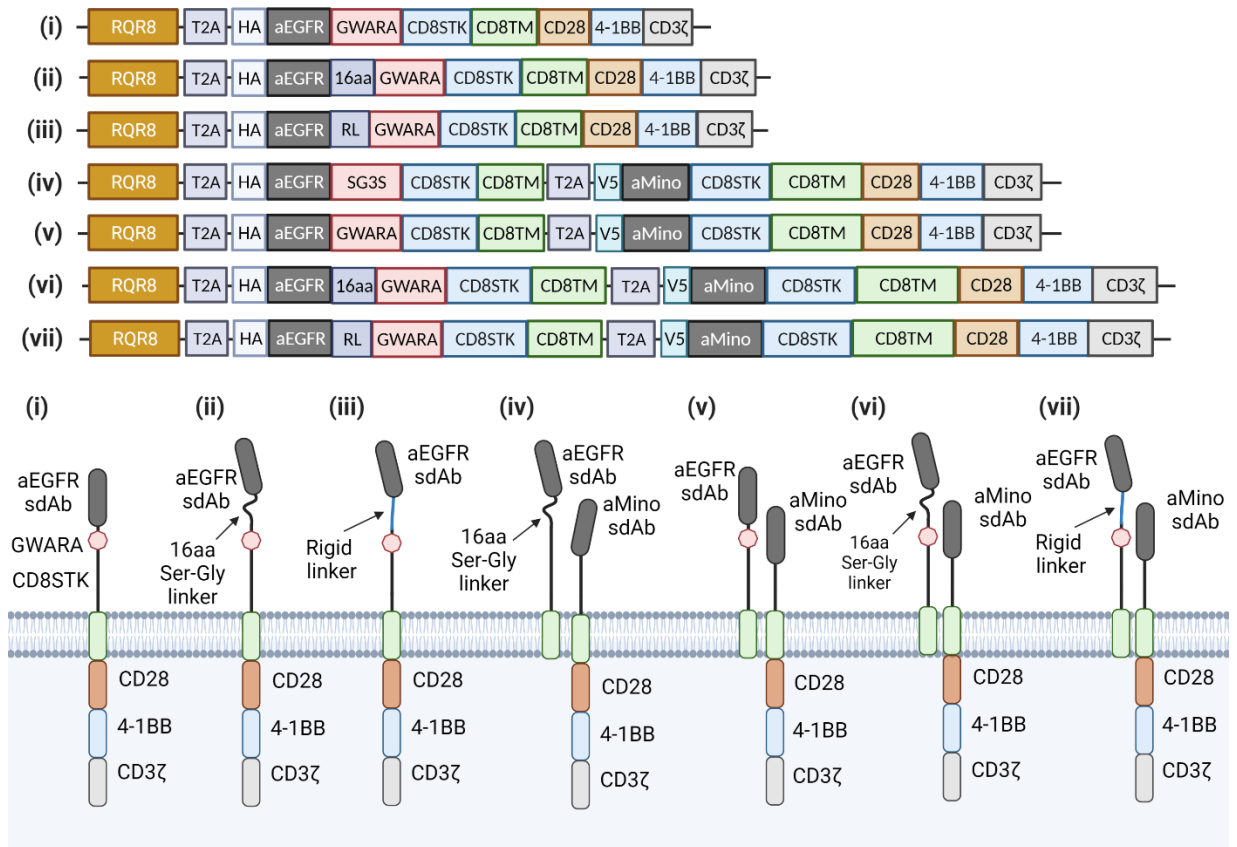
Figure 6.16. Construct design and schematic illustrations of the MinoCAR architectures bearing an N-terminus anti-EGFR sdAb and GWARA peptide-spacer region on the antigen-binding subunit and an N-terminus anti-minocycline sdAb expressed on the signaling chain.

Positive controls: (i) aEGFR-GWARA-CD8STK-TM-CD28-41BBζ, (ii) aEGFR-16aa-SG-GWARA-CD8STK-TM-CD28-41BBζ, (iii) aEGFR-RL-GWARA-CD8STK-TM-CD28-41BBζ. Negative control: (iv) aEGFR-SG3S-CD8STK-TM + aMino-CD8STK-TM-CD28-41BBζ. Test constructs: (v) aEGFR-GWARA-CD8STK-TM + aMino-CD8STK-TM-CD28-41BBζ, (vi) aEGFR-16aa-SG-GWARA-CD8STK-TM + aMino-CD8STK-TM-CD28-41BBζ and (vii) aEGFR-RL-GWARA-CD8STK-TM + aMino-CD8STK-TM-CD28-41BBζ. The anti-EGFR sdAb was expressed with a HA-tag and the anti-minocycline sdAb was expressed with a V5-tag. Predicted effector outputs were also indicated. Each subunit was expressed as a single polypeptide chain separated by a 2A self-cleavage peptide (indicated by + sign). RQR8 was used as a transduction marker.

PBMCs were separately transduced, and the respective cell surface expression profile of each construct was confirmed by flow cytometry (Fig. 6.17). The effector function was tested by carrying out a flow cytometry-based cytotoxicity assay against SupT1-EGFR+ cells at an effector to target ratio (E:T) of 1:2 for 24 hours and 72 hours, in the absence and presence of minocycline (1 µM and 10 µM). At 24 hours and 72 hours, the positive control CAR structures bearing serine-glycine linkers (i, ii) showed significant kill response against SupT1-EGFR+ cells irrespective of minocycline concentration, whereas the inclusion of a rigid-linker bearing positive controls (iii) reduced the kill response. Furthermore, minimal background kill against SupT1-NT was observed. These results indicate the incorporation of GWARA upstream of the CD8α spacer permits T cell activation and cytotoxic response in CAR T cells. Although the transduction profile of the functional test constructs (v, vi and vii) indicated high levels of cell-surface stability and expression, each construct failed to carry out its effector function against SupT1-EGFR up to 72 hours.

A
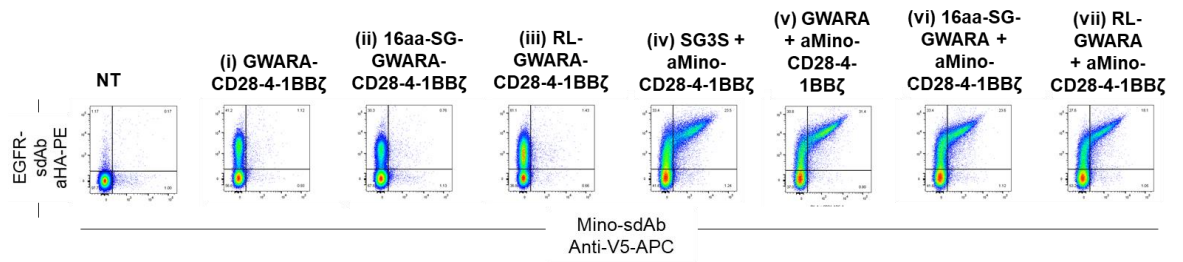
B
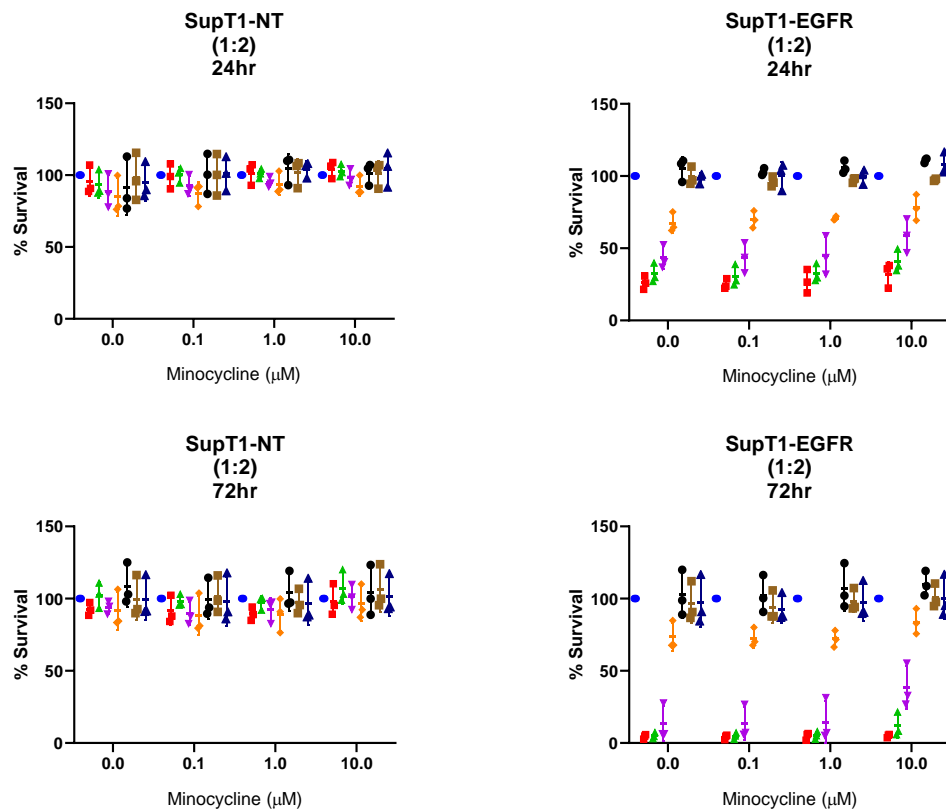
- NT
- aEGFR-GWARA-CD8STK-TM-CD28-41BBζ
- aEGFR-16aa-SG-GWARA-CD8STK-TM-CD28-41BBζ
- aEGFR-RL-GWARA-CD8STK-TM-CD28-41BBζ
- aEGFR-SG3S-CD8STK-TM + aMino-CD8STK-TM-CD28-41BBζ
- aEGFR-GWARA-CD8STK-TM + aMino-CD8STK-TM-CD28-41BBζ
- aEGFR-16aa-SG-GWARA-CD8STK-TM + aMino-CD8STK-TM-CD28-41BBζ
- aEGFR-RL-GWARA-CD8STK-TM + aMino-CD8STK-TM-CD28-41BBζ

Figure 6.17. Cytotoxicity of MinoCAR architectures bearing an N-terminus anti-EGFR sdAb and GWARA peptide-spacer region on the

antigen-binding subunit and an N-terminus anti-minocycline sdAb expressed on the signaling chain.

(A) Transduction profiles were determined by staining cells with anti-HA-PE and anti-V5-APC to test for expression of the anti-EGFR antigen-binding chain and anti-minocycline sdAb signaling chain respectively. Anti-CD34-AF488 was used to detect the transduction marker, RQR8. Based on RQR8 expression, transduction efficiency was normalised to 30% prior to co-culturing with SupT1-NT and SupT1-EGFR+ cells. Transduction efficiency gating strategy was as follow: Singlets (FSH/FS)>Live cells (SYTOX-Blue)>anti-HA-PE/anti-V5-APC/Anti-CD34-AF488. One donor is shown as a representative example. (B) Transduced effector cells were co-cultured with 50,000 target cells at a E:T ratio of 1:2. with and without minocycline (0.1 μM, 1 μM and 10 μM) for 24 hours and 72 hours. The percent of live tumour cells was determined using the MACSQuant X Flowcytometry Analyzer and normalised to non-transduced (NT) PBMCs (n=3). Flow cytometry-based killing gating strategy was as follows: Singlets (FSH/FSA)>Live cells (SYTOX blue)>Anti-CD3-PeCy7.

6.3.11 Incorporating combinations of co-stimulatory domains to the MinoCAR Fab antigen-binding domain increases MinoCAR effector function whilst maintaining tuneability

In order to enhance the cytokine secretion mediated by the MinoCAR, constructs were designed which incorporated various combinations of co-stimulatory domains on both the antigen-binding subunit and the signaling subunit of the MinoCAR structure (Fig. 6.18). Specifically, I introduced the CD28 or CD28-4-1BB co-stimulatory domains to the antigen binding chain whilst the signaling chain expressed a combination of CD3ζ alone, 4-1BB-CD3ζ or CD28-4-1BB-CD3ζ. Figure 6.18 shows the design of each variant of constructs (i) CD28+CD3ζ, (ii) CD28+4-1BB-CD3ζ, (iii) CD28+CD28-4-1BB-CD3ζ, (iv) CD28-4-1BB+CD28-4-1BB-CD3ζ. Each subunit was expressed as a single polypeptide chain separated by a 2A self-cleavage peptide (indicated by + sign). Unlike previous experiments, as each chain had various combinations of co-stimulatory and signaling domains, an equivalent negative control was not used to normalise any non-specific kill response, therefore for the purpose of screening the MinoCAR variants, non-transduced T cells were

used as a negative control. A conventional anti-EGFR CAR made up of an anti-EGFR sdAb fused to Ig-Kappa and the anti-minocycline sdAb fused to CH1, CD28TM and CD28-4-1BB-CD3ζ intracellular co-stimulatory and signaling domains (aEGFR-CD28-4-1BB-CD3ζ) was used as a positive control and gold-standard for CAR T cell activation.
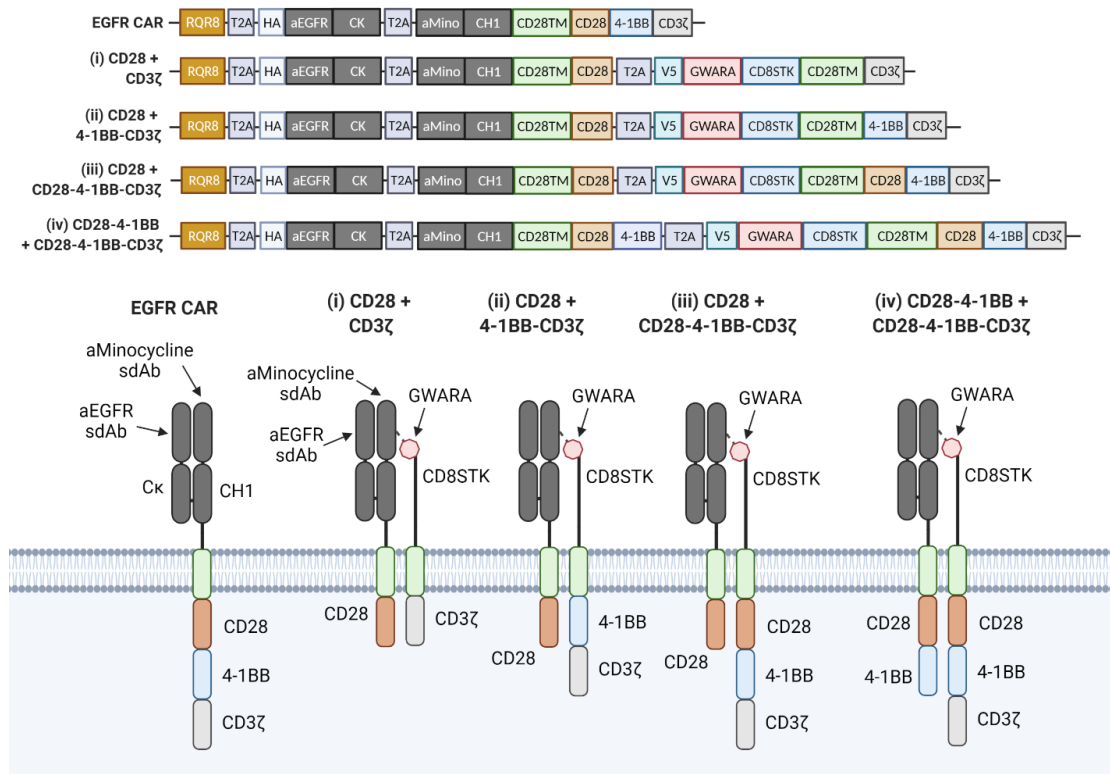
Figure 6.18. Construct design and corresponding schematic illustration of the bipartite MinoCAR structures with various combination of co-stimulatory domains.

Each component was expressed as a tricistronic construct of RQR8, an antigen binding subunit and a signaling subunit separated by 2A self-cleavage peptide sequences. RQR8 was used as an independent transduction marker. The structure of each CAR construct was made up of a heterodimerization binding subunit composed of an anti-EGFR sdAb fused to Ig-Kappa and the anti-minocycline sdAb fused to CH1 and anchored to the membrane via a CD28 transmembrane domain with various intracellular co-stimulatory domains (CD28 alone or CD28-4-1BB) which was expressed with a physically separated T cell signaling chain containing an C-terminus GWARA fused to a human CD8α spacer (CD8STK), CD28 transmembrane domain (CD28TM)

and various combinations of co-stimulatory and intracellular signaling domains (CD3ζ signaling domain alone, 4-1BB costimulatory domain + CD3ζ intracellular or CD28-4-1BB costimulatory domains and a CD3ζ intracellular signaling domain). A conventional anti-EGFR CAR made up of an anti-EGFR sdAb fused to Ig-Kappa and the anti-minocycline sdAb fused to CH1, CD28TM and CD28-4-1BB-CD3ζ co-stimulatory/signaling domains was used as a positive control.

72 hours post transduction, the retroviral transduction efficiencies and profile of primary human lymphocytes expressing the transduction marker RQR8 and each MinoCAR variant were determined. Figure 6.17 indicates high transduction efficiencies and stable expression of antigen-binding and signaling subunits. Additionally, the transduction profile shows each chain is expressed to equal ratios. Based on RQR8 expression, the transduction efficiencies were normalised to 30% prior to proceeding to cytotoxicity and cytokine release assay (Fig. 6.18 and Fig. 6.19).
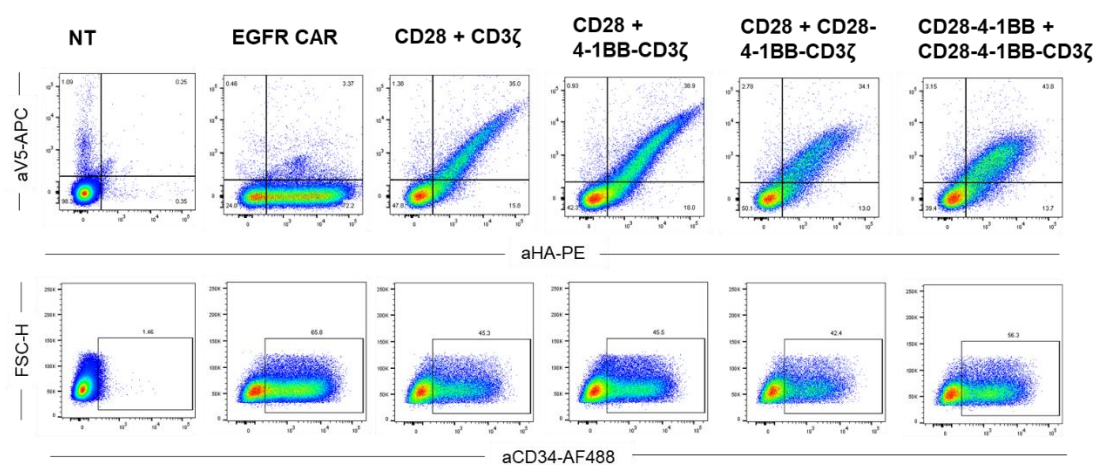
Figure 6.19. Flow cytometry analysis of the transduction efficiency and profile of MinoCAR variants with a combination of co-stimulatory and intracellular signaling domains.

PBMCs were stained using anti-HA antibody conjugated to PE (anti-HA-PE) and anti-V5 antibody conjugated to APC (anti-V5-APC) was used to test for the expression of the anti-EGFR binding subunit and GWARA bearing signaling subunit, respectively. Anti-human CD34 conjugated to AF488 (QBend10-AF488) was used to detect the independent transduction marker,

RQR8. Gating strategy was as follow: Singlets (FSH/FS)>Live cells (SYTOX-Blue)>anti-HA-PE/anti-V5-APC/Anti-CD34-AF488. One donor is shown as a representative example out of three donors.

The efficacy of MinoCAR with various combinations of co-stimulatory and intracellular signaling domains on each constituent subunit was tested by setting up a 24 hours and 72 hours co-culture assay against SupT1-NT and SupT1-EGFR+ cells at an effector to target ratio of 1:2, with and without minocycline supplementation (1 µM and 10 µM). CAR T cell mediated cytotoxicity was determined by staining the co-cultures with anti-CD3 antibody conjugated to PeCy7 to differentiate T cells from targets. Using flow cytometry, target cells were gated, and the total number of viable target cells were counted and normalised to the total viable target cells in co-culturing conditions with non-transduced (NT) T cells.

At 24 hour and 72 hours, we show in the absence of minocycline, cytotoxic killing of SupT1-EGFR+ target cells were observed, with the MinoCAR variants CD28+CD3ζ, CD28+4-1BB-CD3ζ, CD28+CD28-4-1BB-CD3ζ, CD28-4-1BB+CD28-4-1BB-CD3ζ eliminating SupT1-EGFR+ cells to levels equivalent to that of the conventional EGFR-CAR at each respective time-point (Fig. 6.20). Therefore, confirming antigen-specific T cell mediated cytotoxicity was directly comparable to a conventional EGFR-CAR.

Performing co-cultures in the presence of minocycline at concentrations of 1 µM and 10 µM, demonstrated a dose-dependent reduction in cytotoxicity by the MinoCAR constructs as measured by increased SupT1-EGFR+ target cell survival, with MinoCAR CD28+4-1BB-CD3 showing the overall optimum kill response in the absence of minocycline and sensitivity to minocycline at 1 µM and 10 µM in reducing cytotoxicity of target cells at 24 hours and 72 hours post co-culture. These data therefore suggest the minocycline-mediated displacement of the bipartite CAR subunits showing a dose dependent reduction in CAR T cell effector function and maintaining the 'OFF'-switch titratable control of tumour cell lysis even with the inclusion of various co-stimulatory domains on the MinoCAR binding subunit. Furthermore, non-

specific killing of target cells lacking antigen (SupT1-NT) was not observed at 24 hours or 72 hours in each culture condition.
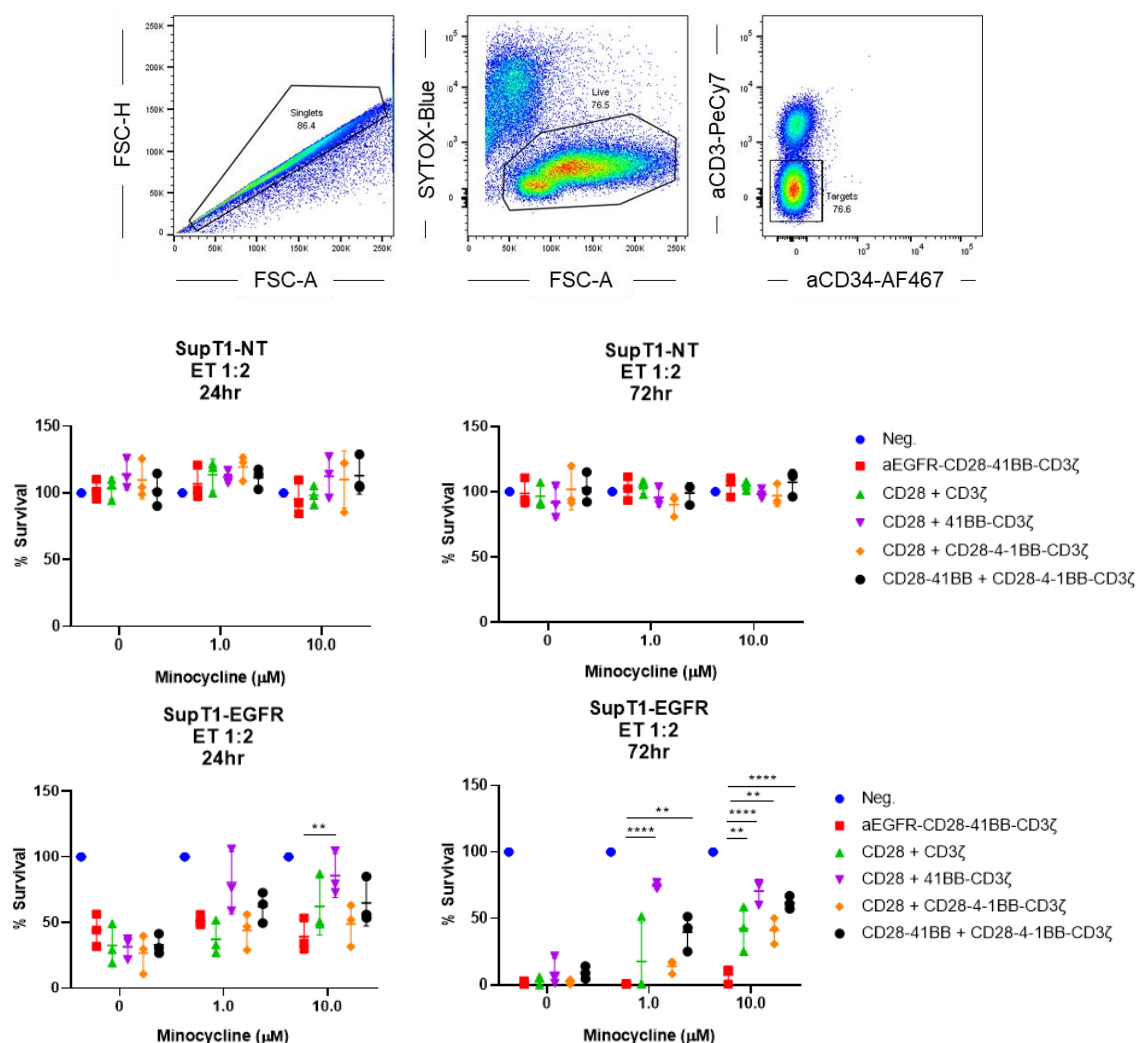
Figure 6.20. Cytotoxicity of the bipartite MinoCAR structures bearing various combination of co-stimulatory and signalling domains on the antigen-binding chain and signaling chains.

Flow cytometry-based cytotoxicity assay of PBMCs transduced with MinoCAR variants (CD28+CD3ζ, CD28+4-1BB-CD3ζ, CD28+CD28-4-1BB-CD3ζ, CD28-4-1BB+CD28-4-1BB-CD3ζ) and a conventional anti-EGFR CAR positive control (EGFR-CAR). Non-transduced Sup-T1 cells (SupT1-NT) and Sup-T1 cells expressing EGFR (SupT1-EGFR+) were used as target cells. Effector cells were co-cultured with target cells at a ratio of 1:2 with varying concentrations of minocycline (1 µM and 10 µM) for 24 hours and 72 hours. The percent of live target cells was determined using the MACSQuant X Flowcytometry Analyzer and normalised to non-transduced (NT) PBMCs

*(n=3). Gating strategy was as follows: Singlets (FSH/FSA)>Live cells (SYTOX blue)>Anti-CD3-PeCy7. Data represented as mean ± SD, n=3, ** p<0.005, *** p=0.0005, **** p<0.0001, two-way ANOVA (Dunnetts's multiple comparisons test).*

Once the ideal OFF-switch CAR cytotoxicity was confirmed, analysis of secreted IFN-γ and IL-2 levels in the supernatant was undertaken. Supernatant from 24 hours and 72 hours co-culture were collected and an IFN-γ and IL-2 ELISA assay was carried out. At 24 hours and 72 hours, IFN-γ and IL-2 levels of each MinoCAR variant in the absence of minocycline were directly comparable to the conventional EGFR CAR with MinoCAR variant CD28+CD28-4-1BB-CD3ζ displaying highest level of IFN-γ secretion and Mino CAR variant CD28+4-1BB-CD3ζ displaying the highest level of IL-2 secretion. Furthermore, co-culturing conditions with minocycline supplementation, the titratable cytokine secretion profile was seen to vary between each MinoCAR variant, with MinoCAR CD28+CD28-4-1BB-CD3ζ maintaining highest levels of IFN-γ secretion (Fig. 6.21). IFN-γ and IL-2 production of each MinoCAR variant when co-cultured with SupT1-NT was not detectable (data not shown). Overall, the MinoCAR CD28+4-1BB-CD3ζ showed the most ideal effector function (target cell cytotoxicity, IFN-γ and IL-2 secretion) whilst maintaining dose-dependent minocycline-mediated tuneability as a measure of reduced target cell cytotoxicity and cytokine release.
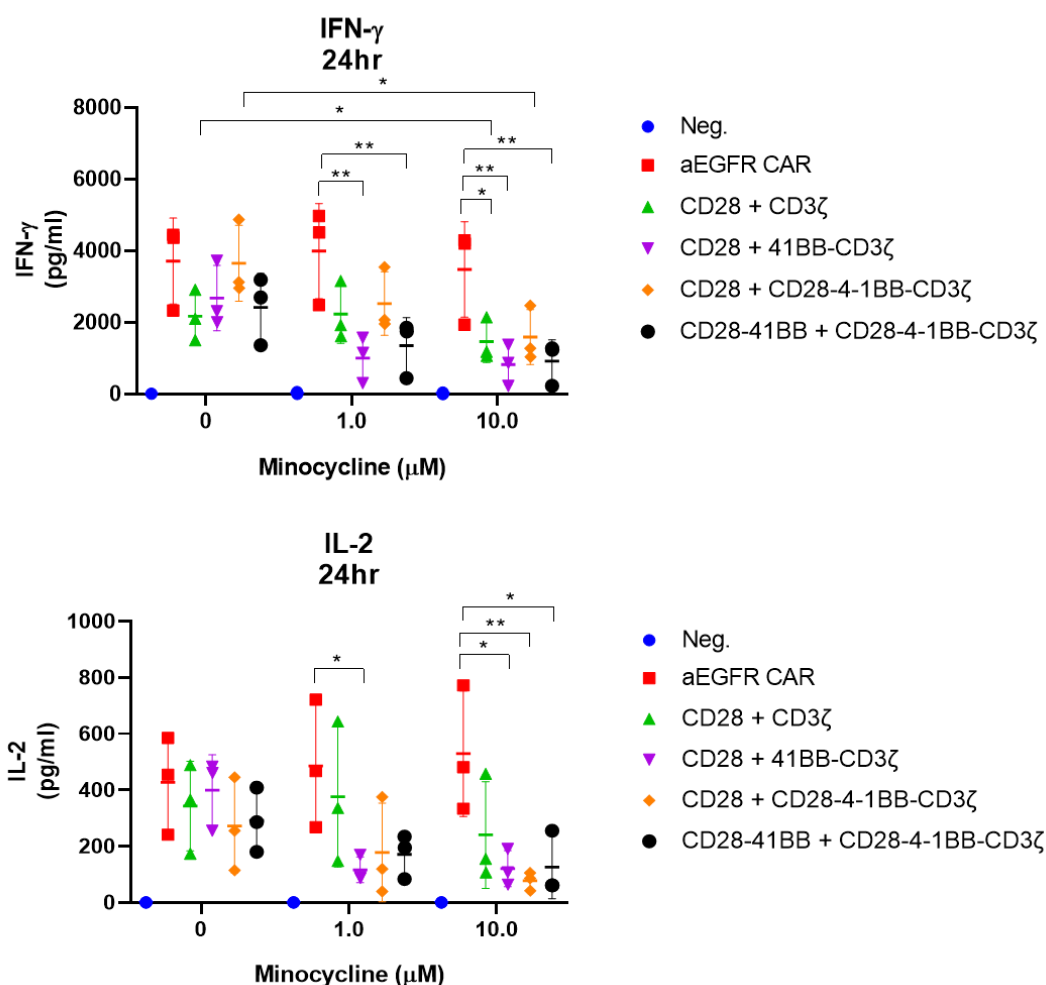
Figure 6.21. Cytokine secretion (IFN-γ and IL-2) of bipartite MinoCAR structures bearing various combination of co-stimulatory and signalling domains on the antigen-binding chain and signaling chains.

Supernatant was collected from the co-cultures of MinoCAR variants (CD28+CD3ζ, CD28+4-1BB-CD3ζ, CD28+CD28-4-1BB-CD3ζ, CD28-4-1BB+CD28-4-1BB-CD3ζ) and a conventional anti-EGFR CAR positive control (EGFR-CAR) against target cells (SupT1-NT and SupT1-EGFR+) at an E:T ratio of 1:2 with varying concentrations of minocycline (1 µM and 10 µM) at 24 hours and 72 hours. Cytokine analysis was carried out using IFN-γ and IL-2-specific ELISA. Data represented as mean ± SD, n=3, * p<0.05, ** p<0.005, two-way ANOVA (Dunnetts's multiple comparisons test).

6.3.12 MinoCAR T cells shows optimal cytotoxicity and cytokine release with dose-dependent CAR inactivation

The MinoCAR CD28+4-1BB-CD3ζ variant, which was termed MinoCAR moving forward, was identified as having the most desirable characteristics in terms of cytotoxicity and cytokine release against tumour target cells in the absence of minocycline and ideal response to minocycline. Therefore, I set out to characterise the tuneablity and reversibility of the MinoCAR. An appropriate negative control was also included in the subsequent experiments. The negative control was composed of an identical structure to the minoCAR with a non-specific Ser-Gly peptide in place of GWARA.

To test whether the latest design of the MinoCAR would perform as strongly as the monolithic conventional CAR structure against a range of cell lines, I performed cytotoxicity, cytokine release assays, tunability and reversibility characterisation against cell lines engineered to express EGFR (SupT1) as well as natively expressing EGFR+ cells (Skov3 cell line).

As expected, at 24 hours and 72 hours, I show in the absence of minocycline, cytotoxic killing of SupT1-EGFR+ target cells were observed, with the MinoCAR eliminating SupT1-EGFR+ cells to levels equivalent to that of the conventional monolithic EGFR-CAR at each respective time-point (Fig. 6.22), further confirming antigen-specific T cell mediated cytotoxicity was directly comparable to a conventional monolithic EGFR-CAR. Co-cultures in the presence of minocycline at concentrations of 1 µM and 10 µM, demonstrated a dose-dependent reduction in cytotoxicity by the MinoCAR constructs as measured by increased SupT1-EGFR+ target cell survival. Non-specific killing of target cells lacking antigen (SupT1-NT) was not observed at 24 hours or 72 hours in each culturing condition. Analysis of MinoCAR IFN-γ and IL-2 secretion 24 hours and 72 hours post co-culture with tumour targets, confirms in the absence of minocycline, levels to be comparable to the conventional EGFR CAR. With minocycline supplementation showing dose-dependent reduction in cytokine secretion by the MinoCAR (Fig. 6.23).
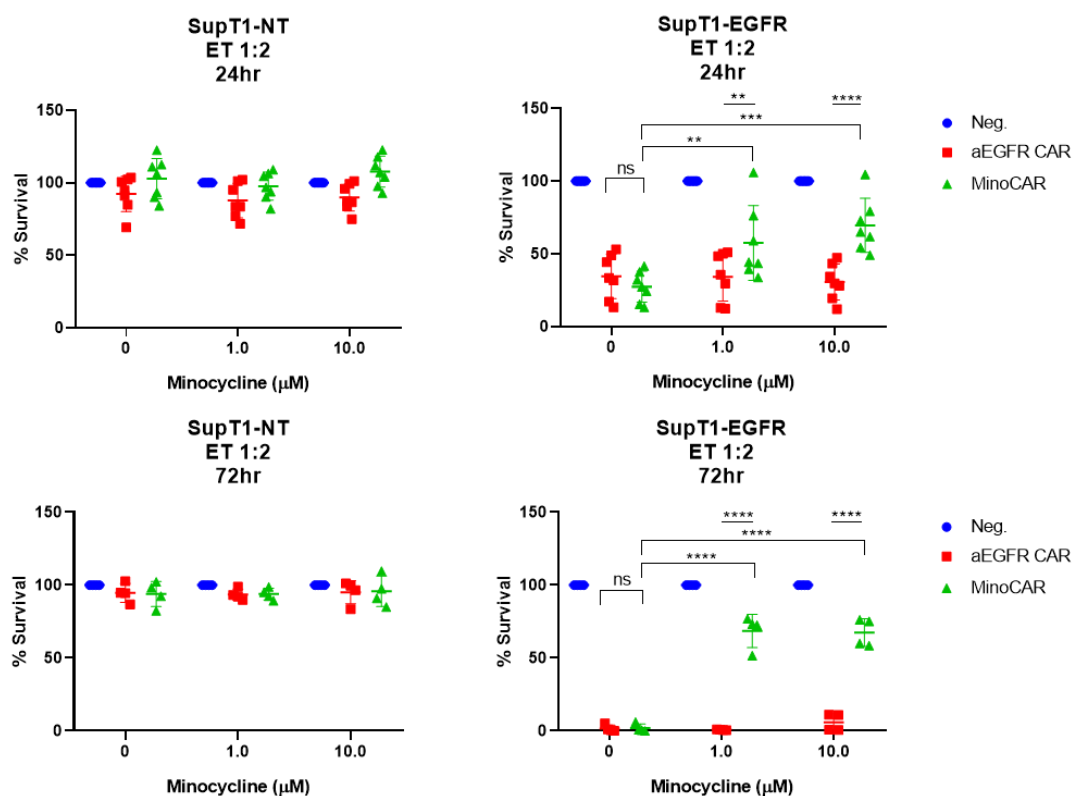
Figure 6.22. Cytotoxicity of the MinoCAR CD28+4-1BB-CD3ζ variant.

Flow cytometry-based cytotoxicity assay of PBMCs transduced with MinoCAR and a conventional anti-EGFR CAR positive control (EGFR-CAR). Non-transduced Sup-T1 cells (SupT1-NT) and Sup-T1 cells expressing EGFR (SupT1-EGFR+) were used as target cells. Effector cells were co-cultured with target cells at a ratio of 1:2 with varying concentrations of minocycline (1 µM and 10 µM) for 24 hours and 72 hours. The percent of live target cells was determined using the MACSQuant X Flowcytometry Analyzer and normalised to non-transduced (NT) PBMCs (n=4-7). Gating strategy was as follows: Singlets (FSH/FSA)>Live cells (SYTOX blue)>Anti-CD3-PeCy7. Data represented as mean ± SD, n=4-7, ** p<0.005, *** p=0.0001, **** p<0.0001, two-way ANOVA (Dunnetts's multiple comparisons test).
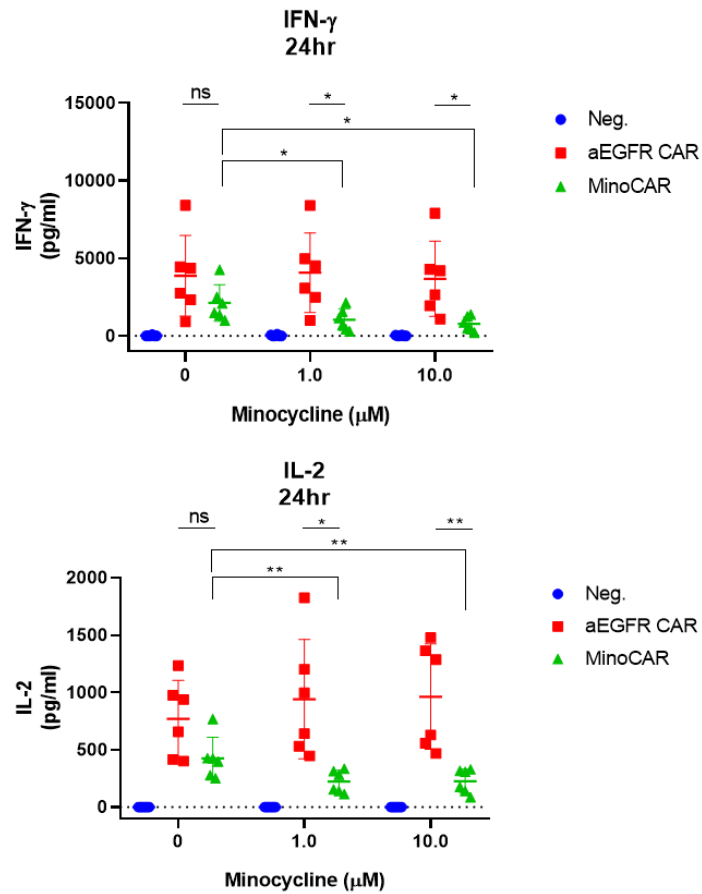
Figure 6.23. Cytokine secretion (IFN-γ and IL-2) of MinoCAR CD28+4-1BB-CD3ζ variant.

*Supernatant was collected from the co-cultures of MinoCAR and the conventional anti-EGFR CAR positive control (EGFR-CAR) against target cells (SupT1-NT and SupT1-EGFR+) at an E:T ratio of 1:2 with varying concentrations of minocycline (1 µM and 10 µM) at 24 hours. Cytokine analysis was carried out using IFN-γ and IL-2-specific ELISA. Data represented as mean ± SD, n=6, * p<0.05, ** p<0.01, two-way ANOVA (Dunnetts's multiple comparisons test).*

6.3.13 MinoCAR effector kinetics and reversibility real-time imaging incucyte assay

An essential feature of the MinoCAR T cells is that following activation they can be rapidly and completely inhibited by exposure to minocycline and that following minocycline removal the cells are able to recover full cytolytic activity within a short time frame. Live-cell imaging was used to gain an understanding of the complete dynamic function of MinoCAR. I sought to validate the reversibility of the MinoCAR by investigating the ability of minocycline to inhibit a pre-activated MinoCAR (ON-OFF rate) as well as the ability of the MinoCAR to recover and to activate after inhibition with minocycline (OFF-ON rate). Specifically, the ON-OFF rate was measured by exposing the MinoCAR T cells to the target antigen before exposing the MinoCAR T cells to antigen expressing target cells in the presence and absence of minocycline. The MinoCAR T cells were pre-incubated for 2 hours on plates pre-coated with 10 µg/ml recombinant EGFR, as this was the concentration which saturated the MinoCAR T cells for maximum activation as a measure of IFN-γ secretion. Once the MinoCAR T cells were activated, the subsequent CAR "Switch-OFF" rate was determined by co-culturing the pre-activated MinoCAR T cells with antigen expressing EGFR+ Skov cells previously transduced to express the mKate2 red reporter gene (Skov-mKate EGFR+ cells) (Fig. 6.24) with and without minocycline supplementation (10 µM). This strategy mimics the MinoCAR dynamics once exposed and activated by tumour cells and then switched OFF by administration of the drug.

Additionally, the reversibility of the system was determined by inhibiting the T cells with minocycline prior to exposure to EGFR+ Skov-mKate cells. To estimate the impact of switching OFF the MinoCAR T cells prior to exposure to antigen, an experiment was set-up to measure the OFF-ON rate of the MinoCAR T cells. For measuring the OFF-ON rate, the T cells were pre-incubated in media supplemented with minocycline (10 µM), washed, and then exposed to 10^4 EGFR+ SKOV3-mKate target cells with or without minocycline (10 µM). Thus, showing the capacity of MinoCAR to perform cytotoxic killing of tumour cells following exposure to minocycline and its subsequent removal. A summary schematic of the experimental set up to determine the ON-OFF

and OFF-ON kinetics is illustrated on Fig. 6.25. In both cases the rate of killing of SKOV3-mKATE cells with pre-activated or pre-inhibited MinoCAR T cells was compared with that of MinoCAR T cells which had not been previously exposed to minocycline or target antigen.
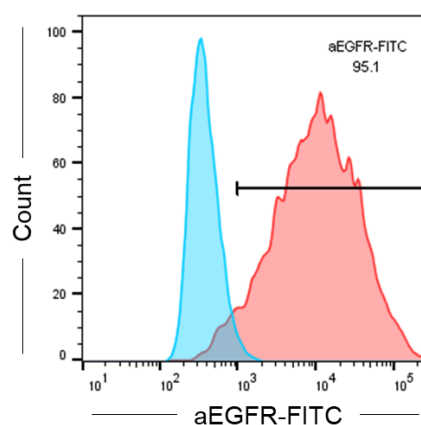
Figure 6.24. SKOV3-mKate2 cell line characterisation.

The human hypodiploid epithelial-like cells derived from adenosarcoma, SKOV-3 cells natively express EGFR and were used in live-cell imaging by transducing cells to express mKate. EGFR expression was determined by staining cells with anti-EGFR antibody conjugated to FITC. Unstained SKOV-3 (blue histogram) and stained SKOV-3 cells (red histogram).
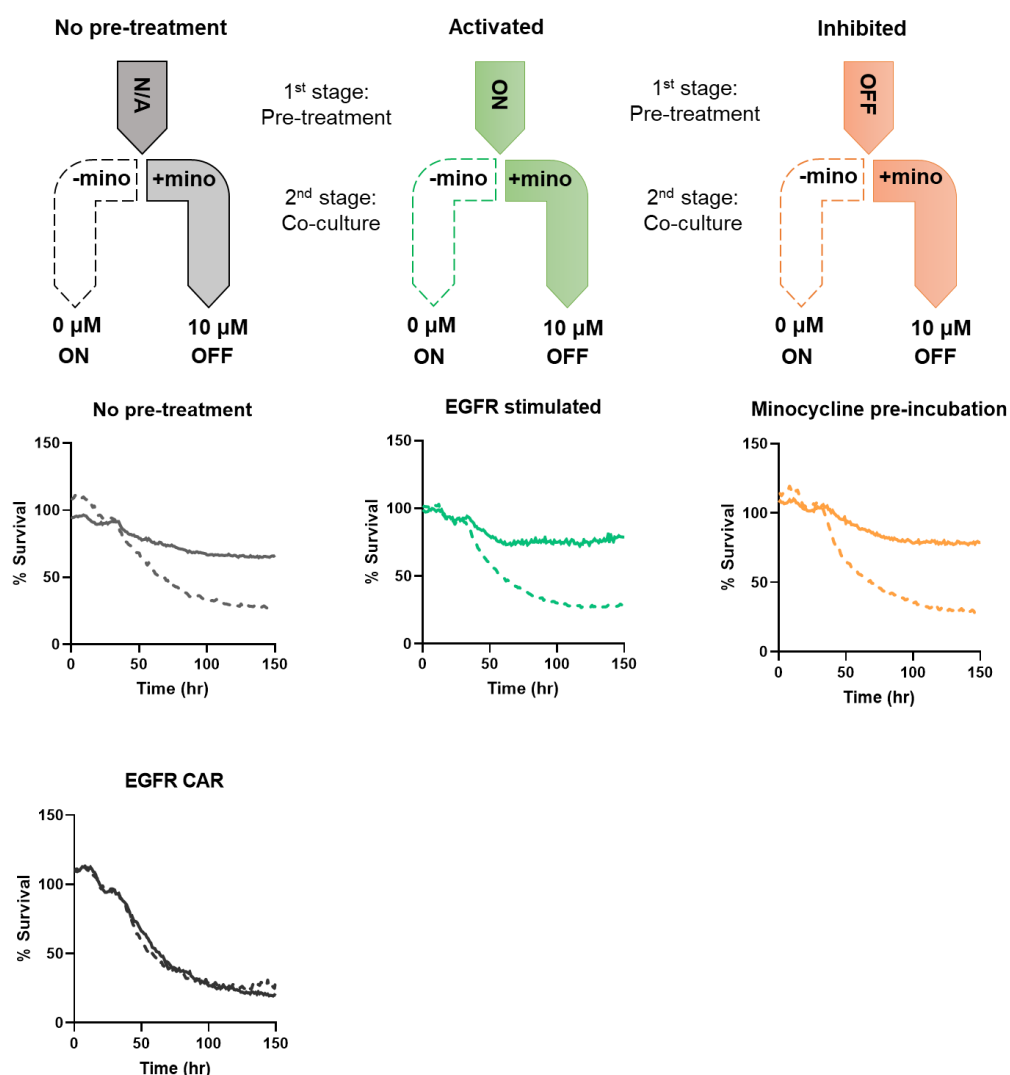
Figure 6.25. Cytotoxicity kinetics using the IncuCyte real-time imager to determine the ON-OFF and OFF-On cytotoxicity rate of the MinoCAR targeting EGFR+ SKOV3-mKate cells.

Schematic of real-time Incucyte assay set up to determine the ON-OFF and OFF-ON rate of the MinoCAR targeting EGFR+SKOV3 cells labelled to express the fluorescent protein mKate. ON-OFF kinetics were determined by pre-activating CAR T cells by incubating cells on plates pre-coated 10 µg/ml recombinant EGFR for 2 hours. Cells were then washed with PBS and incubated with EGFR+SKOV3-mKate target cells with 10 µM minocycline (solid line) and without minocycline (dashed line). OFF-ON kinetics determined by inhibiting CAR T cells by incubating cells in RPMI supplemented with 10% FBS, 1% GlutaMAX and 10 µM minocycline. Cells were then washed with PBS and incubated with EGFR+SKOV3-mKate target

cells with and without minocycline (10 µM). Untreated CAR T cells were also co-cultured with EGFR+SKOV3-mKate target cells. ON-OFF and OFF-ON cytotoxicity rate of the MinoCAR targeting EGFR+ SKOV3-mKate cells. EGFR+ SKOV3-mKate were seeded at $1.0×10^4$ cells per well of a 96-well plate and were used as target cells in the co-culture with transduced PBMCs expressing the MinoCAR and EGFR-CAR (positive control). Co-culture was carried out at effector to target ratio of 1:2. Image capture rate of each condition was set at 1 hour for 150 hours.

From Figure 6.25 I observe, in pre-activated CAR T cells, both the EGFR CAR and MinoCAR showed comparable killing kinetics in the absence of the drug. Whereas in the presence of minocycline, MinoCAR showed a reduction in cytotoxicity relative to the EGFR CAR. Despite prior activation through exposure to antigen the rate and degree of inhibition seen when pre-activated cells were exposed to minocycline was comparable to the inhibition seen when cells lacking pre-treatment were exposed to the drug. This suggests that minocycline can rapidly and completely inhibit activated MinoCAR T cells

In the drug pre-treated CAR T cells, MinoCAR cytotoxicity was restored to normal levels within 24 hours with similar cytolytic kinetics of CAR T cells previously untreated with minocycline. These results confirmed that inhibition is rapidly reversed upon clearance of the drug and that previously inhibited MinoCAR T cells can quickly regain full capacity to kill antigen-bearing target cells to a degree comparable to MinoCAR T cells which had not experienced prior inhibition.

6.3.14 MinoCAR effector tuneablity using real-time imaging incucyte assay

In addition to confirming the reversibility of MinoCAR, I sought out to carry out a comprehensive assessment of the tuneability of MinoCAR by investigating the impact of various concentrations of minocycline (0.625 µM, 0.125 µM, 2.5 µM, 5 µM and 10 µM) on cytotoxic function using the incucyte real-time imaging. In the absence of minocycline, the cytotoxicity kinetics of minoCAR were comparable to the monolithic EGFR CAR. With increasing

concentrations of minocycline from 0.625 µM to 10 µM, dose-dependent tuneablity of CAR deactivation was observed (Fig. 6.26).
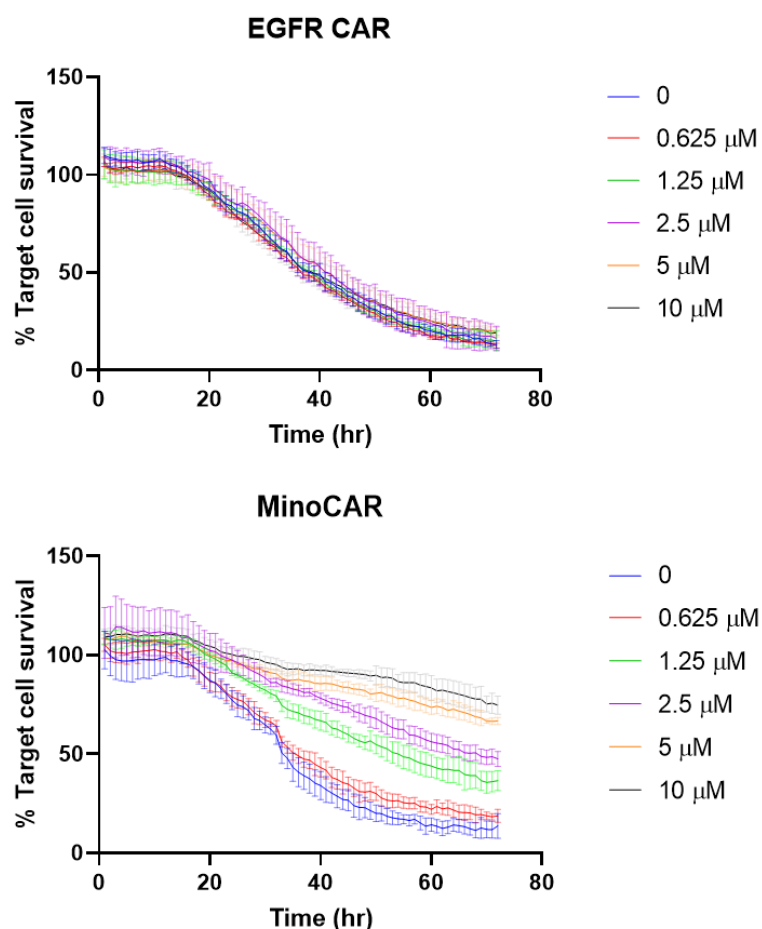
Figure 6.26. Cytotoxicity kinetics using real-time imager Incucyte to determine the tuneable cytotoxicity rate of MinoCAR targeting EGFR+ SKOV3-mKate cells.

Cytotoxicity rate of the MinoCAR targeting EGFR+ SKOV3-mKate cells. EGFR+ SKOV3-mKate were seeded at 1.0×10⁴ cells per well of a 96-well plate and were used as target cells in the co-culture with transduced PBMCs expressing the MinoCAR and EGFR-CAR (positive control). Co-culture was carried out at effector to target ratio of 1:2 and in the absence and presence of minocycline (0.625 µM, 1.25 µM, 2.5 µM, 5 µM, 10 µM). Image capture rate of each condition was set at 1 hour for 72 hours. Data represented as mean ± SD, n=3.

6.3.15 MinoCAR 'OFF'-switch effector function is highly specific to minocycline

Real world use of the MinoCAR would require the system to be highly specific to the small molecule. Use of small molecule drugs which bear similar chemical structures to minocycline could interfere with MinoCAR T cell therapy by inadvertently deactivating the CAR T cell. Therefore, I tested the binding of anti-minocycline sdAb to a range of similar small molecules such as doxycycline, tetracycline, methotrexate, and caffeine. Binding was tested using SPR by immobilizing the murine-Fc conjugated anti-minocycline sdAb to a CM5 Biacore chip, with each drug used as the analyte which confirmed lack of binding to the doxycycline, tetracycline, methotrexate, and caffeine (data not shown). Moreover, a functional cytotoxicity was carried out by testing cytotoxicity response when co-cultured with SupT1-EGFR cells and each drug (0.1 µM, 1 µM and 10 µM). As expected, minocycline dosing shows MinoCAR deactivation as a measure of target cell survival. Doxycycline, tetracycline, methotrexate, and caffeine did not improve SupT1-EGFR cell survival, thus indicating small molecule drugs which have a similar structure to minocycline does not cause displacement of each MinoCAR subunit and a functional heterodimer is maintained (Fig. 6.27).
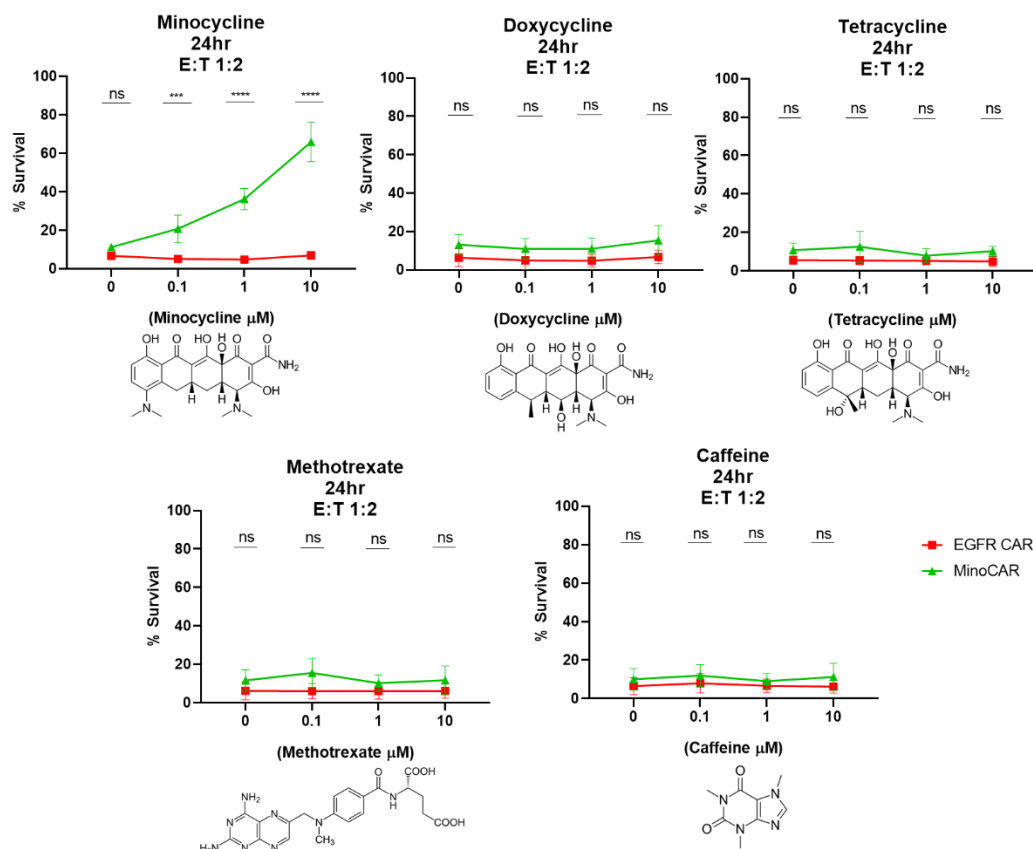
Figure 6.27. MinoCAR 'OFF'-switch effector function is highly specific to minocycline.

Flow cytometry-based cytotoxicity assay of PBMCs transduced with MinoCAR and a conventional anti-EGFR CAR positive control (EGFR-CAR). Sup-T1 cells expressing EGFR (SupT1-EGFR+) were used as target cells. Effector cells were co-cultured with target cells at a ratio of 1:2 with varying concentrations of the indicated drug (0.1 µM, 1 µM and 10 µM) for 24 hours. The percent of live target cells was determined using the MACSQuant X Flowcytometry Analyzer and normalised to negative control. Gating strategy was as follows: Singlets (FSH/FSA)>Live cells (SYTOX blue)>Anti-CD3-PeCy7. Data represented as mean ± SD, n=4, *** p=0.0006, **** p<0.0001, two-way ANOVA (Sidak's multiple comparisons test).

6.4 Discussion

In this chapter, I describe the engineering process for the development of a novel synthetic OFF-switch CAR T cell which enables exogenous small-molecule based control of T cell activity, anti-tumour cytotoxicity and cytokine release using minocycline at or below therapeutic concentrations (5-10 µM).[349,350] Minocycline is the ideal small molecule for such a remote-controlled system based on a range of factors. Minocycline is a cheap, well-tolerated, widely available, non-immunosuppressive, FDA approved drug. Minocycline is easily administered with 100% bioavailability via oral dosing. In addition, the drug is rapidly absorbed showing peak serum concentration 2-3 hours post administration.[349,350] Compared to other tetracycline derivatives, minocycline is lipophilic, therefore readily crosses the blood brain barrier,

User-based remote-controlled therapeutics could permit the use of strategies which utilise highly potent receptors, proteins and drugs which would otherwise present a high risk of toxicity if constitutively active.[351] Traditionally, the use of suicide genes has such as iCasp9 and RQR8 have acted as remote-controlled safety mechanism for CAR T cell therapy. In recent times, small-molecule drug inducible CAR T cells have been described. Initial work began with the use of inducible split CAR designs (ON-switch CARs) whereby a small molecule drug was required for the functional heterodimerisation of an antigen-binding domain and a signaling domain. Later, more convenient OFF-switch CARs were developed where the presence of a disrupting small molecule would result in the displacement of two interacting subunits therefore rendering the CAR incapable of signaling and activation. Similarly, use of inducible degrons fused to the CAR structure can permit the controlled degradation of CARs. However, previously described OFF-switch CAR proteins or the small molecule drug required to control the CAR T cells may limit their widespread clinical application. These systems utilise non-human/immunogenic components, use of immunosuppressant drugs such as rapamycin which could undesirably dampen T cell activation and efficacy, as well as small-molecule drugs which have yet to be FDA approved which may also inhibit the anti-apoptotic protein, BCLxL.[346] Specifically, the key

disadvantage of the TetCAR system is the potential of immunogenicity due to the bacterial TetRB protein utilised as a part of the protein-protein interaction required for a fully signaling CAR. Efforts at minimising the immunogenicity of TetRB protein have been made, although these have resulted in immune responses against other TetRb epitopes further indicating the inevitable immunogenicity to TetRB.[189] Therefore, the development of a system containing a non-immunogenic anti-minocycline binder can reap the benefits of using minocycline as the controlling small molecule for feasible clinical application of an OFF-switch CAR. Non-human sequences of the MinoCAR mainly reside within the VHH domains, however, VHH domains present high sequence similarity (~80%) with the VH3 domains of humans, thus have shown to present particularly low immunogenicity.[193,352] If future concerns arise over the use of a camelid derived antibody sequences, humanization of the anti-minocycline sdAb may be carried out to further reduce immunogenic potential.[353–355]

Previous work on split CARs has shown reduced signal transduction resulting in poor cytokine secretion and proliferation relative to a monolithic CAR structure.[342,346,356] Therefore, in this work, the initial development of a small molecule based OFF-switch CAR was based on a CAR-TCR hybrid due to the many structural advantages of TCRs have over CARs in T cell therapy. TCRs utilise co-stimulation to enhance receptor signaling (CD3, 41BB and CD28), possess greater number of subunits (10 in TCRs compared to 1 in CARs) and contain more ITAMs (10 in TCRs compared to 3 in CARs).[357]

The TCR structure, specifically those which utilise the TCR signaling subunits have emerged as engineering targets to improve the efficacy of immunotherapy. For example, ImmTACs (immune-mobilising monoclonal TCRs against cancer), T Cell Receptor Fusion Constructs (TRuCs) and T Cell Antigen Coupler (TACs) have aimed to utilise the potent signalling capacity of the full TCR complex. Reprogramming of the TCR has been achieved by introducing new target specificity in an HLA-independent mode of T cell activation. TRuCs bear an extracellular N-termini antibody-based tumour antigen-binding domain fused to T cell receptor (TCR) subunits (TCRa, TCRβ,

CD3e, CD3g and CD3d). Once the TRuC has been transduced, the TRuC integrates within the native TCR complex. Hence, not only allowing for the engineered T cells pre-determined target specificity and tumour cell killing in an HLA independent manner, but also utilising the full signaling machinery and capacity of the TCR complex.[358] Therefore, showing improved tumour clearance compared to second-generation CARs, which achieve signaling via a single isolated CD3z cytoplasmic tail.[359] The TAC platform also incorporates the endogenous TCR signalling and effector function to target tumour antigens in an MHC-independent manner and initiate a potent anti-tumour response with reduced toxicity.[360] The TAC system couples with the TCR via an anti-CD3 binding domain which is fused to a tumour antigen-binding domain at the N-termini. Thus, the resulting TCR/CD3 complex is triggered through antigen engagement to achieve robust anti-tumour T cell responses.[360,361] It has been demonstrated that TAC-engineered T cells showed potent T cell effector function and solid tumour infiltration. Based on the success of incorporating the full TCR for maximal signaling output, I believed the poor cytokine secretion and proliferation of previously described split CARs could be overcome through the development of a controllable OFF-switch CAR-TCR chimeric platform (Fig. 6.3). Where instead of having the antigen-binding domain directly interacting with CD3 via an anti-CD3 antibody as described using the TAC platform, this interaction would take place using a chimeric TCR CD3ε chain bearing an N-terminus GWARA peptide interacting with the antigen binding domain via anti-minocycline sdAb. Hence, allowing for remote-control using minocycline. However, the GWARA bearing chimeric CD3ε failed to carry out tumour directed cytotoxicity due to lack of chimeric GWARA-CD3ε expression.

Two potential design platforms were then conceptualised based on a bi-partite CAR structure separated into antigen-binding and T cell activation/signaling subunits which would form a functional heterodimer in the absence of minocycline. The hetrodimerisation of antigen-binding and signaling domains on distinct, separate receptors is a key feature of previously reported drug-controlled CARs which allows their association and function to be controlled, positively or negatively by a relevant small molecule.

As previously mentioned in Section 6.3.3.1, recent CAR designs have utilised sdAbs as the antigen-binding domain. Since the first MUC-1 targeting sdAb-based CAR T cell,[362] other sdAb based CAR platforms have been developed which provided the justification for the design choices described in this chapter. For example, a modular universal CAR termed UniCAR was developed to control T cell effector function using an adaptor protein via a protein-protein interaction. The CAR had specificity towards a short peptide known as 5B9 and an adaptor known as the targeting module was made up of a tumour antigen targeting sdAb tagged with the peptide 5B9.[363] Control of CAR T cell activity was achieved through the protein-protein interaction between the CAR once the targeting module was present. A sdAb-based anti-EGFR adapter has also been described, where a CAR module targets a short peptide epitope E5B9 via an anti-E5B9 scFv. The presence of the targeting module (an anti-EGFR sdAb fused to the E5B9 peptide) led to CAR T cell mediated cytotoxicity of EGFR+ cells and cytokine release.[364] Additionally, a bivalent anti-EGFR targeting module made up of two sdAb fused via E5B9 showed also improved affinity towards EGFR and increased cytokine secretion as a part of the UniCAR.[365] Multiple bi-partite CAR structures have been described where the heterodimerisation via a drug inducer or protein-protein interaction takes place intracellularly.[189,342,346] However, intracellular use of the GWARA was restricted due to the cysteine constrained nature of peptide formation. Therefore, the bi-partite structures contained extracellular sdAb and GWARA peptide. Leung et al showed the development of a successful drug controlled bipartite CAR structure which achieved functionality through extracellular receptor dimerization. Therefore, two bipartite CARs were designed and tested: the peptide spacer MinoCAR and prototype Fab MinoCAR, each containing variations in extracellular receptor dimerisation.

A Fab structure for the antigen binding domain of the MinoCAR was chosen due to the independent function of the anti-EGFR sdAb (tumour target binding) and anti-minocycline sdAb (GWARA binding). Functional dual-sdAb Fab structures known as bispecific Fabs have previously been described. Rozan et al showed that fusing an anti-FcγRIII sdAb and anti-CEA sdAb C17 to the

CH1 and Ck heterodimerization motif, triggered IL-2 and IFN-γ release via CD16 clustering present on CEA+ colon cancer cells as well as potent NK cytotoxicity against CEA+ cells in vitro and inhibition of tumour growth in vivo.[366] A similar dual-sdAb Fab structure was also described by Turini et al using the anti-CEA sdAb and an anti-Her2 sdAb. Compared to the anti-Her2 mAb, Trastuzumab, the dual Fab showed enhanced cytokine release and similar Her2+ breast cancer growth inhibition in vivo.[367] More recently, other bi-partite CARs have shown improved expression of Fab antigen-binding domains over scFv based antigen-binding domains.[189] In all, the Fab structure was chosen as the antigen-binding domain for the MinoCAR and showed stable expression and detection of both the anti-EGFR sdAb and anti-minocycline sdAb on the cell-membrane.

The rationale behind the design of the peptide spacer MinoCAR was as follows: In the absence of minocycline ('ON'-state), the interaction between the antigen-binding spacer region bearing the GWARA sequence and anti-minocycline sdAb on the signaling chain allows for the formation of a functional heterodimer and thus signaling upon antigen engagement. Such a design was attractive due to a reduced DNA encoding region compared to the prototype Fab MinoCAR described in 6.3.3.1, which would not only reduce the transcriptional burden on T cells, but also allow scope for the future development via the introduction of additional components to be placed within the limited real estate of the DNA plasmid cassette. Most importantly, the key motivation for such a design was the possibility to introduce multiple GWARA sequences as a part of the antigen-binding subunit spacer region to allow interaction/binding to multiple anti-minocycline sdAb-signaling subunits resulting in the concatenation of the signaling chain, leading to the enhancement of signaling via the recruitment and signaling through multiple co-stimulatory and signaling domains/ITAMs. It has previously been shown that increasing the number of ITAMs in CARs through the addition of an extra CD3ζ (3 ITAMs to 6 ITAMs) lead to increased number of activated cells, T-cell proliferation, IL-2 release and in vivo anti-tumour response.[361,362] Additionally, functional repercussions of spacer design alterations have been reported in the literature. Changes in the spacer region can regulate the synaptic cleft

distances and kinetic segregation. Generally, optimum synapse distances are achieved when shorter spacers are used for membrane-distal epitopes, whereas longer spacers require membrane-proximal epitopes.[370] Besides limiting inhibitory phosphatases, longer synaptic cleft can lead to diminished transport of granzymes and perforins to the tumour cell. In T cell-target cell engagement, a dense immune synapse impedes diffusion of lytic granules which results in the increased membrane pore formation via transport of granzymes and perforins.[371] Although CAR T cells do not utilise an identical immune synapse as TCRs, transport of lytic granules and kinetic segregation are essential CAR T cell signaling and effector function.[372] Therefore, changes to the spacer region of a CAR can have a significant effect on CAR T cell signaling. Designing an antigen-binding chain where alternations to the spacer length could be made through the insertion or deletion of in-cis GWARA sequences for optimal tumour epitope targeting was also attractive for this reason.

In addition, spacer domain alterations may alter the structural conformation of CARs. In this work I modified the CD8a through the fusion of GWARA. Previous work has been carried out on altering the length of the CD8a spacer through the addition or deletion of residues, which yielded CARs with varied structural conformations resulting in considerable in vitro and in vivo responses.[373] Even though the mechanism of these changes of altering the CD8a spacer is not well understood, it highlights the importance of the spacer to CAR T cell signaling and function. From these results, I showed addition of the GWARA peptide as a part of the spacer region of an anti-EGFR CAR (aEGFR-GWARA-CD8STK-TM-CD28-41BBζ) maintained potent cytotoxicity against EGFR+ cells, corroborating the feasibility of the addition residues to the CD8a spacer to generate a functional CAR. However, the lack of signalling from variants of the bipartite peptide spacer MinoCARs (aEGFR-GWARA-CD8STK-TM + aMino-CD8STK-TM-CD28-41BBζ) indicates GWARA within the spacer region of the antigen-binding chain was sterically inaccessible or the binding angle was constrained and unable to bind to the anti-minocycline sdAb on the signalling chain. The importance of epitope accessibility for CARs has been described previously with suboptimal effector function of an anti-

MUC1 CAR was shown to be ascribed to glycosylation independent steric hindrance of the binding epitope.[104]

In comparison to the peptide-spacer MinoCAR configuration the initial Fab MinoCAR showed good cytotoxicity towards target cells however, despite this, did not appear to induce full activation of the T cells as noted by low cytokine release. As IL-2 is the main proliferative cytokine[374] which requires a greater threshold for initiation compared to cytotoxic killing[347,348] multiple Fab MinoCAR architectures were designed and tested comparing the effector function, particularly IL-2 secretion, to that of a conventional CAR architecture. Previously, split CAR systems have shown to lack the potency to that of conventional CARs, which required significant structural optimisations and novel engineered components.[189,342] In all, architectures which fused various intracellular co-stimulatory domains (CD28 alone or CD28-4-1BB) to the antigen-binding chain show significantly improved overall effector function compared to those which lack co-stimulatory domains on the antigen-binding subunit. Wu and colleagues described a split CAR with a suboptimal CAR effector function when utilizing an antigen-binding chain lacking a physically linked co-stimulatory domain. This group demonstrated the use of a co-stimulatory domain fused to the antigen-binding chain improved CAR effector function to levels comparable to conventional CAR architectures.[342] More recently, Hotblack et al also presented work showing the incorporation of costimulatory domains fused to the antigen-binding domain, specifically using a membrane-proximal CD28, resulted in cytokine secretion and proliferation directly comparable to its respective monolithic CAR architecture.[189] In accordance with these reports, the MinoCAR structure CD28+4-1BB-CD3ζ, which expressed a membrane proximal CD28 co-stimulatory domain on the antigen-binding chain, showed enhanced effector function (target cell cytotoxicity, IFN-γ and IL-2 secretion) whilst maintaining dose-dependent minocycline-mediated tuneability as a measure of reduced target cell cytotoxicity and cytokine release. This further corroborates the requirement of membrane proximal co-stimulation of the antigen-binding chain as described in other split CARs.[342,346,356]

Unlike other co-stimulatory domains, CD28 is present on resting and activated T cells.[92] CD28 can elicit potent T cell activation even without TCR engagement.[92] CD28 ligation leads to recruitment of phosphatidylinositol 3-kinase (PI3K), the adaptor protein involved in signal transduction known as Growth factor receptor-bound protein 2 (Grb2), the protein tyrosine kinases Lck and Itk and the protein phosphatase 2 (PP2).[92] It's cytoplasmic motif (YMNM) interacts and activates PI3K and Grb2 leading to enhanced IL-2 release which enhances T cell persistence and prevents AICD, which is also facilitated through the upregulation and secretion of T helper type 1 cytokines such as IFN-γ, IL-10, TNF-a and GM-CSF.[92] Besides potentiating a powerful T cell signaling and cytokine response, CD28 also activates actin polymerisation mediated through the activity of Vav guanine nucleotide exchange factor 1 (Vav1), cell division control protein 42 homolog (Cdc42) and actin related protein 2/3 complex.[92] Actin polymerisation has been suggested to employ membrane rafts to the immune synapse. This results in assembly of Lck and LAT to the TCR potentiating a greater level of TCR signalling. CD28 activation of PI3K/Akt signalling pathway is inhibited if membrane raft formation is halted.[375] Thus, I enhanced MinoCAR cytokine secretion through the additional of CD28 to the binding chain.

Previous work carried out by Milone and colleagues indicates positioning the 4-1BB co-stimulatory domain closer to the membrane compared to other endodomains provides optimum CAR function.[376] Therefore, I believe expressing the MinoCAR signalling chain which contained the 4-1BB-CD3ζ costimulatory and signaling chains also improved effector function due to the membrane proximal 4-1BB intracellular co-stimulatory domain.

Even though the MinoCAR mediated target cell lysis was comparable to the conventional CAR T cell, and the cytokine secretion concentration were within the range expected for CAR T cells, cytokine (IFN-γ and IL-2) levels were slightly lower than the conventional EGFR CAR. However, a CAR T cell which is precisely remote-controllable which produces slightly lower levels of cytokines may turn out to be safer at higher doses and when targeting tumour antigens with safety concerns. Alternative strategies for increasing T cell

signalling and effector function of split CAR structure has been the incorporation of the ectodomain of DNAX activating protein 10 (DAP10) to the signalling chain. DAP10 can initiate homodimersation of the signaling chains thus doubling the ITAMs and downstream signalling potency.[377–379] If required in the future against challenging targets, such a strategy may be used for the MinoCAR signalling chain to increase the copy number of ITAMS of the functional heterodimerisation unit as well as increase avidity interaction of the signaling chain homodimer.

With regards to the signalling chain of all variations of the MinoCAR, the CD8a spacer region was chosen over other spacers such as CD28. Previously, both the CD8a and CD28 hinge regions have shown clinical efficacy. However, Alabanza et al. showed the use of an CD28a hinge region as a part of an anti-CD19 CAR spacer region showed higher levels of activation-induced cell death (AICD) relative to a CD8a spacer; with elevated levels of IFNg and TNFa reported with CD28 spacer bearing CAR-T cells but no substantial difference in tumour cytotoxicity.[380] These differences were suggested to be assigned this to the greater propensity for CD28 to dimerise compared to CD8a. Therefore, this group suggested the increased CD28 dimerisation resulted in increased signalling and ACID. However, in recent times, Majzner et al. showed a CD19 CAR bearing a CD28 spacer and transmembrane domains reduced the threshold of antigen-density required for T-cell signaling relative its CD8a spacer counterpart. Moreover, Rodgers et al showed introducing structural dimerisation of CARs using an IgG4 spacer with an S228P mutation resulted in in vitro cytotoxicity as well as in vivo tumour clearance.[381] In contradiction to previous reports, this study presents evidence indicating spacer dimerization enhanced CAR effector function.[380] Due to the remote controlled, tuneable, and reversible nature of the MinoCAR, future development could utilise the CD28 spacer or IgG4 hinge spacer bearing the S228P mutation to allow dimerisation and thus increased number of ITAMS of the MinoCAR signalling chain without concerns over AICD.

This MinoCAR OFF-switch system, in which the drug switches off CAR activity, functions solely through tumour specific antigen engagement and does not

rely on continuous small-molecule administration to reap therapeutic benefits as required when using ON-switch CAR T cell approaches. At a low therapeutic minocycline dosing (1 - 10 µM) which is well-tolerated in humans, the MinoCAR showed significant inhibition of cytotoxicity and cytokine secretion. Complete dynamic function of MinoCAR was also carried out to validate the tunability and reversibility of the MinoCAR using live-cell imaging of MinoCAR T cells treated in various conditions. By pre-activating the MinoCAR T cells (ON-OFF rate) and carrying out the co-culture against tumour cells, I aimed to mimic the MinoCAR being exposed to and activated by tumour cells and assess the degree and rate at which T cell activation is halted. Additionally, I showed switching OFF the MinoCAR T cells prior to exposure to tumour cells had minimal impact on MinoCAR's capacity to perform cytotoxic function subsequently upon the removal of minocycline. Therefore, this work demonstrated that the MinoCAR system has the potential to provide on-demand tuneable and reversible user input based on real-time patient indicators of toxicity without concerns over impacting the functionality of CAR T cells. Additionally, CRS is typically observed within the first 7 days upon CAR T cell infusion.[148,149] Particularly, patients with high disease burden and comorbidities present the greatest risk of severe CRS which can onset within 3 days upon CAR T cell infusion.[328,330] Minocycline can not only be applied during the manufacturing process but also titrated upon infusion to introduce therapeutic effects in a controlled fashion to prevent the sudden onset of severe toxicities. Precise optimisation of the MinoCAR and minocycline regimen will be essential for future applications and against novel targets.

Beyond facilitating methods of alleviating potential toxicity, the MinoCAR system allows therapeutic prospects which may in fact enhance CAR T cell function. CAR T cell exhaustion severely restricts immune responses against tumour cells and is a of major setback with the use of conventional CAR T cell therapy. Weber and colleagues demonstrated transient inhibition of CAR T cell signalling was shown to enhance CAR-T cell functionality by avoiding T cell exhaustion.[382] The induction of transient rest using drug controlled down-regulation of CAR proteins led to the expansion of a memory phenotype, transcriptional and epigenetic changes and re-established functionality in CAR

T cells previously showing signs of tonic signalling and exhaustion.[382] Using the MinoCAR system, minocycline can also be used to periodically inhibit CAR signalling and enhance the overall function and potency of CAR-T cell therapy by preventing T cell exhaustion, compared to more potent constitutively active CAR T cells. Furthermore, it has also been shown T cells which present markers of exhaustion can be reversed through resting T cells signalling indicating the concept that exhaustion is not epigenetically fixed.[382]

The protein-protein displacement principle forms an overall cellular control mechanism for incorporating autonomous user control. As the field of immunotherapy develops more therapies with novel technologies which produce potent response against solid tumours, the risk of adverse effects is magnified. The repercussions of uncontrolled cellular therapies mean the stakes of adverse toxicities is significantly burdensome and restricts clinical trial progress and approval. Therefore, remote controlled user-based regulation permits clinicians a precise dose, timing, and targeted response to improve safety of adoptive T cell therapies.

6.5 Conclusions

- The split CAR structure composed of (i) antigen-binding chain made up of a C-terminus anti-EGFR sdAb fused to Ig-Kappa and the anti-minocycline sdAb fused to CH1, CD28TM, and a CD28 intracellular co-stimulatory domain expressed with the (ii) signalling chain made of a C-terminus GWARA fused to a human CD8α spacer, CD28TM and 4-1BB-CD3ζ endodomain (MinoCAR CD28+4-1BB-CD3ζ) showed potent cytotoxic killing and cytokine secretion, directly comparable a conventional monolithic CAR.

- OFF-switch CAR architecture shows efficient inhibition of activity mediated by minocycline at therapeutic concentrations.

- MinoCAR cytotoxicity was shown to be tuneable in a dose-dependent manner.

- Live-cell imaging was used to confirm the effector function of MinoCAR was reversible.

7 EXPLORATION OF NOVEL STRATEGIES FOR THE SECRETION OF AN ANTI-TUMOUR PAYLOAD USING A DISPLACEABLE PEPTIDE-PEPTIDE INTERACTION

7.1 Introduction

Due to the success of engineered cell therapy in clinical trials against haematological malignancies such as CD19+ B cell acute lymphoblastic leukaemia (ALL), diffuse large B-cell lymphoma (DLBCL), Chronic lymphocytic leukaemia (CLL), and adult acute myeloid leukaemia (AML),[146,149,383,384] engineered cell therapies have been rapidly expanding to pursue the treatment of solid tumour malignancies.[385] Despite initial optimism, treatment outcomes have been modest with a host of challenges associated with establishing engineered T cell efficacy in the hostile, immunosuppressive conditions of the solid tumour-microenvironment. Numerous reasons have been suggested why solid tumours have been a challenging target for engineered cell therapy compared to lymphoid cancers, for example tumour access, persistence of engineered cells against inhibitory signals and tumour antigen heterogeneity. Specifically, clinical studies on metastatic cancer show a lack of efficacy of current CAR T cell technologies in tackling the inhibitory cellular elements and immunosuppressive cytokines (IL-4, IL-6, LIF, IL-10 and TGF-β), T cell suppression via the infiltration of tumour associated macrophages (TAMs), myeloid derived suppressor cells (MDSCs), regulatory T cells and upregulated tumour-surface expression of programmed death ligand 1 (PD-L1). Although progress has been made in the development of CAR T cells with the addition of extra intracellular costimulatory domains, which have shown promising in vitro activity, these have yet to show substantial improvement against solid malignancies in a clinical setting. Modulating the tumour microenvironment may provide a more favourable environment in which CAR T cells can proliferate, survive and/or engraft. Engineering the CAR T cell cassette to secrete pro-inflammatory cytokines or express soluble or tethered anti-tumour cargos via drug-induced remote-controlled mechanism is pertinent in the development of CAR T cell therapy against non-haematological malignancies. Interleukin-12 (IL-12) is a potent pro-inflammatory immunomodulatory cytokine of particular interest for

regulating the tumour microenvironment and redirecting the immune response against the tumour. IL-12 has shown potent anti-tumour activity and recruitment of T cell mediated inflammatory responses when artificially administrated or expressed locally.[351,386,387] However, systemic IL-12 is toxic therefore mechanisms for secreting IL-12 locally have been described.[387] Previously autologous melanoma tumour infiltrating lymphocytes (TILs) have been transduced to express a gene encoding for a single-chain flexible IL-12 driven by an NFAT promoter. Despite a functionally controlled system for IL-12 release, severe clinical toxicity occurred including high serum levels of IL-12 and IFN-γ, fever, liver failure and sporadic life-threatening hemodynamic instability.[388] A second generation CAR T cell engineered to constitutively secrete the pro-inflammatory cytokine IL-12 targeting the ovarian cancer cell target Muc-16 in vitro and in syngeneic model of murine ovarian peritoneal carcinomatosis has shown disease clearance.[389] T cells constitutively secreting IL-12 and their potential clinical application remains a grave concern within the field due to potential toxicity through the onset of lethal inflammatory syndrome. Technological advancements to overcome IL-12 toxicity are of paramount importance to enable its use in the clinical setting.[390,391] There remains a need for approaches to controllably modulate the tumour microenvironment, which may improve the effectiveness of engineered cytolytic immune cells to proliferate, survive and/or engraft in a microenvironment without unacceptable systemic toxicity in the patient. To this end a system was developed to allow the controllable secretion of IL-12 in response to minocycline.

7.2 Aims

- To present proof-of-concept work for a novel architecture for the retention and controlled release of pro-inflammatory cytokines using the retention of a KDEL-tagged single-domain antibody (sdAb) and a GWARA-tagged IL-12.

7.3 Results

The endoplasmic reticulum (ER) carries out the primary role of protein synthesis, folding, post-translational modifications, transport and secretion as well as instructing protein degradation within eukaryotic cells.[392,393] The ER also bears mechanisms to ensure proteins are correctly folded and transported to appropriate intracellular and extracellular locations. An example of a mechanism which aids in the maintenance of ER proteostasis, is a protein retrieval pathway using the KDEL receptor (KDELR). Synthesised polypeptides which are intended to be secreted enter the ER and are transported to the Golgi apparatus. ER luminal chaperones such as glucose-regulated-protein-78/94 (GRP78/94) and protein disulphide isomerase (PDI) as well as other enzymes involved in correct folding of secretory and membrane proteins are also trafficked to the Golgi apparatus.[394] Therefore, to preserve the activity of folding chaperones and enzymes within the ER, retention of these proteins within the ER itself is essential. Pelham et al. discovered that protein retention was achieved through KDELR-mediated recognition of ER proteins via a C-terminal ER retrieval sequence (ERS) composed of the amino acid sequence Lys-Asp-Glu-Leu (known as the KDEL motif) in mammals and amino acid sequence His-Asp-Glu-Leu (known as the HDEL motif) in yeast.[394,395] This results in the retrieval of proteins in the Golgi via retrograde transport using COPI-coated vesicles back to the ER.[396,397]

Using the sdAb-GWARA displacement platform, I explored the potential application of this system to enable remote-controlled secretion of an anti-tumour cargo such as pro-inflammatory cytokines. In this chapter, the KDEL amino acid motif, which can be used to retain proteins within the ER/Golgi apparatus, was used to tag the minocycline-specific sdAb thus anchoring it to the ER/Golgi apparatus. Tagging a cargo molecule with one of the sdAb specific peptides (GWARA) should cause its retention through interaction with the sdAb. Upon the addition of minocycline, the sdAb-peptide complex will dissociate enabling the secretion of the peptide-tagged protein payload. The work presented here represents the initial proof-of-concept of a minocycline-controlled payload secretion system. However, this technology has the potential to be applied to an engineered T cell approach and could show

enhanced cytotoxicity & proliferation and decreased apoptosis when engaged with immunosuppressive environments of solid tumour malignancies.

7.3.1 Design of a retention system based on anti-minocycline sdAb fused to KDEL and IL-12 fused to GWARA and PWAYS

I hypothesized that utilizing the anti-minocycline sdAb clone 1 and the sdAb specific displaceable peptides linked to IL-12 as an intracellular system could provide a platform for a small molecule remote controlled secretion of IL-12. The KDEL amino acid sequence was used to tag the minocycline specific sdAb thus anchoring it to the ER/Golgi apparatus. IL-12 was separately tagged with the highest affinity sdAb specific peptides, GWARA, to allow for the formation of a peptide-peptide interaction between the IL-12 molecule (Fig. 7.1).

A
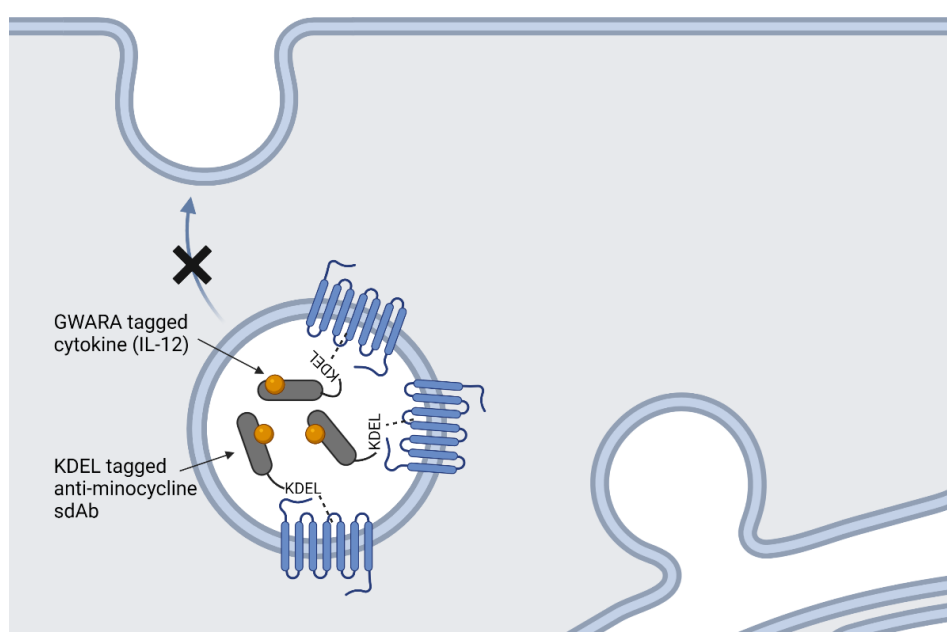
B
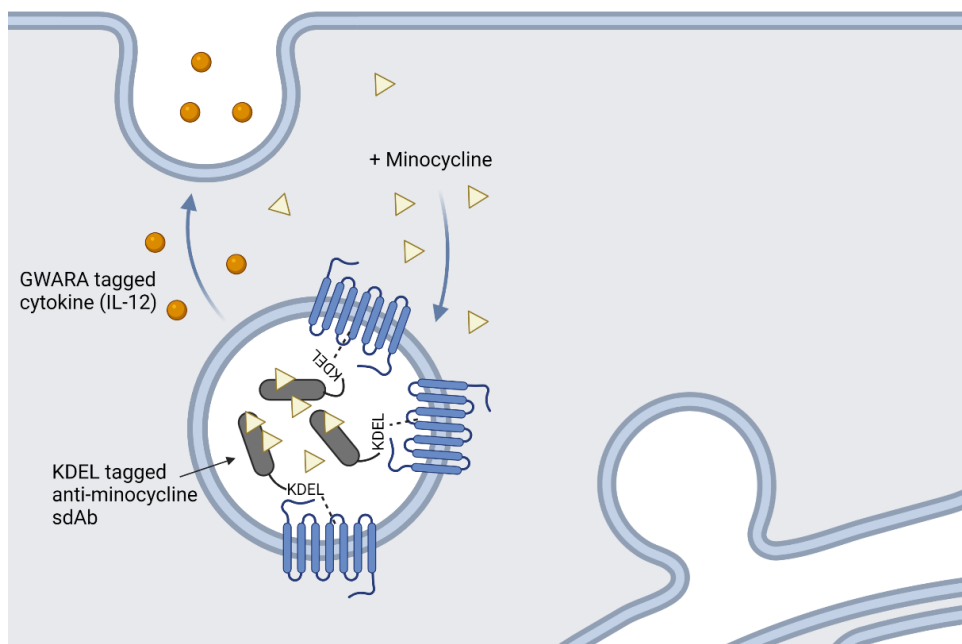
Figure 7.1. Illustration of the anti-minocycline KDEL retention system for the minocycline-mediated secretion of a GWARA tagged anti-tumour cargo in engineered T cells.

The first interaction takes place between GWARA-bearing IL-12 (GWARA-IL-12) and the anti-minocycline sdAb. The second interaction takes place between the anti-minocycline sdAb expressing a C-terminal KDEL retention motif (aMino-sdAb-KDEL) and the KDEL receptor (KDELR). (A) In the absence of minocycline, the first interaction between GWARA-IL-12 and aMino-sdAb-KDEL and the second interaction between aMino-sdAb-KDEL and KDELR results in retention of IL-12 within the endoplasmic reticulum. (B) In the presence of minocycline, the protein:protein interaction between GWARA and aMino-sdAb is disrupted, resulting in IL-12 no longer being retained within the endoplasmic reticulum.

7.3.2 Generation and expression of peptide-IL-12 and sdAb-KDEL constructs

Retroviral vectors were constructed which encoded the following constructs: human IL-12 made up of the p35 and p40 subunit fused together via a flexible linker (flexi-IL-12), GWARA peptide fused-flexiIL-12 (GWARA-flexiIL-12), peptide-flexiIL-12 expressed with the anti-minocycline sdAb separated by the Thosea asigna virus 2A (T2A) self-cleavage peptide (GWARA_flexi-IL12-T2A-sdAb), and peptide-flexi-IL-12 expressed with a C-terminal KDEL-fused anti-minocycline sdAb (GWARA_flexi-IL12-T2A-sdAbKDEL) (Fig. 7.2A).

Flexi-IL-12 and GWARA-flexi-IL-12 were used as positive controls showing the maximal IL-12 secretion achievable in the cell-based assay. GWARA_flexi-IL12-T2A-sdAb was also used as a positive control, expected to show the level of IL-12 secretion with an increased transcriptional and translational burden of a larger open reading frame and IL-12/sdAb complex formation. GWARA_flexi-IL12-T2A-sdAbKDEL was the test construct expected to retain IL-12 in the absence of minocycline.

7.3.3 GWARA_flexi-IL12-T2A-sdAbKDEL shows retention of IL-12 and dose-dependent secretion upon minocycline dosing in primary T cells

The retention capacity of GWARA_flexi-IL12-T2A-sdAbKDEL in PBMCs was measured by detection of secreted IL-12 from retrovirally transduced PBMCs at day 2 and day 7. PBMCs were transduced with Flexi-IL12, GWARA-flexi-IL12, GWARA-flexi-IL12-T2A-sdAb and GWARA_flexiIL12-T2A-sdAbKDEL. Transduction efficiency was determined using anti-HA-PE and cells were normalised to 60% efficiency prior to assay set up (Fig. 7.2B). Transduced T cells were cultured in the absence and presence of minocycline (0.1 µM, 0.5 µM, 1 µM and 2.5 µM). Supernatants were collected at day 2 and day 7 for assessment of IL-12 levels by ELISA.

Figure 7.2C shows the ELISA data of IL-12 levels from each culture condition which indicates GWARA-tagged IL-12 in the context of the GWARA_flexiIL12-T2A-sdAbKDEL construct was retained by forming a complex with the

ER/Golgi anchored KDEL tagged anti-minocycline dAb in the absence of minocycline relatively to IL-12 levels detected from flexi-IL12, GWARA-flexi-IL12 and GWARA-flexi-IL12-T2A-sdAb. Specifically, the results show that in the absence of minocycline, sdAb-KDEL was able to retain IL-12 to levels <200 pg/ml up to day 7 in primary human T cells, whereas the respective control lacking KDEL tagged sdAb showed levels of IL-12 release >10,000 pg/ml.

Upon the incremental addition of minocycline (0.1 µM, 0.5 µM, 1 µM and 2.5 µM), the sdAb-GWARA complex was displaced, enabling the dose-dependent secretion of the peptide tagged IL-12 at day 7 (up to ~2,200 pg/ml). Interestingly, the IL-12 released from the KDEL retained IL-12 in the presence of minocycline, was approximately 5-fold lower than the IL-12 released from the non-KDEL positive control.
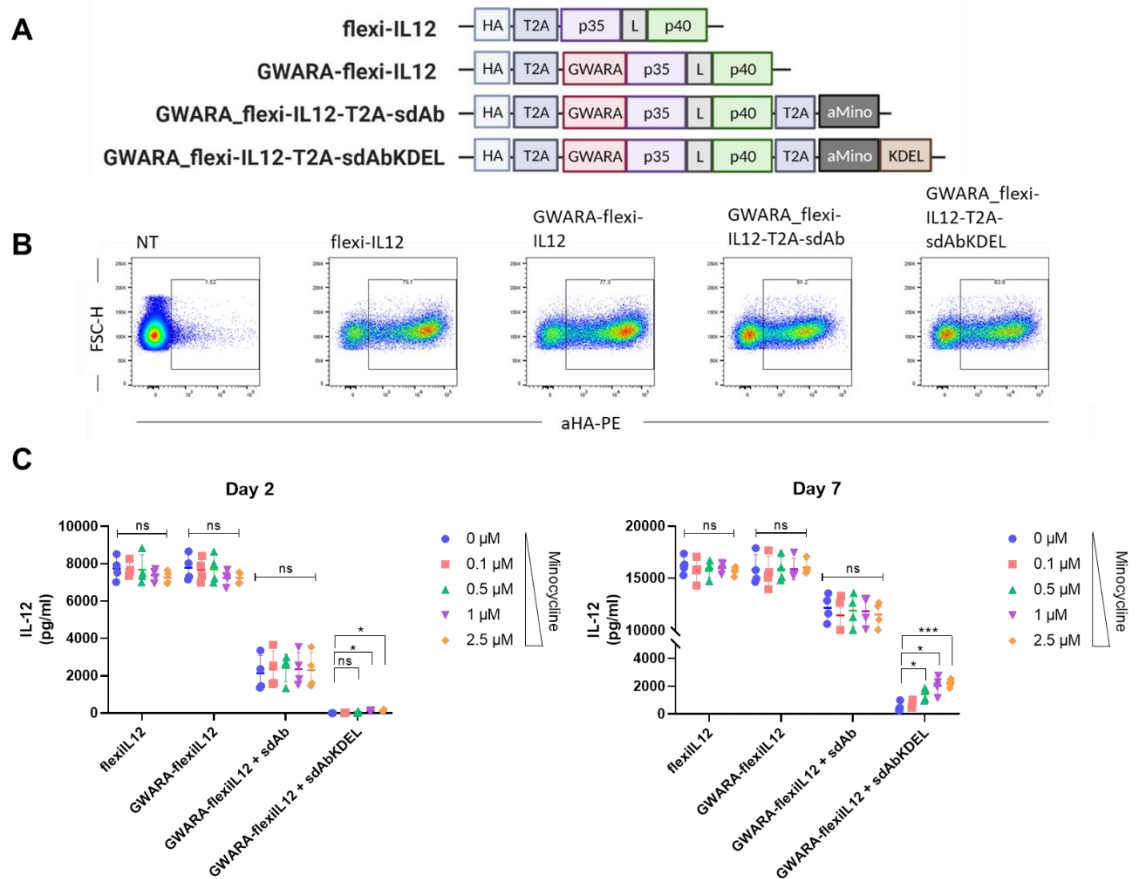
Figure 7.2. Minocycline-induced secretion of ER retained IL12 in T cells.
(A) Schematic diagram illustrating the construct designs of the anti-minocycline KDEL retention system. Each construct is expressed as a single polypeptide chain and separated by the Thosea asigna virus 2A (T2A) self-cleavage peptide. The transfection marker HA was used. (B) PBMCs were transduced with Flexi-IL12, GWARA-flexi-IL12, GWARA-flexi-IL-12-T2A-dAb and GWARA_flexiIL12-T2A-dAbKDEL. Transduction efficiency was determined by staining for the independent HA expression marker using an anti-HA-PE antibody. Cells were normalised to 60% efficiency prior to assay set up. (C) For the assay set up, 50,000 transduced cells were plated in individual wells pre-coated with anti-CD3 and anti-CD28 antibodies at a concentration of 10 µg/ml. Culture media was also supplemented with and without minocycline supplementation (0.1 µM, 0.5 µM, 1 µM and 2.5 µM). The supernatant was collected at day 1 and day 7 for IL-12 ELISA. Data represented as mean ± SD, n=4, * p<0.05, *** p<0.001, two-way ANOVA (Dunnetts's multiple comparisons test).

7.4 Discussion

The use of adoptive T cell therapy has shown efficacy against haematological malignancies. However, success in targeting against solid tumours has been limited. To overcome the hostile, immunosuppressive conditions of the solid tumour-microenvironment, many strategies have been developed to secrete IL-12 and redirect the immune response against the tumour in a controlled manner due to the fact systemic IL-12 presents significant risk of fatal toxicity.[387]

As mentioned in the Section 7.1, the use of inducible IL-12 secretion has been published by many groups. Previous work has shown a C-terminal KDEL retention domain fused to an anti-TCR ScFv to retain and knockout cell-surface expression of TCR.[398] Moreover, Chen et al described the use of an anti-CD7 nanobody fused to the KDEL retention domain to retain CD7 and generate CD7Δ T cells, which were subsequently used to transduce with an anti-CD7 CAR to avoid fratricide.[399] In this work, I carried out a similar approach whereby the KDEL retention domain was utilised to tag a sdAb which interacted with GWARA tagged IL-12 to retain within the ER/Golgi (Fig. 7.2C).

The level of in vitro IL-12 described in this chapter were comparable or less than the in vitro production of IL-12 (<400 pg/ml) using a vector construct expressing a CAR and flexi-IL-12 located from an IRES element; which correlated to <50 pg/ml in mouse models.[400] The IL-12 levels secreted by this system are also lower than reports showing constructs expressing CARs in addition to flexi-IL-12 and flexi-IL-12 secreted using an inducible NFAT promoter ($\sim$5,000 pg/10^6 cells).[401] In the future, the use of an IRES element upstream of the GWARA-IL-12 could be used to further reduce IL-12 expression if required. As native TCR activation can induce secretion of endogenous IL-12, I carried out an assay whereby the TCR was stimulated, using plate bound anti-CD3 and anti-CD28 antibodies, prior to assessing IL-12 levels. These results show that, in the absence of minocycline, the levels of IL-12 secretion were minimal on day 7. The level of peptide-tagged IL-12 secretion when expressed with the sdAb, was slightly lower than the IL-12 and peptide-tagged IL-12 expressed without the sdAb, which was most likely as a result of the increased transcriptional burden due to the tri-cistronic nature of

the construct expressed with a sdAb. For maximal benefits through the use of IL-12, the in vivo minocycline dosing must be optimised to achieve ideal therapeutic window. Regardless of the low levels of in vitro IL-12 presented, the use of an IL-12 expressing vector remains a major safety concern. Additionally, the impact of IL-12 accumulation within the ER is unknown. Therefore, the use of a suicide gene, such as RQR8, would be essential when using an IL-12 expressing vectors.

7.5 Conclusions

- Initial proof-of-concept work suggesting the minocycline mediated protein-protein displacement system can be applied as a part of an architecture for the retention and controlled release of GWARA-IL12 using KDEL-tagged anti-minocycline sdAb.

8 CONCLUSIONS AND FUTURE WORK

In this chapter I aim to review and summarise the key results of this thesis and suggest directions for future work.

8.1 Conclusions

As the aim was to use the small molecule-mediated protein displacement platform in a clinical setting, minocycline was chosen as the controller molecule due to its wide availability, excellent bio-distribution, and lack of toxicity. Additionally, to minimize immunogenicity in patients, a sdAb was specifically chosen as the binding moiety. In Chapter 3, single domain antibodies (sdAbs) targeting minocycline were generated with the aim to isolate the highest affinity sdAb as the main protein component. In total, I show the isolation of 9 unique sdAbs targeting minocycline.

Using Biacore SPR analysis, the highest affinity sdAb-minocycline binding was measured at 31 nM (KD) with component kinetics of $ka=1.13 \times 10^6 M^{-1}s^{-1}$ and $kd=3.6 \times 10^{-2}s^{-1}$. An affinity of 31 nM was in agreement with affinity ranges of previously described antibiotic-based protein-protein disrupters via a high nanomolar affinity interaction with one of the protein components.[249]

A host of tumour targeting sdAbs have been used as antigen-binding domains in CAR T cell therapies, with many reports indicating clinical efficacy. As the aim was to incorporate the sdAb as a part of a CAR structure, I fused the sdAb to the extracellular region of a CAR and measured expression relative to a marker gene and capacity to bind minocycline in the context of a cell-membrane, thus, confirming optimal transgene expression and sdAb transport to the cell membrane as well as excluding the possibility of membrane induced steric hindrance which may have impaired minocycline binding.

The biophysical studies of the sdAb isolated in Chapter 3 produced favourable affinity ranges, stability and domain folding, and cell-surface expression. Therefore, using the sdAb as a target, a displaceable peptide component was described in Chapter 4. Using a combinatorial phagemid library of cysteine-constrained peptides, 4 unique minocycline-displaceable anti-sdAb peptides

with a homologous consensus motif (Pro-Gly/Gln/His-Trp-Ala-Arg/Met/Gln-Ala/Met/Ala-Phe) were isolated. Previous work has shown the dissociation constants of cystine-constrained cyclic peptides targeting protein to be in the micromolar range.[277–279] In order for the peptide and anti-minocycline-sdAb interaction to be displaceable by minocycline, the binding affinity of the peptide would have to be less than that of 31 nM (the affinity of the sdAb for minocycline). SPR analysis of the binding affinity was carried out to confirm each isolated peptide fit these criteria. Overall, each isolated peptide presented nanomolar affinities for the sdAb, with values ranging from 111-328 nM. The peptide sequence ACPGWARAFC bound the sdAb with an affinity of K_D=111 nM with component kinetics of k_a=1.55x10^5 M^{-1}s^{-1} and k_d=1.7x10^{-2}s^{-1}. Nanomolar affinities were typical for cyclic peptides recently generated through phage display.[294,295] The use of an antibiotic mediated displaceable high affinity protein-protein interaction (K_D=640 nM) has been previously described in the development of an OFF-switch split CARs, suggesting the 111 nM sdAb-peptide interaction was also sufficient for split CAR development. [248,296]

Competition ELISA showed a 7-fold reduction in ACPGWARAFC peptide binding to the sdAb in the presence of minocycline relative to no minocycline. Moreover, cell-surface binding assays showed dose-dependent displacement of the ACPGWARAFC-sdAb complex in the presence of minocycline (1 µM - 100 µM). Finally, as the aim was to make the peptide-sdAb interaction reversible, SPR analysis also showed peptide-sdAb rebinding took place upon multiple minocycline-mediated displacement events.

As a part of the characterisation of the displacement platform, understanding the nature of the binding interaction taking place between the sdAb CDRs and minocycline or peptide was also undertaken. Initial attempts at X-ray crystallography failed, therefore, Chapter 5 describes the process of predicting the binding interface using computational antibody-ligand docking validated using experimental alanine scanning mutagenesis. Schrodinger BioLuminate computational homology protein modelling was used to produce a 3D model of the anti-minocycline sdAb to which computational sdAb-minocycline and

sdAb-peptide docking was carried out. SPR binding analysis showed mutant anti-minocycline sdAbs generated through alanine scanning-mutagenesis of the CDRs, that key hotspot residues N38, W110, G111, E112, L115, D116 and Y117 were involved in minocycline binding, either through direct interaction (hydrogen bond, salt bridge, van der Waals bonds) or alterations in CDR loop folding. Moreover, sdAb residues R28, S35, S36, G40, W58, R64 and R108 were shown to be involved in GWARA binding. These results suggested minocycline and GWARA do not target mutual CDR residues. Although in-silico modelling encompasses a degree of error, based on the in-silico docking models, I indicate each ligand occupies and competes for the same binding pocket within the sdAb.

This work describes the development of a novel minimally immunogenic, minocycline controlled, protein displacement system. This platform has several applications in controlling numerous engineered cellular therapy approach. Such control systems permit increased safety and control of engineered cell therapies.

As mentioned in Chapter 1, current published systems proposed to manage CAR T-cell induced toxicities are centred around (i) selective depletion of CAR T-cells using monoclonal antibodies, (ii) suicide genes to induce apoptosis of CAR T-cells, (iii) use of small molecule drugs such as rapamycin and tetracycline to dimerization/activate two components of a bipartite CAR and 'ON-switch' CAR T-cells or to displace/inactivate two components and 'OFF-switch' CAR T-cells, respectively. These strategies are associated with a host of potential adverse side effects or limitations such as the cost and adverse side effects associated with the use of monoclonal antibodies in the clinic. Eradicating CAR-T cells through apoptosis induction may be very effective at reversing effects of CRS, but the lack of tumour control post intervention remains a threat to patients as well as warrants reinfusion of CAR T-cells which may not be economically viable. Use of small molecules such as rapamycin have been shown to be immunosuppressive and components responsive to tetracycline are bacterial derivatives and therefore concerns over immunogenicity remain. The characteristics of the MinoCAR system such

as the minimally immunogenic nature, the tunability and reversibility of CAR cytotoxicity, the availability, effective tissue penetration and pharmacokinetics of minocycline as well as its inert nature against T-cells, tackle many of the problems facing current technologies and make this OFF-switch system potentially an alternative safe, economical, and progressive control approach for CAR activity in vivo. Using the protein-protein displacement system, Chapter 6 shows the development and optimisation of a minocycline mediated OFF-switch split CAR (MinoCAR) architecture where transient suppression of T cell activity was achieved through displacement of the functional CAR heterodimer via the administration of minocycline (0.1 µM – 10 µM). Structural refinement and optimisation experiments showed the MinoCAR bearing an antigen-binding chain composed of an anti-EGFR sdAb fused to Ig-Kappa and the anti-minocycline sdAb fused to CH1, CD28TM, and a CD28 intracellular co-stimulatory domain expressed with the signalling chain composed of GWARA fused to a CD8STK, CD28TM domain and 4-1BB-CD3ζ endodomain had potent cytotoxic potential and cytokine secretion (IFN-γ and IL-2) against tumour target cells comparable to a conventional monolithic CAR. Additionally, MinoCAR effector function was inhibited and tuned in a dose-dependent and reversible manner. This work has presented evidence of the in vitro remote-controlled user-based regulation of a novel minimally immunogenic OFF-switch split CAR using a cheap, well-tolerated, widely available, non-immunosuppressive, FDA approved drug. Although in vivo characterisation of the MinoCAR was not completed for this thesis, this work has potential to be translated to the clinic which may permit clinicians to precisely control the timing and intensity of the tumour targeted response, thus improving the safety of adoptive T cell therapies.

8.2 Future work

In order to fully assess the cytotoxicity, minocycline-mediated control, treatment efficacy, and safety profile of the CAR generated in this work, I suggest evaluating the efficacy, activation and inhibition of minoCAR in vivo. I propose using NALM6 cells transduced to express EGFR and firefly luciferase to engraft NSG mice. Upon tumour engraftment, cohorts would be treated with either 5×10^6, 1×10^6, 0.5×10^6 NT, EGFR CAR, or MinoCAR T cells in the

presence or absence of minocycline. As previously reported, minocycline dosing for mice will be given at ~16 mg/kg via intraperitoneal route every 24-48 hours.[189] I aim to demonstrate that the MinoCAR functions as well as a conventional monolithic CAR in the absence of minocycline, as well as maintaining the tuneable OFF-switch property which is reversible. Once a suitable CAR T dose had been identified and in vivo control by minocycline confirmed experiments would be carried out to further define the tunability and reversibility of the system. Mice bearing tumour and treated with the MinoCAR would be exposed to increasing amounts of minocycline to determine whether a correlation exists between the level of drug administered and therapeutic efficacy. Additionally, models would be carried out in which suppressive levels of minocycline were administered immediately following CAR T infusion and then subsequently halted to determine if CAR activity is recovered once minocycline is permitted to wash out from the system.

Further models could measure reversibility whereby minocycline is administered once evidence of tumour rejection by the MinoCAR had been observed to ensure active CAR T cells can be switched off. Once evidence of tumour recovery has been noted minocycline treatment would be halted to ascertain recovery of CAR T activity and subsequent suppression of tumour growth.

Investigating the tuning of MinoCAR selectivity to challenging but clinically relevant antigens which are expressed on healthy tissue at low levels will also be significant. Developing in vivo models which investigates whether tumour antigen selectively of the MinoCAR can be tuned down to target only high antigen-expressing tumour tissue whilst preserving a low antigen-expressing healthy tissue will be valuable to the field of CAR T cell therapy. The use of an EGFR targeting sdAb as the antigen-binding moiety was sufficient in the development of a novel OFF-switch CAR structure. The application to targeting other antigens is important, however MinoCAR may be limited to the use of tumour targeting sdAbs. Therefore, generating a panel of dAbs targeting a range of antigens and showing their functional utility as CAR binding domains will be important. Alternatively, chimeric Fab spacers bearing a ScFv

antigen-binding domain fused to constant kappa, instead of a sdAb may also be explored.

As the preservation of the CAR immunological synapse is essential to an optimally functional CAR, where a longer spacer is ideal for membrane-proximal epitopes whilst shorter spacer region is favoured for membrane-distal epitopes. Variations in the chimeric Fab structures such as IgK-scFv will allow optimal epitope distances which differ vastly from EGFR.[106]

In Chapter 7, I describe a proof-of-concept work for the minocycline-mediated secretion of GWARA-tagged IL-12 from previously retained KDEL tagged anti-minocycline sdAb. IL-12 is known to be a highly potent immune stimulant typically produced by dendritic, macrophage and neutrophil cells. Systemic use of IL-12 produces highly toxic responses. The in vitro data presented in Chapter 7 suggests the vast majority of IL-12 in this system to be retained within the ER, however I suggest in vivo testing using a mouse model with a xenograft tumour established to test the function of this system in the context of tumour targeting by a CAR T cell for enhanced efficacy as well as safety. I suggest treating with either conventional CAR alone, CAR constitutively expressing IL-12 or CAR with minocycline induced IL-12 secretion. Additionally, the impact of minocycline dosing on the inducible system will be assessed. I hypothesize that at certain CAR T doses or with certain tumour/antigen combinations mice treated with CAR alone will show suboptimal tumour clearance and no IL-12 detection with or without minocycline dosing. Mice treated with CAR with constitutively expressing IL-12 would be expected to show rapid IL-12 toxicity with or without minocycline dosing. In contrast, mice treated with CAR and the inducible IL-12 system would show suboptimal tumour clearance in the absence of minocycline with low/undetectable levels of IL-12 and toxicity. Low levels of minocycline dosing will improve tumour clearance in the absence of toxicity. Further increasing the dose of minocycline will result in further enhanced tumour clearance however the higher levels of secreted IL-12 may lead to the development of additional toxicity. Therefore, I aim to show in vivo tuneability to achieve therapeutic

concentrations of IL-12 without toxicity, and that IL12 retention is sustained over time in the absence of minocycline.

While this thesis was primarily focused on the development of an OFF-switch CAR. The novel displacement platform described in this thesis has many potential applications in cellular therapies. For example, a 'universal' CAR where the administration of a tumour-specific binder fused to the peptide interacts with the membrane presented anti-minocycline sdAb-spacer-signalling domain to form a functional CAR may also be developed.[402] Thus removing limitations on antigen specificity and increasing flexibility of antigen detection and expanding introduction of binders exhibiting various antigen binding kinetics.

Moreover, the system described here may not be suitable for intracellular applications due to the use of cysteine-constrained peptides. In mammalian cells, disulphide bond formation between cysteine residues takes place during the folding of peptides entering the secretory pathway (ER lumen) through the process of covalent linkage catalysed by the protein disulphide isomerase family of enzymes. To drive disulphide bond formation, protein disulphide isomerase enzymes must be oxidized. However, these enzymes can be reduced by thiol glutathione, which is significantly more oxidised within the lumen of the ER than in the cytosol. As a result of reducing cytosolic environment, correct disulphide bonds do not form within the cytosol.

Therefore, re-engineering the peptide component for intracellular based applications may be provide further applications to explore. I suggest carrying this out by excluding the cysteine residues and grafting the GWARA peptide sequence to a bundle of two coiled coil protein pair (α-helices) in an antiparallel relative orientation,[403] using novel linear peptides, or via the generation of novel displaceable sdAbs. If successful, intracellular applications can be explored.

Additionally, Minocycline-controlled secretion of a therapeutic protein payload through the displacement of E1-E2-E3 enzyme complex and thus prevention of poly-ubiquitination and proteasomal degradation can also be explored.

Poly-ubiquitination of proteins results in proteasomal degradation through the attachment of the highly conserved protein Ubiquitin (Ub), to lysine residues on targeted proteins. This process is catalysed through the concerted actions the enzyme ubiquitin thioester cascade, specifically the E1 ubiquitin-activating enzyme, E2 ubiquitin-conjugating enzyme and E3 ubiquitin-protein ligases. E3 specifically binds to the substrate protein and determines specificity of ubiquitination. The formation of the polyubiquitin chain through successive ubiquitination is recognised by the 26S proteasome resulting in protein degradation. By linking the anti-minocycline sdAb to a therapeutic molecule such as IL-12 and the intracellular peptide to the E3 enzyme, the proteasomal degradation pathway may be hijacked to selectively degrade post-translational proteins through the simultaneous binding of a therapeutic protein and the E3 ligase. I suggest, liberation of the therapeutic protein from the E1-E2-E3 enzyme through minocycline mediated displacement prevents proteolysis, thus allowing for the remote-controlled secretion of a therapeutic protein.

9 REFERENCES

1. Kantha, S. S. A centennial review; the 1890 tetanus antitoxin paper of von Behring and Kitasato and the related developments. *Keio J Med* **40**, 35–39 (1991).

2. Walker, J. A. & McKenzie, A. N. J. TH2 cell development and function. *Nat Rev Immunol* **18**, 121–133 (2018).

3. Mauri, C. & Bosma, A. Immune Regulatory Function of B Cells. *Annual Review of Immunology* **30**, 221–241 (2012).

4. Forthal, D. N. Functions of Antibodies. *Microbiol Spectr* **2**, 1–17 (2014).

5. Cohen, S. & Milstein, C. Structure of Antibody Molecules. *Nature* **214**, 449–452 (1967).

6. Charles A Janeway, J., Travers, P., Walport, M. & Shlomchik, M. J. The structure of a typical antibody molecule. *Immunobiology: The Immune System in Health and Disease. 5th edition* (2001).

7. Chiu, M. L., Goulet, D. R., Teplyakov, A. & Gilliland, G. L. Antibody Structure and Function: The Basis for Engineering Therapeutics. *Antibodies (Basel)* **8**, (2019).

8. Nagae, M. & Yamaguchi, Y. Function and 3D Structure of the N-Glycans on Glycoproteins. *International Journal of Molecular Sciences* **13**, 8398–8429 (2012).

9. Mimoto, F., Kuramochi, T., Katada, H., Igawa, T. & Hattori, K. Fc Engineering to Improve the Function of Therapeutic Antibodies. *Curr Pharm Biotechnol* **17**, 1298–1314 (2016).

10. Chothia, C. & Lesk, A. M. Canonical structures for the hypervariable regions of immunoglobulins. *J Mol Biol* **196**, 901–917 (1987).

11.   Padlan, E. A. Anatomy of the antibody molecule. *Mol Immunol* **31**, 169–217 (1994).

12.   Almagro, J. C. Identification of differences in the specificity-determining residues of antibodies that recognize antigens of different size: implications for the rational design of antibody repertoires. *Journal of Molecular Recognition* **17**, 132–143 (2004).

13.   Kabat, E. A., Wu, T. T., Perry, H. M., Foeller, C. & Gottesman, K. S. *Sequences of Proteins of Immunological Interest*. (DIANE Publishing, 1992).

14.   Johnson, G. & Wu, T. T. Kabat Database and its applications: 30 years after the first variability plot. *Nucleic Acids Res* **28**, 214–218 (2000).

15.   Collis, A. V. J., Brouwer, A. P. & Martin, A. C. R. Analysis of the Antigen Combining Site: Correlations Between Length and Sequence Composition of the Hypervariable Loops and the Nature of the Antigen. *Journal of Molecular Biology* **325**, 337–354 (2003).

16.   Charles A Janeway, J., Travers, P., Walport, M. & Shlomchik, M. J. The interaction of the antibody molecule with specific antigen. *Immunobiology: The Immune System in Health and Disease. 5th edition* (2001).

17.   Raghunathan, G., Smart, J., Williams, J. & Almagro, J. C. Antigen-binding site anatomy and somatic mutations in antibodies that recognize different types of antigens. *Journal of Molecular Recognition* **25**, 103–113 (2012).

18.   Persson, H., Lantto, J. & Ohlin, M. A focused antibody library for improved hapten recognition. *J Mol Biol* **357**, 607–620 (2006).

19.   Cobaugh, C. W., Almagro, J. C., Pogson, M., Iverson, B. & Georgiou, G. Synthetic antibody libraries focused towards peptide ligands. *J Mol Biol* **378**, 622–633 (2008).

20.   Almagro, J. C. *et al.* Design and validation of a synthetic VH repertoire with tailored diversity for protein recognition. *J Mol Recognit* **19**, 413–422 (2006).

21.   Heyman, B. & Shulman, M. J. Structure, Function, and Production of Immunoglobulin M (IgM). in *Encyclopedia of Immunobiology* (ed. Ratcliffe, M. J. H.) 1–14 (Academic Press, 2016). doi:10.1016/B978-0-12-374279-7.05001-3.

22.   Chi, X., Li, Y. & Qiu, X. V(D)J recombination, somatic hypermutation and class switch recombination of immunoglobulins: mechanism and regulation. *Immunology* **160**, 233–247 (2020).

23.   Gutzeit, C., Chen, K. & Cerutti, A. The enigmatic function of IgD: some answers at last. *European Journal of Immunology* **48**, 1101–1113 (2018).

24.   Vidarsson, G., Dekkers, G. & Rispens, T. IgG Subclasses and Allotypes: From Structure to Effector Functions. *Frontiers in Immunology* **5**, 520 (2014).

25.   Köhler, G. & Milstein, C. Continuous cultures of fused cells secreting antibody of predefined specificity. *Nature* **256**, 495–497 (1975).

26.   Garcia-Campayo, V., Kumar, T. R. & Boime, I. Thyrotropin, Follitropin, and Chorionic Gonadotropin Expressed as a Single Multifunctional Unit Reveal Remarkable Permissiveness in Receptor-Ligand Interactions. *Endocrinology* **143**, 3773–3778 (2002).

27.   Chow, S. N., Ouyang, P. C., Chu, C. T. & Lee, C. Y. Rapid and simple immunoassays for measurement of human chorionic gonadotropin using monoclonal antibodies. *J Formos Med Assoc* **89**, 792–798 (1990).

28.   Chiswick, E. L., Duffy, E., Japp, B. & Remick, D. Detection and Quantification of Cytokines and Other Biomarkers. *Methods Mol Biol* **844**, 15–30 (2012).

29.   Sgouros, G., Bodei, L., McDevitt, M. R. & Nedrow, J. R. Radiopharmaceutical therapy in cancer: clinical advances and challenges. *Nat Rev Drug Discov* **19**, 589–608 (2020).

30.   Holliger, P. & Hudson, P. J. Engineered antibody fragments and the rise of single domains. *Nat Biotechnol* **23**, 1126–1136 (2005).

31.   Cattaneo, A. & Biocca, S. The selection of intracellular antibodies. *Trends in Biotechnology* **17**, 115–121 (1999).

32.   Ward, E. S., Güssow, D., Griffiths, A. D., Jones, P. T. & Winter, G. Binding activities of a repertoire of single immunoglobulin variable domains secreted from Escherichia coli. *Nature* **341**, 544–546 (1989).

33.   Sanz, L., Cuesta, Á. M., Compte, M. & Álvarez-Vallina, L. Antibody engineering: facing new challenges in cancer therapy. *Acta Pharmacologica Sinica* **26**, 641–648 (2005).

34.   Kim, J., Hayton, W. L., Robinson, J. M. & Anderson, C. L. Kinetics of FcRn-mediated recycling of IgG and albumin in human: Pathophysiology and therapeutic implications using a simplified mechanism-based model. *Clin Immunol* **122**, 146–155 (2007).

35.   Wang, T. & Duan, Y. Probing the stability-limiting regions of an antibody single-chain variable fragment: a molecular dynamics simulation study. *Protein Eng Des Sel* **24**, 649–657 (2011).

36.   Rau, R. Adalimumab (a fully human anti-tumour necrosis factor α monoclonal antibody) in the treatment of active rheumatoid arthritis: the initial results of five trials. *Ann Rheum Dis* **61**, ii70–ii73 (2002).

37.   Szardenings, M. Phage display of random peptide libraries: applications, limits, and potential. *J Recept Signal Transduct Res* **23**, 307–349 (2003).

38.   McCafferty, J., Griffiths, A. D., Winter, G. & Chiswell, D. J. Phage antibodies: filamentous phage displaying antibody variable domains. *Nature* **348**, 552–554 (1990).

39.   Bradbury, A. R. M., Sidhu, S., Dübel, S. & McCafferty, J. Beyond natural antibodies: the power of in vitro display technologies. *Nat Biotechnol* **29**, 245–254 (2011).

40.   Smith, G. P. Filamentous fusion phage: novel expression vectors that display cloned antigens on the virion surface. *Science* **228**, 1315–1317 (1985).

41.   Winter, G. & Milstein, C. Man-made antibodies. *Nature* **349**, 293–299 (1991).

42.   Barderas, R. & Benito-Peña, E. The 2018 Nobel Prize in Chemistry: phage display of peptides and antibodies. *Anal Bioanal Chem* **411**, 2475–2479 (2019).

43.   Breitling, F., Dübel, S., Seehaus, T., Klewinghaus, I. & Little, M. A surface expression vector for antibody screening. *Gene* **104**, 147–153 (1991).

44.   Sidhu, S. S. Engineering M13 for phage display. *Biomol Eng* **18**, 57–63 (2001).

45.   Barbas, C. F., Kang, A. S., Lerner, R. A. & Benkovic, S. J. Assembly of combinatorial antibody libraries on phage surfaces: the gene III site. *Proc Natl Acad Sci U S A* **88**, 7978–7982 (1991).

46.   Galán, A. *et al.* Library-based display technologies: where do we stand? *Mol. BioSyst.* **12**, 2342–2358 (2016).

47.   Mazor, Y., Van Blarcom, T., Mabry, R., Iverson, B. L. & Georgiou, G. Isolation of engineered, full-length antibodies from libraries expressed in Escherichia coli. *Nat Biotechnol* **25**, 563–565 (2007).

48.   Clackson, T., Hoogenboom, H. R., Griffiths, A. D. & Winter, G. Making antibody fragments using phage display libraries. *Nature* **352**, 624–628 (1991).

49.   Pini, A. *et al.* Design and Use of a Phage Display Library. *Journal of Biological Chemistry* **273**, 21769–21776 (1998).

50.   Knappik, A. *et al.* Fully synthetic human combinatorial antibody libraries (HuCAL) based on modular consensus frameworks and CDRs randomized with trinucleotides. *J Mol Biol* **296**, 57–86 (2000).

51.   Willats, W. G. T. Phage display: practicalities and prospects. *Plant Mol Biol* **50**, 837–854 (2002).

52. Alexander, A. *et al.* gamma Heavy chain disease in man: cDNA sequence supports partial gene deletion model. *Proc Natl Acad Sci U S A* **79**, 3260–3264 (1982).

53. Hamers-Casterman, C. *et al.* Naturally occurring antibodies devoid of light chains. *Nature* **363**, 446–448 (1993).

54. Greenberg, A. S. *et al.* A new antigen receptor gene family that undergoes rearrangement and extensive somatic diversification in sharks. *Nature* **374**, 168–173 (1995).

55. Nguyen, V. K., Su, C., Muyldermans, S. & van der Loo, W. Heavy-chain antibodies in Camelidae; a case of evolutionary innovation. *Immunogenetics* **54**, 39–47 (2002).

56. Flajnik, M. F., Deschacht, N. & Muyldermans, S. A Case Of Convergence: Why Did a Simple Alternative to Canonical Antibodies Arise in Sharks and Camels? *PLoS Biol* **9**, e1001120 (2011).

57. Muyldermans, S., Cambillau, C. & Wyns, L. Recognition of antigens by single-domain antibody fragments: the superfluous luxury of paired domains. *Trends Biochem Sci* **26**, 230–235 (2001).

58. Woolven, B. P., Frenken, L. G., van der Logt, P. & Nicholls, P. J. The structure of the llama heavy chain constant genes reveals a mechanism for heavy-chain antibody formation. *Immunogenetics* **50**, 98–101 (1999).

59. Nguyen, V. K., Hamers, R., Wyns, L. & Muyldermans, S. Loss of splice consensus signal is responsible for the removal of the entire C(H)1 domain of the functional camel IGG2A heavy-chain antibodies. *Mol Immunol* **36**, 515–524 (1999).

60.   Lee, Y.-K., Brewer, J. W., Hellman, R. & Hendershot, L. M. BiP and Immunoglobulin Light Chain Cooperate to Control the Folding of Heavy Chain and Ensure the Fidelity of Immunoglobulin Assembly. *Mol Biol Cell* **10**, 2209–2219 (1999).

61.   Vu, K. B., Ghahroudi, M. A., Wyns, L. & Muyldermans, S. Comparison of llama VH sequences from conventional and heavy chain antibodies. *Molecular Immunology* **34**, 1121–1131 (1997).

62.   Gonzalez-Sapienza, G., Rossotti, M. A. & Tabares-da Rosa, S. Single-Domain Antibodies As Versatile Affinity Reagents for Analytical and Diagnostic Applications. *Frontiers in Immunology* **8**, 977 (2017).

63.   Harmsen, M. M. *et al.* Llama heavy-chain V regions consist of at least four distinct subfamilies revealing novel sequence features. *Molecular Immunology* **37**, 579–590 (2000).

64.   Conrath, K. E., Wernery, U., Muyldermans, S. & Nguyen, V. K. Emergence and evolution of functional heavy-chain antibodies in Camelidae. *Dev Comp Immunol* **27**, 87–103 (2003).

65.   Muyldermans, S., Atarhouch, T., Saldanha, J., Barbosa, J. A. R. G. & Hamers, R. Sequence and structure of VH domain from naturally occurring camel heavy chain immunoglobulins lacking light chains. *Protein Engineering, Design and Selection* **7**, 1129–1135 (1994).

66.   Desmyter, A. *et al.* Crystal structure of a camel single- domain VH antibody fragment in complex with lysozyme. **3**, 9 (1996).

67.   Spinelli, S. *et al.* Camelid heavy-chain variable domains provide efficient combining sites to haptens. *Biochemistry* **39**, 1217–1222 (2000).

68. Desmyter, A. *et al.* Crystal structure of a camel single-domain VH antibody fragment in complex with lysozyme. *Nat Struct Biol* **3**, 803–811 (1996).

69. Hozumi, N. & Tonegawa, S. Evidence for somatic rearrangement of immunoglobulin genes coding for variable and constant regions. *PNAS* **73**, 3628–3632 (1976).

70. Matsuda, F. *et al.* The complete nucleotide sequence of the human immunoglobulin heavy chain variable region locus. *J Exp Med* **188**, 2151–2162 (1998).

71. Desiderio, S. V. *et al.* Insertion of N regions into heavy-chain genes is correlated with expression of terminal deoxytransferase in B cells. *Nature* **311**, 752–755 (1984).

72. Nguyen, V. K., Hamers, R., Wyns, L. & Muyldermans, S. Camel heavy-chain antibodies: diverse germline VHH and specific mechanisms enlarge the antigen-binding repertoire. *EMBO J* **19**, 921–930 (2000).

73. Perchiacca, J. M., Bhattacharya, M. & Tessier, P. M. Mutational analysis of domain antibodies reveals aggregation hotspots within and near the complementarity determining regions. *Proteins: Structure, Function, and Bioinformatics* **79**, 2637–2647 (2011).

74. Rajewsky, K., Förster, I. & Cumano, A. Evolutionary and somatic selection of the antibody repertoire in the mouse. *Science* **238**, 1088–1094 (1987).

75. Verheesen, P. *et al.* Reliable and controllable antibody fragment selections from Camelid non-immune libraries for target validation. *Biochim Biophys Acta* **1764**, 1307–1319 (2006).

76.   van der Linden, R. H. J., de Geus, B., Frenken, L. G. J., Peters, H. & Verrips, C. T. Improved production and function of llama heavy chain antibody fragments by molecular evolution. *Journal of Biotechnology* **80**, 261–270 (2000).

77.   Muyldermans, S. & Lauwereys, M. Unique single-domain antigen binding fragments derived from naturally occurring camel heavy-chain antibodies. *J Mol Recognit* **12**, 131–140 (1999).

78.   Wiemann, B. & Starnes, C. O. Coley's toxins, tumor necrosis factor and cancer research: a historical perspective. *Pharmacol. Ther.* **64**, 529–564 (1994).

79.   McCarthy, E. F. The Toxins of William B. Coley and the Treatment of Bone and Soft-Tissue Sarcomas. *Iowa Orthop J* **26**, 154–158 (2006).

80.   Lizée, G. *et al.* Harnessing the power of the immune system to target cancer. *Annu Rev Med* **64**, 71–90 (2013).

81.   Chen, D. S. & Mellman, I. Oncology meets immunology: the cancer-immunity cycle. *Immunity* **39**, 1–10 (2013).

82.   Riechmann, L., Clark, M., Waldmann, H. & Winter, G. Reshaping human antibodies for therapy. *Nature* **332**, 323–327 (1988).

83.   Saxena, M., van der Burg, S. H., Melief, C. J. M. & Bhardwaj, N. Therapeutic cancer vaccines. *Nat Rev Cancer* **21**, 360–378 (2021).

84.   Kantoff, P. W. *et al.* Sipuleucel-T immunotherapy for castration-resistant prostate cancer. *N Engl J Med* **363**, 411–422 (2010).

85.   Russell, S. J., Peng, K.-W. & Bell, J. C. Oncolytic virotherapy. *Nat Biotechnol* **30**, 658–670 (2012).

86.   Abbott, M. & Ustoyev, Y. Cancer and the Immune System: The History and Background of Immunotherapy. *Semin Oncol Nurs* **35**, 150923 (2019).

87.   Schwaber, J. & Cohen, E. P. Human x mouse somatic cell hybrid clone secreting immunoglobulins of both parental types. *Nature* **244**, 444–447 (1973).

88.   Nadler, L. M. *et al.* Serotherapy of a patient with a monoclonal antibody directed against a human lymphoma-associated antigen. *Cancer Res* **40**, 3147–3154 (1980).

89.   Ribatti, D. From the discovery of monoclonal antibodies to their therapeutic application: an historical reappraisal. *Immunol Lett* **161**, 96–99 (2014).

90.   Smith, M. R. Rituximab (monoclonal anti-CD20 antibody): mechanisms of action and resistance. *Oncogene* **22**, 7359–7368 (2003).

91.   Leach, D. R., Krummel, M. F. & Allison, J. P. Enhancement of antitumor immunity by CTLA-4 blockade. *Science* **271**, 1734–1736 (1996).

92.   Esensten, J. H., Helou, Y. A., Chopra, G., Weiss, A. & Bluestone, J. A. CD28 Costimulation: From Mechanism to Therapy. *Immunity* **44**, 973–988 (2016).

93.   Graziani, G., Tentori, L. & Navarra, P. Ipilimumab: a novel immunostimulatory monoclonal antibody for the treatment of cancer. *Pharmacol Res* **65**, 9–22 (2012).

94.   Dudley, M. E. & Rosenberg, S. A. Adoptive-cell-transfer therapy for the treatment of patients with cancer. *Nat Rev Cancer* **3**, 666–675 (2003).

95.   Gross, G., Waks, T. & Eshhar, Z. Expression of immunoglobulin-T-cell receptor chimeric molecules as functional receptors with antibody-type specificity. *Proc Natl Acad Sci U S A* **86**, 10024–10028 (1989).

96.   Eshhar, Z., Waks, T., Gross, G. & Schindler, D. G. Specific activation and targeting of cytotoxic lymphocytes through chimeric single chains consisting of antibody-binding domains and the gamma or zeta subunits of the immunoglobulin and T-cell receptors. *Proceedings of the National Academy of Sciences of the United States of America* **90**, 720–724 (1993).

97.   Gill, S. & June, C. H. Going viral: chimeric antigen receptor T-cell therapy for hematological malignancies. *Immunological Reviews* **263**, 68–89 (2015).

98.   Chmielewski, M., Hombach, A., Heuser, C., Adams, G. P. & Abken, H. T Cell Activation by Antibody-Like Immunoreceptors: Increase in Affinity of the Single-Chain Fragment Domain above Threshold Does Not Increase T Cell Activation against Antigen-Positive Target Cells but Decreases Selectivity. *The Journal of Immunology* **173**, 7647–7653 (2004).

99.   Caruso, H. G. *et al.* Tuning Sensitivity of CAR to EGFR Density Limits Recognition of Normal Tissue While Maintaining Potent Antitumor Activity. *Cancer Res* **75**, 3505–3518 (2015).

100.   Ghorashian, S. *et al.* Enhanced CAR T cell expansion and prolonged persistence in pediatric patients with ALL treated with a low-affinity CD19 CAR. *Nature Medicine* **25**, 1408–1414 (2019).

101.   Eshhar, Z. The T-body approach: redirecting T cells with antibody specificity. *Handb Exp Pharmacol* 329–342 (2008) doi:10.1007/978-3-540-73259-4_14.

102. Faitschuk, E., Nagy, V., Hombach, A. A. & Abken, H. A dual chain chimeric antigen receptor (CAR) in the native antibody format for targeting immune cells towards cancer cells without the need of an scFv. *Gene Ther.* **23**, 718–726 (2016).

103. Rahbarizadeh, F., Ahmadvand, D. & Moghimi, S. M. CAR T-cell bioengineering: Single variable domain of heavy chain antibody targeted CARs. *Adv. Drug Deliv. Rev.* **141**, 41–46 (2019).

104. Wilkie, S. *et al.* Retargeting of human T cells to tumor-associated MUC1: the evolution of a chimeric antigen receptor. *J. Immunol.* **180**, 4901–4909 (2008).

105. Guest, R. D. *et al.* The Role of Extracellular Spacer Regions in the Optimal Design of Chimeric Immune Receptors: Evaluation of Four Different scFvs and Antigens. *Journal of Immunotherapy* **28**, 203–211 (2005).

106. Guest, R. D. *et al.* The role of extracellular spacer regions in the optimal design of chimeric immune receptors: evaluation of four different scFvs and antigens. *J. Immunother.* **28**, 203–211 (2005).

107. Majzner, R. G. *et al.* Tuning the Antigen Density Requirement for CAR T-cell Activity. *Cancer Discov* **10**, 702–723 (2020).

108. Irving, B. A. & Weiss, A. The cytoplasmic domain of the T cell receptor zeta chain is sufficient to couple to receptor-associated signal transduction pathways. *Cell* **64**, 891–901 (1991).

109. Chmielewski, M., Rappl, G., Hombach, A. A. & Abken, H. T cells redirected by a CD3ζ chimeric antigen receptor can establish self-antigen-specific tumour protection in the long term. *Gene Therapy* **20**, 177–186 (2013).

110. Brocker, T. & Karjalainen, K. Signals through T cell receptor-zeta chain alone are insufficient to prime resting T lymphocytes. *J Exp Med* **181**, 1653–1659 (1995).

111. Curran, K. J., Pegram, H. J. & Brentjens, R. J. Chimeric antigen receptors for T cell immunotherapy: current understanding and future directions. *The Journal of Gene Medicine* **14**, 405–415 (2012).

112. Harding, F. A., McArthur, J. G., Gross, J. A., Raulet, D. H. & Allison, J. P. CD28-mediated signalling co-stimulates murine T cells and prevents induction of anergy in T-cell clones. *Nature* **356**, 607–609 (1992).

113. Lenschow, D. J., Walunas, T. L. & Bluestone, J. A. CD28/B7 system of T cell costimulation. *Annu. Rev. Immunol.* **14**, 233–258 (1996).

114. Lamers, C. H. J. *et al.* Gene-modified T cells for adoptive immunotherapy of renal cell cancer maintain transgene-specific immune functions in vivo. *Cancer Immunol Immunother* **56**, 1875–1883 (2007).

115. Park, J. R. *et al.* Adoptive transfer of chimeric antigen receptor re-directed cytolytic T lymphocyte clones in patients with neuroblastoma. *Mol. Ther.* **15**, 825–833 (2007).

116. Kershaw, M. H. *et al.* A phase I study on adoptive immunotherapy using gene-modified T cells for ovarian cancer. *Clin. Cancer Res.* **12**, 6106–6115 (2006).

117. Pule, M. A. *et al.* Virus-specific T cells engineered to coexpress tumor-specific receptors: persistence and antitumor activity in individuals with neuroblastoma. *Nat Med* **14**, 1264–1270 (2008).

118. Lanzavecchia, A. Antigen-specific interaction between T and B cells. *Nature* **314**, 537–539 (1985).

119. Diehn, M. *et al.* Genomic expression programs and the integration of the CD28 costimulatory signal in T cell activation. *PNAS* **99**, 11796–11801 (2002).

120. June, C. H., Ledbetter, J. A., Gillespie, M. M., Lindsten, T. & Thompson, C. B. T-cell proliferation involving the CD28 pathway is associated with cyclosporine-resistant interleukin 2 gene expression. *Mol Cell Biol* **7**, 4472–4481 (1987).

121. Boonen, G. J. *et al.* CD28 induces cell cycle progression by IL-2-independent down-regulation of p27kip1 expression in human peripheral T lymphocytes. *Eur. J. Immunol.* **29**, 789–798 (1999).

122. Radvanyi, L. G. *et al.* CD28 costimulation inhibits TCR-induced apoptosis during a primary T cell response. *The Journal of Immunology* **156**, 1788–1798 (1996).

123. Harding, F. A., McArthur, J. G., Gross, J. A., Raulet, D. H. & Allison, J. P. CD28-mediated signalling co-stimulates murine T cells and prevents induction of anergy in T-cell clones. *Nature* **356**, 607–609 (1992).

124. Maher, J., Brentjens, R. J., Gunset, G., Rivière, I. & Sadelain, M. Human T-lymphocyte cytotoxicity and proliferation directed by a single chimeric TCRzeta /CD28 receptor. *Nat. Biotechnol.* **20**, 70–75 (2002).

125. Maher, J., Brentjens, R. J., Gunset, G., Rivière, I. & Sadelain, M. Human T-lymphocyte cytotoxicity and proliferation directed by a single chimeric TCRζ /CD28 receptor. *Nature Biotechnology* **20**, 70–75 (2002).

126. Brentjens, R. *et al.* CD19-targeted T cells rapidly induce molecular remissions in adults with chemotherapy-refractory acute lymphoblastic leukemia. *Sci Transl Med* **5**, 177ra38 (2013).

127. Kopf, M. *et al.* OX40-deficient mice are defective in Th cell proliferation but are competent in generating B cell and CTL Responses after virus infection. *Immunity* **11**, 699–708 (1999).

128. Croft, M. Costimulation of T cells by OX40, 4-1BB, and CD27. *Cytokine & Growth Factor Reviews* **14**, 265–273 (2003).

129. Hauer, J. *et al.* TNF receptor (TNFR)-associated factor (TRAF) 3 serves as an inhibitor of TRAF2/5-mediated activation of the noncanonical NF-kappaB pathway by TRAF-binding TNFRs. *Proc. Natl. Acad. Sci. U.S.A.* **102**, 2874–2879 (2005).

130. Sabbagh, L., Pulle, G., Liu, Y., Tsitsikov, E. N. & Watts, T. H. ERK-dependent Bim modulation downstream of the 4-1BB-TRAF1 signaling axis is a critical mediator of CD8 T cell survival in vivo. *J. Immunol.* **180**, 8093–8101 (2008).

131. Cannons, J. L., Choi, Y. & Watts, T. H. Role of TNF Receptor-Associated Factor 2 and p38 Mitogen-Activated Protein Kinase Activation During 4-1BB-Dependent Immune Response. *The Journal of Immunology* **165**, 6193–6204 (2000).

132. Barsoumian, H. B., Yolcu, E. S. & Shirwan, H. 4-1BB Signaling in Conventional T Cells Drives IL-2 Production That Overcomes CD4+CD25+FoxP3+ T Regulatory Cell Suppression. *PLoS One* **11**, (2016).

133. Porter, D. L., Levine, B. L., Kalos, M., Bagg, A. & June, C. H. Chimeric Antigen Receptor–Modified T Cells in Chronic Lymphoid Leukemia. *New England Journal of Medicine* **365**, 725–733 (2011).

134.   June, C. H., O'Connor, R. S., Kawalekar, O. U., Ghassemi, S. & Milone, M. C. CAR T cell immunotherapy for human cancer. *Science* **359**, 1361–1365 (2018).

135.   Carpenito, C. *et al.* Control of large, established tumor xenografts with genetically retargeted human T cells containing CD28 and CD137 domains. *Proc Natl Acad Sci U S A* **106**, 3360–3365 (2009).

136.   Zhong, X.-S., Matsushita, M., Plotkin, J., Riviere, I. & Sadelain, M. Chimeric antigen receptors combining 4-1BB and CD28 signaling domains augment PI3kinase/AKT/Bcl-XL activation and CD8+ T cell-mediated tumor eradication. *Mol. Ther.* **18**, 413–420 (2010).

137.   Pulè, M. A. *et al.* A chimeric T cell antigen receptor that augments cytokine release and supports clonal expansion of primary human T cells. *Molecular Therapy* **12**, 933–941 (2005).

138.   Chmielewski, M. & Abken, H. TRUCKs: the fourth generation of CARs. *Expert Opin Biol Ther* **15**, 1145–1154 (2015).

139.   Veillette, A., Bookman, M. A., Horak, E. M. & Bolen, J. B. The CD4 and CD8 T cell surface antigens are associated with the internal membrane tyrosine-protein kinase p56lck. *Cell* **55**, 301–308 (1988).

140.   Rudd, C. E., Trevillyan, J. M., Dasgupta, J. D., Wong, L. L. & Schlossman, S. F. The CD4 receptor is complexed in detergent lysates to a protein-tyrosine kinase (pp58) from human T lymphocytes. *PNAS* **85**, 5190–5194 (1988).

141.   Nika, K. *et al.* Constitutively active Lck kinase in T cells drives antigen receptor signal transduction. *Immunity* **32**, 766–777 (2010).

142. Casas, J. *et al.* Ligand-engaged TCR is triggered by Lck not associated with CD8 coreceptor. *Nat Commun* **5**, 5624 (2014).

143. Chan, A. C., Iwashima, M., Turck, C. W. & Weiss, A. ZAP-70: a 70 kd protein-tyrosine kinase that associates with the TCR zeta chain. *Cell* **71**, 649–662 (1992).

144. Wange, R. L. LAT, the linker for activation of T cells: a bridge between T cell-specific and general signaling pathways. *Sci. STKE* **2000**, re1 (2000).

145. Courtney, A. H., Lo, W.-L. & Weiss, A. TCR Signaling: Mechanisms of Initiation and Propagation. *Trends in Biochemical Sciences* **43**, 108–123 (2018).

146. Maude, S. L. *et al.* Tisagenlecleucel in Children and Young Adults with B-Cell Lymphoblastic Leukemia. *N. Engl. J. Med.* **378**, 439–448 (2018).

147. Maude, S. L. *et al.* Tisagenlecleucel in Children and Young Adults with B-Cell Lymphoblastic Leukemia. *New England Journal of Medicine* **378**, 439–448 (2018).

148. Schuster, S. J. *et al.* Tisagenlecleucel in Adult Relapsed or Refractory Diffuse Large B-Cell Lymphoma. *New England Journal of Medicine* **380**, 45–56 (2019).

149. Neelapu, S. S. *et al.* Axicabtagene Ciloleucel CAR T-Cell Therapy in Refractory Large B-Cell Lymphoma. *N. Engl. J. Med.* **377**, 2531–2544 (2017).

150. Abramson, J. S. *et al.* Lisocabtagene maraleucel for patients with relapsed or refractory large B-cell lymphomas (TRANSCEND NHL 001): a multicentre seamless design study. *The Lancet* **396**, 839–852 (2020).

151. Lee, D. W. *et al.* Current concepts in the diagnosis and management of cytokine release syndrome. *Blood* **124**, 188–195 (2014).

152. Teachey, D. T. *et al.* Identification of Predictive Biomarkers for Cytokine Release Syndrome after Chimeric Antigen Receptor T-cell Therapy for Acute Lymphoblastic Leukemia. *Cancer Discov* **6**, 664–679 (2016).

153. Lee, D. W. *et al.* Current concepts in the diagnosis and management of cytokine release syndrome. *Blood* **124**, 188–195 (2014).

154. Porter, D. L. *et al.* Chimeric antigen receptor T cells persist and induce sustained remissions in relapsed refractory chronic lymphocytic leukemia. *Sci Transl Med* **7**, 303ra139 (2015).

155. Maude, S. L. *et al.* Chimeric Antigen Receptor T Cells for Sustained Remissions in Leukemia. *N Engl J Med* **371**, 1507–1517 (2014).

156. Davila, M. L. *et al.* Efficacy and toxicity management of 19-28z CAR T cell therapy in B cell acute lymphoblastic leukemia. *Sci Transl Med* **6**, 224ra25 (2014).

157. Lee, D. W. *et al.* T cells expressing CD19 chimeric antigen receptors for acute lymphoblastic leukaemia in children and young adults: a phase 1 dose-escalation trial. *The Lancet* **385**, 517–528 (2015).

158. Maude, S. L. *et al.* Chimeric Antigen Receptor T Cells for Sustained Remissions in Leukemia. *New England Journal of Medicine* **371**, 1507–1517 (2014).

159. Neelapu, S. S. *et al.* Chimeric antigen receptor T-cell therapy - assessment and management of toxicities. *Nat Rev Clin Oncol* **15**, 47–62 (2018).

160. Turtle, C. J. *et al.* CD19 CAR-T cells of defined CD4+:CD8+ composition in adult B cell ALL patients. *J. Clin. Invest.* **126**, 2123–2138 (2016).

161. Buie, L. W., Pecoraro, J. J., Horvat, T. Z. & Daley, R. J. Blinatumomab: A First-in-Class Bispecific T-Cell Engager for Precursor B-Cell Acute Lymphoblastic Leukemia. *Ann Pharmacother* **49**, 1057–1067 (2015).

162. Topp, M. S. *et al.* Phase II trial of the anti-CD19 bispecific T cell-engager blinatumomab shows hematologic and molecular remissions in patients with relapsed or refractory B-precursor acute lymphoblastic leukemia. *Journal of Clinical Oncology* **32**, 4134–4140 (2014).

163. Mitchell, C. D. *et al.* Benefit of dexamethasone compared with prednisolone for childhood acute lymphoblastic leukaemia: results of the UK Medical Research Council ALL97 randomized trial. *British Journal of Haematology* **129**, 734–745 (2005).

164. Weber, E. W. *et al.* Pharmacologic control of CAR-T cell function using dasatinib. *Blood Adv* **3**, 711–717 (2019).

165. Tokarski, J. S. *et al.* The Structure of Dasatinib (BMS-354825) Bound to Activated ABL Kinase Domain Elucidates Its Inhibitory Activity against Imatinib-Resistant ABL Mutants. *Cancer Res* **66**, 5790–5797 (2006).

166. Mestermann, K. *et al.* The tyrosine kinase inhibitor dasatinib acts as a pharmacologic on/off switch for CAR T cells. *Science Translational Medicine* **11**, (2019).

167. Chiang, C. L.-L., Benencia, F. & Coukos, G. Whole tumor antigen vaccines. *Semin Immunol* **22**, 132–143 (2010).

168. Rowley, J. D. A New Consistent Chromosomal Abnormality in Chronic Myelogenous Leukaemia identified by Quinacrine Fluorescence and Giemsa Staining. *Nature* **243**, 290–293 (1973).

169. Li, P. *et al.* Elevated serum alpha fetoprotein levels promote pathological progression of hepatocellular carcinoma. *World J Gastroenterol* **17**, 4563–4571 (2011).

170. Cheng, Y.-H., Wong, E. W. & Cheng, C. Y. Cancer/testis (CT) antigens, carcinogenesis and spermatogenesis. *Spermatogenesis* **1**, 209–220 (2011).

171. Morgan, R. A. *et al.* Case Report of a Serious Adverse Event Following the Administration of T Cells Transduced With a Chimeric Antigen Receptor Recognizing ERBB2. *Mol Ther* **18**, 843–851 (2010).

172. Lamers, C. H. J. *et al.* Treatment of Metastatic Renal Cell Carcinoma With Autologous T-Lymphocytes Genetically Retargeted Against Carbonic Anhydrase IX: First Clinical Experience. *JCO* **24**, e20–e22 (2006).

173. Philip, B. *et al.* A highly compact epitope-based marker/suicide gene for easier and safer T-cell therapy. *Blood* **124**, 1277–1287 (2014).

174. Descotes, J. Immunotoxicity of monoclonal antibodies. *MAbs* **1**, 104–111 (2009).

175. Zhou, X. *et al.* Long-term outcome after haploidentical stem cell transplant and infusion of T cells expressing the inducible caspase 9 safety transgene. *Blood* **123**, 3895–3905 (2014).

176. Di Stasi, A. *et al.* Inducible apoptosis as a safety switch for adoptive cell therapy. *N. Engl. J. Med.* **365**, 1673–1683 (2011).

177. Iuliucci, J. D. *et al.* Intravenous safety and pharmacokinetics of a novel dimerizer drug, AP1903, in healthy volunteers. *J Clin Pharmacol* **41**, 870–879 (2001).

178. Straathof, K. C. *et al.* An inducible caspase 9 safety switch for T-cell therapy. *Blood* **105**, 4247–4254 (2005).

179. Quintarelli, C. *et al.* Co-expression of cytokine and suicide genes to enhance the activity and safety of tumor-specific cytotoxic T lymphocytes. *Blood* **110**, 2793–2802 (2007).

180. Bayle, J. H. *et al.* Rapamycin analogs with differential binding specificity permit orthogonal control of protein activity. *Chem. Biol.* **13**, 99–107 (2006).

181. Choi, J., Chen, J., Schreiber, S. L. & Clardy, J. Structure of the FKBP12-rapamycin complex interacting with the binding domain of human FRAP. *Science* **273**, 239–242 (1996).

182. Leung, W.-H. *et al.* Sensitive and adaptable pharmacological control of CAR T cells through extracellular receptor dimerization. *JCI Insight* **4**,.

183. Wu, C.-Y., Roybal, K. T., Puchner, E. M., Onuffer, J. & Lim, W. A. Remote control of therapeutic T cells through a small molecule-gated chimeric receptor. *Science* **350**, aab4077 (2015).

184. Juillerat, A. *et al.* Design of chimeric antigen receptors with integrated controllable transient functions. *Scientific Reports* **6**, 18950 (2016).

185. Leung, W.-H. *et al.* Sensitive and adaptable pharmacological control of CAR T cells through extracellular receptor dimerization. *JCI Insight* **5**, (2019).

186. Li, J., Kim, S. G. & Blenis, J. Rapamycin: one drug, many effects. *Cell Metab* **19**, 373–379 (2014).

187. Giordano-Attianese, G. *et al.* A computationally designed chimeric antigen receptor provides a small-molecule safety switch for T-cell therapy. *Nat. Biotechnol.* **38**, 426–432 (2020).

188. Sun, C. *et al.* THEMIS-SHP1 Recruitment by 4-1BB Tunes LCK-Mediated Priming of Chimeric Antigen Receptor-Redirected T Cells. *Cancer Cell* **37**, 216-225.e6 (2020).

189. Hotblack, A. *et al.* Tunable control of CAR T cell activity through tetracycline mediated disruption of protein–protein interaction. *Sci Rep* **11**, 21902 (2021).

190. Hoogenboom, H. R. *et al.* Multi-subunit proteins on the surface of filamentous phage: methodologies for displaying antibody (Fab) heavy and light chains. *Nucleic Acids Research* **19**, 4133–4137 (1991).

191. Engler, C., Kandzia, R. & Marillonnet, S. A One Pot, One Step, Precision Cloning Method with High Throughput Capability. *PLOS ONE* **3**, e3647 (2008).

192. Engler, C., Gruetzner, R., Kandzia, R. & Marillonnet, S. Golden Gate Shuffling: A One-Pot DNA Shuffling Method Based on Type IIs Restriction Enzymes. *PLOS ONE* **4**, e5553 (2009).

193. Klarenbeek, A. *et al.* Camelid Ig V genes reveal significant human homology not seen in therapeutic target genes, providing for a powerful therapeutic antibody platform. *MAbs* **7**, 693–706 (2015).

194. Nanobody approval gives domain antibodies a boost. https://www.nature.com/articles/d41573-019-00104-w.

195. Fanning, S. W. & Horn, J. R. An anti-hapten camelid antibody reveals a cryptic binding site with significant energetic contributions from a nonhypervariable loop. *Protein Sci* **20**, 1196–1207 (2011).

196. Fleming, J. K., Wojciak, J. M., Campbell, M.-A. & Huxford, T. Biochemical and structural characterization of lysophosphatidic Acid binding by a humanized monoclonal antibody. *J Mol Biol* **408**, 462–476 (2011).

197. MacCallum, R. M., Martin, A. C. & Thornton, J. M. Antibody-antigen interactions: contact analysis and binding site topography. *J Mol Biol* **262**, 732–745 (1996).

198. Ewert, S., Cambillau, C., Conrath, K. & Plückthun, A. Biophysical properties of camelid V(HH) domains compared to those of human V(H)3 domains. *Biochemistry* **41**, 3628–3636 (2002).

199. Akazawa-Ogawa, Y. *et al.* Heat-induced Irreversible Denaturation of the Camelid Single Domain VHH Antibody Is Governed by Chemical Modifications. *J Biol Chem* **289**, 15666–15679 (2014).

200. Ladenson, R. C., Crimmins, D. L., Landt, Y. & Ladenson, J. H. Isolation and characterization of a thermally stable recombinant anti-caffeine heavy-chain antibody fragment. *Anal Chem* **78**, 4501–4508 (2006).

201. Jørgensen, T. Ø. *et al.* The antibody site in Atlantic salmon; phage display and modeling of scFv with anti-hapten binding ability. *Developmental & Comparative Immunology* **26**, 201–206 (2002).

202. Kobayashi, N., Karibe, T. & Goto, J. Dissociation-independent selection of high-affinity anti-hapten phage antibodies using cleavable biotin-conjugated haptens. *Analytical Biochemistry* **347**, 287–296 (2005).

203.   M, T. *et al.* Production and characterisation of monoclonal antibodies against a very small hapten, 3-methylindole. *J Immunol Methods* **240**, 111–124 (2000).

204.   Xu, J. *et al.* Exploratory trial of a biepitopic CAR T-targeting B cell maturation antigen in relapsed/refractory multiple myeloma. *Proc Natl Acad Sci U S A* **116**, 9543–9551 (2019).

205.   De Munter, S. *et al.* Nanobody Based Dual Specific CARs. *International Journal of Molecular Sciences* **19**, 403 (2018).

206.   Xie, Y. J. *et al.* Nanobody-based CAR T cells that target the tumor microenvironment inhibit the growth of solid tumors in immunocompetent mice. *Proc Natl Acad Sci U S A* **116**, 7624–7631 (2019).

207.   Jamnani, F. R. *et al.* T cells expressing VHH-directed oligoclonal chimeric HER2 antigen receptors: towards tumor-directed oligoclonal T cell therapy. *Biochim. Biophys. Acta* **1840**, 378–386 (2014).

208.   Singh, M. K., Srivastava, S., Raghava, G. P. S. & Varshney, G. C. HaptenDB: a comprehensive database of haptens, carrier proteins and anti-hapten antibodies. *Bioinformatics* **22**, 253–255 (2006).

209.   Morel, A., Darmon, M. & Delaage, M. Recognition of imidazole and histamine derivatives by monoclonal antibodies. *Molecular Immunology* **27**, 995–1000 (1990).

210.   Camelid Heavy-Chain Variable Domains Provide Efficient Combining Sites to Haptens | Biochemistry. https://pubs.acs.org/doi/10.1021/bi991830w.

211.   Bever, C. S. *et al.* VHH antibodies: Emerging reagents for the analysis of environmental chemicals. *Anal Bioanal Chem* **408**, 5985–6002 (2016).

212. Alvarez-Rueda, N. *et al.* Generation of llama single-domain antibodies against methotrexate, a prototypical hapten. *Mol Immunol* **44**, 1680–1690 (2007).

213. Yau, K. Y. F. *et al.* Selection of hapten-specific single-domain antibodies from a non-immunized llama ribosome display library. *Journal of Immunological Methods* **281**, 161–175 (2003).

214. Adrian, J., Font, H., Diserens, J.-M., Sánchez-Baeza, F. & Marco, M.-P. Generation of Broad Specificity Antibodies for Sulfonamide Antibiotics and Development of an Enzyme-Linked Immunosorbent Assay (ELISA) for the Analysis of Milk Samples. *J. Agric. Food Chem.* **57**, 385–394 (2009).

215. Doyle, P. J. *et al.* Cloning, expression, and characterization of a single-domain antibody fragment with affinity for 15-acetyl-deoxynivalenol. *Molecular Immunology* **45**, 3703–3713 (2008).

216. Vincke, C. *et al.* General Strategy to Humanize a Camelid Single-domain Antibody and Identification of a Universal Humanized Nanobody Scaffold *. *Journal of Biological Chemistry* **284**, 3273–3284 (2009).

217. Saerens, D. *et al.* Identification of a Universal VHH Framework to Graft Non-canonical Antigen-binding Loops of Camel Single-domain Antibodies. *Journal of Molecular Biology* **352**, 597–607 (2005).

218. Ghahroudi, M. A., Desmyter, A., Wyns, L., Hamers, R. & Muyldermans, S. Selection and identification of single domain antibody fragments from camel heavy-chain antibodies. *FEBS Letters* **414**, 521–526 (1997).

219. Arbabi-Ghahroudi, M. Camelid Single-Domain Antibodies: Historical Perspective and Future Outlook. *Front. Immunol.* **8**, (2017).

220. Genst, E. D. *et al.* Molecular basis for the preferential cleft recognition by dromedary heavy-chain antibodies. *PNAS* **103**, 4586–4591 (2006).

221. Chaplin, D. D. Overview of the Immune Response. *J Allergy Clin Immunol* **125**, S3-23 (2010).

222. *Immunobiology: the immune system in health and disease ; [animated CD-ROM inside]*. (Garland Publ. [u.a.], 2001).

223. Jr, C. A. J. *et al. Immunobiology*. (Garland Science, 2001).

224. Grant, G. A. Synthetic Peptides for Production of Antibodies that Recognize Intact Proteins. *Current Protocols in Immunology* **55**, 9.2.1-9.2.19 (2003).

225. Kafi, K. *et al.* Maleimide conjugation markedly enhances the immunogenicity of both human and murine idiotype-KLH vaccines. *Mol Immunol* **46**, 448–456 (2009).

226. Monnet, C. *et al.* Highly specific anti-estradiol antibodies: structural characterisation and binding diversity. *J Mol Biol* **315**, 699–712 (2002).

227. Burmester, J. *et al.* Selection, Characterization and X-ray Structure of Anti-ampicillin Single-chain Fv Fragments from Phage-displayed Murine Antibody Libraries. *Journal of Molecular Biology* **309**, 671–685 (2001).

228. Niemi, M. H. *et al.* The testosterone binding mechanism of an antibody derived from a naïve human scFv library. *J Mol Recognit* **24**, 209–219 (2011).

229. Spinelli, S., Tegoni, M., Frenken, L., van Vliet, C. & Cambillau, C. Lateral recognition of a dye hapten by a llama VHH domain. *J Mol Biol* **311**, 123–129 (2001).

230.   Sonneson, G. J. & Horn, J. R. Hapten-Induced Dimerization of a Single-Domain VHH Camelid Antibody. *Biochemistry* **48**, 6693–6695 (2009).

231.   Tabares-da Rosa, S., Wogulis, L. A., Wogulis, M. D., González-Sapienza, G. & Wilson, D. K. Structure and specificity of several triclocarban-binding single domain camelid antibody fragments. *J Mol Recognit* **32**, e2755 (2019).

232.   Ding, L. *et al.* Structural insights into the mechanism of single domain VHH antibody binding to cortisol. *FEBS Lett* **593**, 1248–1256 (2019).

233.   Baca, M., Presta, L. G., O'Connor, S. J. & Wells, J. A. Antibody humanization using monovalent phage display. *J Biol Chem* **272**, 10678–10684 (1997).

234.   Muyldermans, S. A guide to: generation and design of nanobodies. *The FEBS Journal* **288**, 2084–2102 (2021).

235.   Maass, D. R., Sepulveda, J., Pernthaner, A. & Shoemaker, C. B. Alpaca (Lama pacos) as a convenient source of recombinant camelid heavy chain antibodies (VHHs). *J Immunol Methods* **324**, 13–25 (2007).

236.   Ponsel, D., Neugebauer, J., Ladetzki-Baehs, K. & Tissot, K. High Affinity, Developability and Functional Size: The Holy Grail of Combinatorial Antibody Library Generation. *Molecules* **16**, 3675–3700 (2011).

237.   Moghaddam, A. *et al.* Identification of scFv antibody fragments that specifically recognise the heroin metabolite 6-monoacetylmorphine but not morphine. *J Immunol Methods* **280**, 139–155 (2003).

238.   Hawlisch, H. *et al.* Site-specific anti-C3a receptor single-chain antibodies selected by differential panning on cellulose sheets. *Anal Biochem* **293**, 142–145 (2001).

239. Hust, M., Maiss, E., Jacobsen, H.-J. & Reinard, T. The production of a genus-specific recombinant antibody (scFv) using a recombinant potyvirus protease. *J Virol Methods* **106**, 225–233 (2002).

240. Davies, J. *et al.* A scanning tunnelling microscopy comparison of passive antibody adsorption and biotinylated antibody linkage to streptavidin on microtiter wells. *J Immunol Methods* **167**, 263–269 (1994).

241. Takakusagi, Y., Takakusagi, K., Sakaguchi, K. & Sugawara, F. Phage display technology for target determination of small-molecule therapeutics: an update. *Expert Opinion on Drug Discovery* **15**, 1199–1211 (2020).

242. Omidfar, K. *et al.* Production of a Novel Camel Single-Domain Antibody Specificfor the Type III Mutant EGFR. *TBI* **25**, 296–305 (2004).

243. Smolarek, D., Bertrand, O. & Czerwinski, M. Variable fragments of heavy chain antibodies (VHHs): A new magic bullet molecule of medicine? *Postępy higieny i medycyny doświadczalnej (Online)* **66**, 348–58 (2012).

244. Martin, D. A. *et al.* Selection of Ig μ Heavy Chains by Complementarity-Determining Region 3 Length and Amino Acid Composition. *J Immunol* **171**, 4663–4671 (2003).

245. Dumoulin, M. *et al.* Single-domain antibody fragments with high conformational stability. *Protein Sci* **11**, 500–515 (2002).

246. Sheedy, C., Yau, K. Y. F., Hirama, T., MacKenzie, C. R. & Hall, J. C. Selection, characterization, and CDR shuffling of naive llama single-domain antibodies selected against auxin and their cross-reactivity with auxinic herbicides from four chemical families. *J Agric Food Chem* **54**, 3668–3678 (2006).

247. Tabares-da Rosa, S. *et al.* Competitive selection from single domain antibody libraries allows isolation of high-affinity antihapten antibodies that are not favored in the llama immune response. *Anal Chem* **83**, 7213–7220 (2011).

248. Klotzsche, M., Berens, C. & Hillen, W. A Peptide Triggers Allostery in Tet Repressor by Binding to a Unique Site*. *Journal of Biological Chemistry* **280**, 24591–24599 (2005).

249. Takahashi, M., Altschmied, L. & Hillen, W. Kinetic and equilibrium characterization of the Tet repressor-tetracycline complex by fluorescence measurements. Evidence for divalent metal ion requirement and energy transfer. *J Mol Biol* **187**, 341–348 (1986).

250. Johnson, C. M. Differential scanning calorimetry as a tool for protein folding and stability. *Arch Biochem Biophys* **531**, 100–109 (2013).

251. Govaert, J. *et al.* Dual beneficial effect of interloop disulfide bond for single domain antibody fragments. *J Biol Chem* **287**, 1970–1979 (2012).

252. Turner, K. B., Zabetakis, D., Goldman, E. R. & Anderson, G. P. Enhanced stabilization of a stable single domain antibody for SEB toxin by random mutagenesis and stringent selection. *Protein Eng Des Sel* **27**, 89–95 (2014).

253. Saerens, D., Conrath, K., Govaert, J. & Muyldermans, S. Disulfide Bond Introduction for General Stabilization of Immunoglobulin Heavy-Chain Variable Domains. *Journal of Molecular Biology* **377**, 478–488 (2008).

254. Hussack, G., Hirama, T., Ding, W., Mackenzie, R. & Tanha, J. Engineered single-domain antibodies with high protease resistance and thermal stability. *PLoS One* **6**, e28218 (2011).

255. Zabetakis, D., Olson, M. A., Anderson, G. P., Legler, P. M. & Goldman, E. R. Evaluation of Disulfide Bond Position to Enhance the Thermal Stability of a Highly Stable Single Domain Antibody. *PLoS One* **9**, e115405 (2014).

256. Akazawa-Ogawa, Y., Uegaki, K. & Hagihara, Y. The role of intra-domain disulfide bonds in heat-induced irreversible denaturation of camelid single domain VHH antibodies. *Journal of Biochemistry* **159**, 111 (2016).

257. van der Linden, R. H. *et al.* Comparison of physical chemical properties of llama VHH antibody fragments and mouse monoclonal antibodies. *Biochim Biophys Acta* **1431**, 37–46 (1999).

258. Liu, X. *et al.* Development of a nanobody-alkaline phosphatase fusion protein and its application in a highly sensitive direct competitive fluorescence enzyme immunoassay for detection of ochratoxin A in cereal. *Anal Chem* **87**, 1387–1394 (2015).

259. Bever, C. R. S. *et al.* Development and utilization of camelid VHH antibodies from alpaca for 2,2',4,4'-tetrabrominated diphenyl ether detection. *Anal Chem* **86**, 7875–7882 (2014).

260. Wang, J. *et al.* Heterologous antigen selection of camelid heavy chain single domain antibodies against tetrabromobisphenol A. *Anal Chem* **86**, 8296–8302 (2014).

261. He, T. *et al.* Nanobody-based enzyme immunoassay for aflatoxin in agro-products with high tolerance to cosolvent methanol. *Anal Chem* **86**, 8873–8880 (2014).

262. Franco, E. J. *et al.* Production and characterization of a genetically engineered anti-caffeine camelid antibody and its use in immunoaffinity

chromatography. *J Chromatogr B Analyt Technol Biomed Life Sci* **878**, 177–186 (2010).

263. Bakhtiari, S. H. A. *et al.* Anti-MUC1 Nanobody Can Redirect T-Body Cytotoxic Effector Function. *Hybridoma* **28**, 85–92 (2009).

264. Sharifzadeh, Z. *et al.* Genetically engineered T cells bearing chimeric nanoconstructed receptors harboring TAG-72-specific camelid single domain antibodies as targeting agents. *Cancer Lett.* **334**, 237–244 (2013).

265. Han, L. *et al.* Safety and efficacy of CAR-T cell targeting BCMA in patients with multiple myeloma coinfected with chronic hepatitis B virus. *J Immunother Cancer* **8**, e000927 (2020).

266. Han, L. *et al.* The phase I clinical study of CART targeting BCMA with humanized alpaca-derived single-domain antibody as antigen recognition domain. *JCO* **37**, 2535–2535 (2019).

267. Zhao, W.-H. *et al.* A phase 1, open-label study of LCAR-B38M, a chimeric antigen receptor T cell therapy directed against B cell maturation antigen, in patients with relapsed or refractory multiple myeloma. *J Hematol Oncol* **11**, 141 (2018).

268. Wang, B.-Y. *et al.* Long-Term Follow-up of a Phase 1, First-in-Human Open-Label Study of LCAR-B38M, a Structurally Differentiated Chimeric Antigen Receptor T (CAR-T) Cell Therapy Targeting B-Cell Maturation Antigen (BCMA), in Patients (pts) with Relapsed/Refractory Multiple Myeloma (RRMM). *Blood* **134**, 579 (2019).

269. Raje, N. *et al.* Anti-BCMA CAR T-Cell Therapy bb2121 in Relapsed or Refractory Multiple Myeloma. *New England Journal of Medicine* (2019) doi:10.1056/NEJMoa1817226.

270. Zorzi, A., Deyle, K. & Heinis, C. Cyclic peptide therapeutics: past, present and future. *Current Opinion in Chemical Biology* **38**, 24–29 (2017).

271. O'Neil, K. T. *et al.* Identification of novel peptide antagonists for GPIIb/IIIa from a conformationally constrained phage peptide library. *Proteins* **14**, 509–515 (1992).

272. McLafferty, M. A., Kent, R. B., Ladner, R. C. & Markland, W. M13 bacteriophage displaying disulfide-constrained microproteins. *Gene* **128**, 29–36 (1993).

273. Noren, K. A. & Noren, C. J. Construction of High-Complexity Combinatorial Phage Display Peptide Libraries. *Methods* **23**, 169–178 (2001).

274. Deyle, K., Kong, X.-D. & Heinis, C. Phage Selection of Cyclic Peptides for Application in Research and Drug Development. *Acc. Chem. Res.* **50**, 1866–1874 (2017).

275. Screening of a Library of Phage-displayed Peptides Identifies Human Bcl-2 as a Taxol-binding Protein | Elsevier Enhanced Reader. https://reader.elsevier.com/reader/sd/pii/S0022283698923038?token=C59 305BEA447517830C9DCE132A663D8899B567734AC6463928D6B9B29 E3E4A73ED6C13201A329341BE49C03C1C1BE70&originRegion=eu-west-1&originCreation=20210710181135 doi:10.1006/jmbi.1998.2303.

276. Whaley, S. R., English, D. S., Hu, E. L., Barbara, P. F. & Belcher, A. M. Selection of peptides with semiconductor binding specificity for directed nanocrystal assembly. *Nature* **405**, 665–668 (2000).

277. Joo, S. H. Cyclic Peptides as Therapeutic Agents and Biochemical Tools. *Biomol Ther (Seoul)* **20**, 19–26 (2012).

278. Krumpe, L. R. H. & Mori, T. The Use of Phage-Displayed Peptide Libraries to Develop Tumor-Targeting Drugs. *Int J Pept Res Ther* **12**, 79–91 (2006).

279. Giebel, L. B. *et al.* Screening of cyclic peptide phage libraries identifies ligands that bind streptavidin with high affinities. *Biochemistry* **34**, 15430–15435 (1995).

280. Duncan, K. E. *et al.* Discovery and characterization of a nonphosphorylated cyclic peptide inhibitor of the peptidylprolyl isomerase, Pin1. *J Med Chem* **54**, 3854–3865 (2011).

281. Roxin, Á. & Zheng, G. Flexible or fixed: a comparative review of linear and cyclic cancer-targeting peptides. *Future Medicinal Chemistry* **4**, 1601–1618 (2012).

282. Nilsson, F., Tarli, L., Viti, F. & Neri, D. Nilsson F, Tarli L, Viti F, Neri DThe use of phage display for the development of tumour targeting agents. Adv Drug Deliv Rev 43: 165-196. *Advanced drug delivery reviews* **43**, 165–96 (2000).

283. Aina, O. H., Sroka, T. C., Chen, M.-L. & Lam, K. S. Therapeutic cancer targeting peptides. *Biopolymers* **66**, 184–199 (2002).

284. Reilly, R. M. *et al.* Problems of Delivery of Monoclonal Antibodies. *Clin. Pharmacokinet.* **28**, 126–142 (1995).

285. Vaughan, T. J. *et al.* Human antibodies with sub-nanomolar affinities isolated from a large non-immunized phage display library. *Nat Biotechnol* **14**, 309–314 (1996).

286. Zhao, Y. *et al.* Discovery and Characterization of a High-Affinity Small Peptide Ligand, H1, Targeting FGFR2IIIc for Skin Wound Healing. *CPB* **49**, 1074–1089 (2018).

287. Jones, K. M. *et al.* Phage Ligands for Identification of Mesenchymal-Like Breast Cancer Cells and Cancer-Associated Fibroblasts. *Front Oncol* **8**, 625 (2018).

288. Wrighton, N. C. *et al.* Small peptides as potent mimetics of the protein hormone erythropoietin. *Science* **273**, 458–464 (1996).

289. Selective Inhibition of Matrix Metalloproteinase-14 Blocks Tumor Growth, Invasion, and Angiogenesis | Cancer Research. https://cancerres.aacrjournals.org/content/69/4/1517.long.

290. Selection and Screening of Antibody Phage Display Libraries | Antibody Drug Discovery. https://www.worldscientific.com/doi/abs/10.1142/9781848166295_0002.

291. Perosa, F., Favoino, E., Vicenti, C., Merchionne, F. & Dammacco, F. Identification of an antigenic and immunogenic motif expressed by two 7-mer rituximab-specific cyclic peptide mimotopes: implication for peptide-based active immunotherapy. *J Immunol* **179**, 7967–7974 (2007).

292. Pescovitz, M. D. Rituximab, an anti-cd20 monoclonal antibody: history and mechanism of action. *Am J Transplant* **6**, 859–866 (2006).

293. Binder, M., Otto, F., Mertelsmann, R., Veelken, H. & Trepel, M. The epitope recognized by rituximab. *Blood* **108**, 1975–1978 (2006).

294. Reichart, F. *et al.* Selective Targeting of Integrin αvβ8 by a Highly Active Cyclic Peptide. *Journal of Medicinal Chemistry* (2019) doi:10.1021/acs.jmedchem.8b01588.

295. Sevy, A. M. *et al.* Computationally Designed Cyclic Peptides Derived from an Antibody Loop Increase Breadth of Binding for Influenza Variants. *Structure* **28**, 1114-1123.e4 (2020).

296. Klotzsche, M., Goeke, D., Berens, C. & Hillen, W. Efficient and exclusive induction of Tet repressor by the oligopeptide Tip results from co-variation of their interaction site. *Nucleic Acids Res* **35**, 3945–3952 (2007).

297. Yu, J. & Smith, G. P. Affinity maturation of phage-displayed peptide ligands. *Methods Enzymol* **267**, 3–27 (1996).

298. Li, X., Keskin, O., Ma, B., Nussinov, R. & Liang, J. Protein-protein interactions: hot spots and structurally conserved residues often locate in complemented pockets that pre-organized in the unbound states: implications for docking. *J Mol Biol* **344**, 781–795 (2004).

299. Moreira, I. S., Fernandes, P. A. & Ramos, M. J. Hot spots—A review of the protein–protein interface determinant amino-acid residues. *Proteins: Structure, Function, and Bioinformatics* **68**, 803–812 (2007).

300. Brooks, B. D. *et al.* Characterizing Epitope Binding Regions of Entire Antibody Panels by Combining Experimental and Computational Analysis of Antibody: Antigen Binding Competition. *Molecules* **25**, 3659 (2020).

301. Renaud, J.-P. *et al.* Biophysics in drug discovery: impact, challenges and opportunities. *Nat Rev Drug Discov* **15**, 679–698 (2016).

302. Abbott, W. M., Damschroder, M. M. & Lowe, D. C. Current approaches to fine mapping of antigen–antibody interactions. *Immunology* **142**, 526–535 (2014).

303. Weiss, G. A., Watanabe, C. K., Zhong, A., Goddard, A. & Sidhu, S. S. Rapid mapping of protein functional epitopes by combinatorial alanine scanning. *PNAS* **97**, 8950–8954 (2000).

304. Hua, C. K. *et al.* Computationally-driven identification of antibody epitopes. *eLife* **6**, e29023 (2017).

305. Dahiyat, B. I. & Mayo, S. L. De novo protein design: fully automated sequence selection. *Science* **278**, 82–87 (1997).

306. Kuhlman, B. *et al.* Design of a Novel Globular Protein Fold with Atomic-Level Accuracy. *Science* **302**, 1364–1368 (2003).

307. Korkegian, A., Black, M. E., Baker, D. & Stoddard, B. L. Computational thermostabilization of an enzyme. *Science* **308**, 857–860 (2005).

308. Lippow, S. M., Wittrup, K. D. & Tidor, B. Computational design of antibody-affinity improvement beyond in vivo maturation. *Nat Biotechnol* **25**, 1171–1176 (2007).

309. Sela-Culang, I., Ofran, Y. & Peters, B. Antibody specific epitope prediction—emergence of a new paradigm. *Current Opinion in Virology* **11**, 98–102 (2015).

310. Ponomarenko, J. V. & Bourne, P. E. Antibody-protein interactions: benchmark datasets and prediction tools evaluation. *BMC Struct Biol* **7**, 64 (2007).

311. Schmitz, K. R., Bagchi, A., Roovers, R. C., van Bergen en Henegouwen, P. M. P. & Ferguson, K. M. Structural Evaluation of EGFR Inhibition Mechanisms for Nanobodies/VHH Domains. *Structure* **21**, 1214–1224 (2013).

312. Duhoo, Y. *et al.* Camelid nanobodies used as crystallization chaperones for different constructs of PorM, a component of the type IX secretion system from Porphyromonas gingivalis. *Acta Cryst F* **73**, 286–293 (2017).

313. Lefranc, M.-P. *et al.* IMGT unique numbering for immunoglobulin and T cell receptor constant domains and Ig superfamily C-like domains. *Dev Comp Immunol* **29**, 185–203 (2005).

314. Lefranc, M. P. Unique database numbering system for immunogenetic analysis. *Immunol Today* **18**, 509 (1997).

315. DeLano, W. L. Unraveling hot spots in binding interfaces: progress and challenges. *Current Opinion in Structural Biology* **12**, 14–20 (2002).

316. Friesner, R. A. *et al.* Glide: a new approach for rapid, accurate docking and scoring. 1. Method and assessment of docking accuracy. *J Med Chem* **47**, 1739–1749 (2004).

317. Halgren, T. A. *et al.* Glide: a new approach for rapid, accurate docking and scoring. 2. Enrichment factors in database screening. *J Med Chem* **47**, 1750–1759 (2004).

318. Marks, C. & Deane, C. M. Antibody H3 Structure Prediction. *Computational and Structural Biotechnology Journal* **15**, 222–231 (2017).

319. Improving Loop Modeling of the Antibody Complementarity-Determining Region 3 Using Knowledge-Based Restraints. https://journals.plos.org/plosone/article?id=10.1371/journal.pone.0154811.

320. Messih, M. A., Lepore, R., Marcatili, P. & Tramontano, A. Improving the accuracy of the structure prediction of the third hypervariable loop of the heavy chains of antibodies. *Bioinformatics* **30**, 2733–2740 (2014).

321. Rodrigues, J. P. G. L. M. *et al.* Defining the limits of homology modeling in information-driven protein docking. *Proteins* **81**, 2119–2128 (2013).

322. Bluestone, J. A. & Bour-Jordan, H. Current and Future Immunomodulation Strategies to Restore Tolerance in Autoimmune Diseases. *Cold Spring Harb Perspect Biol* **4**, a007542 (2012).

323. Kalos, M. & June, C. H. Adoptive T Cell Transfer for Cancer Immunotherapy in the Era of Synthetic Biology. *Immunity* **39**, 49–60 (2013).

324. Sterner, R. C. & Sterner, R. M. CAR-T cell therapy: current limitations and potential strategies. *Blood Cancer J.* **11**, 1–11 (2021).

325. Roybal, K. T. *et al.* Engineering T Cells with Customized Therapeutic Response Programs Using Synthetic Notch Receptors. *Cell* **167**, 419-432.e16 (2016).

326. Fischbach, M. A., Bluestone, J. A. & Lim, W. A. Cell-based therapeutics: the next pillar of medicine. *Sci Transl Med* **5**, 179ps7 (2013).

327. Brentjens, R. J. *et al.* CD19-targeted T cells rapidly induce molecular remissions in adults with chemotherapy-refractory acute lymphoblastic leukemia. *Sci Transl Med* **5**, 177ra38 (2013).

328. Maude, S. L. *et al.* Chimeric Antigen Receptor T Cells for Sustained Remissions in Leukemia. *New England Journal of Medicine* **371**, 1507–1517 (2014).

329. Turtle, C. J. *et al.* CD19 CAR–T cells of defined CD4$^+$:CD8$^+$ composition in adult B cell ALL patients. *J Clin Invest* **126**, 2123–2138 (2016).

330. Davila, M. L. *et al.* Efficacy and Toxicity Management of 19-28z CAR T Cell Therapy in B Cell Acute Lymphoblastic Leukemia. *Science Translational Medicine* **6**, 224ra25-224ra25 (2014).

331. Kochenderfer, J. N. *et al.* B-cell depletion and remissions of malignancy along with cytokine-associated toxicity in a clinical trial of anti-CD19 chimeric-antigen-receptor-transduced T cells. *Blood* **119**, 2709–2720 (2012).

332. Pettitt, D. *et al.* CAR-T Cells: A Systematic Review and Mixed Methods Analysis of the Clinical Trial Landscape. *Molecular Therapy* **26**, 342–353 (2018).

333. Maude, S. L. *et al.* Chimeric Antigen Receptor T Cells for Sustained Remissions in Leukemia. *http://dx.doi.org/10.1056/NEJMoa1407222* https://www.nejm.org/doi/10.1056/NEJMoa1407222 (2014) doi:10.1056/NEJMoa1407222.

334. Chou, C. K. & Turtle, C. J. Insight into mechanisms associated with cytokine release syndrome and neurotoxicity after CD19 CAR-T cell immunotherapy. *Bone Marrow Transplant* **54**, 780–784 (2019).

335. Gust, J., Taraseviciute, A. & Turtle, C. J. Neurotoxicity Associated with CD19-Targeted CAR-T Cell Therapies. *CNS Drugs* **32**, 1091–1101 (2018).

336. Locke, F. L. *et al.* Preliminary Results of Prophylactic Tocilizumab after Axicabtageneciloleucel (axi-cel; KTE-C19) Treatment for Patients with Refractory,Aggressive Non-Hodgkin Lymphoma (NHL). *Blood* **130**, 1547 (2017).

337. Neelapu, S. S. Managing the toxicities of CAR T-cell therapy. *Hematol Oncol* **37 Suppl 1**, 48–52 (2019).

338. Sadelain, M., Brentjens, R. & Rivière, I. The Basic Principles of Chimeric Antigen Receptor Design. *Cancer Discov* **3**, 388–398 (2013).

339. Lanitis, E., Dangaj, D., Irving, M. & Coukos, G. Mechanisms regulating T-cell infiltration and activity in solid tumors. *Ann Oncol* **28**, xii18–xii32 (2017).

340. Adachi, K. *et al.* IL-7 and CCL19 expression in CAR-T cells improves immune cell infiltration and CAR-T cell survival in the tumor. *Nat Biotechnol* **36**, 346–351 (2018).

341. Tang, L. *et al.* Enhancing T cell therapy through TCR-signaling-responsive nanoparticle drug delivery. *Nat Biotechnol* **36**, 707–716 (2018).

342. Wu, C.-Y., Roybal, K. T., Puchner, E. M., Onuffer, J. & Lim, W. A. Remote control of therapeutic T cells through a small molecule-gated chimeric receptor. *Science* **350**, aab4077 (2015).

343. Juillerat, A. *et al.* Modulation of chimeric antigen receptor surface expression by a small molecule switch. *BMC Biotechnol.* **19**, 44 (2019).

344. Lanier, L. L. DAP10- and DAP12-associated receptors in innate immunity. *Immunological Reviews* **227**, 150–160 (2009).

345. Weiss, A. & Littman, D. R. Signal transduction by lymphocyte antigen receptors. *Cell* **76**, 263–274 (1994).

346. Giordano-Attianese, G. *et al.* A computationally designed chimeric antigen receptor provides a small-molecule safety switch for T-cell therapy. *Nat Biotechnol* 1–7 (2020) doi:10.1038/s41587-019-0403-9.

347. Huppa, J. B., Gleimer, M., Sumen, C. & Davis, M. M. Continuous T cell receptor signaling required for synapse maintenance and full effector potential. *Nat Immunol* **4**, 749–755 (2003).

348.   Purbhoo, M. A., Irvine, D. J., Huppa, J. B. & Davis, M. M. T cell killing does not require the formation of a stable mature immunological synapse. *Nat Immunol* **5**, 524–530 (2004).

349.   Garrido-Mesa, N., Zarzuelo, A. & Gálvez, J. Minocycline: far beyond an antibiotic. *Br J Pharmacol* **169**, 337–352 (2013).

350.   Agwuh, K. N. & MacGowan, A. Pharmacokinetics and pharmacodynamics of the tetracyclines including glycylcyclines. *Journal of Antimicrobial Chemotherapy* **58**, 256–265 (2006).

351.   Chiocca, E. A. *et al.* Regulatable interleukin-12 gene therapy in patients with recurrent high-grade glioma: Results of a phase 1 trial. *Sci Transl Med* **11**, eaaw5680 (2019).

352.   Cortez-Retamozo, V. *et al.* Efficient tumor targeting by single-domain antibody fragments of camels. *International Journal of Cancer* **98**, 456–462 (2002).

353.   Bartunek, J. *et al.* Novel Antiplatelet Agents: ALX-0081, a Nanobody Directed towards von Willebrand Factor. *J. of Cardiovasc. Trans. Res.* **6**, 355–363 (2013).

354.   Muyldermans, S. Nanobodies: Natural Single-Domain Antibodies. *Annual Review of Biochemistry* **82**, 775–797 (2013).

355.   Van Bockstaele, F., Holz, J.-B. & Revets, H. The development of nanobodies for therapeutic applications. *Curr Opin Investig Drugs* **10**, 1212–1224 (2009).

356.   Jan, M. *et al.* Reversible ON- and OFF-switch chimeric antigen receptors controlled by lenalidomide. *Sci Transl Med* **13**, eabb6295 (2021).

357. Harris, D. T. & Kranz, D. M. Adoptive T Cell Therapies: A Comparison of T Cell Receptors and Chimeric Antigen Receptors. *Trends Pharmacol Sci* **37**, 220–230 (2016).

358. Alcover, A., Alarcón, B. & Di Bartolo, V. Cell Biology of T Cell Receptor Expression and Regulation. *Annu Rev Immunol* **36**, 103–125 (2018).

359. Baeuerle, P. A. *et al.* Synthetic TRuC receptors engaging the complete T cell receptor for potent anti-tumor response. *Nat Commun* **10**, 2087 (2019).

360. Helsen, C. W. *et al.* The chimeric TAC receptor co-opts the T cell receptor yielding robust anti-tumor activity without toxicity. *Nat Commun* **9**, 3049 (2018).

361. Arnett, K. L., Harrison, S. C. & Wiley, D. C. Crystal structure of a human CD3-epsilon/delta dimer in complex with a UCHT1 single-chain antibody fragment. *Proc Natl Acad Sci U S A* **101**, 16268–16273 (2004).

362. Iri-Sofla, F. J., Rahbarizadeh, F., Ahmadvand, D. & Rasaee, M. J. Nanobody-based chimeric receptor gene integration in Jurkat cells mediated by φC31 integrase. *Exp Cell Res* **317**, 2630–2641 (2011).

363. Cartellieri, M. *et al.* Switching CAR T cells on and off: a novel modular platform for retargeting of T cells to AML blasts. *Blood Cancer J* **6**, e458 (2016).

364. Albert, S. *et al.* A novel nanobody-based target module for retargeting of T lymphocytes to EGFR-expressing cancer cells via the modular UniCAR platform. *Oncoimmunology* **6**, e1287246 (2017).

365. Albert, S. *et al.* From mono- to bivalent: improving theranostic properties of target modules for redirection of UniCAR T cells against

EGFR-expressing tumor cells in vitro and in vivo. *Oncotarget* **9**, 25597–25616 (2018).

366. Rozan, C. *et al.* Single-domain antibody-based and linker-free bispecific antibodies targeting FcγRIII induce potent antitumor activity without recruiting regulatory T cells. *Mol Cancer Ther* **12**, 1481–1491 (2013).

367. Turini, M., Chames, P., Bruhns, P., Baty, D. & Kerfelec, B. A FcγRIII-engaging bispecific antibody expands the range of HER2-expressing breast tumors eligible to antibody therapy. *Oncotarget* **5**, 5304–5319 (2014).

368. Majzner, R. G. *et al.* Tuning the Antigen Density Requirement for CAR T-cell Activity. *Cancer Discov* **10**, 702–723 (2020).

369. James, J. R. Tuning ITAM multiplicity on T cell receptors can control potency and selectivity to ligand density. *Sci Signal* **11**, eaan1088 (2018).

370. Hudecek, M. *et al.* Receptor affinity and extracellular domain modifications affect tumor recognition by ROR1-specific chimeric antigen receptor T cells. *Clin Cancer Res* **19**, 3153–3164 (2013).

371. Woodsworth, D. J., Dunsing, V. & Coombs, D. Design Parameters for Granzyme-Mediated Cytotoxic Lymphocyte Target-Cell Killing and Specificity. *Biophysical Journal* **109**, 477–488 (2015).

372. Lindner, S. E., Johnson, S. M., Brown, C. E. & Wang, L. D. Chimeric antigen receptor signaling: Functional consequences and design implications. *Science Advances* (2020) doi:10.1126/sciadv.aaz3223.

373. Ying, Z. *et al.* A safe and potent anti-CD19 CAR T cell therapy. *Nat Med* **25**, 947–953 (2019).

374. Dwyer, C. J. *et al.* Fueling Cancer Immunotherapy With Common Gamma Chain Cytokines. *Front Immunol* **10**, (2019).

375. Zumerle, S., Molon, B. & Viola, A. Membrane Rafts in T Cell Activation: A Spotlight on CD28 Costimulation. *Frontiers in Immunology* **8**, (2017).

376. Milone, M. C. *et al.* Chimeric Receptors Containing CD137 Signal Transduction Domains Mediate Enhanced Survival of T Cells and Increased Antileukemic Efficacy In Vivo. *Molecular Therapy* **17**, 1453–1464 (2009).

377. Wu, J. *et al.* An Activating Immunoreceptor Complex Formed by NKG2D and DAP10. *Science* **285**, 730–732 (1999).

378. Irving, B. A., Chan, A. C. & Weiss, A. Functional characterization of a signal transducing motif present in the T cell antigen receptor zeta chain. *Journal of Experimental Medicine* **177**, 1093–1103 (1993).

379. Guy, C. S. *et al.* Distinct TCR signaling pathways drive proliferation and cytokine production in T cells. *Nat Immunol* **14**, 262–270 (2013).

380. Alabanza, L. *et al.* Function of Novel Anti-CD19 Chimeric Antigen Receptors with Human Variable Regions Is Affected by Hinge and Transmembrane Domains. *Molecular Therapy* **25**, 2452–2465 (2017).

381. Rodgers, D. T. *et al.* Switch-mediated activation and retargeting of CAR-T cells for B-cell malignancies. *PNAS* **113**, E459–E468 (2016).

382. Weber, E. W. *et al.* Transient rest restores functionality in exhausted CAR-T cells through epigenetic remodeling. *Science* **372**, eaba1786 (2021).

383. Porter, D. L. *et al.* Chimeric antigen receptor T cells persist and induce sustained remissions in relapsed refractory chronic lymphocytic leukemia. *Sci Transl Med* **7**, 303ra139 (2015).

384. Hofmann, S. *et al.* Chimeric Antigen Receptor (CAR) T Cell Therapy in Acute Myeloid Leukemia (AML). *J Clin Med* **8**, (2019).

385. Martinez, M. & Moon, E. K. CAR T Cells for Solid Tumors: New Strategies for Finding, Infiltrating, and Surviving in the Tumor Microenvironment. *Front. Immunol.* **10**, (2019).

386. Jung, K. *et al.* Heterodimeric Fc-fused IL12 shows potent antitumor activity by generating memory CD8+ T cells. *Oncoimmunology* **7**, e1438800 (2018).

387. Chmielewski, M., Kopecky, C., Hombach, A. A. & Abken, H. IL-12 release by engineered T cells expressing chimeric antigen receptors can effectively Muster an antigen-independent macrophage response on tumor cells that have shut down tumor antigen expression. *Cancer Res.* **71**, 5697–5706 (2011).

388. Zhang, L. *et al.* Improving Adoptive T Cell Therapy by Targeting and Controlling IL-12 Expression to the Tumor Environment. *Mol Ther* **19**, 751–759 (2011).

389. Yeku, O. O. & Brentjens, R. J. Armored CAR T-cells: utilizing cytokines and pro-inflammatory ligands to enhance CAR T-cell anti-tumour efficacy. *Biochemical Society Transactions* **44**, 412–418 (2016).

390. Motzer, R. J. *et al.* Phase I trial of subcutaneous recombinant human interleukin-12 in patients with advanced renal cell carcinoma. *Clin. Cancer Res.* **4**, 1183–1191 (1998).

391. Leonard, J. P. *et al.* Effects of single-dose interleukin-12 exposure on interleukin-12-associated toxicity and interferon-gamma production. *Blood* **90**, 2541–2548 (1997).

392. Schwarz, D. S. & Blower, M. D. The endoplasmic reticulum: structure, function and response to cellular signaling. *Cell. Mol. Life Sci.* **73**, 79–94 (2016).

393. Meusser, B., Hirsch, C., Jarosch, E. & Sommer, T. ERAD: the long road to destruction. *Nat Cell Biol* **7**, 766–772 (2005).

394. Munro, S. & Pelham, H. R. B. A C-terminal signal prevents secretion of luminal ER proteins. *Cell* **48**, 899–907 (1987).

395. Semenza, J. C., Hardwick, K. G., Dean, N. & Pelham, H. R. ERD2, a yeast gene required for the receptor-mediated retrieval of luminal ER proteins from the secretory pathway. *Cell* **61**, 1349–1357 (1990).

396. Gomez-Navarro, N. & Miller, E. Protein sorting at the ER-Golgi interface. *J Cell Biol* **215**, 769–778 (2016).

397. Majoul, I., Straub, M., Hell, S. W., Duden, R. & Soeling, H.-D. KDEL-Cargo Regulates Interactions between Proteins Involved in COPI Vesicle Traffic: Measurements in Living Cells Using FRET. *Developmental Cell* **1**, 139–153 (2001).

398. Maciocia, P., Wawrzyniecka, P., Kassimatis, L. & Pule, M. A Protein-Based Method to Develop Allogeneic Chimeric Antigen Receptor T-Cells. *Blood* **132**, 700 (2018).

399. Chen, D. *et al.* Chimeric antigen receptor T cells derived from CD7 nanobody exhibit robust antitumor potential against CD7-positive malignancies. *Am J Cancer Res* **11**, 5263–5281 (2021).

400. Koneru, M., Purdon, T. J., Spriggs, D., Koneru, S. & Brentjens, R. J. IL-12 secreting tumor-targeted chimeric antigen receptor T cells eradicate ovarian tumors in vivo. *Oncoimmunology* **4**, e994446 (2015).

401. Chinnasamy, D. *et al.* Local delivery of interleukin-12 using T cells targeting VEGF receptor-2 eradicates multiple vascularized tumors in mice. *Clin Cancer Res* **18**, 1672–1683 (2012).

402. Zhao, J., Lin, Q., Song, Y. & Liu, D. Universal CARs, universal T cells, and universal CAR T cells. *Journal of Hematology & Oncology* **11**, 132 (2018).

403. Oakley, M. G. & Kim, P. S. A Buried Polar Interaction Can Direct the Relative Orientation of Helices in a Coiled Coil [†]. *Biochemistry* **37**, 12603–12610 (1998).